Development and Characterization of Polymer Gel as Self-driven Actuators

by

Liangxi Li

A dissertation submitted to the Graduate Faculty of
Auburn University
in partial fulfillment of the
requirements for the Degree of
Doctor of Philosophy

Auburn, Alabama
August 7, 2021

Keywords: Marangoni effect, self-driven actuator,
chemomechanical, polymer gels

Approved by

Committee Members
Zhongyang Cheng, Chair, Professor of Materials Engineering
Edward Davis, Assistant Professor of Materials Engineering
Pengyu Chen, Assistant Professor of Materials Engineering
Xinyu Zhang, Associate Professor of Chemical Engineering

Abstract

Actuators are objects that can transfer energy or signal to mechanical energy and are widely used in our daily life. Most of actuators are actuated by external energy suppliers that make the device big. Self-powered actuators, which are able to provide directional motion without external energy input, are extremely desirable for some special applications.

In this study, a new type of self-powered and rechargeable actuators composed of polymer gel are developed and studied. These actuators can move at the water-air interface, liking some microorganisms that can move around without external energy suppling unit. To deepen the understanding of self-driven gel actuator, a systemic study of their characteristics was carried out. First of all, it is experimentally confirmed that self-driven motions of gel actuators at the air-water interface is a universal phenomenon. When the solvent in get is completely consumed (i.e., diffused to water), the gel actuators can be recharged by placing gel in solvent. Gel actuators with large mass result in larger mass loss and longer duration of motion. Both solvent diffusion and surface tension contribute to the observed self-driven motions. Solvent diffusion is the main driven force for the self-driven motion of gels, while surface tension makes a minor contribution. The diameter of beaker has an effect on the motion of gel actuators, while the water depth and volume of water has little effect on the motion.

Next, the change in the gel's characteristics during its motion at the air-water surface were characterized. Based on the experimental results, it is concluded that the mass of the gel decreases with time as solvent in gel diffusing into water. In addition, the gel actuators shrink after motion.

The transparency of the gel decreases as motion at the air-water interface. Compared to the gels exposed to the air, gel actuators loss mass more, shrink faster and became less transparency after motions. The gel actuators undergo bending downward once placed at the air-water interface and transform to bending upward gradually during motion.

Furthermore, a process to quantify the gel motion was established by taking the advantage of digit videos. Using this process, various variables/parameters about the motion of gel at the air-water surface: velocity, acceleration, kinetic energy and their time dependence are able to be obtained. Motion modes and motion variables of gel actuators can be clearly illustrated as function of time. It was found that the velocity of gel actuator decreases as it moves toward the wall of glass beaker and increases as it moves away from the wall of glass beaker. The motion in the first a few seconds is irregular, and the first few seconds are not used for the motion mode study. Based on the experimental results, it is concluded that the shape/geometry of the gel actuators plays an important role on their motion mode. For example, gel in rectangle shapes with a higher length/width ratio have the tendency of spin motions; gel in circle and square shape have the tendency of orbital motions. Based on the geometry dependent results, gels built in 3D printed mold in a fan shape with releasing windows were designed and fabricated, which have controlled motion modes. Thanks to the digitalized results, friction force of gel motion at the air-water interface was studied and it is confirmed that the friction force obeys $F = -\alpha v^2$, where v is the velocity of the gel.

Fourthly, energy conversion through the actuation process was studied. Self-driven gels convert stored chemical energy into mechanic motions. The consumption of the kinetic energy of a gel during the motion reflects the contribution of the friction force. The kinetic energy and work down

by the friction force are obtained from experiment. The chemical energy change of gel actuators is linked with the mass loss of actuators originated by solvent diffusion. A new model was derived that considers one-dimensional diffusion into semi-infinite bar. This model can help us understand the trend of mass loss as function of time. Based on the experimental results, mass loss as function of time has two segments of time, i.e., Period – I and Period – II. A set of equation was derived to describe the mass loss in the two time periods. An empirical equation based on Eq. (5.8) can be used to predict mass loss as function of time in Period – I and a simplified equation from Eq. (5.28) can be used to predict mass loss as function of time in Period – II. This can be used for the future study to determine the velocity of solvent eject by the gel actuators, which is a step forward for the understanding of self-driven gels.

Acknowledgments

I would like to express my most sincere thanks to my advisor Dr. Zhongyang Cheng. I had little knowledge with the real research when I enrolled in Auburn University. I am confused and had hard time with projects. And I cannot reach my achievements without Dr. Cheng's guidance, support and encouragement. What I learn these years will benefit me in the whole lifetime. I would like to express my sincere thanks to my committee member, Dr. Edward Davis, Dr. Pengyu Chen, Dr. Xinyu Zhang and the outside-department dissertation reader, Dr. Tae-Sik Oh, for their guides, time and efforts. I appreciate their valuable suggestions on my research and dissertation.

I would like to express my sincere thanks to the staff in Materials Engineering. Many thanks to technician Mr. Steven Moore for offering me help, training, lab supplies purchase and technical supports.

I would like to express sincere thanks to my group member: Dr. Lin Zhang, Dr. Patrick Bass, Dr. Zhizhi Sheng, Dr. Yang Tong, Dr. Hossein Talebinezhad, Dr. Farrukh Najmi, Jiachen Liu, Yancen Cai, Jindong Wei, Weiye Wang, Jialiang Shen. Many thanks for their support and help. I am so happy to work, study and make progress together. Special thanks to Dr. Farrukh Najmi for helping on equation derivation, Yuzhe Sun for the coding supports and Wen Yang for helping me fabricating 3-D print molds. Many thanks to my colleagues and friends, Dr. Yuanyuan Zhang, Jiajia Hu, Dr. Anqi Zhang, Yan Chen, Dr. Xingxing Zhang, Dr. Songtao Du, Dr. Yuzhe Liu, Dr. Lang Zhou, Dr. Pu Deng, Xue Li, Dr. Xin Sha, Dr. Yang shen, Zi Yan, Jing Zhao and Shijia Wang.

Table of Contents

List of Figures

19

List of Table

Chapter I

Introduction

1.1 Overview of actuators

Actuators are essential components for almost all engineering devices and systems. Actuators convert input energy, that can be very different, into mechanical work. Conventional actuators are components of a machine that convert input energy (i.e., electric, magnetic, optical energy) into motion or control. Muscles are natural actuators that transfer calories from food into various forms of mechanical work, such as running, walking, hitting, for instance.

Actuators can be made of materials that are able to respond to external stimuli (i.e., input energy) with a mechanical response. The input energy can be electrical, mechanical, optical, thermal and magnetic energy, which are summarized in Table 1.1. For example, a motor can convert electrical energy to mechanical work; a pneumatic control valve can transform mechanical energy to mechanical motion [1].

Based on the way that input energy is supplied, all actuators can be categorized into two simple groups: external-stimulated actuators and self-driven actuators. The input energy of the self-driven actuators is stored in the actuator and the self-driven actuators exhibit an autonomous motion.

The size of the actuators can vary over a big range from nanometers to meters (e.g., motors) or even tens of meters (e.g., piston in hydraulic cylinder). The size of an actuator is dependent on not only the mechanism, but also the actuator and application. Nowadays, the actuators with sizes down to micrometers, or even nanometers, have been developed, such as the actuators used to

Table 1.1 Energy input and output for actuators

Input Energy	Output	Examples
Mechanical energy		Hydraulic piston, Pneumatic valve
Electrical energy		Electric motor, Piezoelectric actuator, Electrostrictive actuator
Thermal energy	Mechanical work	Shape memory material, Thermal expansion
Magnetic energy		Magnetostrictive actuator, Magnetic actuators
Optical energy		Photostrictive actuators, Photothermal actuators
Chemical energy		Internal combustion engine (chemical reaction) Diffusion (chemical potential)

manipulate single cells[2]. Both organic and inorganic materials have been used to fabricate actuators. Requirements for materials to be used in the actuators include ability of deformation, fatigue resistance, long cycle life and stability. Inorganic materials, such as ceramics and glass, are generally of good chemical stability and thermal stability that allows them to operate under different conditions for actuator applications [3,4]. On the other hand, organic materials, especially polymers, have advantages including large deformation, being resilient with a high mechanical impact under an applied load, high processability, synthetic versatility, inexpensive and light weight. Driven by rapid development of polymer in the late 20th century, polymers have been used to develop actuators [5].

The output of actuators can be linear, rotary, bending, elongation, expansion, oscillation, locomotion, etc. [6,7]. For instance, a hydraulic cylinder or an air cylinder can convert energy into

linear movements. A fan can convert electronic energy into rotary movements. Voice coils in a speaker can convert electric energy into oscillations.

The performance of an actuator can be characterized using many parameters. Parameters that vary from applications to applications, include displacement, bending degree, velocity, force, frequency, etc. Based on the deformation, actuators can be characterized by their elongation and strain. For example, a piezoelectric ceramic actuator is of elongation with 0.1% [17], and a shape memory polymer can exhibit a high strain of 800% [8]. Actuators can be characterized by the speed of motion if they exhibit mechanical motions. For example, a droplet (~2 μL) was observed with a speed of 0.35 μm/s on a solid surface [9], and a liquid metal droplet can have a locomotion rate of 180 mm/s in aqueous phase [10].

1.2 External-stimulated actuators

Numerous materials were able to respond to external stimuli with a mechanical work so that these materials can be used to develop external-stimulated actuators. Aforementioned energy forms (i.e., electric, thermal, magnetic, mechanical, optical and chemical energy) have been used in the various actuations. Nowadays, stimuli-responsive materials play vital roles in emerging actuator applications [11,12,13,14]. Actuators made of various types of materials with stimuli-responsive properties and their mechanisms, advantages and shortages are briefly reviewed here based on the input energy form.

1.2.1 Electric energy

Electric energy is widely used and essential in our daily life and current industries. Materials that can utilize electric energy and undergo actuation processes are plentiful, including polymers, ceramics, single crystal, etc. Ceramic, especially piezoelectric-based ceramic actuators, are relatively mature for commercial applications. They are of good chemical as well as thermal stability and high stiffness. Plus, ceramics have advantages on robust and inexpensive techniques to form films with thickness of a wide range. Nevertheless, ceramics are limited in strain (typical 0.1% in elongation [17]), which constrains their applications as actuators. Polymer actuators, on the opposite side, are flexible and able to generate a large displacement. Ability to undergo large deformation in responding to external stimuli is important in actuation applications. In addition, polymer actuators are characterized by high processability, synthetic versatility and light weight. It should be mentioned that no matter what type of actuator it is, wires are an inevitable component that connects electric power and the actuators.

1.2.1.1 Piezoelectric actuators

Piezoelectric actuators are one type of actuator which have been intensively investigated and are widely used in current industry [15]. Piezoelectric materials as actuators have the following advantages over other electric actuators: rapid response time, low power consumption, less heat and low noise generation [4], and additionally, their ability to work at high frequency and high temperature, which make them suitable for applications in severe conditions [16,17]. Piezoelectric materials exhibit a dimension change when the applied voltage changes and, thus, afford the actuators with enormous promises. Basically, they convert input electrical energy into mechanical

energy and vice versa. Due to the fact that the response of a piezoelectric material is a strain (i.e., change in the percentage of its dimension that is typically in the range less than 0.1% elongation [17]), the shape change or displacement of a piezoelectric actuator can be in the micrometer even nanometer range, dependent on its dimension. Piezoelectric actuators are used in miniature motors, micromanipulators, dispensing systems, precision positioning systems, vibration suppressors, acoustics, etc. Nowadays, research on piezoelectric actuators has been extended to robotic applications, health monitoring applications, acoustic emission techniques, etc [16].

1.2.1.2 Electroactive actuators

Electroactive polymers (EAPs) are another type of electric stimuli-responsive materials that been extensively studied in last three decades [18,19] and is still a hot research area [20,21,22,23]. EAP actuators are capable of undergoing a deformation with response to proper electric stimuli and have promising applications in drug delivery [19], tunable systems [24], artificial muscle [25,26], motor, etc.

EAPs can be divided into two main groups: ionic EAP [27] and electronic EAP. Deformation of ionic EAP relies on stimulated ion or solvent transportation. Ions are randomly distributed in an EAP in absence of an electric field, and the EAP actuator is at its initial shape, such as flat, as shown in Figure 1.1(a). These ions can move through the polymer along the electric field and will move to two different sides when an electric field is applied cross the two sides. The accumulation of cation/ anion on each side, and the size difference between the cation and anion, results in a bending of the EAP actuator as shown in Figure 1.1(b).

Ionic EAP can be driven using a very low electric field/voltage as low as 1 V [19], which is the major advantage of ionic EAP over other electric stimulus-responsive materials. Ionic EAP faces some challenges, such as a short lifetime, slow response speed, and a small diving force.
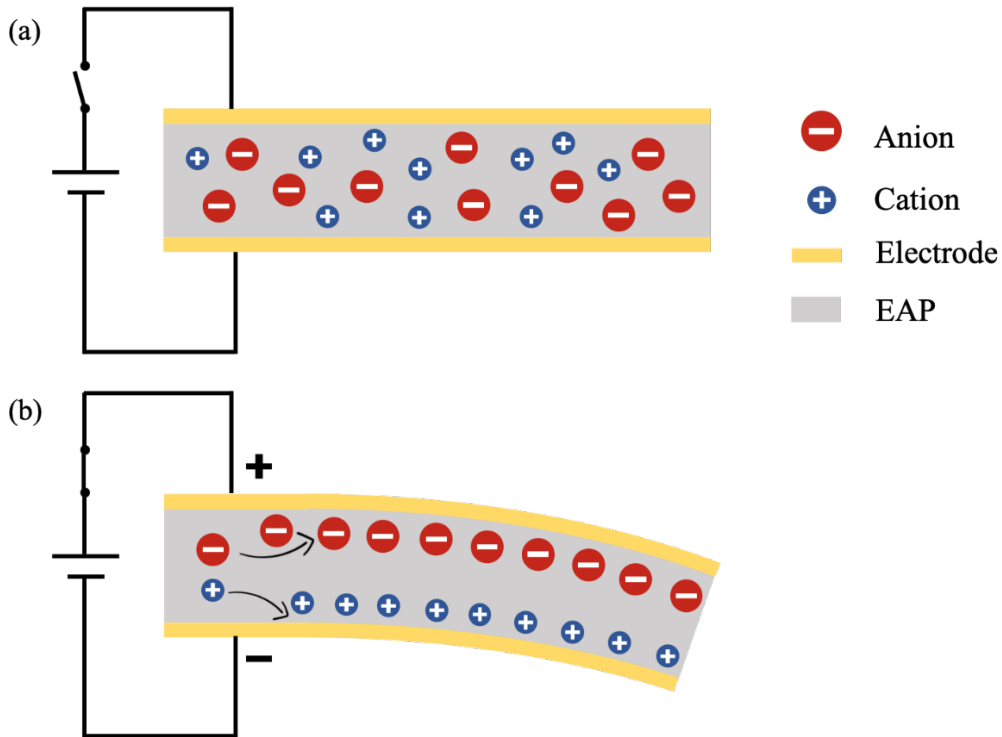
Figure 1.1 Scheme of principal for electroactive polymer actuators

Electronic EAP includes electrostrictive polymer, piezoelectric polymer and dielectric elastomers. Electronic EAP are of a long lifetime, fast respond speed and high strain/stress deformation, while electronic EAP required high a stimulated electric field[19,28], $\sim 10^2$ MV/m.

1.2.2 Thermal energy

Thermal actuators, implied by the name, are powered by thermal energy. Thermal energy input in the study refer to the heat or temperature change. There are different ways to generate the heat. For example, photothermal effect (i.e., optical energy is converted into heat) and electrothermal

effect (i.e., electrical energy is converted into heat) have been used to generate the heat and trigger an actuation process.

Shape memory materials (SMMs) have been used to fabricate various actuators. SMMs possess the ability to return to their original shape and size with thermal stimulus. This phenomenon makes the SMMs remember their former configuration. Among different types of SMMs, shape memory alloy (SMA) and shape memory polymer (SMP) are two vital ones. Performances of all SMMs can be evaluated using the ability or degree of materials to return to their original state, induced by a proper stimulus [29]. SMMs are able to offer a considerable range of motion and usually lots of circles for actuators applications [30].

SMAs are very sensitive to precise composition, grain size and processing conditions [31, 32]. Thus, they can be tailored to various applications, for instance automotive systems, energy conversion, aerospace applications (adaptive aircraft), biomedical applications, etc. Three methods have been used to heat up SMAs: (1) electrical current through SMA, (2) electrical current through high-resistance wire wrapped around SMA, and (3) by air/water or other medium around SMA [32]. To date, only a limited number of patented SMAs are commercially available [33]. The limited commercial success of SMA applications is due to a limited operation temperature, load or stress. SMPs, as soft materials, can undergo a much large deformation. SMPs are based on the phase-separated structures between their hard and soft segments. SMPs have the ability of being transparent, which is needed by some particular applications, and ability to be tailored by blending fillers or varying compositions. The shape memory effect of SMPs can be induced by temperature [34,35,36] that can be induced by light [37,38,39], electrical field [40,41,42], magnetic field [43,44], etc.

A water-driven SMP was developed by Huang *et al.* [36]. This actuator was able to be bent at 40 °C and recover gradually in room-temperature water. The drawbacks of SMPs mainly are: (1) requiring a change in ambient temperature and (2) difficulty to control the quantitative supply of heat. Development of electroactive SMPs, magnetic induced SMPs or light induced SMPs can solve part of the problems mentioned above. A future prospect lies in the development of various new material systems to meet different specific demands [38].

Besides SMM, thermal responsive polymers can also be used to develop thermal-stimulated actuators [45, 46]. Thermal responsive polymers are polymers that exhibit conformational changes in response to temperature, and the conformational changes induce a discontinuous change of their physical properties. For example, Stoychev et al. [47] fabricated microcapsules that were able to fold and unfold in response to temperature, utilizing a thermal-responsive polymer.

1.2.3   Optical energy

Light energy has attracted a great deal of attention since it is an abundant, sustainable and renewable energy which is widely distributed on earth. In nature, plants can convert optical energy into chemical energy through photosynthesis. The chemical energy can be further used for organism activities. However, it is known that natural sunlight is unstable and may be affected by weather, climate, season or unexpected incidents.

Photo-actuators are able to be remotely and precisely controlled without wires [48, 49]. Thus, actuators powered by light have potential applications in nano- and microscale devices/systems [50]. Generally, natural light is utilized as input energy input in the development of actuators

triggered by light. There are some reports focused on infrared (IR) and near-infrared (NIR) light as the input energy [51, 52, 53]. The output of photoactuators can be an oscillation [54], bending [55], or helical motion [56], etc. For example, J. Mu et al. [57] fabricated a graphene monolayer paper that can be stimulated by sunlight. Their multi-responsive material exhibits a rapid, powerful and controllable response with a representative of light. It can curl up and grip an object powered by optical energy. Kumar et al. [58] fabricated a film that has continuous chaotic oscillations stimulated by sunlight.

1.2.4 Magnetic energy

Magnetically-responsive actuators have the same advantages as discussed for photoactuators, namely they can be remotely and precisely controlled. In addition, a magnetic field is able to penetrate a wide range of materials and the response of the actuators is relatively fast compared to other types of actuations [59,60]. Torques are generated on materials filled with magnetic particles when subjected to a magnetic field [61,62]. Magnetic materials can exhibit magnetostrictive, magnetoelastic and piezomagnetic effects. All of these effects can result in a dimension change or a physical deformation in a magnetic material when the magnetic material is subjected to a magnetic field. Magnetic actuators are beneficial when working in a confined space and are promising for applications including drug delivery [63], microrobotics [64], microfluidics [65], lab-on-a-chip devices, etc. However, magnetic coils are essential to generate a magnetic field.

1.2.5 Chemical energy

Chemical energy is another type of energy that has been used as input energy. The process that directly converts chemical energy to mechanical energy is the so-called the "chemomechanical'' process. A chemomechanical process generally involves chemical reactions and a chemical potential difference in the system. Chemical reactions as energy input are of great advantage of high energy density. An explosion is a chemical reaction process that generates gases that expand rapidly so that chemical energy is converted into mechanical work. Internal combustion engines can be characterized as actuators that convert energy generated from chemical reactions into mechanical work.

Among different chemical reactions that induce/generate mechanical work, Belousov-Zhabotinsky (BZ) reactions that are main group that has been extensively studied in recent years [66,67,68,69]. BZ is generally known as an oscillating reaction consisting of organic acids, oxidizing agents and a metal catalyst [70,71]. BZ reactions are mostly in solution and induce autonomous motion without the on-off switching of external stimuli. Chemical energy from BZ reactions is converted into mechanical energy. Self-oscillating actuations powered by BZ reactions are controlled by changing the composition, temperature and size of gel [72]. Motions of self-oscillating systems triggered by BZ reactions are available among ciliary motion [73], self-walking [74, 21], intestine-like motion [75], periodic reciprocating motion [70], etc. Applications of those self-oscillating gels lie in artificial motors, artificial muscles, biomimetic robots, mass transportation, etc. However, BZ reactions require crucial operating conditions where a strong acid and oxidant coexist [76]. There is

a challenge on BZ self-oscillating system operating under physiological environments, thus systems of these actuations should be improved for them to be used in practical applications [77].

Besides the aforementioned motions powered by chemical reaction, BZ reactions for example, there are motions that can be triggered by chemical potential differences in a system. Some actuators were fabricated with a function on motion generated by solvent vapor or moisture [78,79]. Cheng et al. [80] fabricated a torsional graphene-fiber motor that is able to respond to moisture. Its moisture-responsive actuation allows applications of humidity switches and electric generators. The method that exploits chemical potential differences in a system is also a strategy for self-driven actuation. All in all, different from other energy inputs, actuators powered by chemical energy are able to generate self-driven motions.

1.3 Self-driven actuators

There are materials that exhibit self-driven motions without external power. Self-driven motions/actuators were widespread in the biological world and aroused great research interests [81,82,83]. Studies of the self-driven motion help us not only understand autonomous motions in biological systems, but also aid in designing motors or actuators to mimic living systems. In addition, self-driven motions/actuators have promising applications in drug delivery, lab-on-a-chip devices, sensors, etc.

Inspired by living organisms, chemomechanical conversion was exploited to develop actuators exhibiting self-driven motions [84,85]. The isothermal conversion of chemical energy into mechanical energy or motion is ubiquitous in living organisms across many length scales. This

process is greatly different from thermal engines that provide mechanical energy with heat generation. Therefore, this type of conversion can be more efficient and may meet the demand to develop environmentally friendly energy devices [86,87]. In addition, chemomechanical systems may have promising applications where power supply is limited, for example, under water or in space [88].

A strategy to fabricate artificially autonomous actuators is taking advantage of synesthetic polymers instead of utilizing biomolecules from living organisms. Thus, the study of chemomechanical systems based on synthetic materials is essential for the growth of self-driven actuators and robotics.

1.3.1 Mechanisms of self-driven motion

Living organisms work through the dissipation of chemical energy under almost isothermal condition, which is the so-called chemomechanical process mentioned above. It exhibits a specific spatiotemporal mode in a self-organized manner under a thermodynamically open condition. Dynamics of the motion is vital for fundamental and technological studies. Moreover, to mimic moving living objects or designing novel artificial motors that adapt to the environment, the understanding of the mechanism of their self-motion is needed.

Marangoni effect is a phenomenon that the chemical energy is directly converted into mechanical motions. Fundamental behind self-driven motion is the imbalance of surface tension around actuators, or broken the symmetry at front and rear of actuators [147,167].

Although the Marangoni effect has been extensively discussed in recent years, it still attracts a great deal of research interests recently due to its potential for various applications. Additionally, the mechanism behind the Marangoni effect has not been fully unraveled [89,90,91,92,93,94]. This process can be analogous to the processes in living organisms and the studies about the Marangoni effect to employ chemical engines is important in modern science [95].

Besides the Marangoni effect, conservation of momentum should be taken into consideration. An actuator can be pushed forward by expelling substance in the opposite direction. A good example is a rocket that is pushed forward by expelling exhaust at a high speed.

1.3.2   Surface tension

Surface tension is an inevitable term through the discussion of the Marangoni effect. Interior molecules are pulled equally in every direction because of cohesive force, leading to a net force of zero. While molecules at the liquid–air interface lack of pulls on the air side, those molecules are pulled inward, which is shown in Figure 1.2 (a). Therefore, the surface of liquid contracts to a minimum area and this tendency is the so-called surface tension.
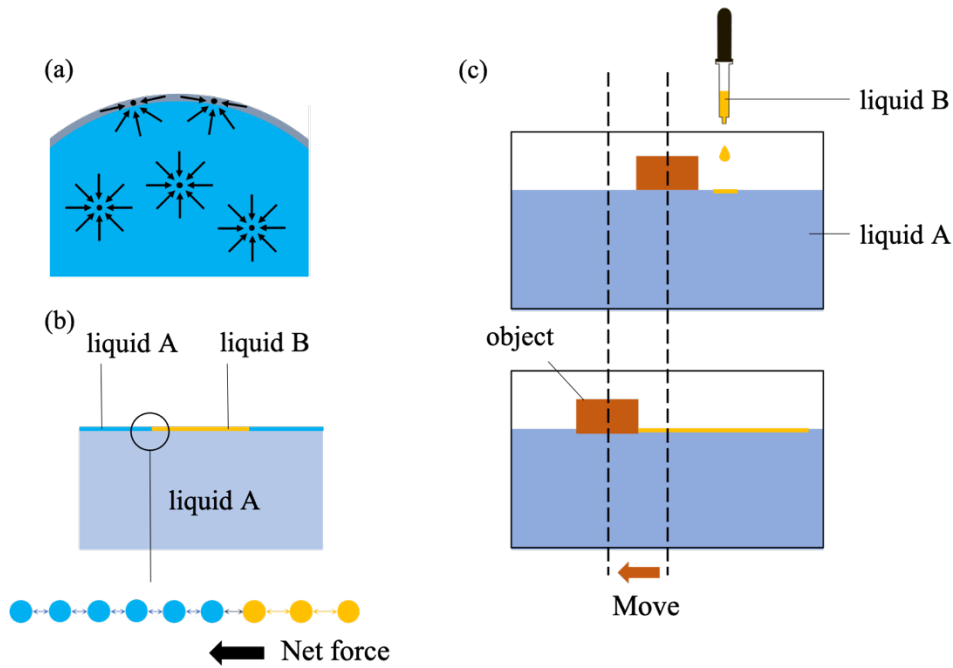
Figure 1.2 Scheme of forces on liquid molecules and fundamental of Marangoni effects

In addition to cohesive force, energy is another aspect to understand surface tension. Interior molecules have a lower energy because they are surrounded by molecules as many as they can possibly have. Compared to interior molecules, the molecules at the liquid–air interface lack neighbors and thus results in a higher energy. The number of molecules at the liquid–air interface is minimized in order to minimize the overall energy, which leads to a minimum surface area. Compared to interior molecules, molecules at the surface of liquid form stronger bonds due to surface tension. Surface tension of a liquid is proportional to the contractile force of molecules on the surface. A high surface tension of a liquid corresponds to a high contractile force. If a drop of liquid B with a lower surface tension is placed on liquid A with higher surface tension, contractile force of liquid A is higher than that of liquid B. Therefore, the surface tension of liquid A is stronger than the surface tension of liquid B. This results in a net force from the region with a

lower surface tension (liquid B area) to the region with a higher surface tension (liquid A area), which was shown in Figure 1.2 (b). If an object is placed on the surface of liquid A and then liquid B was applied on one side of the object, aforementioned net force is able to push the object forward, which was shown in Figure 1.2 (c).

1.3.3 Marangoni Effect

As discussed above, the net force from the region with a lower surface tension to the region with a higher surface tension is known as the Marangoni flow. The spontaneous spreading arisen from Marangoni flow is known as the Marangoni effect. This phenomenon was first identified by Carlo Marangoni in 1865, and thereby, this general effect was named after him.

The Marangoni effect is generated by surface tension gradient resulting in either mass or heat transfer along an interface. Basically, the surface tension depends on both the temperature and chemical potential. The Marangoni effect generated by a concentration gradient was named as solutal Marangoni effect. The Marangoni effect generated by a thermal gradient was named as thermal Marangoni effect, also known as thermocapillary instabilities [96, 97, 98]. In some systems, thermal and chemical Marangoni convection exist simultaneously. Thus, there are studies to clarify features of flow caused by thermal Marangoni convection and chemical Marangoni convection [99,100].

As stated above, it is clear that the Marangoni effect can be triggered by the local inhomogeneity of the surface tension gradient along the direction perpendicular to the interface. Although, the Marangoni effect has been known for more than a century and is studied experimentally and

theoretically, a universal onset criterion of the Marangoni effect was still not developed due to the complexity of systems, including geometry, boundary condition, solvent properties, etc [101]. Most of self-driven motions generated by the Marangoni effect were generally random agitation with regard to both spatial and temporal changes. To regular the motion of actuators, efforts were made by applying geometrical constraints or controlling size and shape of actuators. Marangoni flow or Marangoni convection can be observed in a water droplet utilizing fluorescent particles [102]. And numerical studies of sessile droplets during evaporation process was still being investigated recently [103, 104]. Regulations of these types of flow are important in industrial and biological applications, microfluidic analysis device for example [105]. Research on the Marangoni effect is dedicated to exploring interphase mass transfer which is much complicated than interphase heat transfer. Moreover, the Marangoni effect is also important for versatile applications including clean dry process, self-assemble process, spontaneous locomotion, crystal growth, miniature robot [106,107,108,109,110] etc.

Marangoni effect is prevalent in our daily life. When placing a drop of detergent on the water surface, a rapid spread of detergent is observed. Plus, a well-known example of the Marangoni effect is 'tears of wine' or 'wine legs', which was shown in Figure 1.3. Evaporation of alcohol at thin layer on the wall is faster due to the large specific surface area. Therefore, alcohol concentration of the thin layer on the wall is smaller compared to the bulk. The surface tension of the layer on the wall is higher than that of the bulk since the surface tension increases with alcohol decrease. Difference in the surface tension pulls wine up continuously, which makes wine

accumulate at the top of thin film. 'Tears' or 'legs' form as weight of wine at the top exceeds the force of effect.

Figure 1.3 Illustration of 'tears of wine' or 'wine legs' [111]

Another phenomenon pertaining the Marangoni effect is the coffee-ring effect. Coffee-ring [112] is a ring-like deposit of a spill with the color darkening from inside to outside. During the process of droplet dry, liquid that evaporates faster at the edge will be replenished by interior liquid. Marangoni flow, or Marangoni convection, was induced by the different evaporation rate across a drop. The flow can carry suspended substances to the edge. The substance accumulates during the evaporation, forming a ring pattern. Mechanisms of the coffee-ring effect and Marangoni flow are still a research topic for the investigations in recent studies [113,114]. In fact, the coffee-ring effect mentioned in most investigations is generally referred to as the process described above. However, suspended particles can be redistributed back to the center of the drop with a stronger Marangoni flow, which is the so-called reverse coffee-ring effect. Studies of both the coffee-ring effect and reversed coffee-ring effect contributed to processes related to deposition, evaporation and mass

transfer [115,116]. Manipulation of Marangoni flow [117,118,119,120] and evaporation control of droplets [121, 122, 123] are important in industrial and biological areas, such as biochemical assays, drug delivery, crystal growth, ink-jet printing, etc.

1.3.4   Research on self-driven motion powered by Marangoni effect

1.3.4.1   Gel

A gel is a soft material that can undergo a large deformation without damage or plastic deformation. It is consisted with the physically or chemically cross-linked network and liquid that is dispersed in the interstitial spaces of the network. Although the mass of a gel is mostly liquid, it behaves like a solid due to the three-dimensional network. The ability of a gel to swell and de-swell is a remarkable property, which is very promising to develop gels into actuators. And gels are of potential to mimic motor in living organisms since living systems are largely made of gels except for bones, teeth, nails and the out layer of skin [124].

Gel is able to exhibit self-driven motion powered by the Marangoni effect. Yoshihito Osada et al. [125,126] investigated self-driven motion of a hydrophobic-hydrophilic polymer gel at the air-water interface. They stated that "we have discovered that cross-linked hydrophobic-hydrophilic copolymer gels swollen in organic solvent undergo spontaneous motion when immersed in water" and "these motions are observed ***only*** for amphoteric copolymer gels capable of forming organized structure and not for hydrophilic ones such as poly (AA) and hydrophobic ones such as poly (SA)". They claimed that this amphoteric polymer gel [127] has a special structure to squeeze solvent out during the motion. They believed both the osmotic pressure and hydrostatic pressure contributed

to the solvent diffusion, which in turn induced Marangoni flow to propel gel motion. The study also pointed out that "the smaller the gel, the faster it moves" and that "the duration of the motion was found to increase with an increase in the weight." A gel with mass in about 200 mg exhibited a duration of motion of 150 minutes. They stated that the motion modes were largely dependent on the shape of gels: disc-shaped or sphere gels exhibit a translational motion, while triangle or square shaped gels exhibit a rotational motion. However, photographs about various motion modes were only within 1 s. A disc gel (4 mm in the diameter and 2 mm in the thickness) exhibits a maximum velocity of 5 cm/s, illustrated by a curve of velocity versus time within 4 s. A triangle gel (10 mm in side and 4 mm in the thickness) exhibits 6-8 rounds per second in the first 20-30 s, no curve presented. A square gel (2mm in the length and 2 mm in the thickness) exhibits 400-500 rpm, illustrated by a curve of rotation rate versus time within 1s. They considered the work done by two-dimensional spreading of solvent by $E = nRT$, where n is the molar number of organic solvents making two-dimensional spreading, R is gas constant and T is temperature in Kelvin. Then the work done by a square-shaped gel for rotational motion was calculated by integral of resistance force times angular velocity within 10 min. Thus, the energy efficiency of a gel motion, which is defined as the ratio of work done by the gel motion and to the work done by two-dimensional spreading of solvent, was estimated as of $1.5 \times 10^{-5}\%$. They also attempted to control the motion modes, rotational motion or translational motion, by covering gel with foil, leaving one window in the rear for solvent diffusion [128,129].

Noy Bassik et al. [130] investigated with the self-driven behavior of poly-N-isopropylacrylamid (PNIPAm) gels. They took the advantages of lithographically fabrication to get gels precisely shaped. The size of gel was decreased to mm scale and shape of gel actuators can be arbitrary. Reports of gels exhibit self-driven motion are very limited. Mechanisms behind the gel motion can be the Marangoni effect. While the discussion about how the Marangoni effect has an influence on the gel motion is limited. In addition, the discussions about how the external condition affects the gel motions and how the energy is converted during the actuation process are very limited.

1.3.4.2   Droplet

Besides gels, other self-driven objects powered by the Marangoni effects were studied [131, 132]. Droplet motion is a typical group. Basically, studies about self-motion of droplets can be classified into two categories: crawling on a solid substrate [133,134,135,136] and motion on another liquid [137,138,139]. The velocity of a silane droplet crawling on the substrate can range from 1 mm/s to 100 mm/s [140]. And the velocity of a droplet of PVDF/DMF solution on water can reach 90 mm/s [141]. More variables should be taken into the consideration for a droplet motion in the aqueous phase, compared with the gel motion. Liquid droplets were able to deform during motion and interplay between two sides at the liquid-liquid interface is intricate. The same as motion modes of gels, self-driven motion of the droplet on an aqueous surface are random agitations. Motion modes of a droplet was able to be controlled by the volume of droplets [142, 143], applying a boundary [144,145,146], etc.

Yong-Jun Chen et al. [147] investigated the self-driven of aniline oil on water surface. The velocity of oil on water can reach 50 mm/s. They stated that "the interaction between a droplet and the wall

is subtle". The oil droplets moved circularly along the wall when they were deposited close to the circular wall, while oil droplets moved translationally when they were deposit far from the circular wall. Modes may switch from translational motion to circular motion after hitting the wall. When the droplet approaches the wall, the decrease in its velocity was observed. A simulation study also illustrated the flow around a droplet with vortices at the rear [148]. Discussion of flow around a droplet and internal convection in the droplet were limited [149].

Shogo Oshima et al. [150] experimentally measured distribution of surface tension in the front and rear of a droplet moving in a circular channel. The study presented numerical data to illustrated surface tension gradient in the front and rear of the droplet. And the surface tension gradient in the front of droplet was steep compared to that in the rear of a droplet.

1.3.4.3 Camphor

Self-motion of camphor on the surface of water was observed more than a hundred years ago [151]. Camphor is a good object to study self-driven motion of a solid on a liquid at interface. Basically, camphor molecules diffusing into water decrease the surface tension around the camphor. Thus, anisotropic distribution of camphor layer made a surface tension gradient around camphor heterogeneous [152,153]. The Marangoni flow is generated and in turn propel the motion.

Satoshi Nakata's research group investigated camphor's self-motion process experimentally and theoretically during the past 20 years [155-171]. The velocity of camphor on water surface ranges from 50 mm/s to 100 mm/s. The motions of camphor can be affected by both internal factors (size and shape of camphor) and external environment (pH of an aqueous phase [154,155,156], surfactant in an aqueous phase [157,158], shape of a vessel [159]). Motion modes of a camphor, including rotation

and uni-directional translation, were able to be controlled by its shape [160].In addition, motion mode-switch is dependent on the boundary, or shape of vessel [161,162,163,164,165,166,167]. Satoshi Nakata et al. attempted to make convection flow visualized by plastic beads or uranin [168,169]. Marangoni flow can be affected by the depth of water [170,171,172,173] and also can be affected by chemicals in the aqueous phase [174,175,176]. Regarding the depth dependence of Marangoni flow, Yui Matsuda et al. stated that "The maximum flow speeds increased with an increase in the water depth in the one-dimension system increased." and "The speeds of a camphor disk in the one-dimension system increased with increasing water depth." However, they pointed out that flow speeds were independent of the water depth and radial flow was observed around the camphor disk in the two-dimensional system.

In addition, the simulation indicated that an estimated diffusion coefficient constant of camphor molecules at the air-liquid surface is around 10^{-3} m^2s^{-1}[177]. This value is six orders of magnitude larger than diffusion coefficient of molecules under equilibrium conditions, which is 10^{-9} m^2s^{-1} [178].

1.3.4.4   Summary

Spontaneous motion triggered by the Marangoni effect was widely discussed. Self-driven motion of a droplet on aqueous surface is random agitation within a container. Motion modes selection was investigated by using the size or shape of actuators, boundary conditions, etc [125,126, 141-146, 154-167]. It is clear that imbalance of surface tension around an actuator triggered the motion. Recently, the surface tension at the front and rear of an actuator were measured during its motion in an annular channel [150]. The Marangoni convection plays the vital role during self-driven motions of

an actuators on air-aqueous interface. The surface tension gradient distribution around an actuator may accelerate or decelerate a certain motion depending on the structure of actuators. At last, studies about the motion of actuators, especially gels actuators, on water were very limited. Energy conversion between energy stored in actuators and kinetic energy was not thoroughly investigated.

1.4   Friction in actuators

A moving body faces a friction force whose direction is always in opposite to the relative motion direction. Therefore, the friction slows the moving body down. For a moving solid object on a solid surface, the friction force acting on a moving solid object obeys the Amonton's law: $F = \mu W$, where F is the friction force(N), W is the normal force(N) and μ is the friction coefficient(unitless). Friction coefficient is independent of the velocity and contact area. It only depends on the materials, which usually lies in the range 0.3-1.0 [179,180].

However, for a gel moving on the water surface, the friction force acting on the gel cannot be simply interplayed by Amonton's law. The gel consists of the 3-dimentional network filled with liquid. Gel is neither solid nor liquid, thus, the friction force is very complex for a gel moving on a solid surface. It was known that the friction is much weaker when a thin layer of water exists between two solid surfaces [181]. Yoshihito Osada et al. [182,183] investigated the friction force acting on a gel moving on solid surfaces. They found that the friction force is strongly dependent on the velocity of the gel and that the friction coefficient of a gel moving on a solid surface decreases to a scale as low as 10^{-3}, which cannot be reached by the friction between two solid surfaces. In addition, Giuseppe Pucci et al. studied motion of a centimeter-size object sliding on a water surface

[184] and they concluded that the motion on water was strongly influenced by the boundary layer in fluid under the object. Besides the surface properties of solid substrate, even the chemical composition of a gel should be taken into consideration through the friction discussion [185,186].

1.5   Research Motivation

1.5.1   Objective I: Development of polymer gels as self-driven actuators

Actuators are essential in our daily life. Self-driven actuators can directly convert stored energy to mechanic motions with a long displacement that is orders larger than the external stimulated actuators such as piezoelectric actuators. Osada's group illustrated the gel motion on the water surface and stated that "these motions are observed only for amphoteric copolymer gels." The research work in this dissertation was intended to demonstrate that the self-driven of gel motion on the water surface is more universal and then, to quantify the related variables including mass loss, dimension and factors that control the gel motion. The quantified results will provide a solid database for the future study of the phenomenon and help to deepen our understanding of the actuators.

1.5.2   Objective II: Quantification of motion and study friction of gel motions

To deepen the understanding, and to characterize the output, of self-driven actuators, the research under this objective is to quantify the variables about the motion: velocity, acceleration, and their time dependence. A method is developed to retrieve spatial and temporal data during the motion of a gel on the water surface. Trajectory and coordinate points are obtained from the video. Thus, linear or angular velocity, and distance change as time were able to be quantified. The digitalized

actuation behavior of gels makes it is possible to determine the friction of gel motion on water surface, which is one of the objectives for this study.

1.5.3 Objective III: Study of energy conversion during gel motions

Energy conversion through the actuation process was rarely discussed. Self-driven gels convert stored chemical energy into mechanic motions. Under this objective, the kinetic energy converted from chemical energy will be studied. The consumption of the kinetic energy of a gel during the motion reflects the contribution of the friction force. The research work here is intended to discuss the energy source and energy conversion during the motion of a gel, which means a step forward for the understanding of self-driven gels.

Chapter II

Preparation and characterization methods

2.1 Raw material introduction

Poly(vinylidene fluoride) (PVDF) is a highly nonreactive semicrystalline fluoropolymer. The fluorine is of great electronegativity and is able to form strong bonds with hydrogen and carbon [187]. PVDF are known as a polymer of high mechanical strength, chemical resistance, thermal stability, highly hydrophobic, good biocompatibility and piezoelectric [188,189]. The mean length of PVDF chain increases as increasing temperature [190], which may affect interaction between polymer chains and thus, further affect properties.

PVDF mainly has four crystal structures, namely α (form II), β (form I), γ (form III) and δ (form IV). And typically, PVDF crystallinity ranges from 35% to 70% [189]. Generally, the crystallinity, crystalline structure, and morphology have a strong influence on the properties of PVDF, especially mechanical strength and impact resistance [191].

Crystalline of a polymer is greatly dependent on the process conditions, processing temperature, solvents used for instance. The α-phase is the most thermodynamically stable among different crystal structure of PVDF [192]. W Ma et al. [193] fabricated a PVDF film by the solution cast of PVDF with good solvent N,N-dimethylformamide (DMF). They stated that PVDF film from this single solvent system exhibited dominantly β-phase crystalline. However, samples from good swelling agents, tetrahydrofuran (THF) for example, showed α-phase crystalline with some amount of β-phase crystalline. X. Wang et al. [194] formed PVDF membranes via immersion

precipitation. The results indicated membrane precipitated at 60℃ exhibited typical α phase crystalline. While at 15℃, membrane crystallites are the mixture of α and β crystalline.

PVDF is able to form gel on cooling, which is the so-called thermoreversible gel [187,195]. Gel morphology can be affected by process conditions [187] and solute concentrations [196]. M. Tazaki [197] stated that spherulites were formed by slowly cooling hot polymer solutions (180 ℃) while no spherulites were observed by rapidly cooling hot polymer solution (180 ℃) in a 30 ℃ water bath.
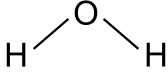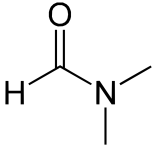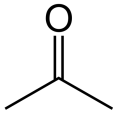
Polyacrylonitrile (PAN) is a semicrystalline organic polymer synthesized from radical polymerization by using acrylonitrile as the monomer. Due to the existence of nitrile group, PAN is N-containing and thus has high polarity in its molecule structure, which means it is soluble in polar solvents, such as DMF, dimethylacetamide (DMA), dimethyl sulfoxide (DMSO), etc [198]. Based on this property, PAN can be firstly dissolved and then extruded in coagulation bath to form PAN fibers, which is an important fiber precursor for high-performance carbon fibers [199]. Physical gel, or thermoreversible gel, can form in PAN solution either after a long period of aging or at a low temperature [200].

2.2 Experiment procedure

Gels in this study were formed by PVDF and PAN. PVDF powder (Mw~534000, SIGMA ALDIRICH), PAN (Mw~150000, SIGMA ALDIRICH), acetone (VWR, 99.5%) and DMF (fisher chemical, 99.8%) were directly used as received without further processes. DI waster was obtained

by E-purity system (D4641) from Thermo Scientific, resistance of DI water utilized in the test is above 18 MΩ. Both acetone and DMF are polar organic solvents, and they are miscible with water.

Table 2.1 Characteristics of H_2O, DMF and acetone

	Density/ (g/cm^3)	Surface tension at 20°C/(mN/m)	dipole moment	Relative Polarity	Molecule structure
H_2O	1	72.8	1.85D	1	
DMF	0.948	37.1	3.86D	0.386	
Acetone	0.785	25.2	2.91D	0.355	

2.2.1 Solution preparation

PVDF gels were prepared by two different polymer solutions, one uses DMF only, the other uses DMF and acetone with the volume ratio of acetone to DMF being 1.5:1.0. First, 0.9g PVDF powder was added into 5 mL DMF to form 16wt.% PVDF/DMF solution. 0.81g PVDF powder was added into the mixture of 2 mL DMF and 3mL acetone to form 16wt.% PVDF/DMF-acetone solution. They were stirred (400 rpm) for 4 hours at 60℃ to form uniform polymer solutions.

PAN gels were prepared by using 10wt.% PAN solutions. 0.525 g PAN powder was added into 5 mL DMF to form the polymer solution. It was stirred (400 rpm) for 4 hours at 80℃ to form uniform polymer solutions. All polymer solutions were formed in glass vials with the cap as illustrated in Figure 2.1. Glass vials are of 60mm in height, 15 mm in inner diameter and 17 mm in outer diameter.

Figure 2.1 Uniform polymer solution formed in a glass vial

After 4 hours heating and stirring at 60 ℃, vials with polymer solutions were placed on the leveled table at room temperature (~20℃) for 20 mins in order to cool down naturally.

2.2.2   Gel preparation

Bulk gels were formed on standing in glass vials with the cover shown in Figure 2.1 by keeping the vials at room temperature for 24 hours. The gels were taken out by tweezers and manually cut into pieces by blades.

Film gels were formed by casting uniform polymer solutions, which were prepared at 60 ℃, on glass substrates. Solution cast was conducted right after the solution was cooling down at room temperature (~20℃) for 20 mins. Glass substrates were put on a stable and leveled workbench, which was shown in Figure 2.2. On one glass substrates of 22 mm × 22 mm, 0.4 mL, 0.6 mL, 0.8 mL and 1 mL PVDF/DMF-acetone solution was casted, respectively, in the preliminary test to control the thickness of film gels. After the gel was formed, their thicknesses were measured to be 0.30 mm, 0.50 mm, 0.70 mm and 0.85 mm, respectively. When 4 mL and 6 mL PVDF/DMF-acetone polymer solutions were casted on one glass substrate of 75 mm × 50 mm to form gel films, the thickness was 0.36 mm and 0.62 mm, respectively. Similarly, when 4 mL and 6 mL

PVDF/DMF polymer solutions were also casted on one glass substrate of 75 mm × 50 mm, the thickness was 0.70 mm and 1.2 mm, respectively. Additionally, when 4mL PAN polymer solution was cast on one glass substrate of 75 mm × 50 mm, and its thickness was 1.4 mm. To provide a relatively stable condition for gel formation, a glass cover with a diameter of 10 cm was put over glass substrate right after solution cast for the formation of all the gels mentioned above.
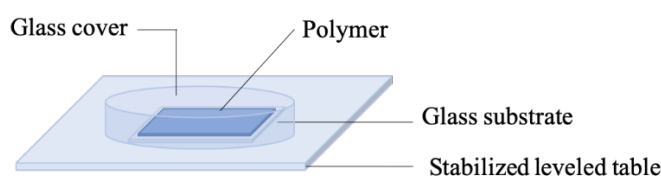
Figure 2.2 Polymer solution and gel in sealed glass beaker

PVDF-based gel films were cut and tested 12 hours after solutions cast. PAN based gel films were cut and tested 24 hours after solution cast. Gel films were manually cut into squares, rectangles and triangles in shape with various sizes by using blades. Gel films in the circle shape were cut by metal pipes.

For the actuation characterization, shaped gels (i.e., gel actuators) were placed on the water surface by metal tweezers.

2.2.3   Gels in 3-D print molds

3D print mold was made of PLA filament (Polyactic Acid, 3D Solutech). Cuboid molds were made of 7 mm in length, 4 mm in width and 3 mm in height for its outside. The thickness of the wall was 0.5 mm. Two types of molds were prepared: two holes on one side, shown in Figure 2.3(a); and two holes on the opposite side, shown in Figure 2.3(b). The radius of each hole was 1 mm.
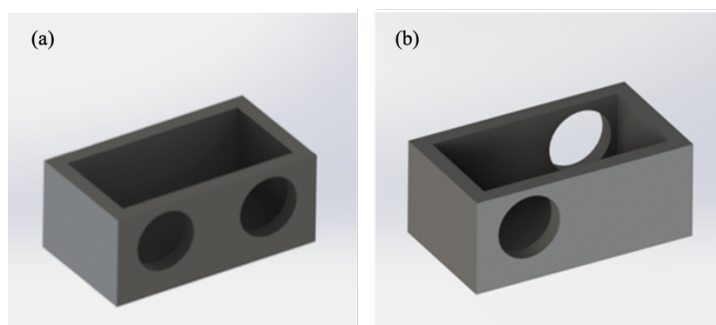
Figure 2.3 Scheme of rectangular 3D print molds

3-D print fan-shape molds with three holes were also prepared as shown in Fig. 2.4. Three holes were on three surfaces. The thickness of the wall is 0.5 mm. Radius of each hole was 1 mm.
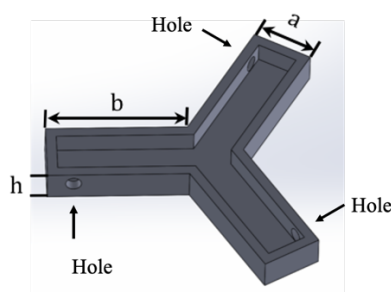
Figure 2.4 Scheme of 3-D print fan shape mold. a = 4 mm, b = 10 mm and h = 3 mm

Solution was cast into mold to form the gel. The mold with solution was put on a stable and leveled workbench. A glass cover was put on the top over the mold right after solution cast. Gel was formed in the mold and test was conducted 20 mins after solution cast. Mass of the mold, polymer solution with the mold, gel with the mold were measured for each test. The mold filled with gel was tested as an actuator by placing it at the air-water interface.
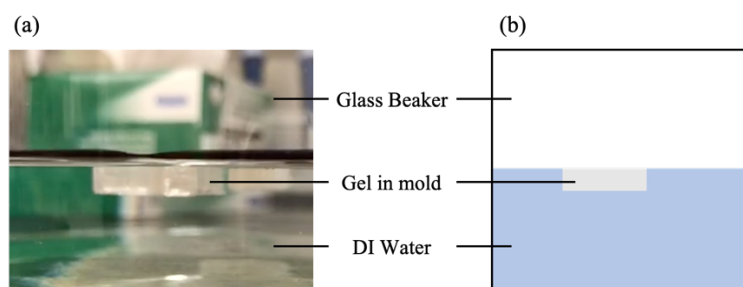
Figure 2.5 (a) Photo during test and (b) scheme of 3-D print mold at the air-water interface

3-D printed molds were placed on the water surface with open side up as shown in Figure 2.5. Since the mold was hydrophobic, mold will be tilted when placed on the water surface. Tweezers were used to make the top (open side) of the 3-D print mold horizontal.

2.2.4 Recharge process

All gel actuators studied here including gels and gel-filled 3-D print molds, can be recharged after their motion/actuation on the water surface. After a gel actuator moved on the water surface, the actuator was recharged as followings. Actuators/gels after motion were placed on a substrate with glass covers as illustrated in Figure 2.2. Then, excess amount solvent of corresponding to each type of gels were added dropwise. For example, solvent amount of a gel with size of 6mm × 3 mm is 0.3 mL. Similarly, a glass cover with a diameter of 10 cm was put over the glass substrate right after adding solvents.

2.2.5 Detergent water

The influence of chemicals on the behavior of self-driving actuators was studied by adding chemicals in water. In the study, detergent (Dishwashing Liquid Soap, Dawn) was directly used without further process. Detergent water was prepared by adding 103.3 mg detergent into 20 mL

DI water. Detergent water was stirred (400 rpm) at room temperature for 10 min to prepare a uniform solution with detergent concentration of 0.052 mg/mL. The detergent water was added into water for gel motion by the pipette.

2.2.6   Friction test

Friction is inevitable for all mechanical motion. The friction force facing self-driving actuator was studied as the following. Friction test and simulation was conducted by a gel in mold sample (6 mm × 3 mm) that already actuated on water and stopped moving. The sample was put on the water and then, a tweezer was used to push the actuator to initiate the motion (i.e., initial velocity is created). Thus, the actuator moved on the water surface. Since there is no driving force during the motion, the acceleration of the actuation would be the direct result of the friction force. The mass of this gel was 6.1 mg.

2.3 Characterization method

All the actuators including the gels and gel-filled 3-D print molds, were tested by placing it on the water surface in a glass beaker with diameter of 190 mm. Depth of water was 14 mm. All samples were tested on the water at room temperature (around 20 °C) with humidity of 19%-22%.

For motion quantification purpose, two scotch markers in different color were put on the top surface of each gel/actuator for easy measurement as shown in Figure 2.6. The mass of two markers was around 1mg.
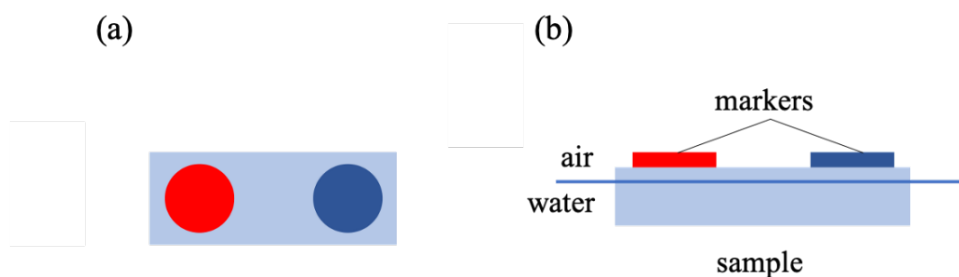
Figure 2.6 (a) Top view and (b) side view of markers on a gel.

2.3.1   Actuation record

When a gel actuator was placed on water surface, its motion was video-taped by a camera (iPhone X) that took photos every 1/60 second (top view), which was shown in Figure 2.7. The speed of gel motion changes with time. It was found that the motion speed of an actuator on water surface eventually reduces to zero and that at the final stage, the motion is in a pulse mode with the interval between two motion periods increasing with the time. The video record was stopped when the interval between two motion periods reached 15 sec.
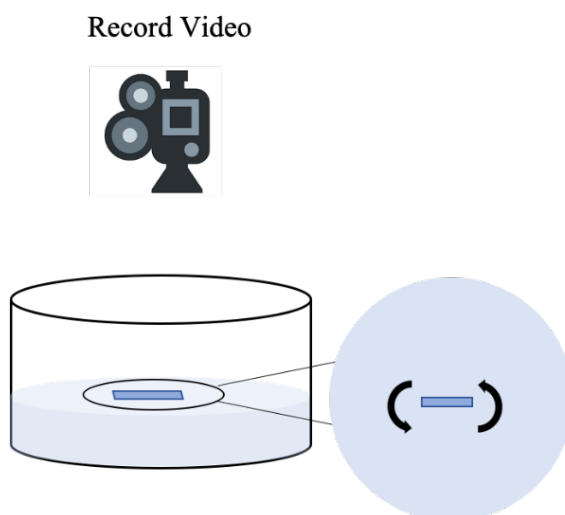
Figure 2.7 Scheme of video record

2.3.2 Mass

All the samples were weighted by balance (Mettler Toledo XS105DU) before and after actuation to determine the change of actuator's mass. For the mass measurement, gel samples were gently wiped out excess solvent/water without squeezing for each measurement. For those gels with markers, the measured mass was total mass with makers on gels.

2.3.3 Vacuum

Figure 2.8 Image of VWR Thermo Scientific Vacuum Oven Model 6291

Dry mass of a gel was measured after putting the sample in the vacuum (VWR Thermo Scientific Vacuum Oven Model 6291) for 24 hours at 1084 Pa.

Chapter III

Changes in properties of gel during autonomous motion at air-water interface

Self-driven motion of gel as actuator moves at the air-water interface. The process was archived and quantified. Changes, especially the difference between before and after actuation, in the properties of gel, such as mass loss, shrink and transparency were observed/measured for different gels. Mass loss as well as rate of mass loss through actuation process are important information for the fundamental understanding since they are correlated with energy transfer (i.e., loss of solvent into environment such as water). The results may be beneficial to screen out the basic energy-conversion mechanism of gel motion at the air-water interface. The study of mass loss for gel actuators was devoted to future energy calculation and mechanism exploration. In addition, factors that controls the gel motion were studied.

3.1 Experimental

In the beginning, the tests were mainly about bulk gels. Bulk gels were taken out from the glass beaker carefully and cut into pieces for actuation test. These experiments demonstrated that the PVDF gels can be used as self-driven actuators. Except for several attempts in an early stage, all other samples utilized in this study were gel films since their shapes are much controllable than the bulk gel actuators. The bulk gels have the problem in controlling both the thickness and cross section through the cutting process.

Gel films were prepared using the process as described in Section 2.2.2 and cut manually by blades into different shapes including square, rectangle and circle with various sizes: rectangles (6 mm

× 3 mm, 6 mm ×1 mm), squares (6 mm × 6 mm, 9.7 mm × 9.7 mm, 12 mm × 12 mm) and circles (diameter in 3.82 and 7.82 mm, respectively). Figure 3.1 presents a group of gel films actuators in the shape of the rectangle, square and circle. The fan shaped gel actuators in mold were also prepared using the process described in Section 2.2.3.
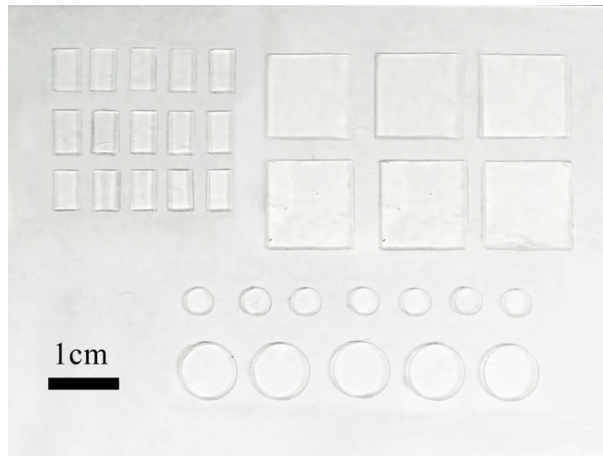
Figure 3.1 Gel actuators in rectangle, square and circle shape cut from gel films

Weights of these gel actuators before and right after motion at the air-water interface were measured as described in Section 2.3.2. The mass loss of a gel actuator is defined as the mass difference between these two values. The mass loss percentage is defined as mass loss divided by mass of the gel actuators before motion at the air-water interface.

Solvent percentage in a gel is defined as the mass ratio of the solvent in the gel to the entire gel. Solvent percentage in a gel is defined as the mass ratio of the solvent in the gel to the mass of the whole gel. The mass of the solvent in a gel is measured by the mass difference between the fresh gel and the dried gel. The dried gel was obtained by placing the gel in the vacuum at room temperature (~20 °C) for 12 hours in order to remove the solvent. The mass of fresh gels and dried gels was measured by balance.

Two durations were defined. Duration of continuous motion on the water surface was denoted as t_1. After that, the gels exhibited pulse motion and the interval between two motions increase as time. As was mentioned in Chapter II, the video record was stopped when the interval between two motions reached 15 sec. The duration includes this pulse motion was denoted as t_2.

3.2 Results and discussion

3.2.1   Self-driven motion of gel

Table 3.1 shows the summary of study of self-driven motion of gel actuators. Some of them are not reported by others, location influence, mass loss in the air, pulsive motion, effect of container size, dimension change of gels, motion modes in longer time period included.

Table 3.1 Summary of study on self-driven motion of gel actuators

Object	Comments
Multiple polymer/ solvent	Self-driven motion of gel is a universal phenomenon
Rechargeability	The actuators are rechargeable
Location influence	Motion is observed on surface and no motion in bulk water and on the bottom of beaker
Mass loss	Losses mass both in the water and in the air
Duration	Continuous duration and pulsive motion
Size of container	Depth/diameter of container
Transparency	Becomes translucent after motions
Shrinkage	Shrink faster after motion on water surface
Dimension change	Bended downwards and then upwards during motion
Motion modes	Studied shape dependent motion modes in longer time period. controlled by 3-D printed molds

Both PVDF gel actuators and PAN gels actuators with two organic solvents (i.e., DMF and acetone) exhibit self-driven motions at the air-water interface. The motion of these gel actuators takes place immediately after the gel actuator was placed at the air-water interface. Thus, the self-driven motion of gel at the air-water interface is a universe phenomenon.

All actuators, gels and gel-filled 3-D print molds, can be recharged after motion on water surface followed the process described in section 2.2.4. Measurements were conducted to explore whether there is polymer loss through recharge process. Gels with size of 12 mm × 12 mm and 6 mm × 3 mm were recharged 5 times. Dried mass of gel was measured before each recharge process. Mass of each dried sample before recharge process is shown in Figure 3.2. The curves show that mass loss through recharge process is limited.
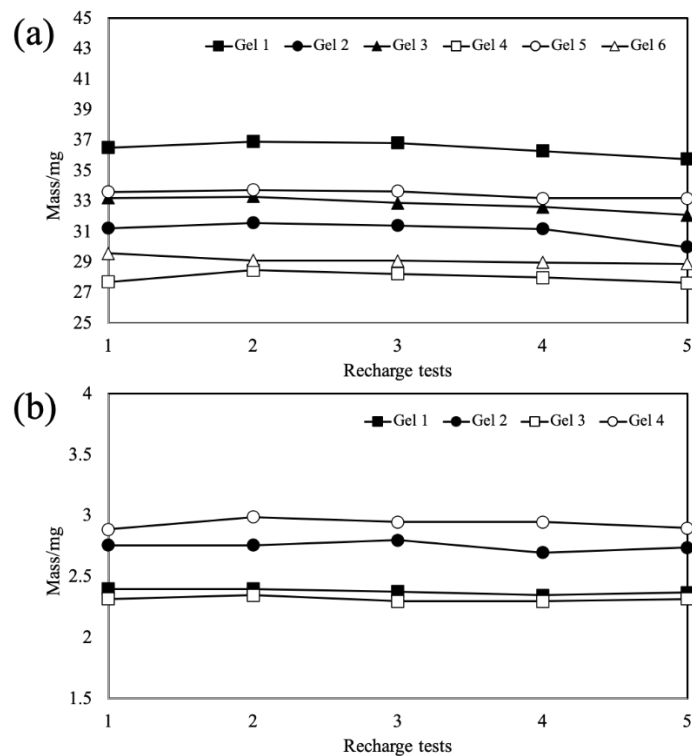
Figure 3.2 Dry mass of gels before recharge. (a) 12 mm × 12 mm and (b) 6 mm × 3 mm.
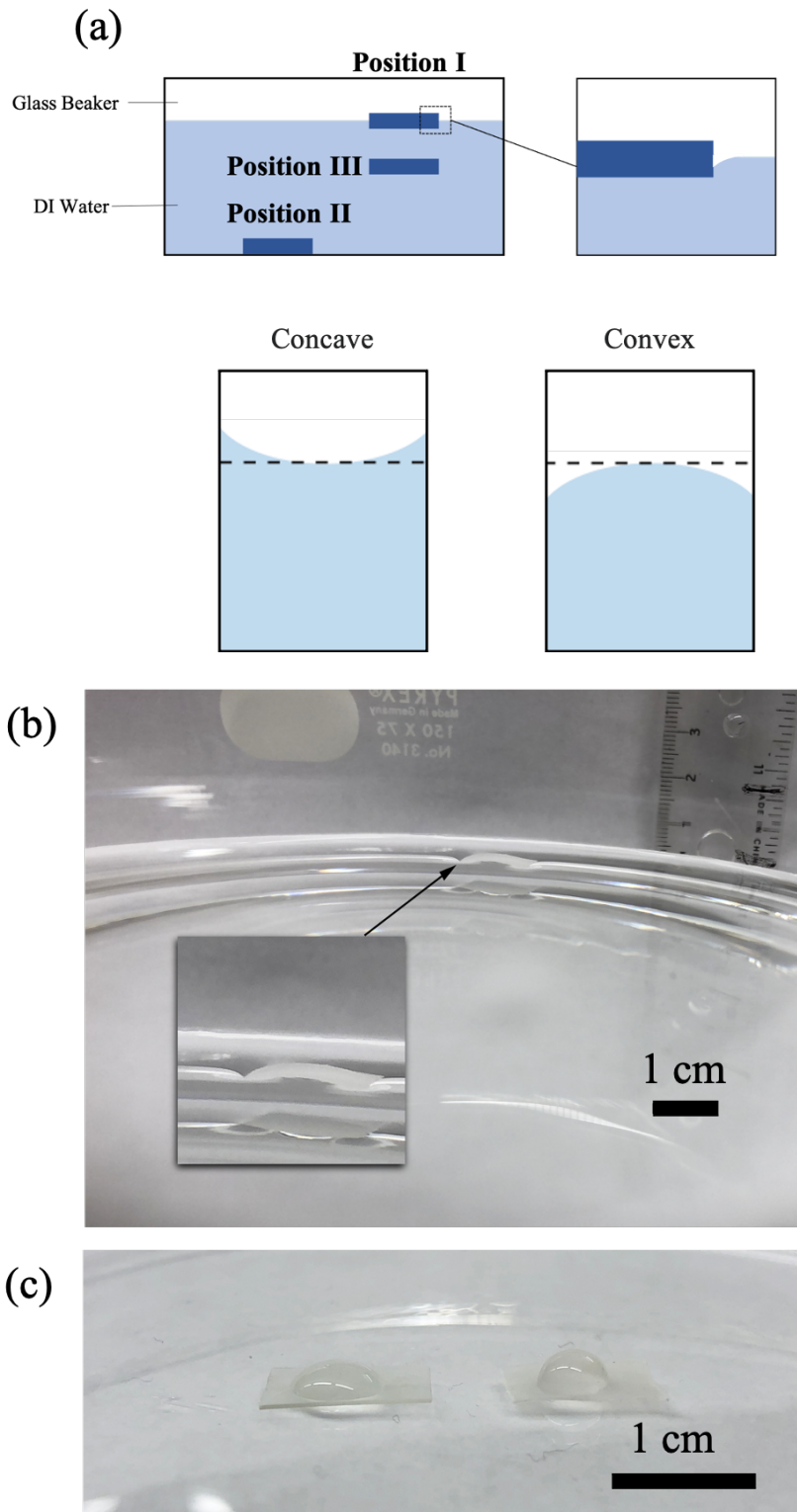
Figure 3.3 (a) Scheme of gel actuators on or in the water; (b) Photograph of a gel actuator at the air-water interface, PVDF gel, 6 mm × 12 mm and (c) 30 µL DI water on a fresh gel (left) and a used gel (right), PVDF gel, 6 mm × 12 mm.

Interface between gel actuators and water is shown as Figure 3.3 (a) and (b), which was observed in the self-driven motion process. The concave meniscus and convex meniscus are illustrated as in Figure 3.3 (a). Figure 3.3 (c) shows 30 µL DI water on a fresh gel (left) and a used gel (right), which further confirm the convex meniscus of a PVDF gel actuator through self-driven motion at the air-water interface.

Self-driven motion happens at the air-water interface as Position-I shown in Figure 3.3 (a). When the gel actuator was placed on the bottom of glass container as Position-II shown in Figure 3.3 (a), no motion was observed. In addition, no motion was observed when the gel actuator was in the middle of water as Position-III shown in Figure 3.3 (a). A gel actuator was place on stones in the water shown in Figure 3.4. No motion was observed even the gel actuator was close to the air-water interface. However, the gel shown in Figure 3.4 was able to move when it was taken out of water and placed at the air-water interface.

Figure 3.4 A gel actuator on a stone in the DI water with Position-III.

Gel actuators at all three positions – Position-I, Position-II and Position-III – loss mass, meaning the solvent in gel actuators diffusing into water during motion at the air-water interface. Mass loss of gels at Position-I and Position-II were shown in Table 3.2 and Table 3.3 respectively. m_1 is the mass of gel actuator before the test, m_2 is the mass of gel actuator after 30 minutes, and Δm is the mass difference before and after the test. $\Delta m/m_1$ is the rate of mass loss of the gel actuator. There is no remarkable difference between the mass loss of gel at Position-I and Position-II. Gel also losses mass with Position-III. A gel with mass of 70.93 mg has a mass loss of 13.13 mg for 10 minutes.

Table 3.2 Mass loss of gels at Position-I

	m_1 (mg)	m_2 (mg)	Δm (mg)	$\Delta m/m_1$ (%)
Sample 1	20.24	16.22	4.02	19.86
Sample 2	60.76	51.3	9.46	15.56
Sample 3	70.22	56.78	13.44	19.14
Sample 4	74.95	63.51	11.44	15.26
Sample 5	68.79	58.14	10.65	15.48
Sample 6	86.53	70.74	15.79	18.24

Table 3.3 Mass loss of gels at Position-II

	m_1 (mg)	m_2 (mg)	Δm (mg)	$\Delta m/m_1$ (%)
Sample 1	25.28	18.50	6.78	26.82
Sample 2	63.28	47.08	16.20	25.60
Sample 3	76.04	59.00	17.04	22.41
Sample 4	100.17	77.18	22.99	22.95
Sample 5	75.3	57.45	17.85	23.70
Sample 6	72.98	60.38	12.60	17.27

Regarding the diffusion of solvent in the gel into water, the diffusion occurs at the edges and also the bottom surface at Position-I, but the diffusion occurs at the edges and also the bottom surface of the gel as well as the top surface of the gel at Position-II and Position-III. Regarding the friction force acting on the gel sample, at Position-I there are friction forces on the edges and bottom surface, but at Position-II and Position-III there are friction forces on the edge and both bottom and top surfaces of the gel. For Position-II, it is possible that the friction force on the bottom surface (gel-glass connection) is much higher than that in water. For example, it is well known that a rubber on a solid surface exhibit a much higher friction force than a solid on a solid surface [201,202]. That is, comparing to the gel sample at Position-I, the gel sample at Position-II faces a much higher friction force. The driven force is not high enough to overcome the friction force and trigger the motion when same the amount of water diffusing from gel into water. This may be the reason that the gel at Position-II does not move. All these contribute to the experimental results – no motion was observed when gel samples are placed at Position-II and Position-III.

3.2.2   Mass loss and duration of motions

This study focuses on gel motion at the air-water interface (i.e., Position-I). There is mass loss for the motion of gel actuators. Mass loss of gel actuators is an evidence that solvent diffused to water during motion at the air-water interface. Both DMF-acetone based and DMF based PVDF gels were examined in mass loss tests. In addition, gel films were cut into different shapes including rectangle, square and circle. A large number of samples were measured and obtained the trend that the mass loss increases as mass of gel increases as shown in Figure 3.5 (a) and (b).
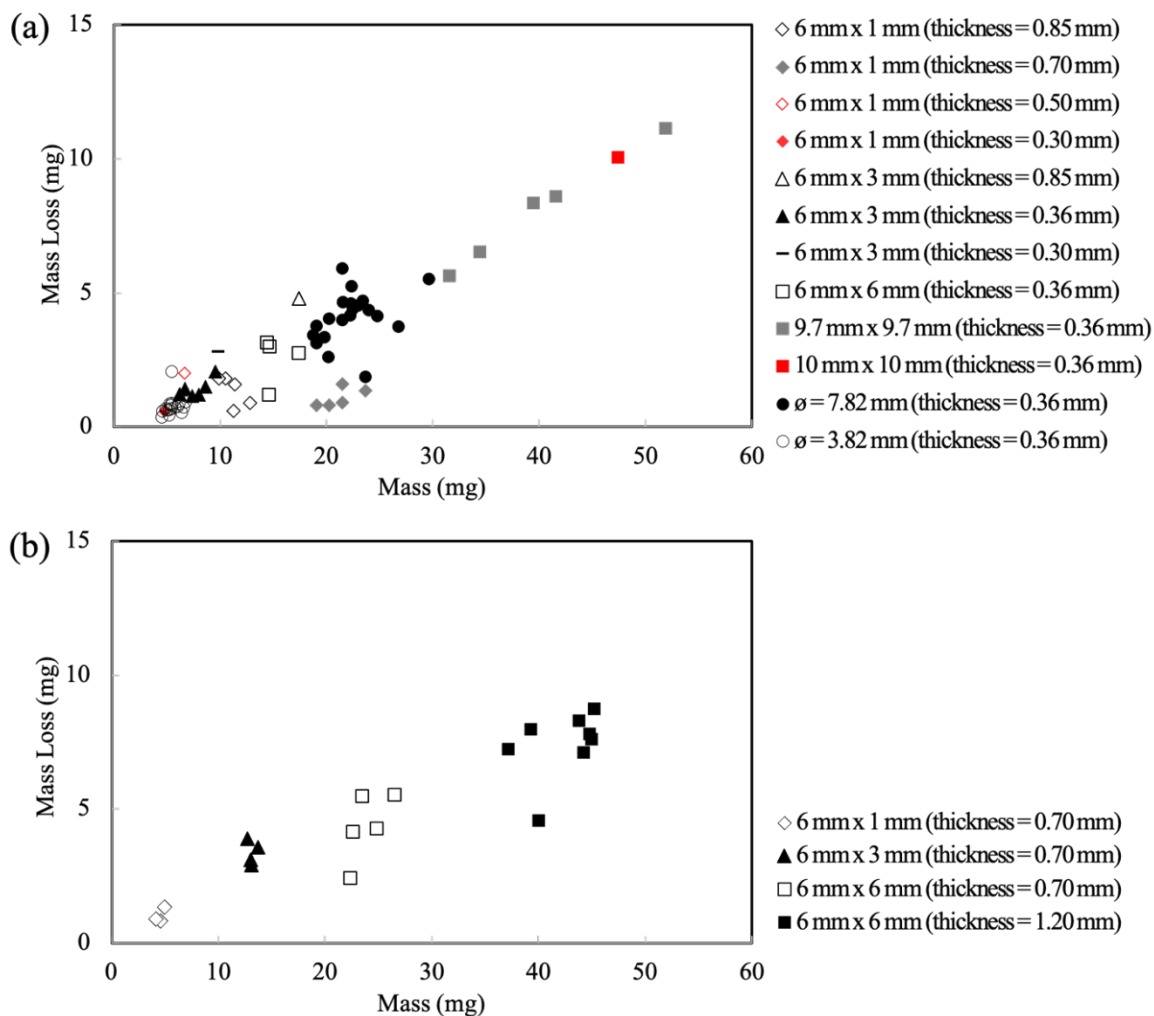
Figure 3.5 Mass loss changes as sample mass. (a) PVDF-DMF/acetone gel actuators and (b) PVDF-DMF gel actuators

A summary of mass, mass loss and mass loss percentage of different gel actuators was shown in Table 3.4 (a) and (b). Average mass of 6 mm × 1 mm DMF-acetone based gels was 8.01 mg, with mass loss less than 2 mg. Average mass loss of 6 mm × 3 mm DMF-acetone based gels was 10.82 mg, with mass loss of 2.02 mg. This is an obvious evidence that a larger gel has a larger mass loss. The trend is same for square and circle shaped gels. Mass loss percentage of various types of gel actuators range from 15 % to 25%. Overall, the results indicated that a large mass of gel results in a large mass loss.

Table 3.4 (a) Summary of average mass loss percentage of PVDF/DMF-acetone gels

Shape	Size	Mass (mg)	Mass loss (mg)	Mass loss percentage (%)
Rectangle	6 mm × 1 mm	8.01	1.23	15.38
	6 mm × 3 mm	10.82	2.02	18.66
Square	6 mm × 6 mm	15.22	2.54	16.70
	9.7 mm × 9.7 mm	39.77	8.06	20.26
Circle	Ø = 3.82 mm	5.53	0.78	14.16
	Ø = 7.82 mm	22.31	4.11	18.41

(b) Summary of average mass loss percentage of PVDF/DMF gels

Shape	Size	Mass (mg)	Mass loss (mg)	Mass loss percentage (%)
Rectangle	6 mm × 1 mm	4.46	1.03	23.00
	6 mm × 3 mm	13.26	3.38	25.46
Square	6 mm × 6 mm	35.31	6.26	17.73

Dry mass of gel was measured after 24 hours dried in vacuum. The percentage of solute in the gel was calculated from many gels with an average of 19.6 wt.%. This result inferred that there is average 80.4 wt.% organic solvent in the fresh gels before motion. However, the mass loss percentage of gel after motion is about 20 wt.%. This indicates that there is still large amount of organic solvent remaining in gel when its motion ceases, assuming no water diffusing into the gel during motion.

To obtained mass loss curves, 8 gels in circular shape with a diameter of 7.82 mm (thickness = 0.35 mm) were measured before motion and every 1 minute during motion for 10 minutes. Mass of gel actuators decreased gradually when they move at air-water interface as shown in Figure 3.6 (a) and (b). The normalized mass is the ratio of the mass at each moment to the mass before the actuation. In order to explore the influence of wipes on each test, 4 gels were measured before

motion and 10 minutes after motion at the air-water interface. The mass loss of these 4 gels is shown in Figure 3.6 (c) and (d).

The mass loss percentage in this test is the mass difference of gel before and after 10 mins motion divided by mass of the gel before motion on water. Average mass loss percentage of the 8 gels wiped every 1 minutes (i.e., wiped 11 times totally) is 23.5%, compared to an average mass loss percentage of 19.2% the 7 gels wiped only before and after the motion (i.e., wiped 2 times totally) as shown in Figure 3.6 (e). There is only 4% in the difference of the mass loss percentage between the two groups of gels. The difference in mass loss percentage may be attributed to the wipe of each measurement. If wipe is the only reason leads to the difference, 4% is accumulated by 9 times wipes. That is, mass loss originated by each wipe is about 0.44%, which is far less than the mass loss of around 20% due to motion at the air-water interface. Therefore, the wipe process before mass measurement in this study does not introduce apparent mass loss, i.e., the wipe process almost does not affect the mass measurement.

Gel may loss solvents through air besides wipe of each measurement. The gels measured every 1 minute experiencing longer time exposing to the air, which may also result in the different in mass loss from the gels measured only before and after motion. To explore the evaporation of solvents from top surface of gel, mass of a gel placed on a glass substrate was measured.
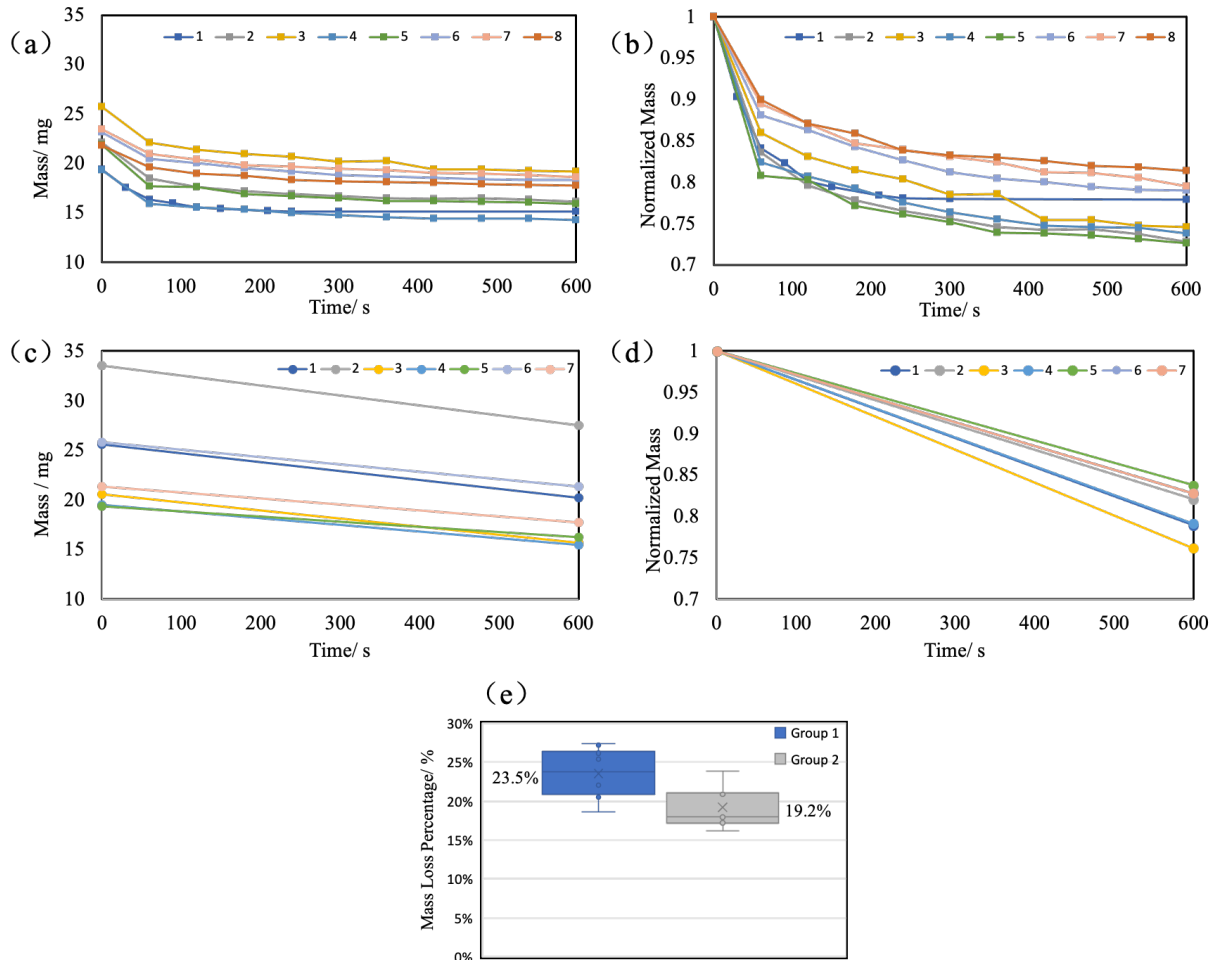
Figure 3.6 (a) Mass of gel as function of time during motion on water surface in group 1;
(b) Normalized mass of gel varies as time in group 1; (c) Mass of gel as function of time during
motion on water surface in group 2; (d) Normalized mass of gel varies as time in group 2 and (e)
Mass loss percentage of gels with duration of 10 minutes in two groups.
Group 1: Mass was measured before motion and every 1 minute during motion for 10 minutes.;
Group 2: Mass was measured before motion and 10 minutes after motion

Mass of gel on the glass substrate losses linearly as function of time as shown in Figure 3.7 with

solid dots. There is 3% mass loss in 10 minutes and 6% mass loss in 20 minutes. Compared to the

gel on glass substrate, the gel loss mass faster when moving at the air-water interface as shown in

Figure 3.7 with open dots. This shows that gel losses solvent by two paths: one is diffusion into

water through edges and bottom surface, the other is evaporation into air through top surface.
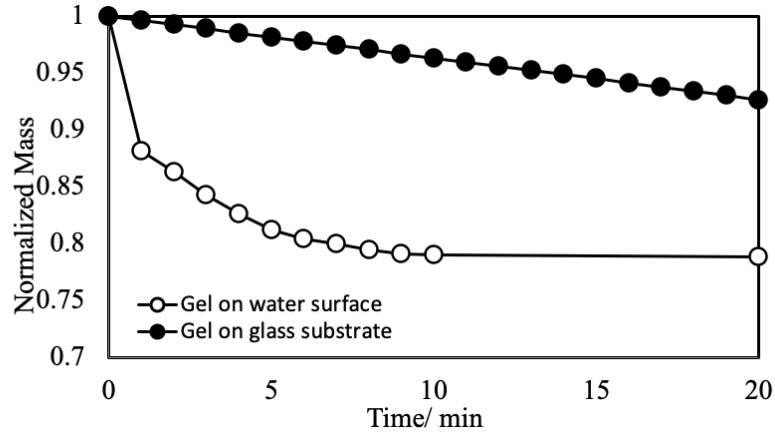
Figure 3.7 Normalized mass of gel at the air-water interface and on a glass substrate within 20 minutes

Velocity of gel actuator decreases as time and it stops at a certain time. Then, the gel actuator exhibits pulse motion and the interval between two motions increase as time. The pulse motion is a typical phenomenon observed from many gels, which is not reported by other yet. This phenomenon is possible originated from the non-uniform distribution of solvents in the gels. And it takes time for the solvent diffusion through the gels. In addition, there is no surface tension difference at the gel-water interface when the gel is stop. Therefore, surface tension may not be the only driven force.

Two durations, t_1 and t_2 are defined as the duration of continuous motion and duration of pulse motion, respectively. The duration of gel actuators moving at the air-water interface varies as mass was shown in Figure 3.8 and Figure 3.9. PVDF/ DMF-acetone gel actuators range from 4 mg to 50 mg with various shapes were tested. t_2 of a gel actuator with size of 45 mg reached 1500 seconds. t_2 of a gel actuator with size of 5 mg was around 300 seconds. Both t_1 and t_2 of PVDF/ DMF-acetone gel actuators increase as mass of gels increase shown in Figure 3.8 (a) and (b). Compared to t_2, t_1 is relatively consistent for gel actuators in one size. t_2 is diverse although the interval

between two motion periods increases with the time. This is an evidence that solvent diffusion from gel into water randomly from side of gel actuators. The tendency is the same for PVDF/ DMF gel actuators shown in Figure 3.9 (a) and (b).
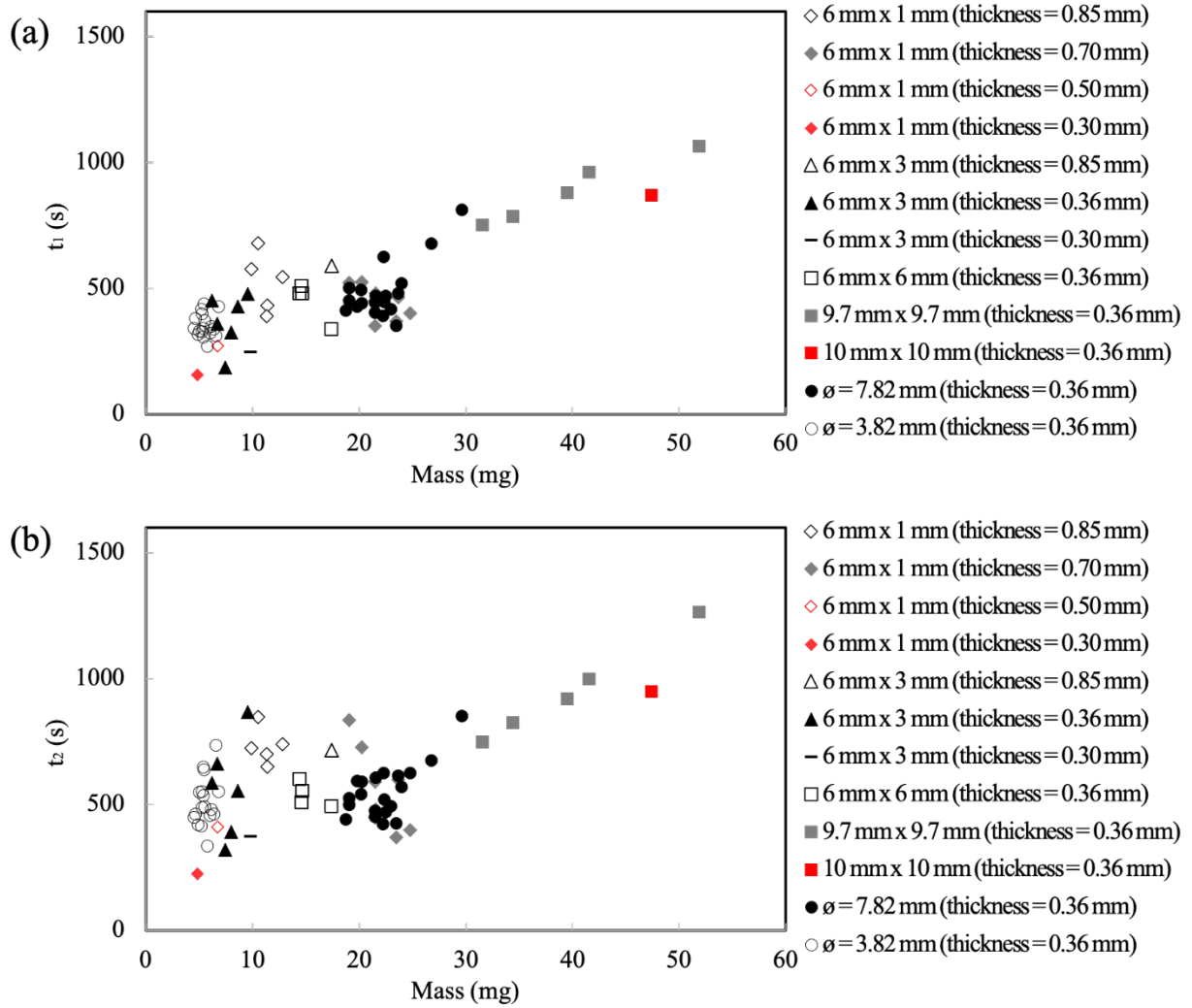
Figure 3.8 (a) t_1 and (b) t_2 of PVDF/ DMF-acetone gel actuators
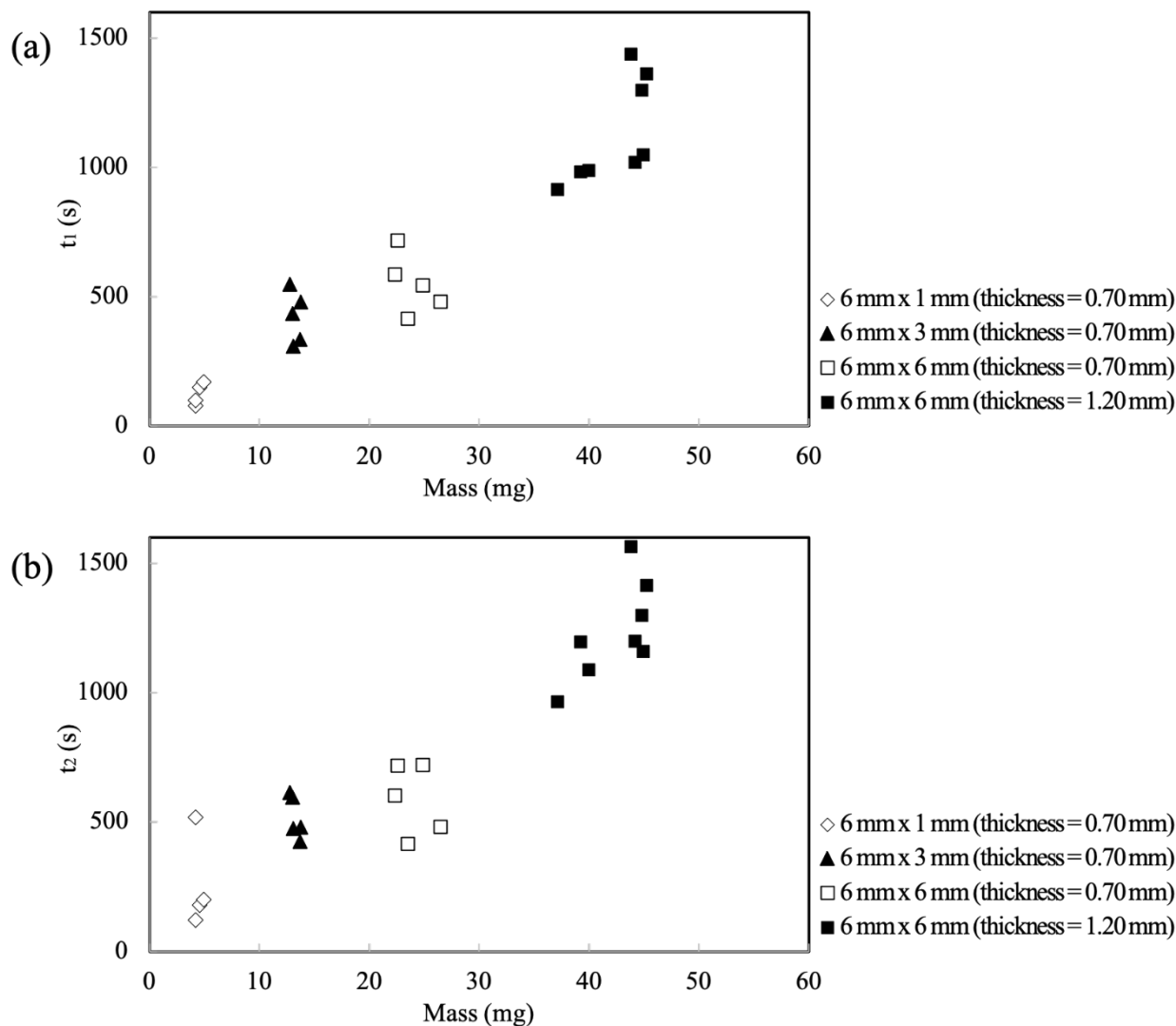
Figure 3.9 (a) t_1 and (b) t_2 of PVDF/ DMF gel actuators

3.2.3　Motion mode control

A fan shaped gel actuator was cut from gel film and tested at the air-water interface. Instead of an

anticipation of spin motion, the result showed a translational motion. This may be attributed to

imperfect of hand craft and random diffusion of solvent from gel into water. Therefore, a gel built

in 3D printed mold was utilized. The mold had three windows open for solvent to pass through as

shown in Figure 2.4. Thus, the gel actuator has a relative standard structure and a constant solvent

diffusion from with 3 windows. In addition, translational motion and spin motion were achieved by rectangular mold with two holes on one side and two holes on opposite sides as shown in Figure 2.3, respectively.

The fan shaped gel in mold exhibited spin motion on water with initial angular velocity of 32 rpm and then reduced gradually as shown in Figure 3.10. Solvent diffusing from three windows at the end of arms on the fan shape mold produced a net force to trigger a prolonged spin motion. Mass of 3-D print mold was around 260mg and a total mass of 430 mg with gel in mold, which was a heavy load of gel motion on water. A higher angular velocity is expected with lighter mold.

At about 40 minutes, its angular velocity is about 2 rpm. At this point, the actuator was taken out of container and immediately placed at the air-water interface of another container (i.e., second container) with fresh DI water. A steep increase of angular velocity to a value of 11 rpm and then the velocity gradually reduced. After angular velocity gradually reduced to around 4 rpm, the actuator was taken out from second container and immediately placed on the water surface of another container with fresh water (i.e., third container). Again, a steep increase in angular velocity of 7.3 rpm was observed.
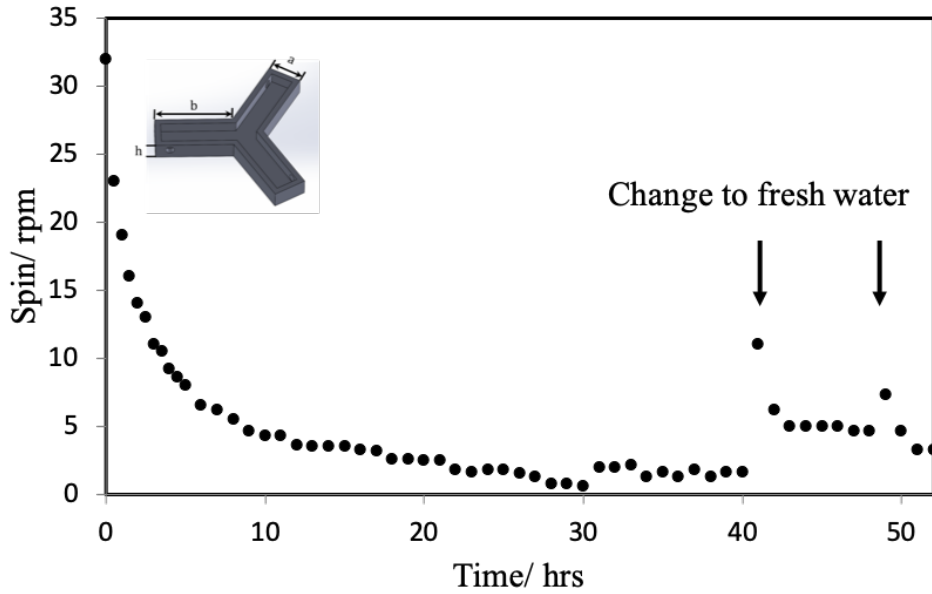
Figure 3.10 Spin rate of gel in 3D printed mold of self-driven motion on water

The velocity reduce should be attributed to both the friction and the lower difference between the gel actuator and water as more solvent diffused into water. The latter is related to the difference in the chemical potential of solvent in gel and water and also decreases surface tension difference, which is believed as the driven force. In addition, the results pointed out that a ceased actuator was able to restart when placed on a fresh DI water surface, which indicate the importance of the difference between the water and gel.

Assume the potential of solvent in water is $\mu_{water}(T, n_s)$ that is dependent on the concentration of solvent ($n_{s,w}$) in water and the temperature of water and the potential of solvent in gel is $\mu_{gel}(T, n_{s,g})$ that is dependent on the concentration of solvent ($n_{s,g}$) in gel and the temperature of gel, the difference in the chemical potential of solvent in water and gel is $\mu_{gel}(T, n_{s,g}) - \mu_{water}(T, n_{s,w})$. Here we can assume that the temperature of water and gel is the same and does not change so that $\mu_{gel}(T, n_{s,g})$ increases with increasing $n_{s,g}$ and $\mu_{water}(T, n_{s,w})$ increase with increasing $n_{s,w}$. As the gel

actuator moves on the water surface, solvent diffused into water as demonstrated and discussed in section 3.2.2 above. Therefore, as a gel actuator moves on the water surface in a container, $\mu_{gel}(T, n_{s,g})$ decreases, while $\mu_{water}(T, n_{s,w})$ increases, with time so that $\mu_{gel}(T, n_{s,g}) - \mu_{water}(T, n_{s,w})$ decreases with time. When the actuator stopped in a container, it means the difference $\mu_{gel}(T, n_{s,g}) - \mu_{water}(T, n_{s,w})$ is so small or even be zero. However, if this actuator is placed on the water surface of another container with fresh water, even though $\mu_{gel}(T, n_{s,g})$ is the same, $\mu_{water}(T, n_{s,w})$ is zero, so that difference $\mu_{gel}(T, n_{s,g}) - \mu_{water}(T, n_{s,w})$ is bigger so that the actuator moves again. Certainly, all the kinetic energy loses as heat due to the friction. All these demonstrate that it is the difference in chemical potential of solvent in gel and water, $\mu_{gel}(T, n_{s,g}) - \mu_{water}(T, n_{s,w})$, rather than the concentration of the solvent in gel that is the driving force for the self-driven actuators. The results also indicate that a gel actuator would have a longer motion duration in a container with more DI water.

3.2.4 Mechanism of self-driven motion

A fresh gel actuator with size of 6 mm × 3 mm was placed at the air-water interface and wait until no motion is observed. Then, the used gel was place at the air-DMF interface. The same procedure was conducted on another fresh gel actuator with size of 6 mm × 3 mm and then it was place at the air-acetone interface.

Motion was observed when a used gel was placed on the surface of DMF or acetone (i.e., at air-DMF/acetone interface) as shown in Figure 3.11. The used gel moved slowly on the DMF surface in the first 20 seconds. There is no surface tension difference for a gel that is already stop at the

air-water interface. However, there is solvent diffusing into gel for this case. Thanks to the

conservation of momentum, the used gel actuator moves on the DMF surface. This is an evidence

that solvent diffusion contributes to the self-driven motions of gel actuators. The slow motion of

used gel on the DMF surface is understandable since the solvent diffuses into gel slowly.
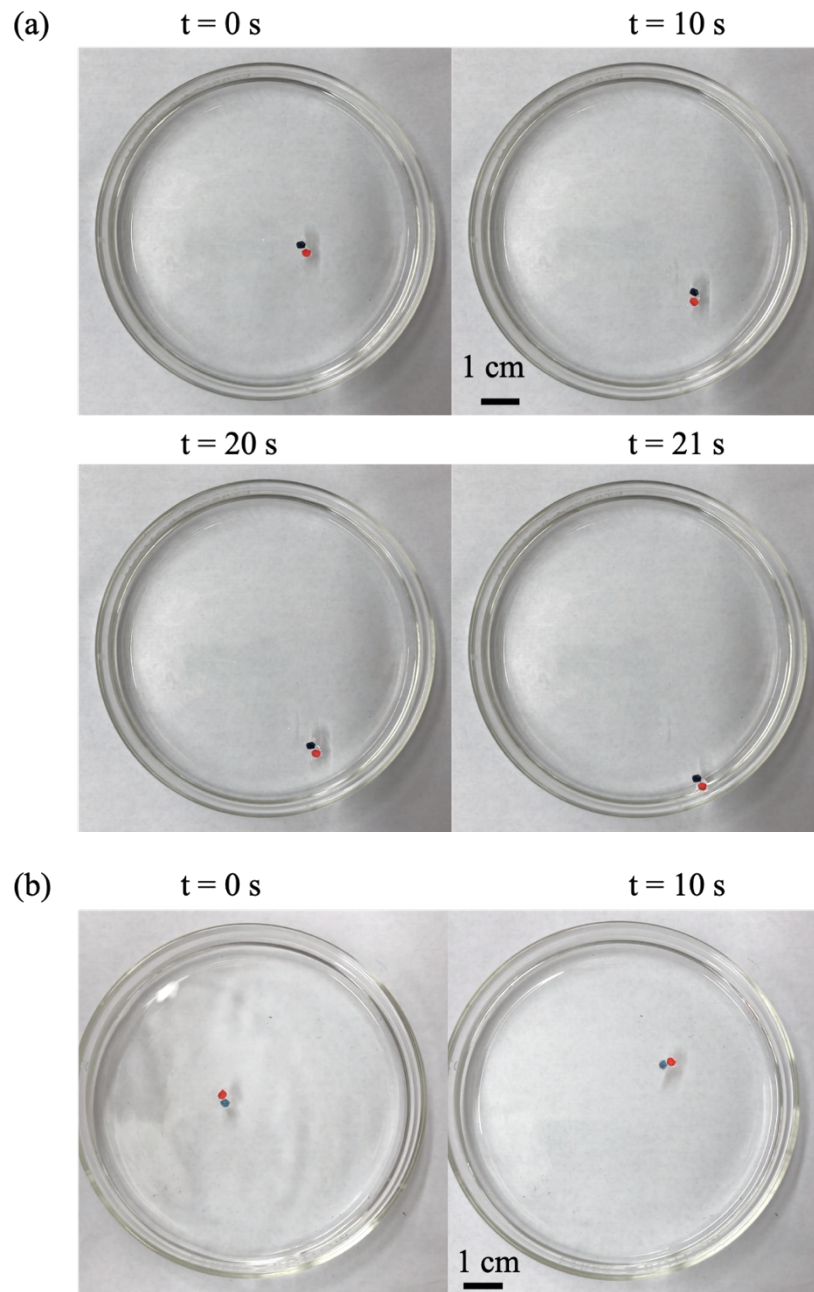
Figure 3.11 Used gel actuators on the surface of (a) DMF and (b) acetone

At the last 1 second, the used gel approached the wall rapidly. This could be attributed to the asymmetry of surface tension on the two side of gel. By observation, the meniscus for both gel actuators and glass is concave as shown in Figure 3.12. Figure 3.12 (a) directly shows a concave meniscus of PVDF gel at the DMF-air interface. 30 μL DMF and acetone was placed on the used PVDF gel as shown in Figure 3.12 (c) and (d). Contact angle of DMF on the PVDF gel and the fact that acetone on the PVDF gel is flat indicates that the menisci is concave for the used PVDF gel on DMF or acetone surface. The contact angle of DI water, DMF and acetone on the glass beaker is shown in Figure 3.12 (b), which indicates that the menisci of DI water, DMF and acetone in the glass beaker are concave. The capillary force is attractive when the menisci around two objects are similar, which is the case of a PVDF on DMF surface in the glass beaker. Therefore, the used gel moved rapidly towards the wall of beaker when it is closed to the wall.
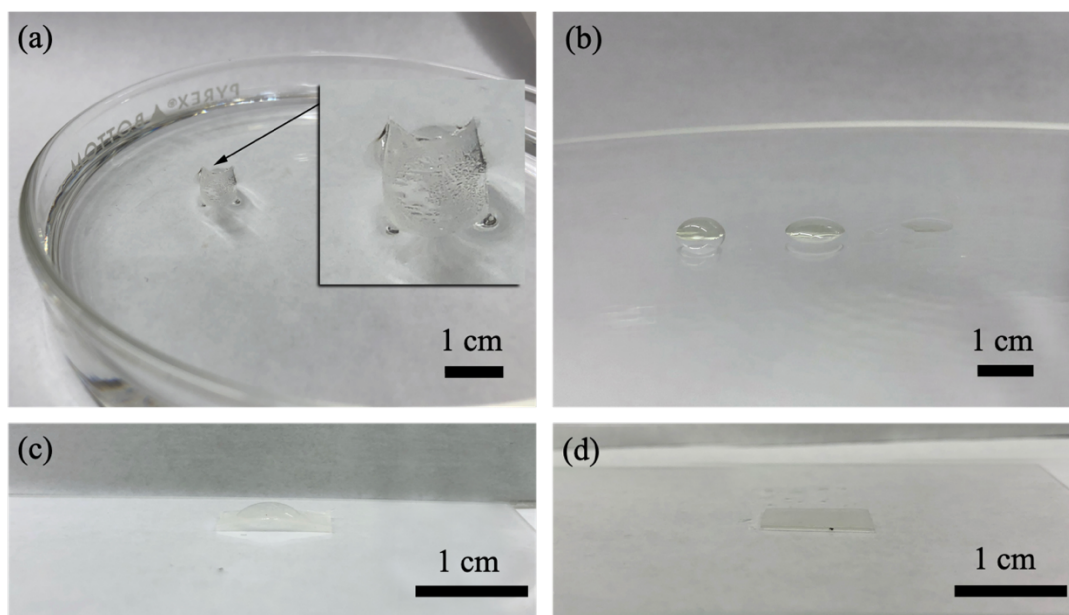
Figure 3.12 (a) A used gel actuators on the surface of DMF, PVDF gel, 6 mm × 12 mm; (b) 30 μL DI water (left), DMF (middle) and acetone (right) on the glass beaker; (c) 30 μL DMF on used PVDF gel, 6 mm × 12 mm and (d) 30 μL acetone on used PVDF gel, 6 mm × 12 mm

Consider the case that an object without solvent diffusion placed at air-water interface, it may exhibit self-driven motion but will not last long. However, the self-driven motion at air-water interface is prolonged. Therefore, solvent diffusion is the main driven force for the self-driven motion of gels, while surface tension makes a minor contribution.

3.2.5   Diameter of the container

To explore whether the performance of gel actuators affected by the diameter of glass beaker, the gel actuators with the size of 6 mm × 3 mm were tested in two glass beakers with different diameters (i.e., 150 mm and 190 mm). The water depth with different amount of water in two glass beakers were shown in Table 3.5. With 400 mL DI water in glass beaker, the water depth of large glass beaker ($\emptyset$ = 190 mm) was 14 mm and the water depth of small glass beaker ($\emptyset$ = 150 mm) was 22.5 mm.

Table 3.5 Diameter and water depth of two glass beaker with different amount of DI water

	Water depth (mm)	DI water volume (mL)
Large beaker ($\emptyset$ = 190 mm)	14	400
	28	800
	56	1600
Small beaker ($\emptyset$ =150 mm)	11	200
	22.5	400
	45	800

A fresh gel film (i.e., Gel 1) was tested in the large glass beaker. Then, Gel 1 was recharged and tested in the small glass beaker. Another fresh gel (i.e., Gel 2) was tested in the small glass beaker, followed by recharged Gel 2 tested in the large glass beaker.

The duration of motion and mass loss of gel actuators in the glass beakers were shown in Table 3.6. Linear velocity at the very beginning was denoted as υ_0. Results presented that both t_1 and t_2 in the large beaker is longer. Figure 3.4 illustrated difference in t_1 of gel motions in two beakers. The duration of the gel actuator in the large beaker is longer than that of the gel actuator in the small beaker in DI water as shown in Figure 3.4 (a), no matter the gel is fresh one or recharge one.

Table 3.6 Mass loss, durations and initial velocity of gel actuators with DI water

Sample	Beaker	Δm (mg)	υ_0 (mm/s)	t_1 (s)	t_2 (s)
Gel 1	Large beaker	1.34	167	392	504
Recharged Gel 1	Small beaker	1.38	156	320	474
Gel 2	Small beaker	1.33	160	307	460
Recharged Gel 2	Large beaker	1.89	150	357	506

1 mL DMF was added into 400 mL DI water and gel actuators with the size of 6 mm $\times$ 3 mm were tested after the organic solvent was added. A fresh gel film (i.e., Gel 3) was tested in the large glass beaker, then recharge and teste it in the small glass beaker. A fresh gel (i.e. Gel 4) was tested in the small glass beaker, then recharge and teste it in the large glass beaker. The same procedure was conducted on two fresh gel films (i.e., Gel 5 and Gel 6) with the size of 6 mm $\times$ 3 mm using acetone as the solvent.

The duration of motion and mass loss of gel actuators in the glass beakers were shown in Table 3.7 and Table 3.8. Similarly, both t_1 and t_2 in the large beaker is longer when DMF or acetone was added. Compare to DI water, the difference in t_1 between two beakers it is larger when DMF or acetone was added as shown in Figure 3.13. Considering the volume of water and solvent added

were the same for both breakers, the experimental results indicates that either the height of water

or the surface area (diameter of the beaker) has a strong influence on the behavior of the actuator.

Table 3.7 Mass loss, durations and initial velocity of gel actuators when 1 mL DMF was added into DI water

Sample	Beaker	Δm (mg)	v_0 (mm/s)	t_1 (s)	t_2 (s)
Gel 3	Large beaker	1.16	21(spin)	332	560
Recharged Gel 3	Small beaker	1.02	128	177	203
Gel 4	Small beaker	0.97	143	207	352
Recharged Gel 4	Large beaker	1.53	148	300	413

Table 3.8 Mass loss, durations and initial velocity of gel actuators when 1 mL acetone was added into DI water

Sample	Beaker	Δm (mg)	v_0 (mm/s)	t_1 (s)	t_2 (s)
Gel 5	Large beaker	1	141	279	410
Recharged Gel 5	Small beaker	1.36	98	145	188
Gel 6	Small beaker	0.78	151	170	259
Recharged Gel 6	Large beaker	1.46	104	276	293
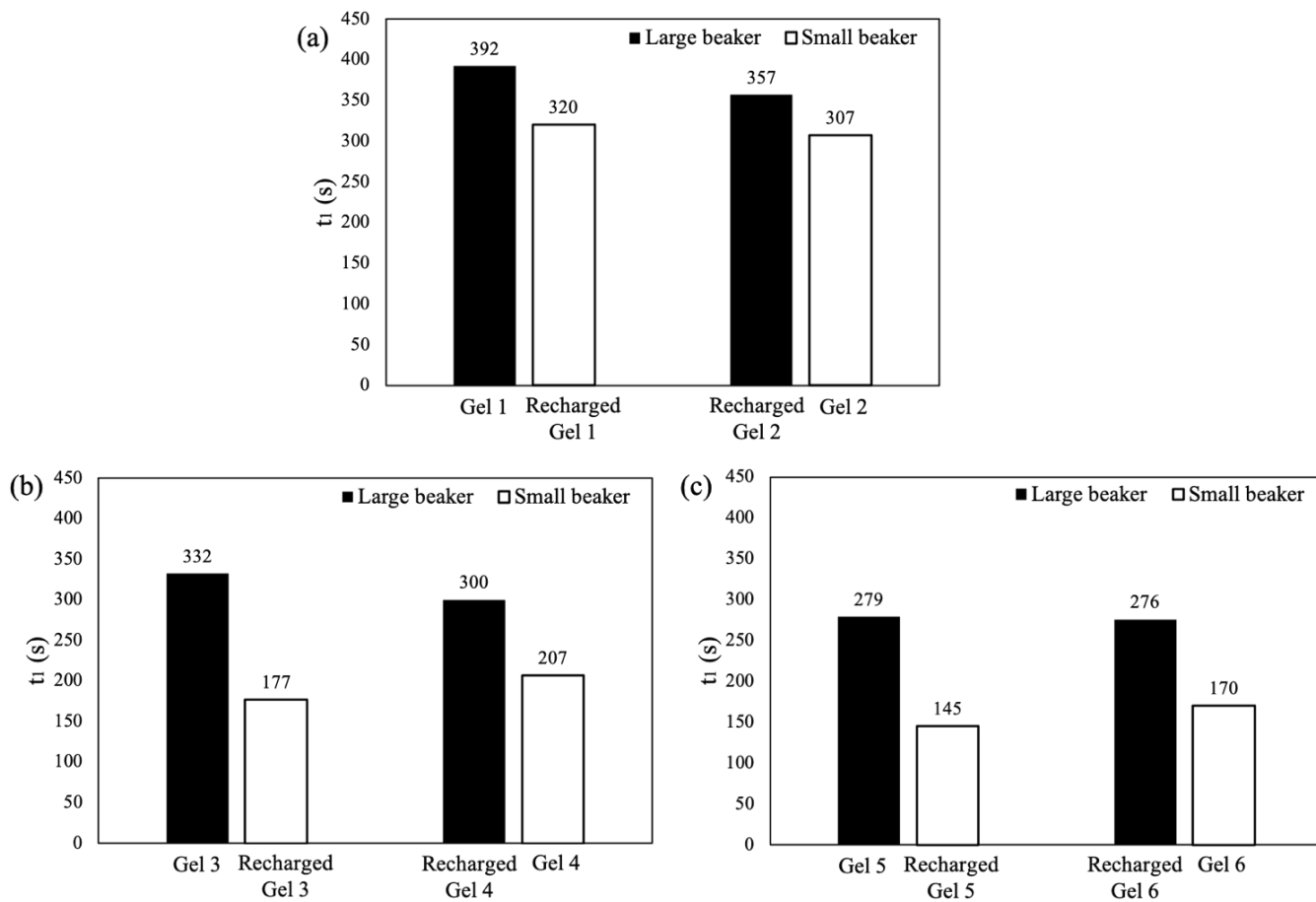
Figure 3.13 Duration, t_1, of gel actuators in two glass beakers with (a) into DI water and when adding (b) 1mL DMF and (c) 1mL acetone into DI water

As mentioned above, the depth of water in the of large glass beaker ($\emptyset$ = 190 mm) and the small glass beaker ($\emptyset$ = 150 mm) was 14 mm and 22.5 mm, respectively. There is a difference in water depth between two glass beakers when volume of water was the same in both beakers. Yui Matsuda et al. pointed out that speeds of camphor disks were independent of the water depth in the two-dimensional system [170] , but it is not clear how the water depth influence on motions of gel actuators. A series of tests was designed to explore whether the water depth affects the gel motions, in addition, to confirm the effect of diameter of the beaker on the gel motion.

Three parameters include the diameter of glass beakers, the water depth and the volume of DI water. In addition, the water depth and volume of DI water are correlated. In order to explore how the three parameters influence on the motions of gel actuators, three volume of DI water were used in each glass beaker. They are 400 mL, 800 mL and 1600 mL DI water in the large glass beaker and 200 mL, 400 mL and 800 mL DI water in the small glass beaker. The water depth corresponding to each volume of DI water was shown in Table 3.5. 1 mL DMF was added into 400 mL DI water. To maintain the same solvent concentration, 0.5 mL, 1 mL, 2mL and 4 mL organic solvent was added into 200 mL, 400 mL, 800 mL and 1600 mL DI water.

Gel actuators with the size of 6 mm × 3 mm were tested when DMF added. A fresh gel film (i.e., Gel 1) was tested in the large glass beaker with 400 mL water. Then, Gel 1 was recharged and tested in the larger glass beaker with 800 mL DI water. At last, the recharged Gel 1 was recharged again and tested in the larger glass beaker with 1600 mL DI water. Another fresh gel (i.e., Gel 2) was tested in the large glass beaker with opposite sequence, i.e., 1600 mL, 800 mL and 400 mL. Similarly, Gel 3 was tested in the small glass beaker with sequence of 200 mL, 400 mL and 800 mL, and Gel 4 was tested in the small glass beaker with sequence of 800 mL, 400 mL and 200 mL. The same procedure was conducted on Gel 5 and Gel 6 in the large glass beaker and Gel 7 and Gel in the small glass beaker using acetone as the solvent. Duration of motions and mass changes of gel actuators in the glass beakers were shown in Table 3.9 to Table 3.12. NA in the table means data not available.

Table 3.9 Mass loss, initial velocity and durations of gel actuators when 1 mL DMF was added into water in a beaker with ø = 190 mm

Depth	Sample	m_1 (mg)	m_2 (mg)	Δm (mg)	υ_0 (mm/s)	t_1 (s)	t_2 (s)
15 mm	Gel 1	10.24	7.48	2.76	142	284	433
30 mm	Recharged Gel 1	11.47	7.51	3.96	137	314	351
60 mm	Recharged Gel 1	8	6.85	1.15	135	247	355
60 mm	Gel 2	11.94	8.1	3.84	135	333	482
30 mm	Recharged Gel 2	11.96	7.59	4.37	144	445	464
15 mm	Recharged Gel 2	10.5	8.05	2.45	15(spin)	276	445

Table 3.10 Mass loss, initial velocity and durations of gel actuators when 1 mL DMF was added into water in a beaker with ø = 150 mm

Depth	Sample	m_1 (mg)	m_2 (mg)	Δm (mg)	υ_0 (mm/s)	t_1 (s)	t_2 (s)
12.5 mm	Gel 3	10.91	8.12	2.79	24.3(spin)	190	420
25 mm	Recharged Gel 3	10.94	7.32	3.62	168	157	282
50 mm	Recharged Gel 3	10.48	8.15	2.33	143	263	371
50 mm	Gel 4	11	7.94	3.06	148	345	472
25 mm	Recharged Gel 4	10.12	7.56	2.56	144	342	526
12.5 mm	Recharged Gel 4	10.68	8.21	2.47	125	361	486

Table 3.11 Mass loss, initial velocity and durations of gel actuators when 1 mL acetone was added into water in a beaker with ø = 190 mm

Depth	Sample	m_1 (mg)	m_2 (mg)	Δm (mg)	υ_0 (mm/s)	t_1 (s)	t_2 (s)
15 mm	Gel 5	9.34	6.95	2.39	155	160	295
30 mm	Recharged Gel 5	9.45	6.38	3.07	152	194	259
60 mm	Recharged Gel 5	13.7	8.05	5.65	NA	104	316
60 mm	Gel 6	10.78	7.93	2.85	121	224	310
30 mm	Recharged Gel 6	10.76	7.87	2.89	106	124	269
15 mm	Recharged Gel 6	10.68	8.08	2.6	16.7(spin)	160	416

Table 3.12 Mass loss, initial velocity and durations of gel actuators when 1 mL acetone was added into water in a beaker with ø = 150 mm

Depth	Sample	m_1 (mg)	m_2 (mg)	Δm (mg)	υ_0 (mm/s)	t_1 (s)	t_2 (s)
15 mm	Gel 7	9.54	7.51	2.03	149	252	377
30 mm	Recharged Gel 7	10.6	7.51	3.09	140	216	326
60 mm	Recharged Gel 7	10.48	8.16	2.32	15.1	164	383
60 mm	Gel 8	9.23	7.44	1.79	115	182	288
30 mm	Recharged Gel 8	8.88	7.1	1.78	143	225	424
15 mm	Recharged Gel 8	9.72	7.52	2.2	129	191	311

Figure 3.14 illustrated t_1 of gel motions, where x axis of these figures represents recharge sequence. Figure 3.14 (a) illustrated that t_1 of Gel 1 increases at first and then decreases as volume of DI water increases. However, t_1 of Gel 2 increases at first and then decreases as volume of DI water decreases. In addition, Figure 3.14 (b) presented that t_1 of Gel 4 does not change too much as volume of DI water decrease. Figure 3.14 (c) and (d) presented the t_1 of gel actuators when acetone was added. In addition, there is no clear trend of t_1 when volume of DI water increases or decreases. All in all, the water depth has little effect on the initial velocity and duration of gel motions.
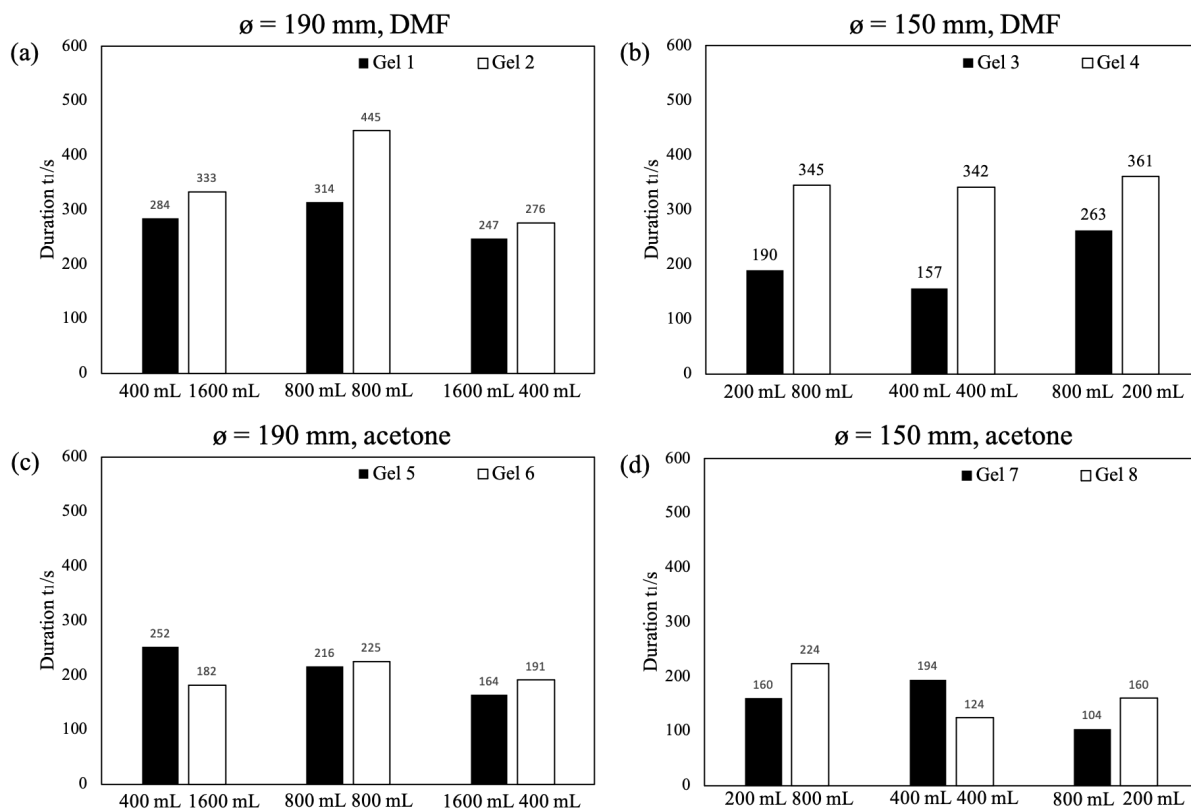
Figure 3.14 Duration, t_1, of gel actuators in glass beakers, x axis represents the recharge sequence. (a) large glass beaker ($\emptyset = 190$ mm), DMF; (b) small glass beaker ($\emptyset = 150$ mm), DMF; (c) large glass beaker ($\emptyset = 190$ mm), acetone and (d) small glass beaker ($\emptyset = 190$ mm), acetone

To obtain more data points about recharge gels on all six conditions (i.e. I. $\emptyset = 190$ mm 1600 mL, II. $\emptyset = 190$ mm 800 mL, III. $\emptyset = 190$ mm 400 mL, IV. $\emptyset = 150$ mm 800 mL, V. $\emptyset = 150$ mm 400 mL and VI. $\emptyset = 150$ mm 200 mL), a series tests was conducted as followings using DMF as the solvent. Six fresh gel actuators with size of 6 mm × 3 mm were tested on six different conditions, recharged and then tested in a certain sequence of the rest five conditions. That is, a fresh gel (i.e., Gel 1) was tested on Condition I. Then, the gel actuator was recharged and tested on Condition II. Thirdly, the gel was recharged and tested on Condition III. The processes were repeated until recharged Gel 1 was tested on Condition VI. Similarly, Gel 2 was tested on Condition II, then,

recharged and tested in the sequence of Condition III, Condition IV, Condition V, Condition VI and Condition I. Gel 3 to Gel 6 were tested starting Condition III, Condition IV, Condition V and Condition VI, respectively. Then they were recharged and tested in a sequence of the rest five conditions. Gel actuators and the sequence of test conditions were shown in Table 3.13.

Table 3.13 Gel actuators and sequence of test conditions.

Sample	Test 1	Test 2	Test 3	Test 4	Test 5	Test 6
Gel 1	I	II	III	IV	V	VI
Gel 2	II	III	IV	V	VI	I
Gel 3	III	IV	V	VI	I	II
Gel 4	IV	V	VI	I	II	III
Gel 5	V	VI	I	II	III	IV
Gel 6	VI	I	II	III	IV	V

Duration of motions and mass changes of gel actuators in six different conditions were shown in Table 3.14 to Table 3.19. NA in the table means data not available. Results showed that the initial velocity of gel actuators are independent of volume of water, or water depth. Mass and mass loss of gel actuators were illustrated in Figure 3.15. It is obvious that the mass loss is correlated with mass of gel actuators. Large gel actuators induce large mass loss. This trend was not affected by the test conditions and recharge processes.

Table 3.14 Mass loss, initial velocity and durations of Gel 1

Condition	m_1 (mg)	m_2 (mg)	Δm (mg)	v_0 (mm/s)	t_1 (s)	t_2 (s)
I. $\emptyset$ = 190 mm 1600 mL	11.4	8.76	2.64	150	280	364
II. $\emptyset$ = 190 mm 800 mL	11.55	8.57	2.98	154	252	403
III. $\emptyset$ = 190 mm 400 mL	9.71	8.36	1.35	NA	349	571
IV. $\emptyset$ = 150 mm 800 mL	9.84	8.73	1.11	137	204	394
V. $\emptyset$ = 150 mm 400 mL	9.43	8.56	0.87	128	294	425
VI. $\emptyset$ = 150 mm 200 mL	9.7	8.52	1.18	15	310	459

Table 3.15 Mass loss, initial velocity and durations of Gel 2

Condition	m_1 (mg)	m_2 (mg)	Δm (mg)	v_0 (mm/s)	t_1 (s)	t_2 (s)
II. Ø = 190 mm 800 mL	10.66	8.04	2.62	157	282	406
III. Ø = 190 mm 400 mL	10.39	7.97	2.42	154	300	403
IV. Ø = 150 mm 800 mL	8.95	7.17	1.78	120	157	340
V. Ø = 150 mm 400 mL	8.83	7.64	1.19	130	289	506
VI. Ø = 150 mm 200 mL	9.32	7.95	1.37	NA	228	406
I. Ø = 190 mm 1600 mL	8.8	7.8	1	132	258	417

Table 3.16 Mass loss, initial velocity and durations of Gel 3

Condition	m_1 (mg)	m_2 (mg)	Δm (mg)	v_0 (mm/s)	t_1 (s)	t_2 (s)
III. Ø = 190 mm 400 mL	10.44	8.23	2.21	152	312	387
IV. Ø = 150 mm 800 mL	11.5	8.1	3.4	165	154	216
V. Ø = 150 mm 400 mL	8.8	7.9	0.9	141	230	408
VI. Ø = 150 mm 200 mL	8.52	7.65	0.87	152	320	540
I. Ø = 190 mm 1600 mL	9.74	8.02	1.72	102	210	285
II. Ø = 190 mm 800 mL	8.52	7.56	0.96	133	358	430

Table 3.17 Mass loss, initial velocity and durations of Gel 4

Condition	m_1 (mg)	m_2 (mg)	Δm (mg)	v_0 (mm/s)	t_1 (s)	t_2 (s)
IV. Ø = 150 mm 800 mL	10.21	8.13	2.08	157	263	524
V. Ø = 150 mm 400 mL	11.44	8.59	2.85	125	98	479
VI. Ø = 150 mm 200 mL	10.03	8.27	1.76	133	270	375
I. Ø = 190 mm 1600 mL	10.27	7.93	2.34	NA	252	388
II. Ø = 190 mm 800 mL	9.26	8.23	1.03	131	246	375
III. Ø = 190 mm 400 mL	9.25	8.23	1.02	20	192	239

Table 3.18 Mass loss, initial velocity and durations of Gel 5

Condition	m_1 (mg)	m_2 (mg)	Δm (mg)	v_0 (mm/s)	t_1 (s)	t_2 (s)
V. Ø = 150 mm 400 mL	10.06	7.56	2.5	152	295	418
VI. Ø = 150 mm 200 mL	11.08	8.23	2.85	108	216	497
I. Ø = 190 mm 1600 mL	9.09	7.87	1.22	134	288	526
II. Ø = 190 mm 800 mL	9.71	8.1	1.61	94	282	509
III. Ø = 190 mm 400 mL	9.34	8.21	1.13	77	257	380
IV. Ø = 150 mm 800 mL	8.77	7.89	0.88	113	136	320

Table 3.19 Mass loss, initial velocity and durations of Gel 6

Condition	m_1 (mg)	m_2 (mg)	Δm (mg)	υ_0 (mm/s)	t_1 (s)	t_2 (s)
VI. $\emptyset$ = 150 mm 200 mL	10	7.85	2.15	180	283	383
I. $\emptyset$ = 190 mm 1600 mL	10.74	8.15	2.59	145	300	441
II. $\emptyset$ = 190 mm 800 mL	9.05	7.8	1.25	121	270	355
III. $\emptyset$ = 190 mm 400 mL	9.4	7.9	1.5	134	283	398
IV. $\emptyset$ = 150 mm 800 mL	8.7	7.78	0.92	155	195	375
V. $\emptyset$ = 150 mm 400 mL	8.78	7.87	0.91	123	200	354

Figure 3.16 illustrated mass and duration, both t_1 and t_2, of gel actuatros. Mostly, a larger t_1 correspond to a larger t_2, although the increment from t_1 to t_2 is not consistent. However, there is some exemption, for example, Gel 4 tested on condition V ($\emptyset$ = 150 mm 400 mL) has a t_1 of 98 s and a t_2 479 s. In this case, t_2 is far more than t_1, compared to Gel 4 tested on condition I ($\emptyset$ = 190 mm 1600 mL) that has a t_1 of 252 s and t_2 of 388 s.

Both t_1 and t_2 decrease when gel actuators change from the large glass beaker to the small glass beaker for all six gels. And both t_1 and t_2 increase when gel actuators change from the small glass beaker to the large glass beaker except for Gel 3 and Gel 4. Thus, the diameter of beaker has an effect on the motion of gel actuators. Therefore, the organic solvents have an effect at the air-water interface during motions.
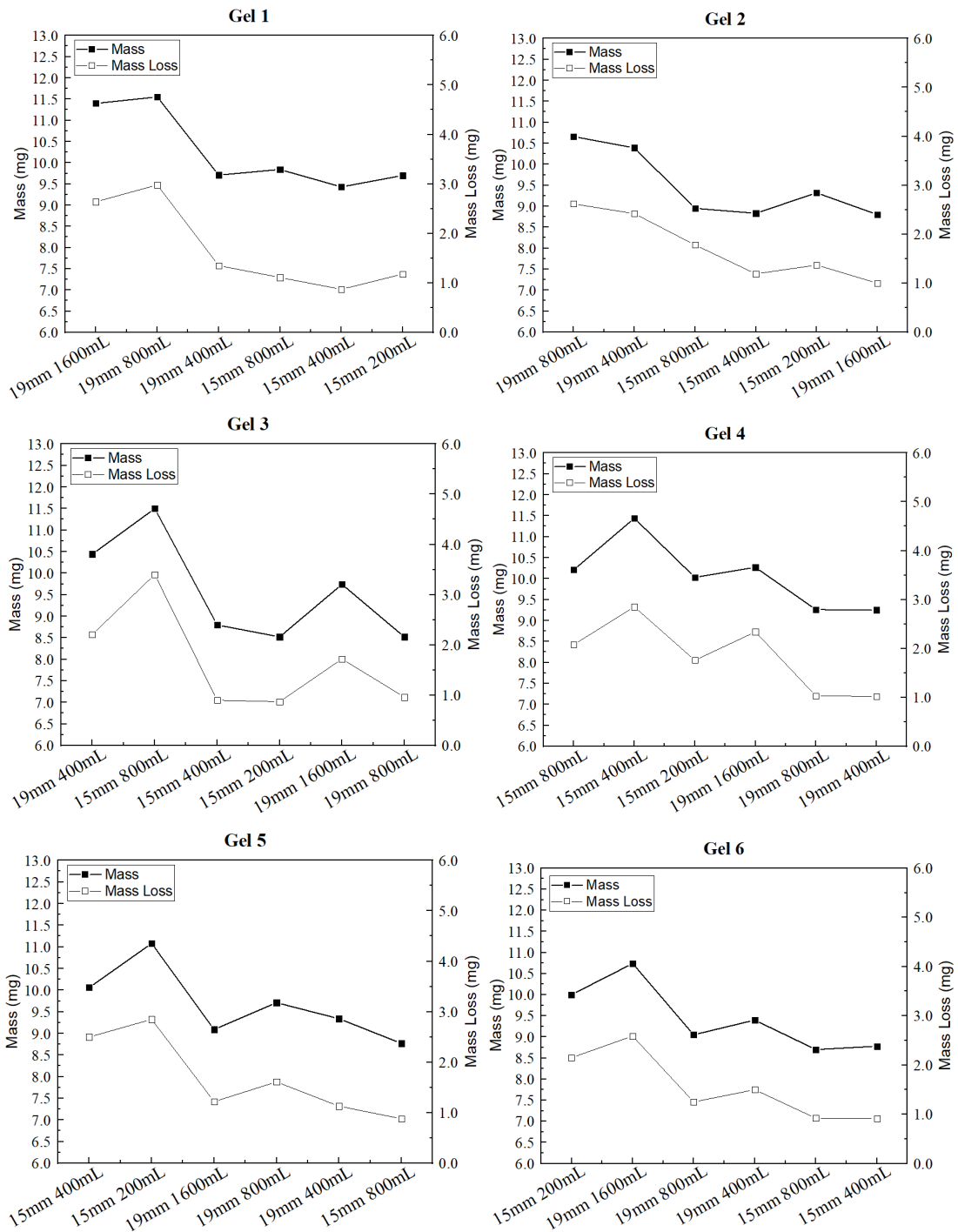
Figure 3.15 Mass and mass loss of gels actuators
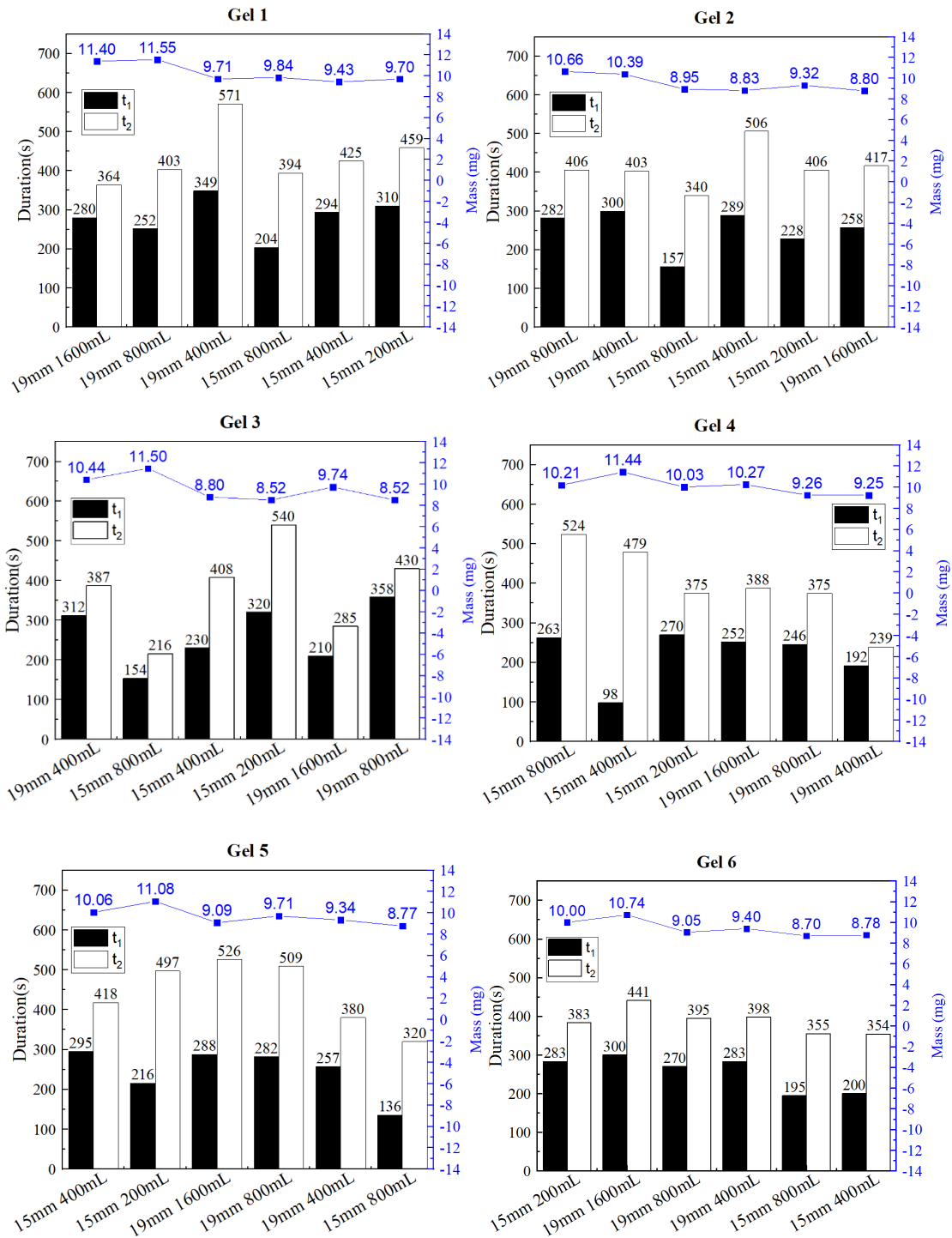
Figure 3.16 Duration, t_1 and t_2, of gel actuators tested on six different conditions, x axis represents the recharge sequence.

(a) Gel 1; (b) Gel 2; (c) Gel 3; (d) Gel 4; (e) Gel 5 and (f) Gel 6.

Based on discussion above, motion of gel at the air-water interface are dependent on the diameter of beaker, instead of the depth or volume of water. Both DMF and acetone is miscible with water. Therefore, the concentration of solvent should be the same when solvent diffusing into same amount of water. However, there are difference in duration in two beakers with different diameter but same amount of water. It is possible that solvent diffusion in the bulk water takes time, resulting in concentration of solvent at the air-water interface is higher than the concentration of solvent in the bulk water. That is, concentration of solvent is higher for a small beaker due to a small surface area at the air-water interface.

3.2.6   Physical changes of gels after motion
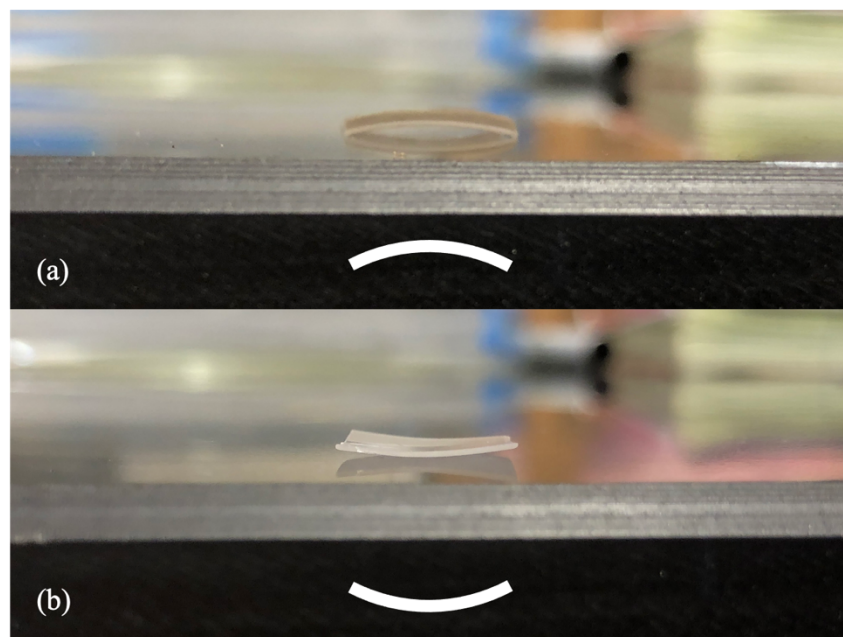
Figure 3.17 The gel actuator in (a) Phase-I and (b) Phase-II.
PVDF/ DMF-acetone gel, size: 12 mm × 12 mm

Flatness of gel actuators: It is found that during the actuation, the flatness of the gel actuator changes. A gel actuator curled down and curled up after motion on water surface as shown in

Figure 3.17. At the very beginning, all gels remain flat before they were placed on the water surface. All samples curled down (phase-I in Figure 3.19) in first 10 s after actuating on the water. Samples gradually transform to curl up (phase-II in Figure 3.19) during moving on the water surface in around 5 minutes. And they will keep this shape till the end of actuation process.

In addition, the gel curved up when placing 100 µL DI water was placed on the top of it as shown in Figure 3.18. That is, the bending is strong enough to overcome the adhesion between the gel and glass substrate.
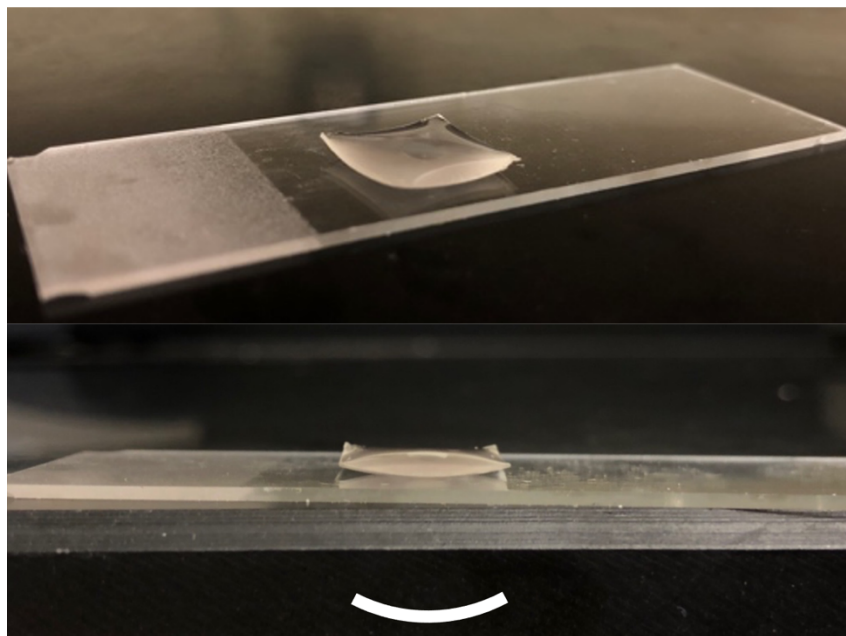
Figure 3.18 100 µL DI water was placed on the top of gel and the gel was placed on a glass substrate. PVDF/ DMF-acetone gel, size: 12 mm × 12 mm

This phenomenon was not reported for other self-driven gel actuators. Certainly, the bending of gels reflects some kind of asymmetry of the gel actuator. Logically, first would be considered is the fabrication of gel film. The gel film was cast on a glass substrate. One may link this asymmetry to two surfaces of the gel film during cast: one faced air, the other was in contact with glass

substrate. To explore the relationship between this phenomenon and asymmetry of gel between air side and glass side, tests were conducted as following. Both air side (case-I) and glass side (case-II) of samples were tested on water. The test showed sequence of phase-I and Phase-II is identical for two cases, which is shown in Figure 3.19. Thus, one concludes that the bending of a gel during actuation on the water surface is not originated from the fabrication process of the gel. The next factor would be the changes during the actuation. That is, bending of gel was originated from organic solvent diffusion from gel into water during the motion.
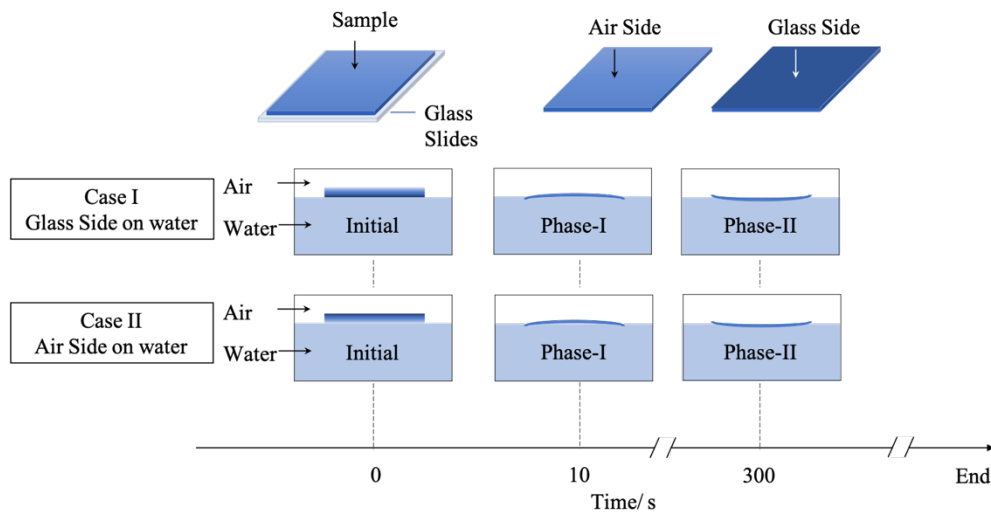
Figure 3.19 Scheme of gel actuators bend when moving at the air-water interface

It was well known that for ionic EAP, the EAP film remains flat when absence of electric field due to randomly distributed ions including both positive and negative ions. However, when an electric field is applied on the ionic EAP film, ions are forced to move so that positive and negative ions are separated into two different sides, which results in a bending actuation due to the size difference between two types of ions [203,204]. In addition, studies indicated that bending of a thin film can depend on the moisture gradient across the film [205,206,207].
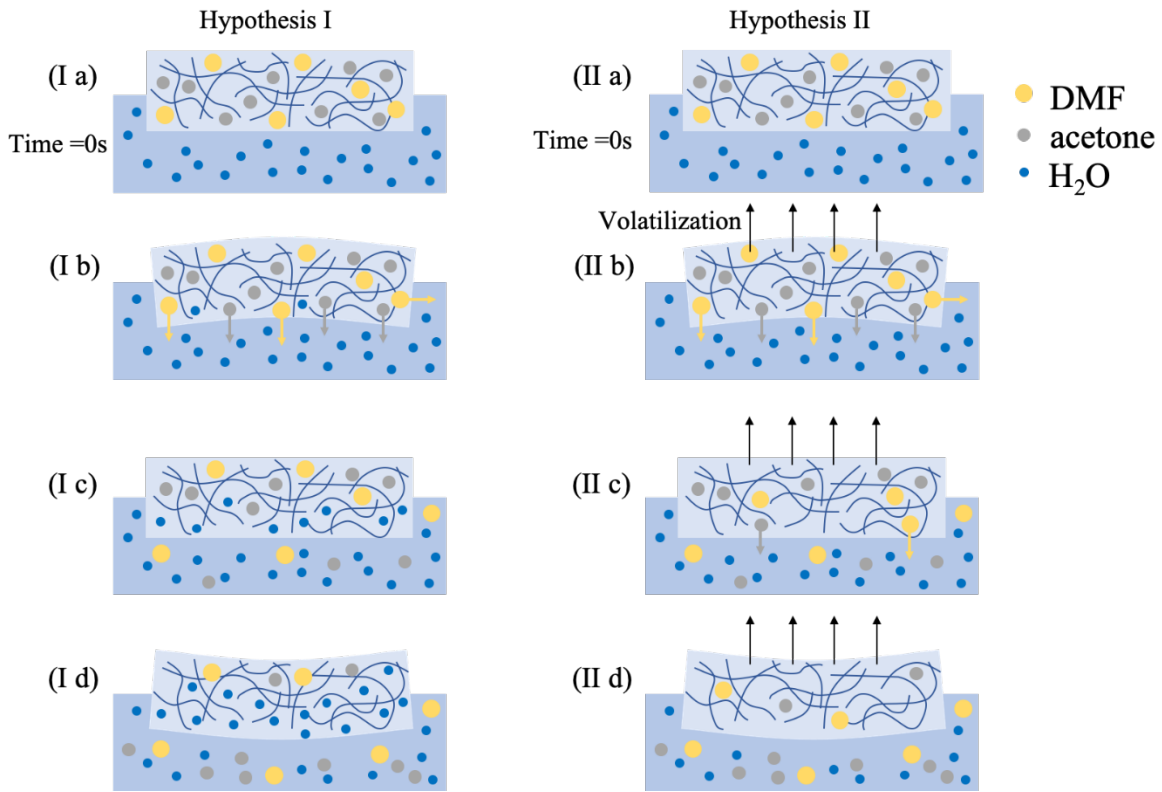
Figure 3.20 Two hypotheses of gels bend during the motion on the water surface.

Inspired by aforementioned research on the ionic EAP, two hypotheses are proposed for the mechanism that is responsible for Phase-I and Phase-II bending of gel actuators during their actuation/motion at the air-water interface as below and illustrated in Figure 3.20. Gels has 3-D networks of the polymer matrix (i.e., PVDF), in which the interstitials (i.e., free volume) are filled with organic solvent molecules. For the PVDF gels studied here, solvent was either only DMF or the mixture of DMF and acetone. Once a gel actuator is placed at the air-water interface, the chemical potential of the solvent in the actuator is higher than that in water since the chemical potential of solvent in the pure DI water is zero. Therefore, the solvent in the actuator diffuses into water as expected from thermodynamics, which is experimentally proved as discussed above. As discussed above, the diffusion of solvent from a gel actuator into water occurs through edges and

bottom surface of the gel actuator, which results in the reduction in the concentration of solvent at edges and bottom surface of the gel actuator. That is, there will be a gradient in the concentration of solvent in the gel actuator. Assuming that the lower concentration of the solvent in the gel, the smaller the dimension of the gel, one can get that a gel actuator at the air-water interface experiences a shrinkage on edges and also the bottom surface, which results in Phase-I bending observed in the experiments as shown in Figure 3.20 (I b). That is, the at the beginning, the organic solvent in a gel actuator diffuses from bottom surface of the gel into water, which results in a crease in the concentration of solvent in the layer near the bottom surface. In other words, there is a concentration gradient along the thickness with a lower concentration at bottom surface for the solvent in gel. This would result in the downward bending of gel as observed for Phase-I as shown in Figure 3.20 (I b). If this was the only process (i.e., solvent in gel diffuses into water), the downward bending of a gel actuator will be enhanced with time initially and, then, weakened with time. That is, slowly the solvent in the gel actuator diffuses from higher concentration regions into lower concentration regions, which would reduce the concentration difference between different regions in the gel actuator. However, this process would not result in Phase-II: upward bending of gel actuator observed in all the experiments. For Phase-II, there are two possibilities: one is water diffusing into gel, the other is the evaporation of solvent from top surface to air. For the former, the diffusion of solvent from the gel actuator into water results in more free space in 3-D network of the gel, which make it is possible for water molecules diffuse into gel through bottom surface of gel. In this case, the upward bending will become strong with time and then weaker. Eventually, the gel should show a very week upward bend. That is, film gel gradually turns back from Phase-

I (downward bend) to flat and then to upward bend that increases initially and the decrease. Eventually, the gel should show a weak upward bend. Another possibility for the observed phenomena is that it was not water molecules diffusing into gel network, but there is some kind interaction between the solvent molecule and water molecules, such as the formation DMF-H_2O. Therefore, a layer of DMF-H2O is formed in gel around the bottom surface. The size of DMF-H_2O is bigger than DMF molecule so that the bottom surface of the gel actuator expands, which would result in an upward bending (i.e., Phase-II). In this case, the upward bending will keep. That is, even a gel actuator stops motion, it will keep the upward bending. This is different with last case - water diffusing into gel network. From the experimental observation, upward bending of the gel actuator increase and will keep.

Five dried PVDF films were soaking in DI water for 24 hours to test whether water solvent can diffuse into PVDF gels. Mass of films were measured before and after soaking, shown in Table 3.20. It showed that water absorption of dried PVDF film is very limited.

Table 3.20 Mass of PVDF film before and after 24 hours soaking in DI water

	Sample 1	Sample 2	Sample 3	Sample 4	Sample 5
m_1*	12.40	22.42	29.20	21.48	7.05
m_2**	12.42	22.45	29.30	21.55	7.13

* m_1- mass of film before soaking
** m_2- mass of film after 24 hours soaking

For latter one, the evaporation of solvent from top surface of gel has an observable influence. That is, gel losses solvent by two paths: one is diffusion into water through edges and bottom surface, the other is evaporation into air through top surface. It has to be mentioned for either diffusion or

evaporation, not all solvent in gel will be lost since there is a minimum concentration. If the minimum concentration for evaporation is lower than that of diffusion, eventually, the solvent concentration in gel will have a lower concentration at top and a higher concentration at bottom, which results in the upward bend. Certainly, there is a possibility that both contribute to the experimental observation.

Evaporation of organic solvent was taken into consideration in hypothesis II. When the gel was placed at the air-water interface, amount of solvent diffused into water is much more than amount of solvent evaporation, which induced gel bending downward and was depicted in Figure 3.20 (II b). While film will bend to the opposite direction when amount of solvent evaporation is much more than amount of solvent diffused into water, which was depicted in Figure 3.20 (II d).

Based on experiment results, the dried gel is flat after placing on a glass substrate and exposing to the air even for 90 minutes. It is possible that rate of solvent evaporation is slow, which makes solvent in the gel have enough time to diffuse. Concentration different between the top and bottom layer is so small, or gets close to an equilibrium state, that does not introduce bending. However, the adhesion between the gel and glass substrate may prevent the gel from bending. A PVDF/ DMF gel was placed on the surface of silicone oil as shown in Figure 3.21 (a). The bottom of gel is immersed in the silicone oil and the top of gel is exposed to the air. DMF in the gel is immiscible with silicone oil. Therefore, there is no solvent diffusion through the bottom of gel. The only way that the gel losses mass is through the solvent evaporation from the tope of gel. And the liquid (i.e., silicone oil) allows the gel bend as it was placed on water surface. No bending of the gel was observed when PVDF/ DMF gel was placed on the silicone oil surface. It remained flat from the

very beginning to 30 minutes, compared to a gel bended downwards after placing on water surface for 20 seconds as shown in Figure 3.21 (b). This result demonstrated that evaporation of solvent from top of gel is not strong enough to generated bending. Therefore, the Hypothesis I is more reasonable.
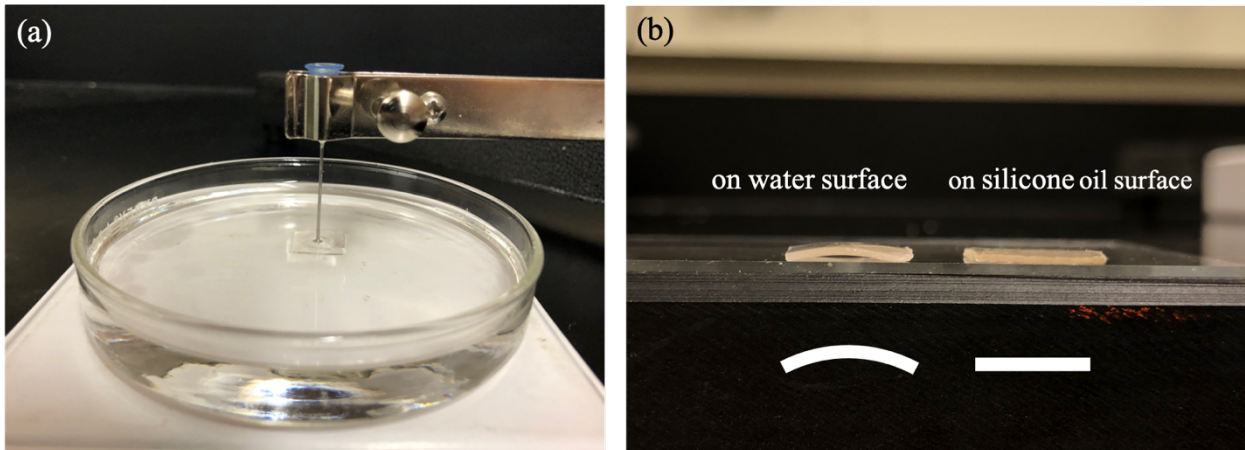
Figure 3.21 (a) A gel placed on the silicane oil surface; (b) A gel after placing on the water surface for 20 seconds (left) and a gel after placing on the silicone oil surface for 30 minutes (right). PVDF/ DMF gel, size: 12 mm × 12 mm

Dimension and Transparency of gel actuator: As indicated by the photo shown in Figure 3.22 (a) fresh gel actuators (i.e., before the gel was placed at the air-water interface) are transparent. However, after the motion at the air-water interface, the transparency is clearly reduced as shown in Fig 3.22 (b) where several gel actuators after motions (i.e., the ones marked with white dotted line) were put together with fresh gel actuators. The fresh gel actuators are transparent, the Auburn logo is clear even it was under the gel. The Auburn logo is blur under the gel actuators after motion at the air-water interface. Thus, transparency gel actuators reduced during actuation process. In addition, side length reduce was pointed out by red arrow in Figure 3.22 (b). Therefore, gel actuators shrink during actuation process.
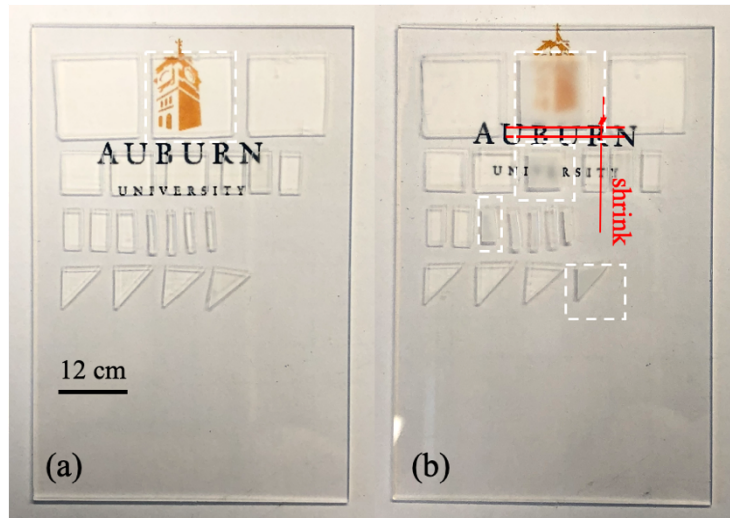
Figure 3.22 Illustration of gels before and after actuation. (a) Gels before actuations; (b) Gels circled by dash lined were samples after actuation.

Three PVDF/DMF-acetone gels with size in 12mm×12mm are shown in Figure 3.23. Figure 3.23 (a) – (f) are photos taken at 10 mins, 20 mins, 30 min, 40 mins, 50 mins 60 mins and 90 mins. The gel on the left was the sample kept in the container with cover. It remained transparent for 90 minutes. The gel in the middle was the sample exposed to the air for 90 minutes. The degree of transparency of this gel decreased gradually in 90 minutes. In addition, gel shrank slowly during the time. The gel on the right was the sample placed at the air water interface for 10 mins and then exposed air. The gel actuator became translucent after motion at the air-water interface. When exposed to the air for the same time, degree of transparency of the gel after motion decreased rapidly, compared to the gel exposed to the air from the beginning to end.
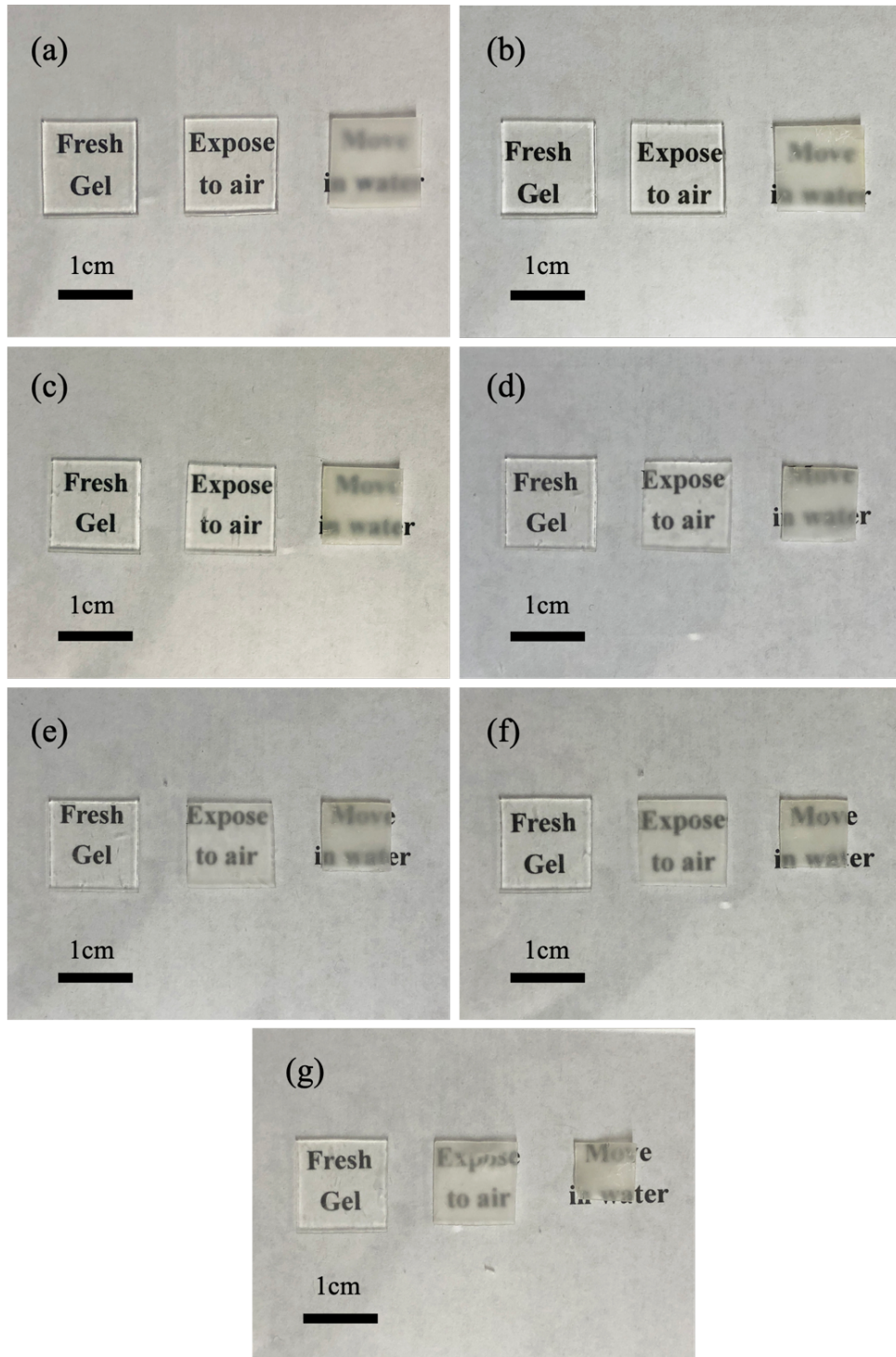
Figure 3.23 Three gel samples with time in (a) 10 minutes; (b) 20 minutes; (c) 30 minutes; (d) 40 minutes; (e) 50 minutes; (f) 60 minutes and (g) 90 minutes.

Compared to the fresh gel, there is an average shrinkage of 10 % in dimension or 19 % in area for gel actuators after 10 minutes motion on water. When exposed to the air for the same time, the gel after motion shrank more compared to the gel exposed to the air from the beginning to end. After 90 minutes, there is shrinkage of 10 % in dimension for gel exposed to air, compared to a shrinkage of 40 % in dimension for gel actuators after motion on water. There is an average shrinkage of 41 % in dimension or 65 % in area for the gels that was dried in vacuum.

Normalized mass of the gel actuators moved on water and gel exposed to air were shown in Figure 3.24. There was 21% mass loss for the gel actuator after 10 minutes motion on water. Totally, there was 68% mass loss at 90 minutes for the gel actuator exposed to air after motion. While there was only 26% mass loss for the gel exposed to air for 90 minutes. Compared to the gels exposed to the air, gel actuators loss mass more and shrink faster, and became less transparency after motions at the air-water interface.
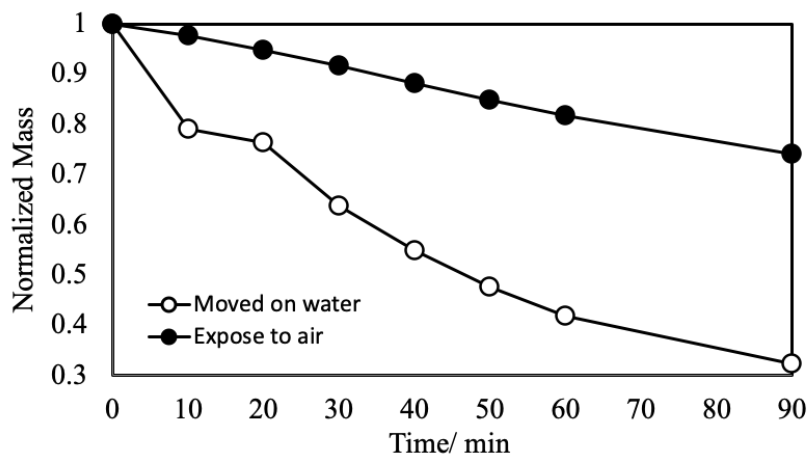
Figure 3.24 Normalized mass of the gel exposed to air (black dots) and moved on water (white dots)

3.2.7 Gel actuators affected by materials of beaker

All gel actuators discussed above were tested in the glass beaker. Self-driven motion of gel actuators at the air-water interface in a glass beaker is prolonged. However, results are different in a plastic beaker. A glass beaker and a plastic beaker with size shown in Table 3.21 were utilized. There is no motion for a gel actuator when placed at the air-water interface in a plastic beaker (i.e., beaker I). This gel actuator was able to move at the air-water interface in a glass beaker (i.e., beaker II) after it was taken out from beaker I. Then, the gel actuator did not move again when it was put back to the plastic beaker (beaker I) from the glass beaker (beaker II). The gel actuator is able to move slowly if beaker I is washed 10 days using DI water. In addition, a droplet of PVDF polymer solution can move rapidly when placed at the air-water interface in plastic beaker, no need to be washed.

Table 3.21 Diameter and water depth of two beakers

	Diameter (mm)	Water depth (mm)	DI water volume (mL)
Glass beaker	150	35	600
Plastic beaker	100	90	600

There is mass loss for the gel at the air-water interface in plastic beaker, although no motion was observed. Figure 3.25 demonstrated normalized mass of three PVDF/ DMF-acetone gels. Two gels at the air-water interface loss mass gradually with similar rate, compared to the gel exposed to the air on a glass substrate. That is, solvent diffused from gel into water continuously during the time even it was in the plastic beaker.
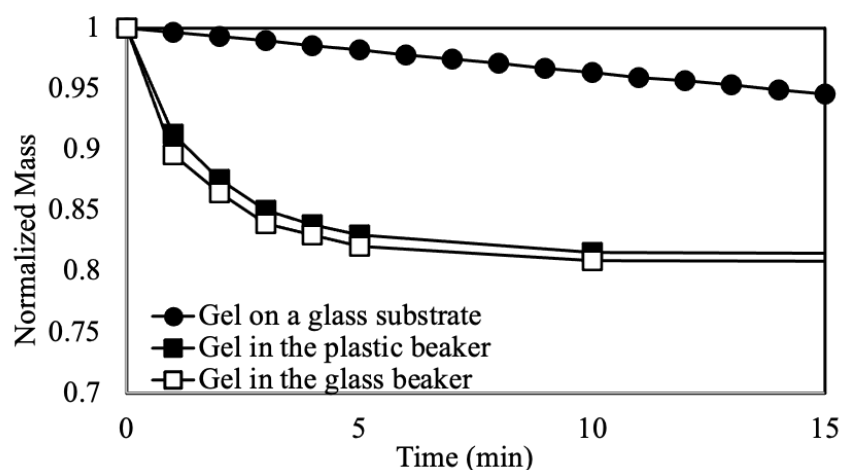
Figure 3.25 Normalized mass of gel on a glass substrate, gel in the plastic beaker and gel in the glass beaker.

It was considered that motion of gel actuators could be affected by chemical in the water. To explore how sensitive the motion of gel actuators is to the chemical in water, detergent was added into water and figure out the critical concentration that gel actuators do not move.

Table 3.22 Amount of soap added into DI water and soap concentration

Volume of Detergent Water (mL)	Detergent Concentration ($\times 10^{-5}$%)	Duration (s)	Mass Loss (mg)
0	0	600	2.26
0.01	1.73	350	2.02
0.02	3.47	306	1.89
0.03	5.20	198	1.85
0.04	6.92	93	1.70
0.05	8.65	58	1.44
0.06	10.38	30	1.00
0.07	12.11	7	0.54
0.075	12.98	0	-
0.08	13.84	0	-

- data not available

Duration of gel actuators varies as amount of detergent in water was presented as Figure 3.26. Detergent in water makes motion of gel actuators harder. The gel motion was very sensitive to the detergent in water and there is no motion of gel actuator at detergent concentration of 12.98×10^{-5} wt.%. Figure 3.26 (b) presented duration of gel motion varies as mass loss. There is a trend that larger mass loss is correlated with a longer duration of motion on water, which is consist with results in Section 3.2.2.
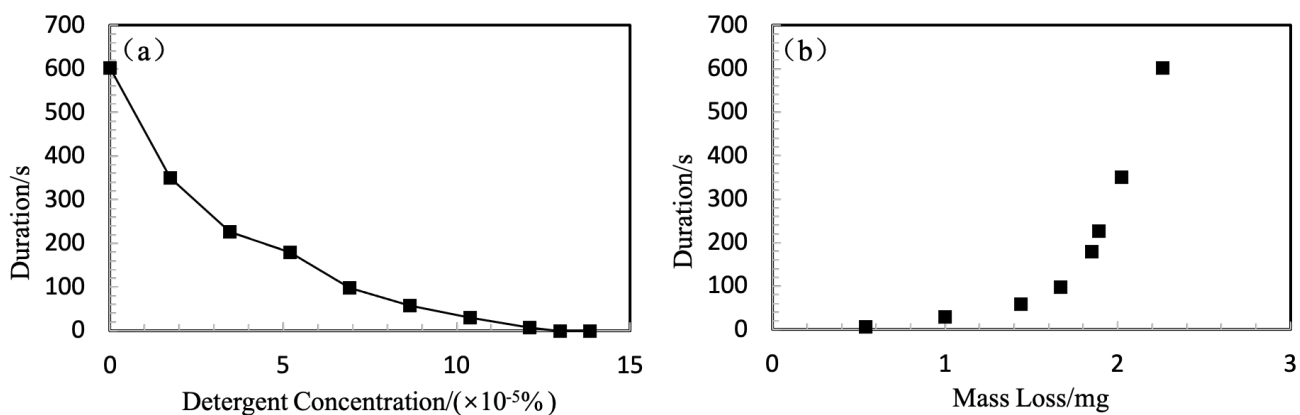
Figure 3.26 (a) Durations of gel motions on water change as detergent concentration and (b) Duration of motion on water varies as mass loss

3.3 Conclusion

This experimentally confirmed that self-driven motions of gel actuators at the air-water interface are a universal phenomenon. When the solvent in get is completely consumed (i.e., diffused to water), the gel actuators can be recharged by placing gel in solvent. No motion of gel was observed when they are placed in bulk water. Based on the experimental results, it is concluded that the mass of the gel decreases with time as solvent in gel diffusing into water. Large gel actuators result in large mass loss and durations of gel actuators increase as mass of gels increases. In addition, the

gel actuators shrink after motion. The transparency of the gel decreases as motion at the air-water interface. Compared to the gels exposed to the air, gel actuators loss mass more, shrink faster and became less transparency after motions. The gel actuators undergo bending downward once placed at the air-water interface and transform to bending upward gradually during motion.

Gels built in fan shape 3D printed mold in a fan shape was designed and fabricated, exhibiting prolonged spin motion. Moreover, translational motion and spin motion were achieved by gel built in the rectangular mold with two holes on one side and two holes on opposite sides. A ceased actuator was able to restart when placed on a fresh DI water surface. This demonstrates that it is the difference in chemical potential of solvent in gel and water, rather than the concentration of the solvent in gel that is the driving force for the self-driven actuators. It also provided a potential method to extend duration of motions.

Both solvent diffusion and surface tension contribute to the observed self-driven motions. Solvent diffusion is the main driven force for the self-driven motion of gels, while surface tension makes a minor contribution. The diameter of beaker has an effect on the motion of gel actuators, while the water depth and volume of water has little effect on the motion.

Chapter IV

Friction of Gel Moving on Water

Based on the experimental results, motion modes of gel actuators include translational motions, spin motions and orbital motions. The actuation mode is critical for future applications and also important for the fundamental study of self-driven gel actuators. Among these motion modes, there are three characteristic variables: the linear velocity, orbital rate and spin rate of samples. All these three variables change with time during the motion. It is not feasible to manually calculate these three variables for spatiotemporal motion of tens samples. Moreover, motion duration of samples varies from 10 minute to an hour, which also makes the manually calculation of rate infeasible. In order to characterize the performance of self-driven actuators, quantifications of these three variables about the motion: velocity, acceleration, and their time dependence are needed. Additionally, the digitalized actuation behavior of gel actuators makes it is possible to determine the friction of gel motion on water surface that is also a critical factor for the performance of an actuator.

Motion of an object is slowed down by friction. Friction force for an object moving at the air-water interface is different from the friction between solids that conforms to Amonton's law [181,187,208,209]. An object moving on water surface experiences a drag force from fluid. And this force is strongly dependent on the velocity of object with respect to the surrounding fluid. The Reynolds number (Re) is the ratio between inertial forces and viscous forces, which is subjected to the fluid velocity (v). The force is dominated by viscous forces and is proportional to v for small Re. While inertial

force is dominant for large Re and drag force is proportional to v^2 [185]. Figuring out the type of friction of gel actuators at the air-water interface would help understanding self-driven motion of objects on water surface.

4.1 Experimental

The actuation of gel at the air-water interface has different motion modes including spin, orbital motion, translational motion as shown in Figure 4.1. Certainly, the geometry of gel actuator plays an important role on the motion mode. In this study, gels in different shapes, such as rectangular with different length/width ratios, square with different sizes, circular with different diameters, were fabricated and studied to explore the relationship between geometry and motion modes or the factors that control the motion mode.
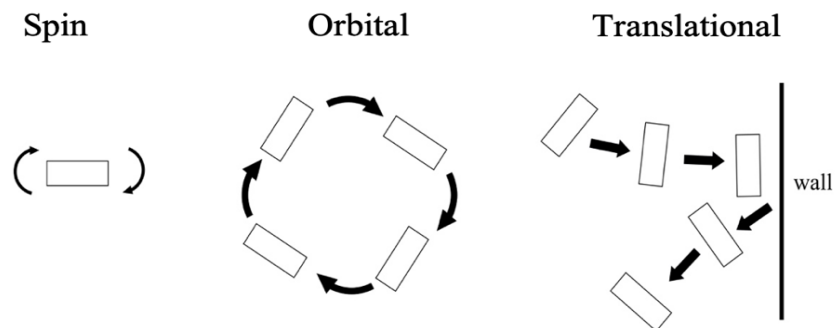
Figure 4.1 Motion modes of gels

Definition of motion mode: Spin is rotation with an axis inside of the body. Spin of a 6 mm × 3 mm gel was shown in Figure 4.2 (a). Orbital motion is rotation with an axis outside of the body. Orbital motion of a circle sample with diameter in 7.82mm was shown in Figure 4.2 (c). Translational motion of a 6mm×3mm gel was shown in Figure 4.2 (b)

(a)

t= 0s	$t=\frac{1}{30}$ s	$t=\frac{1}{15}$ s
$t=\frac{1}{10}$ s	$t=\frac{2}{15}$ s	$t=\frac{1}{6}$ s

5 cm

(b)

5 cm

6s $6\frac{1}{3}$s $6\frac{2}{3}$s   7s $7\frac{1}{3}$s $7\frac{2}{3}$s   8s

(c)
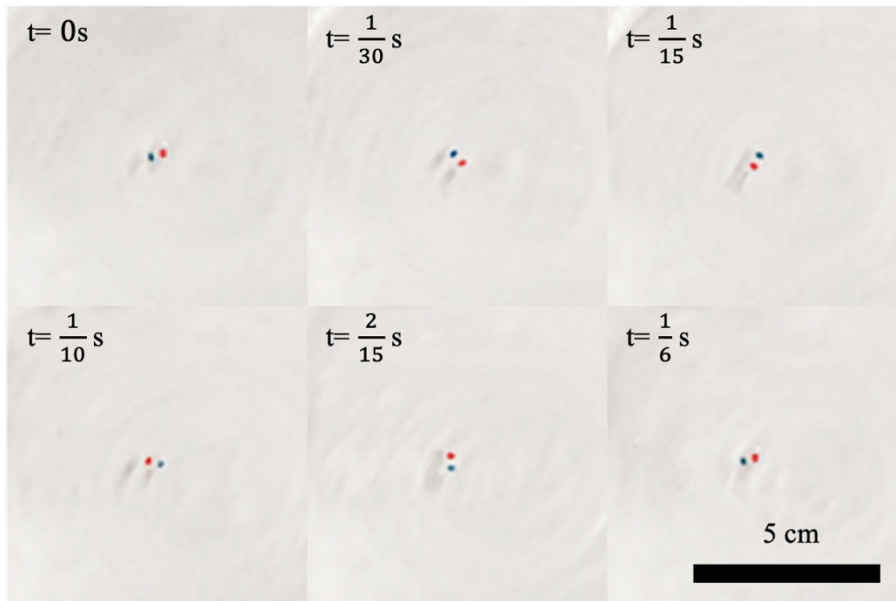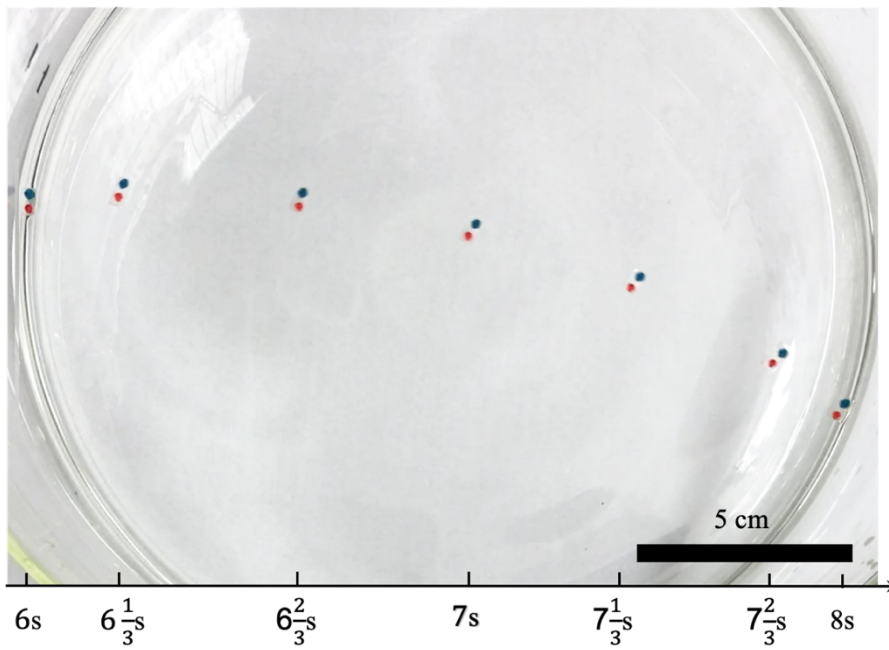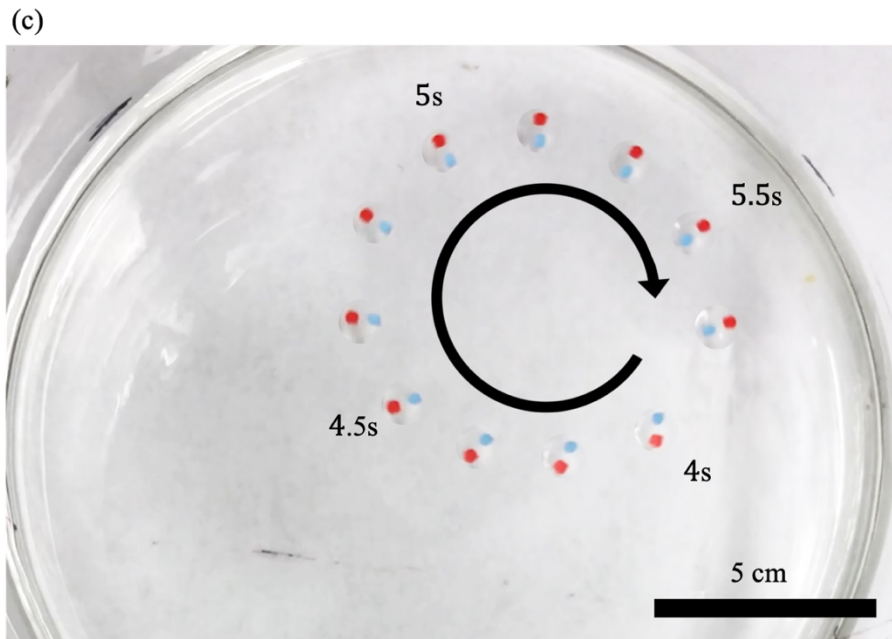
Figure 4.2 Trajectory of (a) a rectangle gel in 6 mm × 3 mm; (b) a rectangle gel in 6 mm × 3 mm and (c) a circle gel with diameter of in 7.82 mm

Quantification of a motion can provide more information about the motion that can be useful for the fundamental study of self-driven gel actuators. Python and R language [210,211] were utilized to in this research to quantify the motion of gels. Scotch markers in two different colors, illustrated in Figure 2.6, were put on gel. Recognition of the two markers in the video was conducted by Python using CV2 and imutils packages [212], the process of which is illustrated in Figure 4.3.
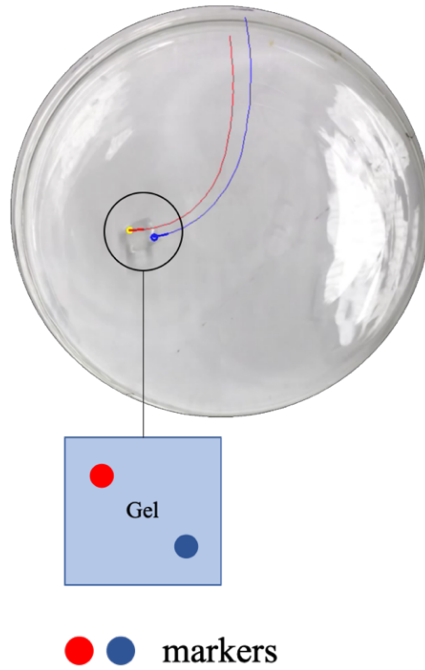
Figure 4.3 Illustration of two markers recognized by Python program for a square sample

Using digitalized video, the coordinate locations of these two marks were determined as the function of time. These digitalized results were also used to calculate the displacement, linear velocity, orbital rate and spin rate of the gel motion. Figures were generated using ggplot2 package in R language.

Definition of motion parameters: Gel motion depicted in the XY axis is shown in Figure 4.4, 1) where a rectangle with side length in a and b is utilized to illustrate translational motion as shown in Figure 4.4 (a), 2) while a circle with a diameter of 2r is utilized to illustrate orbital motion as shown in Figure 4.4 (b). O_i is mass center (i.e., geometrical center since the gel has a uniform thickness) of the sample at time t_i. Linear velocity is the rate of displacement change with respect to time during motion. Linear velocity was calculated by Eq. (4.1).

$$v = \frac{O_{i+1}O_i}{t_{i+1}-t_i}$$

Equation 4.1
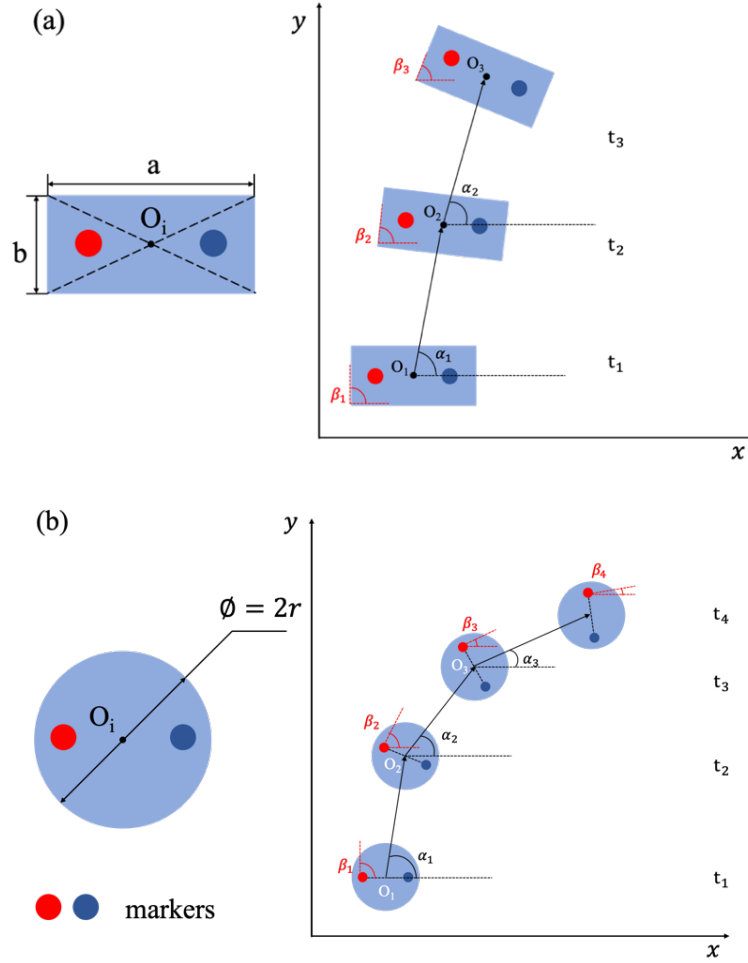
Figure 4.4 Illustration of motion of a (a) rectangle sample and (b) a circle sample

α_i and β_i at each moment, t_i, was show in Figure 4.4. Then, orbital speed, ω_1, and spin speed, ω_2, were calculated through Eq. (4.2) and Eq. (4.3).

$$\omega_1 = \frac{\alpha_{i+1}-\alpha_i}{t_{i+2}-t_{i+1}} \qquad \text{Equation 4.2}$$

$$\omega_2 = \frac{\beta_{i+1}-\beta_i}{t_{i+1}-t_i} \qquad \text{Equation 4.3}$$

The kinetic energy (E) of a gel during motion was calculated by Eq. (4.4)

$$E = \frac{1}{2}mv^2 + \frac{1}{2}I\omega_2^2 \qquad \text{Equation 4.4}$$

where *m* is the mass of the gel, *I* is the moment of inertia. *I* for a rectangle sample (the side length is a and b) and a circle sample (the radius is r) was calculated by Eq. (4.5) and (4.6), respectively.

$$I = \frac{1}{12}m(a^2 + b^2)$$ Equation 4.5

$$I = \frac{1}{2}mr^2$$ Equation 4.6

Parameters, symbols and their units were summarized in Table 4.1

Table 4.1 Parameters in digitalized results

Symbol	Unit	Definition
v	mm/s	Linear Velocity
α	°	Orbital Angle
ω_1	rpm	Orbital Speed
β	°	Spin Angle
ω_2	rpm	Spin Speed
E	nJ	Kinetic Energy

4.2 Result and Discussion

4.2.1 Digitalized data

Velocity and kinetic energy of a sample during the motion were determined as a function of time using the software mentioned above. Figures of trace, velocity, orbital speed, spin speed as the function of time for a sample can be plotted using the digitalized results as demonstrated in Figure 4.5 using one sample (PVDF/DMF-acetone gel, circle shaped, ø = 7.82 mm), where the circle in black solid line in left figure reflects the boundary of glass beaker. Each arrow represents the sample at each moment and timeline was depicted by color variation. The velocity, orbital speed

and spin speed curves of the sample are presented in the right of Figure 4.5. Similarly, color variation of the curves reflects the timeline.

Figure 4.5 Trace (left) and motion parameters (right) including the velocity, orbital speed, spin speed and energy change as the function of time for a circle sample with diameter in 7.82 mm (sample 1) for the *first ten seconds*.

Circle samples, ∅ = 7.82 mm

For gel actuators in circle shape with a diameter of 7.82 mm, thirteen samples were studied, and the results are summarized in Table 4.2, where v_0 is the initial value of the linear velocity at the very beginning of motion.

Table 4.2 Mass (m_1 and m_2 are the mass of gel before and after the motion, respectively) and initial velocity (v_0) of circle samples with diameter in 7.82 mm

Sample	m_1 (mg)	m_2 (mg)	v_0 (mm/s)	Motion modes
1	19.07	15.32	194	
2	21.47	17.48	149	
3	20.24	16.21	168	
4	21.51	15.59	125	
5	22.21	18.05	158	
6	22.98	18.45	114	
7	29.61	24.09	160	Orbital motion
8	18.73	15.30	140	
9	22.36	17.12	155	
10	22.46	18.06	146	
11	19.79	15.31	157	
12	22.32	17.72	190	
13	19.05	15.93	172	

The gel exhibited translational motion in the first 2 seconds before proceeding to prolonged orbital motion in the remaining time as shown in Figure 4.5. *This is a typical phenomenon that occurs on other samples*. The translational motion is slowly changed to orbital motion as shown in Figure 4.6 and Figure 4.7. That is, in the beginning, there are a few seconds in which the motion is more irregular and then, the gel actuator exhibits a more regular motion. The irregular motion in the first a few seconds may be induced by the way the gel was placed on to the surface of water. Therefore, the study of motion modes based on a few seconds results is not reliable. The first few seconds are not used in this study about motion modes.

Figure 4.6 Trace (left) and motion parameters (right) including the velocity, orbital speed, spin speed and energy change as the function of time for a circle sample with diameter in 7.82 mm (sample 3) in the *time period from 0 to 30 second*.

Figure 4.7 Trace (left) and motion parameters (right) including the velocity, orbital speed, spin speed and energy change as the function of time for a circle sample with diameter in 7.82 mm (sample 9) in the *time period from 0 to 20 second*.

To have a detailed look at the motion of gel, the results from a circle gel (i.e., sample 1) with a mass of 19.07 mg are shown in Figure 4.5 and Figure 4.8- 4.10, where each figure shows a small time window during the motion: from 0 to 10 second in Figure 4.3; from 10 to 50 second in Figure 4.4; from 50 to 80 second in Figure 4.5. Clearly, the linear velocity decreases gradually with time, but the velocity exhibits a periodic fluctuation as shown in the figures. In order to show this period fluctuation clearly, trace and velocity of this sample during time period from 15 to 25 second are plotted in Figure 4.10.

The periodic fluctuation for both spin speed curves and orbital speed curves is originated by the definition. There is 360 degree (i.e., from -180 ° to 180 °) in a round and a new round will start when one is finished.

Figure 4.8 Trace (left) and motion parameters (right) including the velocity, orbital speed, spin speed and energy change as the function of time for a circle sample with diameter in 7.82 mm (sample 1) in the *time period from 10 to 50 second.*

118

Figure 4.9 Trace (left) and motion parameters (right) including the velocity, orbital speed, spin speed and energy change as the function of time for a circle sample with diameter in 7.82 mm (sample 1) in the *time period from 50 to 80 second*.

Figure 4.10 Trace (left) and motion parameters (right) including the velocity, orbital speed, spin speed and energy change as the function of time for a circle sample with diameter in 7.82 mm (sample 1) in the *time period from 15 to 35 second*.

As mentioned above and detailed in Figure 4.10, there are periodic fluctuations in the velocity, spin speed and kinetic energy curves. A systemic analysis of these fluctuations was carried out. The data analysis indicates that the valley values of velocity (i.e., minimum velocity points) correspond to the positions of the gel actuator close to the wall of glass beaker, while the peak value of velocity (i.e., the maximum velocity points) are obtained at the positions of the gel actuator away from the wall of glass beaker. That is, the velocity of gel actuator decreases as it moves toward the wall of glass beaker, and while the velocity of gel actuator increases as it moves away from the wall of glass beaker. The trace of another two samples exhibited orbital motion and also showed the similar behavior - periodic fluctuations of velocity curves, which were shown in Figure 4.11 and Figure 4.12.

Figure 4.11 Trace (left) and motion parameters (right) including the velocity, orbital speed, spin speed and energy change as the function of time for a circle sample with diameter in 7.82 mm (sample 11) in the *time period from 20 to 30 second*.

120

Figure 4.12 Trace (left) and motion parameters (right) including the velocity, orbital speed, spin speed and energy change as the function of time for a circle sample with diameter in 7.82 mm (sample 5) in the *time period from 30 to 40 second*.

Two hypotheses are proposed to explain this phenomenon. Hypotheses-I focuses on randomly solvent diffusion through each edge of a gel actuator. Solvent diffusion from gel into water is also the key to the motion of self-driven gel actuator, thanks to the conservation of momentum. The thrust at the wall side of gel actuator increases as it moves toward the wall. Therefore, the gel actuators slowdown as it is approaching the wall. Besides, the area of water surface at wall side is reducing when the gel moves towards the wall, resulting a higher concentration of solvent on the water surface. Thus, the diffusion on the side closer to the wall is reducing, and the surface tension at the wall side is smaller when similar amount of solvent was diffused into water, both of which result in an external force pushing the gel actuator away from the wall.

Hypotheses-II focuses on the capillary force between two objects on water surface. This force is attractive when the menisci around two objects are similar (i.e., both of them are concave or convex) as shown in Figure 4.13 (a) and (b). The force is repulsive when the menisci around two objects are opposite (i.e., one is concave while the other is convex) as shown in Figure 4.13 (c) [213,214,215]. It will be very easy to understand by a phenomenon in daily life – cereals tend to stick together in the milk. Menisci around the gel actuators at the air-water interface are convex as depicted in Figure 3.3. The meniscus between the water and glass is concave. Therefore, there is a repulsive force between the gel actuator and wall of glass beaker due to opposite menisci.

Both hypotheses can explain the experimental results – velocity of the gel actuator deceases as it moves towards the wall of glass beaker.
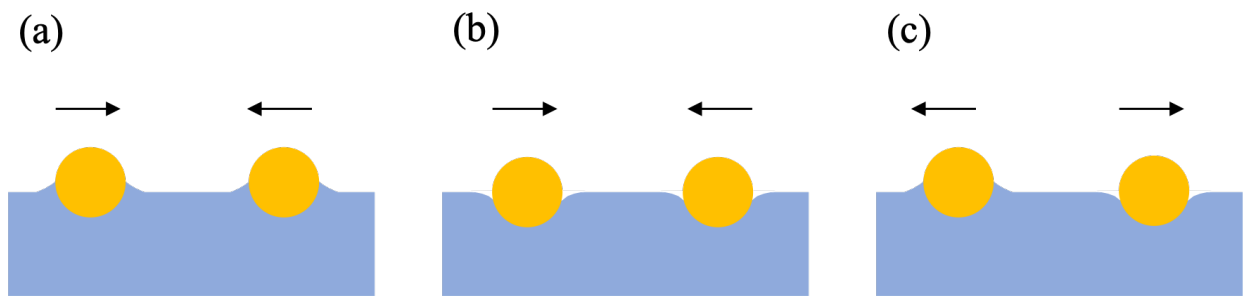
Figure 4.13 Scheme of the repulsive force and attractive force between two objects on water surface.

The trace was not always a standard circle and can be ellipse, which was shown in Figure 4.8. Moreover, the diameter of a circle for traces varied as time, shown in Figure 4.9, and also varied from samples to samples as shown in Figure 4.11 – 4.12, Figure 4.14 – 4.15.
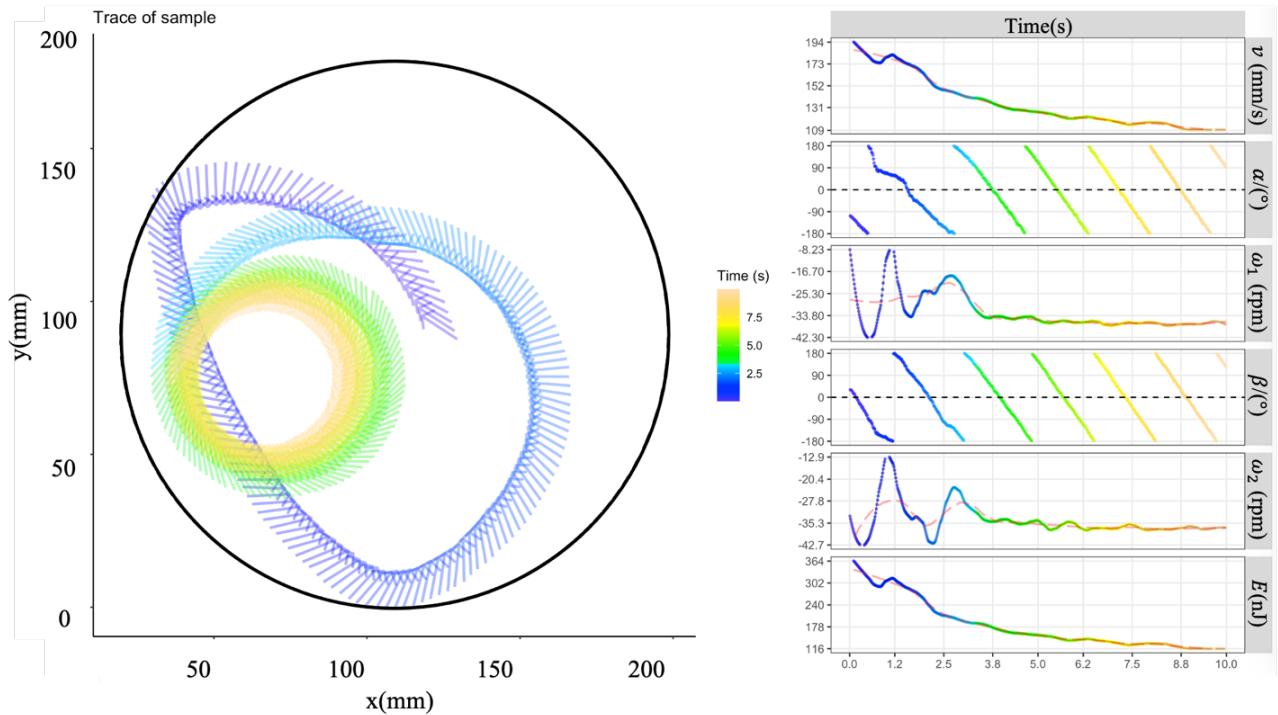
Figure 4.14 Trace (left) and motion parameters (right) including the velocity, orbital speed, spin speed and energy change as the function of time for a circle sample with diameter in 7.82 mm (sample 8) in the *time period from 10 to 20 second*.
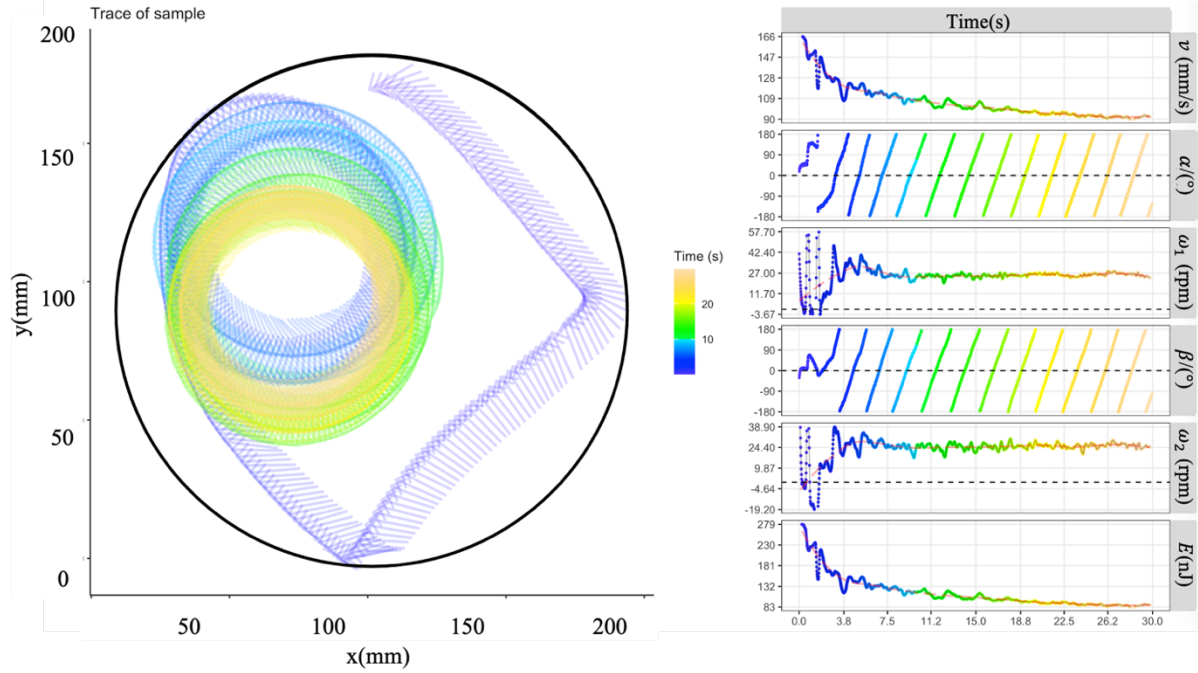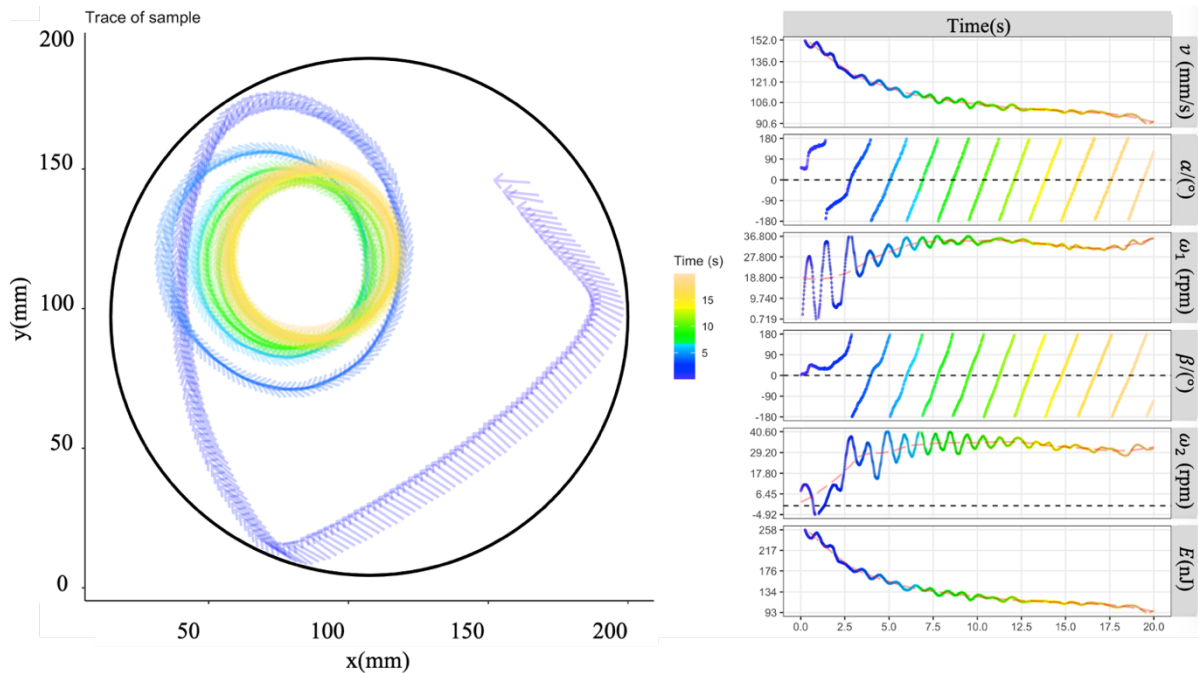

Figure 4.15 Trace (left) and motion parameters (right) including the velocity, orbital speed, spin speed and energy change as the function of time for a circle sample with diameter in 7.82 mm (sample 2) in the *time period from 25 to 105 second*.

Trace of sample 2 showed the gel moving along wall of container as shown in Figure 4.15. Decrease in the velocity during motion was relatively steady compared to what was shown in Figure 4.8.

In addition, the kinetic energy (E), which can be calculated using Eq. (4.4): $E = \frac{1}{2}mv^2 + \frac{1}{2}I\omega_2^2$ of gel actuators during motion was mainly dominated by the linear velocity. Thus, both translational energy and rotational energy were taken into consideration for kinetic energy calculation. While it was found that $E \sim t$ curve and $v \sim t$ curve are in phase, while $E \sim t$ curve and $\omega_2 \sim t$ curve are out of phase, especially Figure 4.11, Figure 4.12 and Figure 4.14.

Circle samples, $\emptyset = 3.82$ mm

Six circle gel actuators in a diameter of 3.82 mm were studied. The basic characteristics of these six gel actuators are summarized in Table 4.3, where m_1 and m_2 are the mass of the gel before and after, initial velocity (v_0). The motion mode of these circle samples is also presented in Table 4.3.

Table 4.3 Mass and initial velocity of circle samples with diameter in 3.82 mm

Sample	m_1 (mg)	m (mg)	v_0 (mm/s)	Motion mode
1	5.77	5.03	182	
2	4.62	4.02	170	
3	5.20	4.55	97	Orbital motion
4	4.51	4.13	168	
5	5.49	4.61	154	
6	6.16	5.30	160	

Results of these circle samples with a diameter of 3.82mm are shown in Figure 4.16 – 4.22. Patterns of circle sample with a smaller diameter were diverse, comparing with the results from circle samples with a diameter of 7.82 mm. Orbital motion of sample 1 is shown in Figure 4.16

and Figure 4.17. The diameter of orbital increases with time and finally reaches the wall of container. While the orbital trace of sample 3 is in a similar diameter during time period from 0 to 100 second, which was illustrated in Figure 4.19. Moreover, the center of orbital trace moves as time.

The trace of sample 2 exhibited a pattern of flower, which was shown in Figure 4.20 and Figure 4.21. This pattern was categorized into the orbital motion since it can be split into many orbital motion segments that were alternated when hitting to the wall of container. Similar trace occurs on sample 6, which was shown in Figure 4.22.
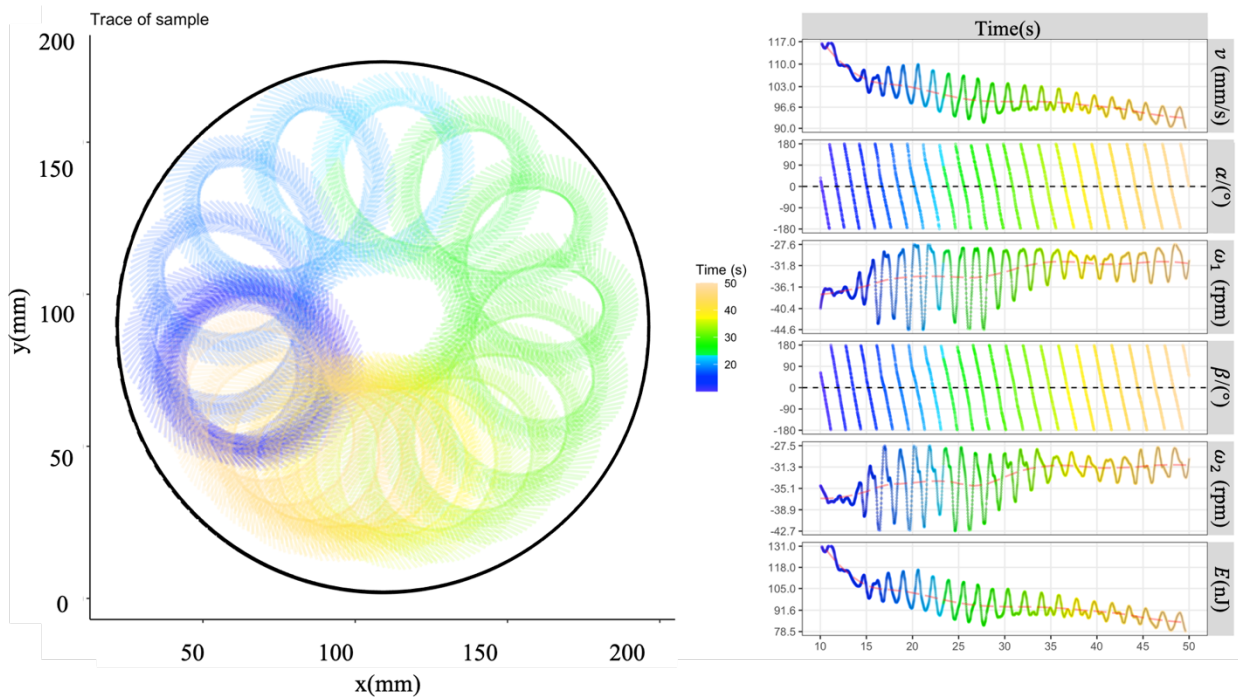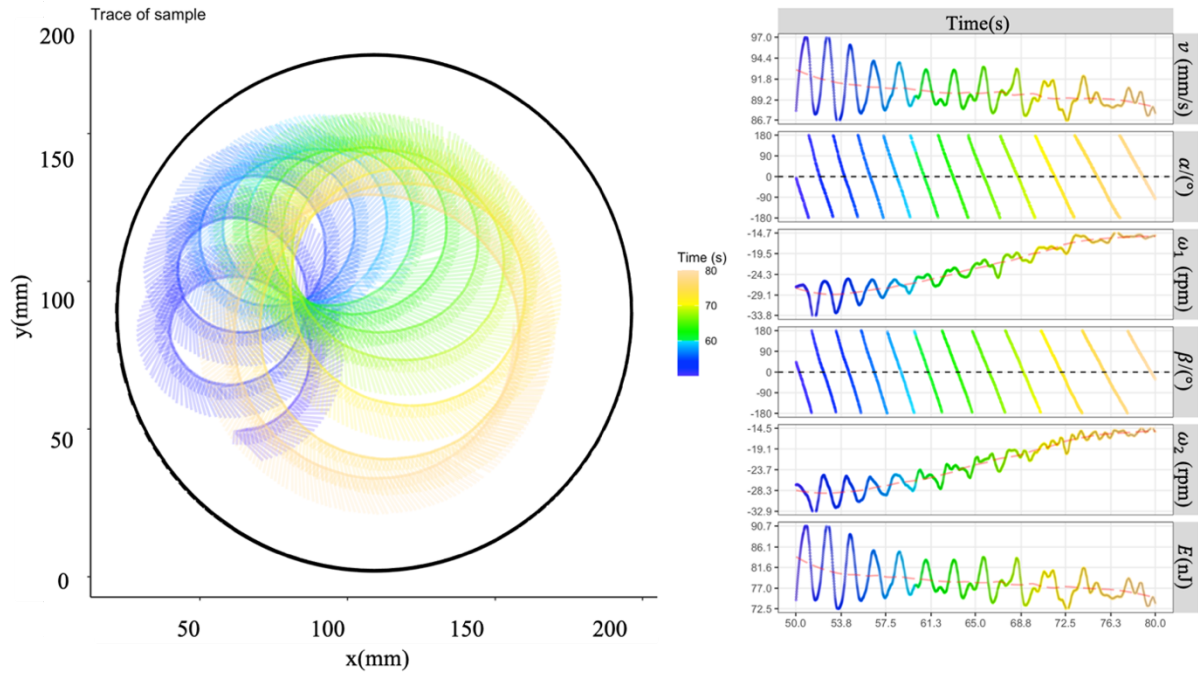

Figure 4.16 Trace (left) and motion parameters (right) including the velocity, orbital speed, spin speed and energy change as the function of time for a circle sample with diameter in 3.82 mm (sample 1) in the *time period from 0 to 10 second*.
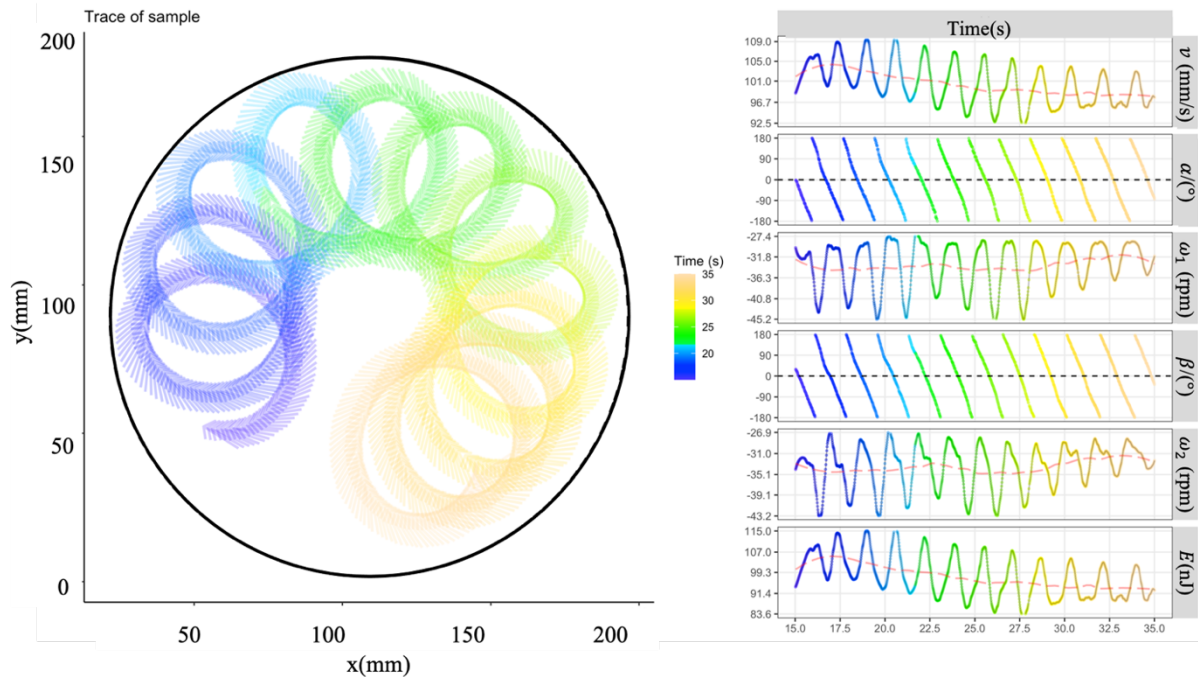
Figure 4.17 Trace (left) and motion parameters (right) including the velocity, orbital speed, spin speed and energy change as the function of time for a circle sample with diameter in 3.82 mm (sample 1) in the *time period from 0 to 100 second*.

Figure 4.18 Trace (left) and motion parameters (right) including the velocity, orbital speed, spin speed and energy change as the function of time for a circle sample with diameter in 3.82 mm (sample 3) in the *time period from 0 to 10 second*.

Figure 4.19 Trace (left) and motion parameters (right) including the velocity, orbital speed, spin speed and energy change as the function of time for a circle sample with diameter in 3.82 mm (sample 3) in the *time period from 0 to 100 second*.

Figure 4.20 Trace (left) and motion parameters (right) including the velocity, orbital speed, spin speed and energy change as the function of time for a circle sample with diameter in 3.82 mm (sample 2) in the *time period from in 0 to 15 second*.

Figure 4.21 Trace (left) and motion parameters (right) including the velocity, orbital speed, spin speed and energy change as the function of time for a circle sample with diameter in 3.82 mm (sample 2) in the *time period from 0 to 75 second*.
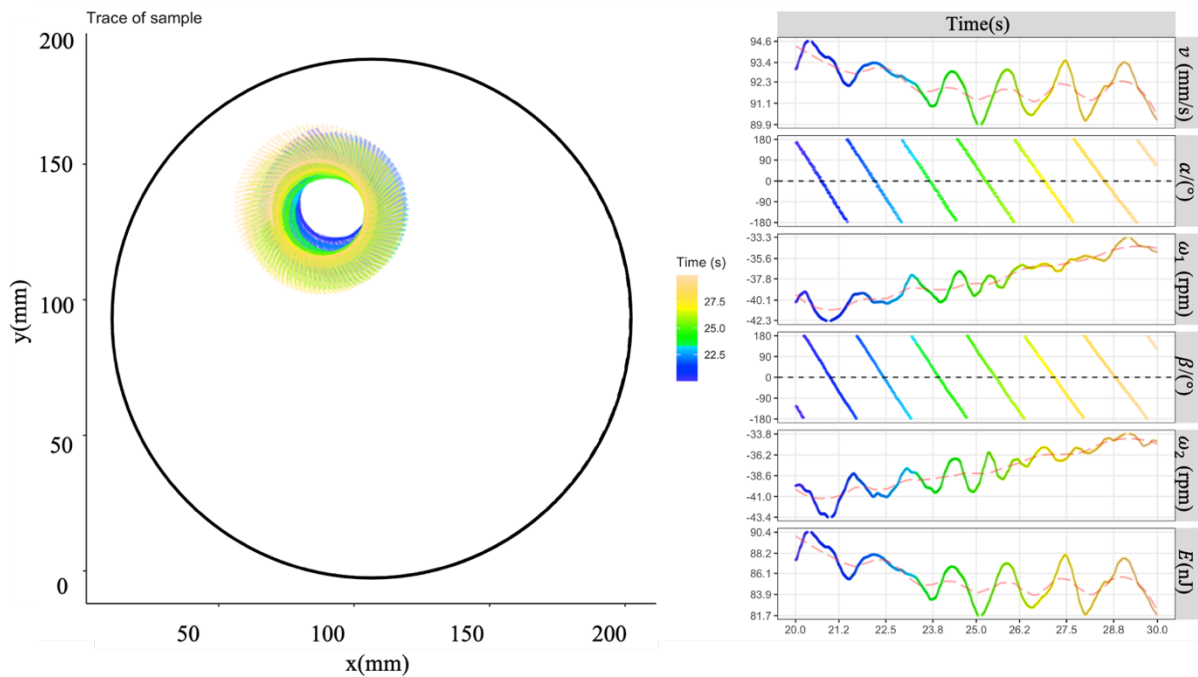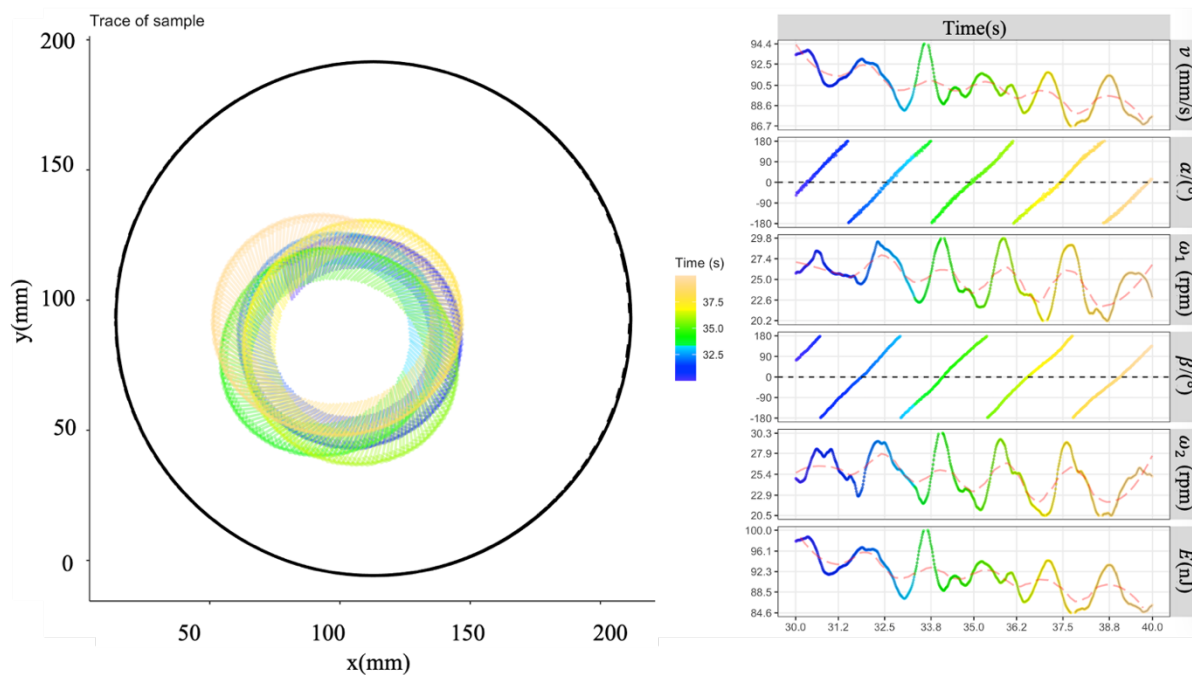

Figure 4.22 Trace (left) and motion parameters (right) including the velocity, orbital speed, spin speed and energy change as the function of time for a circle sample with diameter in3.82 mm (sample 6) in the *time period from 20 to 40 second*.

Square samples

Table 4.4 Mass and initial velocity of square samples with various size

Sample	Size	m_1 (mg)	m_2 (mg)	v_0 (mm/s)
1	9.7 mm × 9.7 mm	51.87	40.72	134
2	9.7 mm × 9.7 mm	41.55	32.95	128
3	9.7 mm × 9.7 mm	31.53	25.88	159
4	9.7 mm × 9.7 mm	34.46	27.87	156
5	9.7 mm × 9.7 mm	39.48	31.12	155
6	10 mm × 10 mm	47.38	37.32	141
7	6 mm × 6 mm	17.34	14.57	174

The basic parameters of square gel actuators tested are presented in Table 4.4. Again, m_1 and m_2 are the mass before and after motion, respectively, and v_0 is the initial velocity. The digitalized results are shown in Figure 4.23 – 4.30. Based on the experimental results, it is found that square samples were of high possibility of orbital motion. The typical phenomenon that the translational motion is slowly changed to orbital motion is shown in Figure 4.23. And the phenomenon of periodic fluctuations of velocity curves are shown in Figure 4.24 – 4.30. Similarly, the diameter as well as center of orbital trace varied as time as shown in Figure 4.25 – 4.28.

Figure 4.23 Trace (left) and motion parameters (right) including the velocity, orbital speed, spin speed and energy change as the function of time for a square sample with side length in 9.7mm (sample 1) in the *time period from 0 to 10 second*.

Figure 4.24 Trace (left) and motion parameters (right) including the velocity, orbital speed, spin speed and energy change as the function of time for a square sample with side length in 9.7mm (sample 1) in the *time period from 10 to 40 second*.

Figure 4.25 Trace (left) and motion parameters (right) including the velocity, orbital speed, spin speed and energy change as the function of time for a square sample with side length in 9.7mm (sample 2) in the *time period from 10 to 100 second*.

Figure 4.26 Trace (left) and motion parameters (right) including the velocity, orbital speed, spin speed and energy change as the function of time for a square sample with side length in 9.7mm (sample 3) in the *time period from 15 to 45 second*.
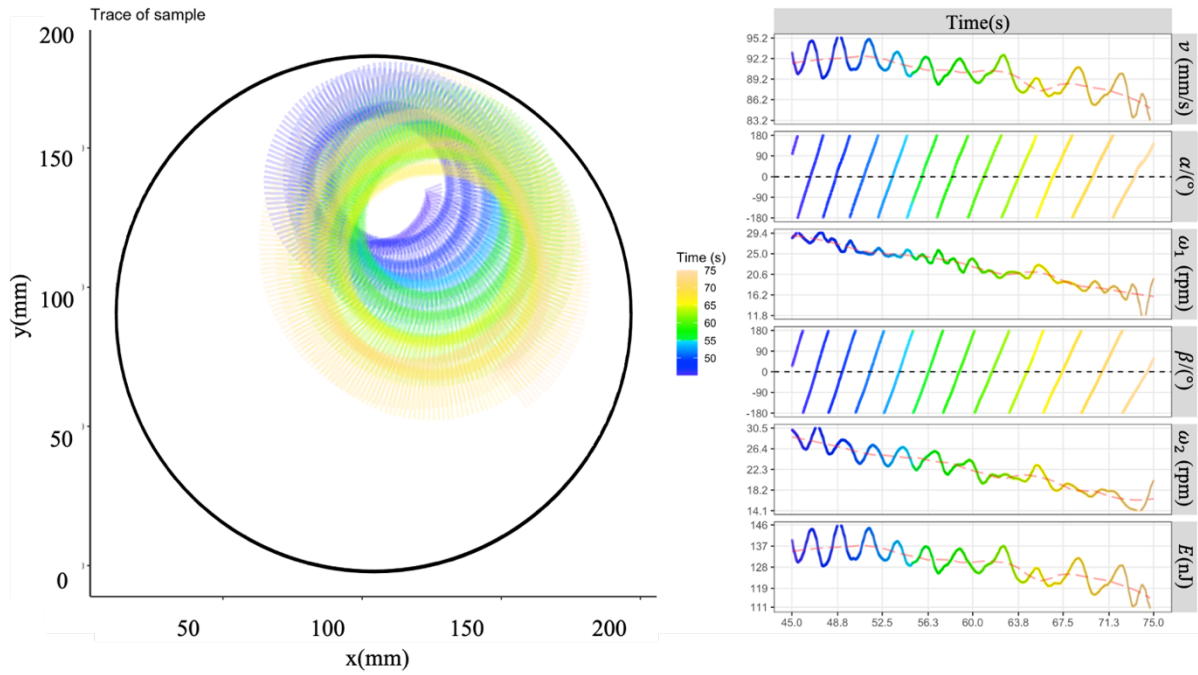
Figure 4.27 Trace (left) and motion parameters (right) including the velocity, orbital speed, spin speed and energy change as the function of time for a square sample with side length in 9.7mm (sample 3) in the *time period from 45 to 75 second*.
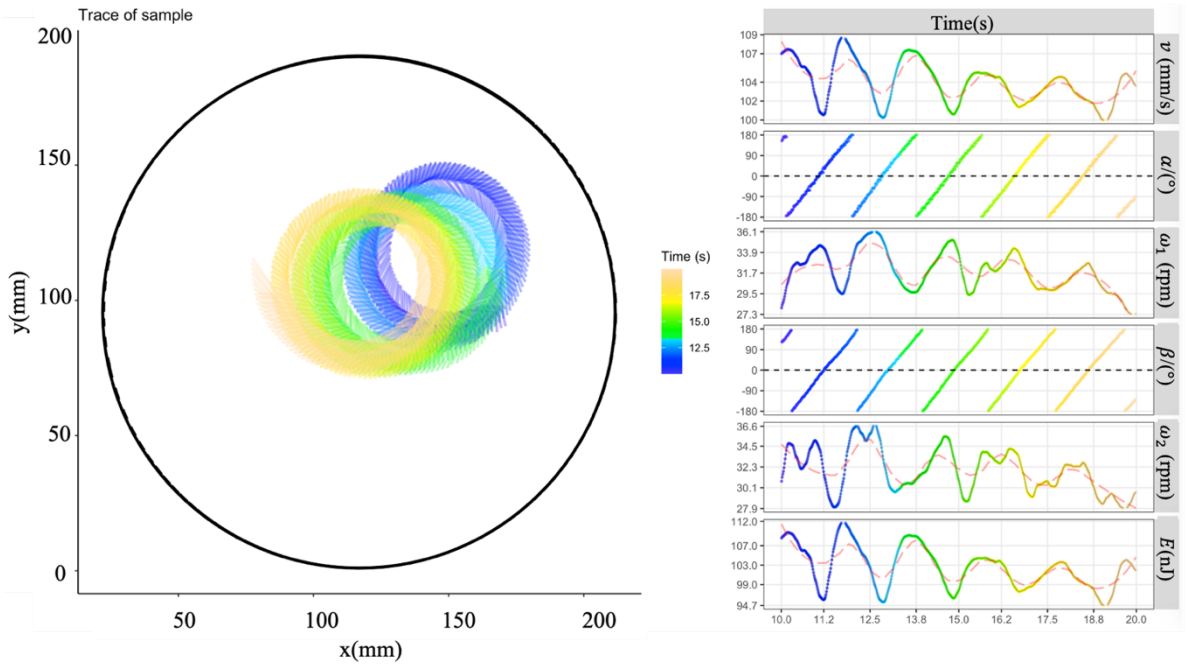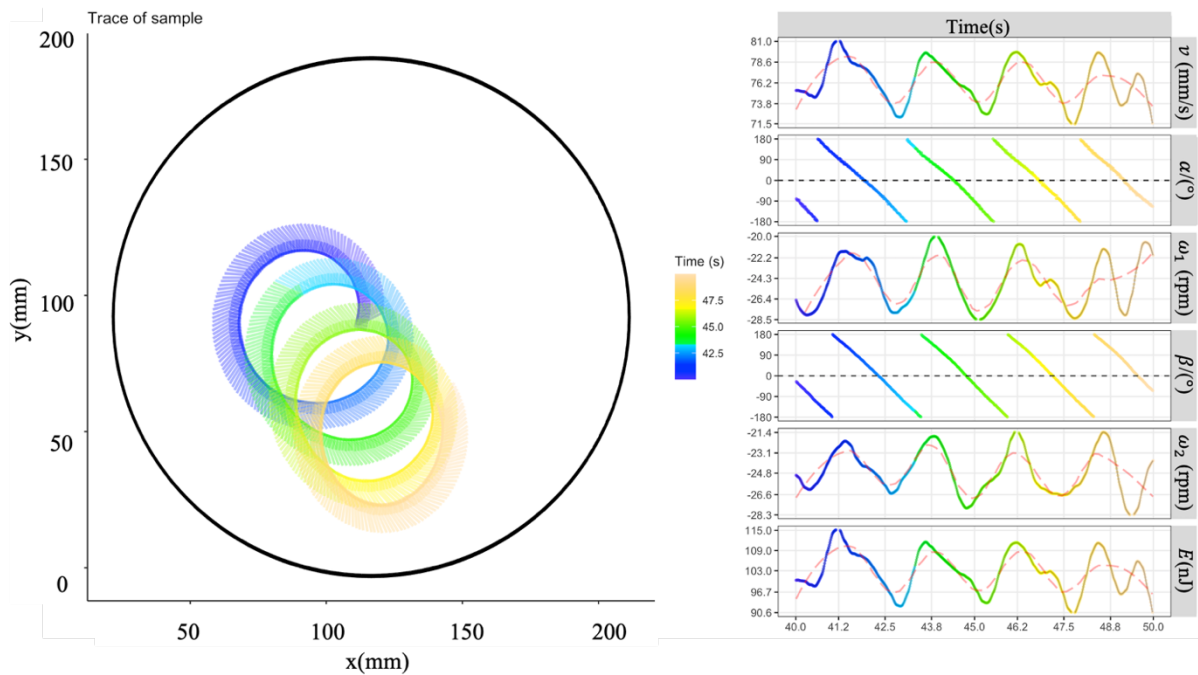

Figure 4.28 Trace (left) and motion parameters (right) including the velocity, orbital speed, spin speed and energy change as the function of time for a square sample with side length in 9.7mm (sample 4) in the *time period from 40 to 50 second*.
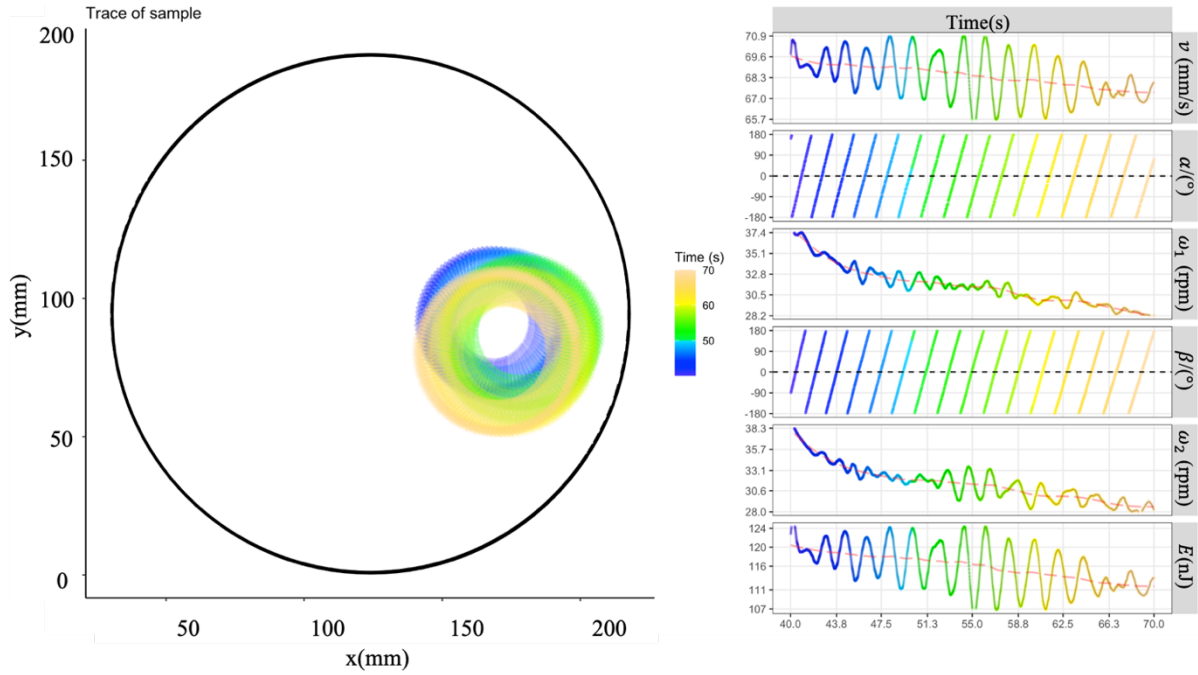
Figure 4.29 Trace (left) and motion parameters (right) including the velocity, orbital speed, spin speed and energy change as the function of time for a square sample with side length in 9.7mm (sample 6) in the *time period from 40 to 70 second*.
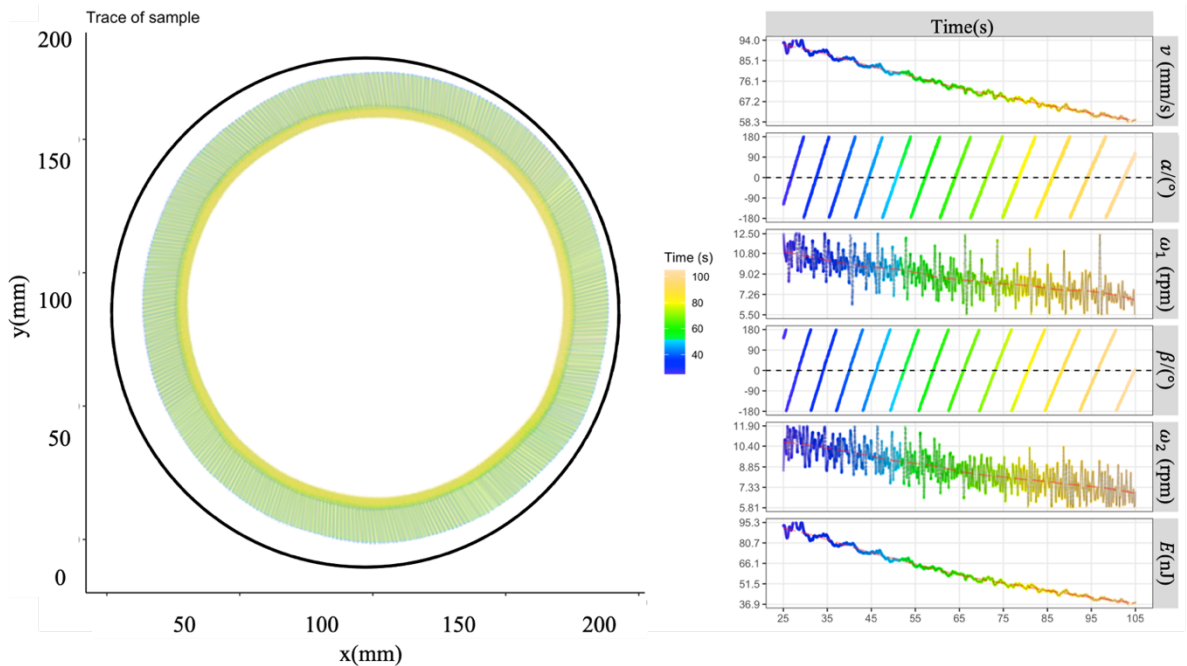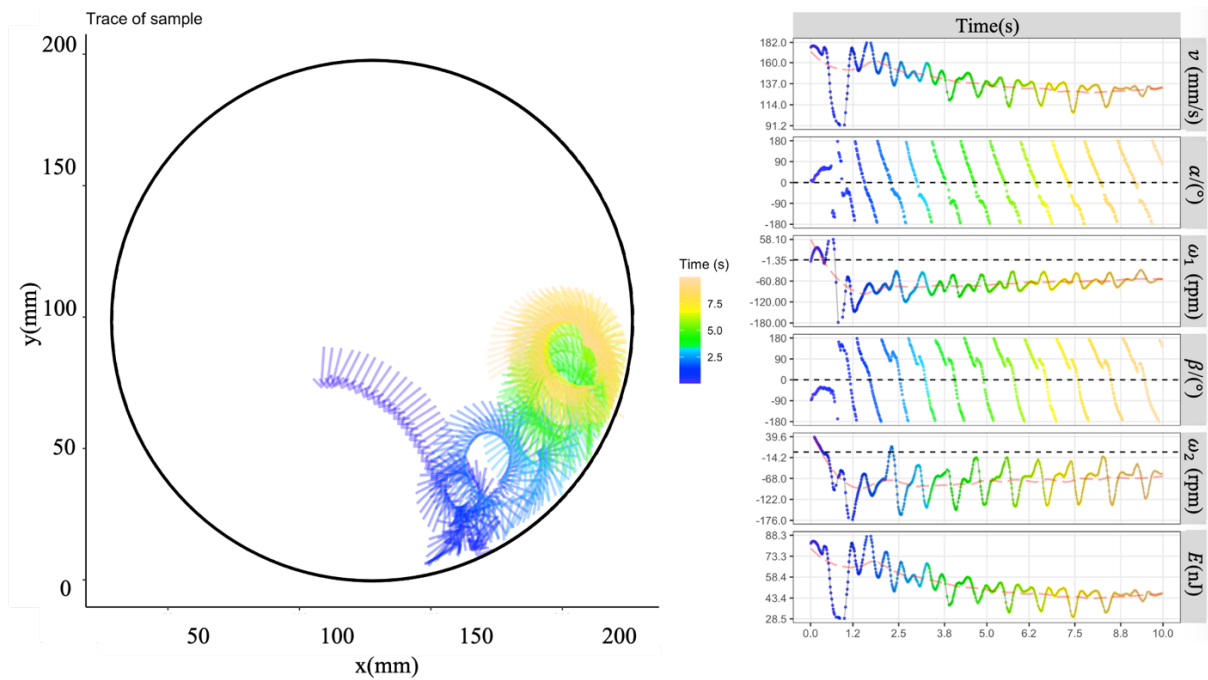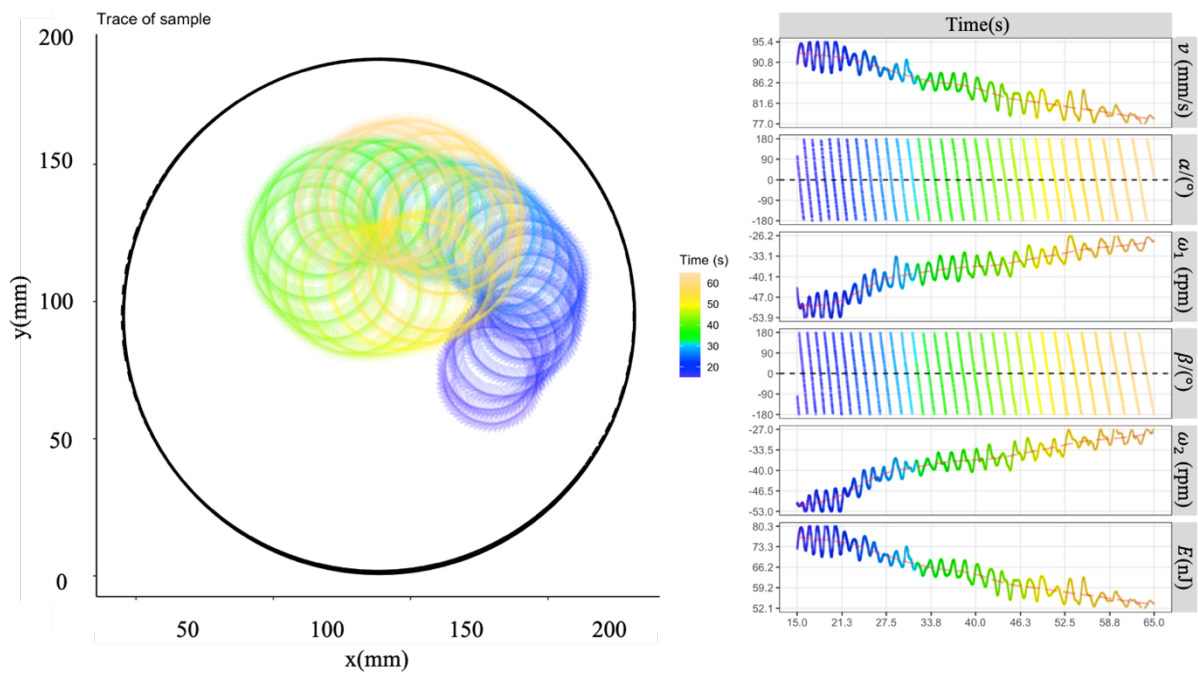

Figure 4.30 Trace (left) and motion parameters (right) including the velocity, orbital speed, spin speed and energy change as the function of time for a square sample with side length in 9.7mm (sample 7) in the *time period from 15 to 65 second*.

Rectangle samples，6 mm × 3 mm

Based on experiment results, rectangle gel actuators (6 mm × 3 mm) showed high probability of the translational motion and very small number of gels showed spin and orbital motion. The motion modes of rectangle gel actuators are different from circle and square ones that exhibited high probability of orbital motion. In addition, rectangle gels with size in 6 mm × 1 mm were of even higher probability of spin motion, compared to gel actuators with size in 6 mm × 3 mm. Mass before and after motion, initial velocity and motion modes of gel actuators with size in 6 mm × 3 mm were shown in Table 4.5.

Table 4.5 Mass and initial velocity of rectangle samples with size in 6 mm × 3 mm

Sample	m_1 (mg)	m_2 (mg)	v_0 (mm/s)	Motion Mode
1	10.98	7.96	21.5	Spin
2	12.65	10.57	24.8	Spin
3	6.63	4.97	28.9	Spin
4	10.98	7.64	117	Orbital
5	10.39	7.40	75.1	Orbital
6	8.55	6.61	161	Translational
7	10.68	8.31	153	Translational
8	10.04	8.14	171	Translational
9	9.70	7.41	150	Translational
10	9.99	8.13	171	Translational
11	9.76	7.75	156	Translational
12	9.32	7.70	137	Translational
13	8.55	7.11	171	Translational
14	9.12	7.74	177	Translational
15	8.80	7.41	188	Translational
16	9.28	7.9	185	Translational
17	9.24	8.00	165	Translational
18	7.09	5.57	171	Translational
19	6.80	5.22	163	Translational
20	8.90	7.14	160	Translational
21	8.93	7.09	168	Translational
22	7.00	5.45	179	Translational
23	6.27	4.27	185	Translational
24	7.29	5.23	181	Translational
25	6.65	5.07	165	Translational
26	6.78	5.12	177	Translational

Regarding to the spin motion, it is experimentally found that the spin speed decreases gradually with time. Spin motion of two rectangle gel actuators (6 mm × 3 mm) were shown in Figure 4.3 – 4.34. Sample 1 and sample 2 started with a spin speed of 380 rpm and 417 rpm, respectively. Minus value of spin speed (i.e., ω_2 in Figure 4.31 and Figure 4.32) of sample 2 means the anticlockwise direction of spin, while sample 1 exhibited clockwise direction of spin. That is, spin direction varied from samples to samples.
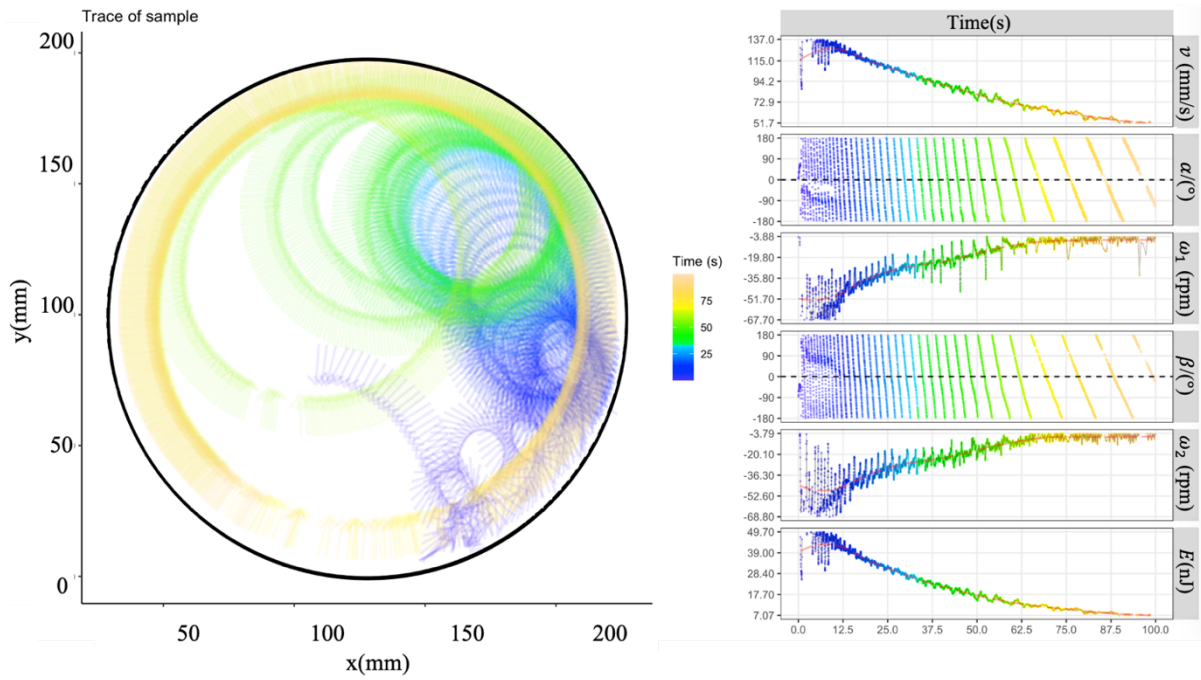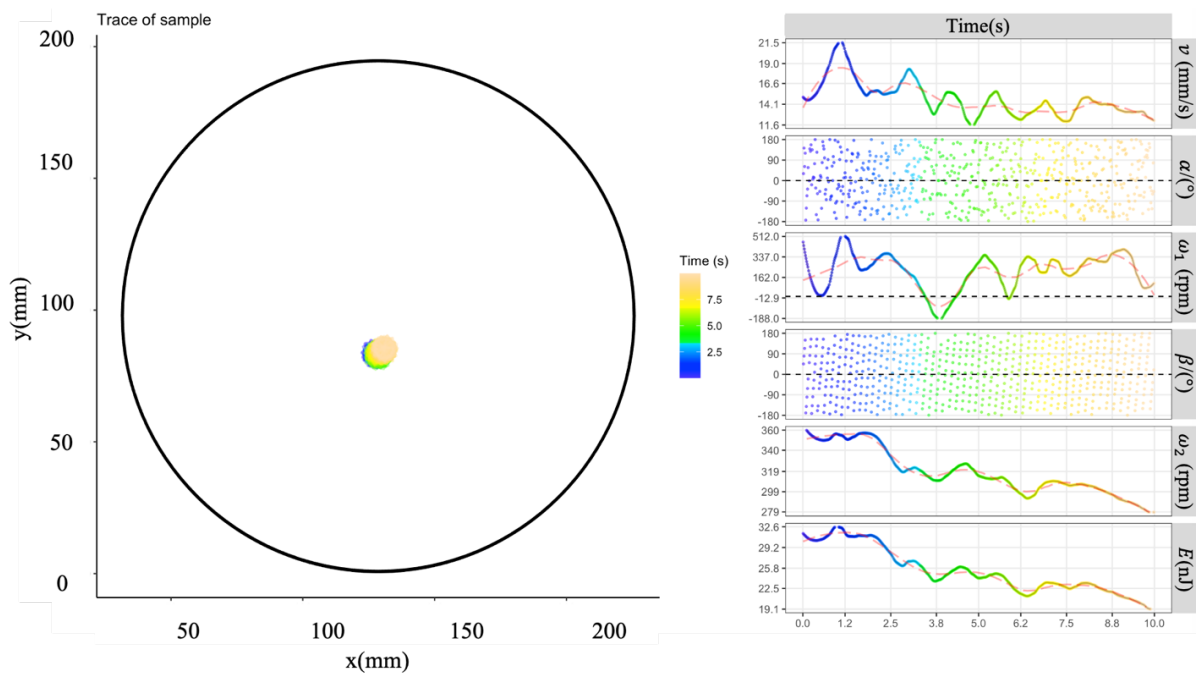

Figure 4.31 Trace (left) and motion parameters (right) including the velocity, orbital speed, spin speed and energy change as the function of time for a rectangle sample with size in 6 mm × 3 mm (sample 1) in the *time period from 0 to 10 second*.
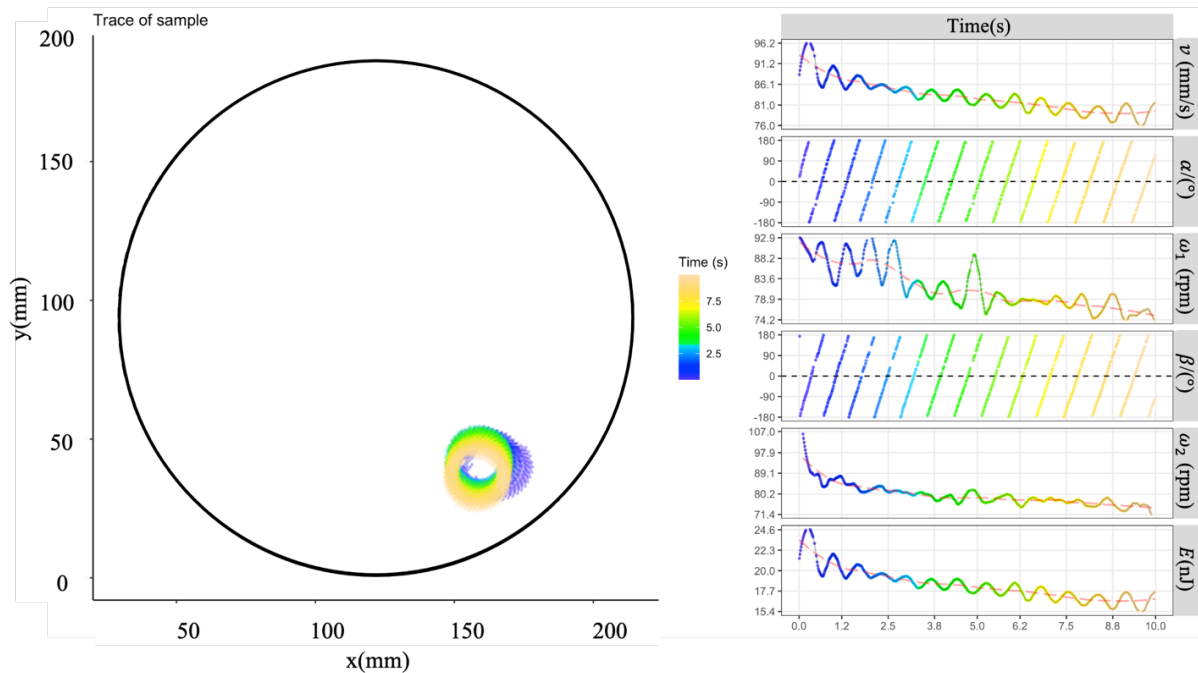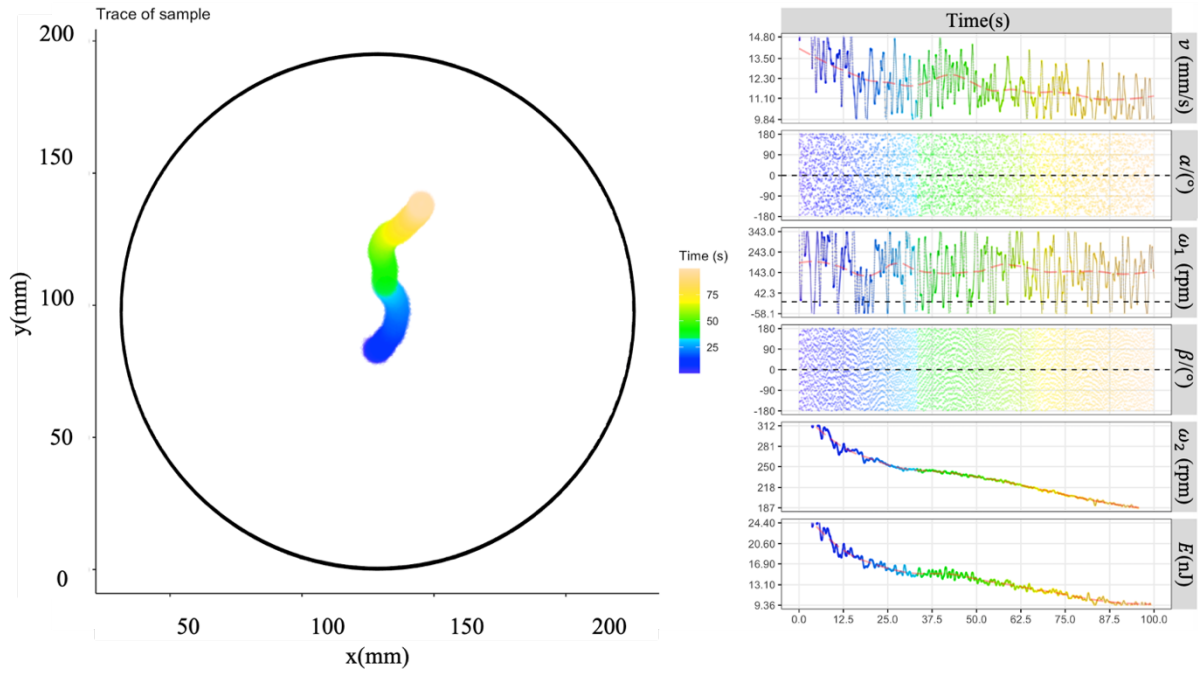
Figure 4.32 Trace (left) and motion parameters (right) including the velocity, orbital speed, spin speed and energy change as the function of time for a rectangle sample with size in 6 mm × 3 mm (sample 1) in the *time period from 10 to 100 second*.
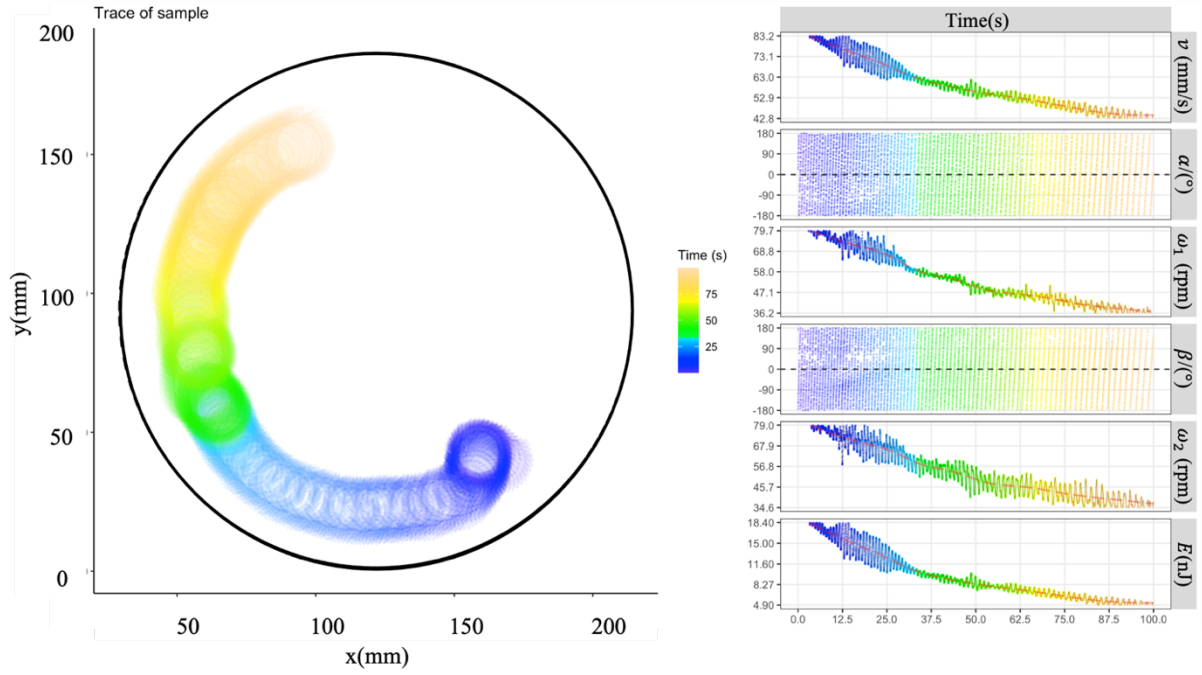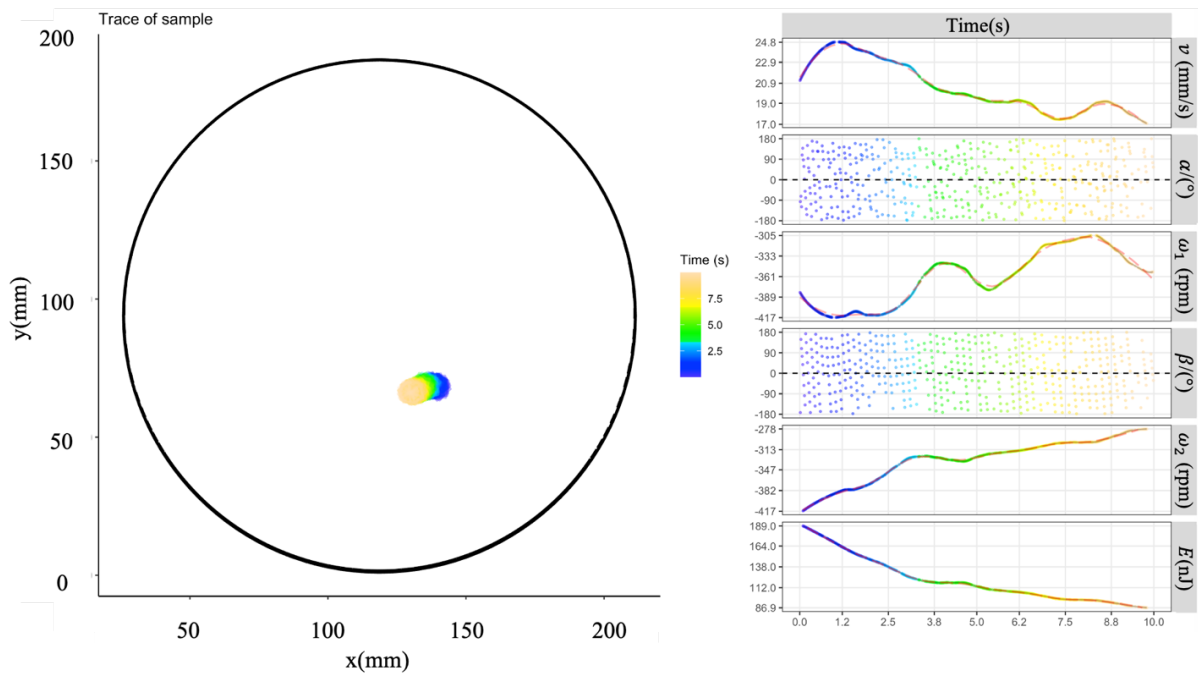

Figure 4.33 Trace (left) and motion parameters (right) including the velocity, orbital speed, spin speed and energy change as the function of time for a rectangle sample with size in 6 mm × 3 mm (sample 2) in the *time period from 0 to 10 second*.
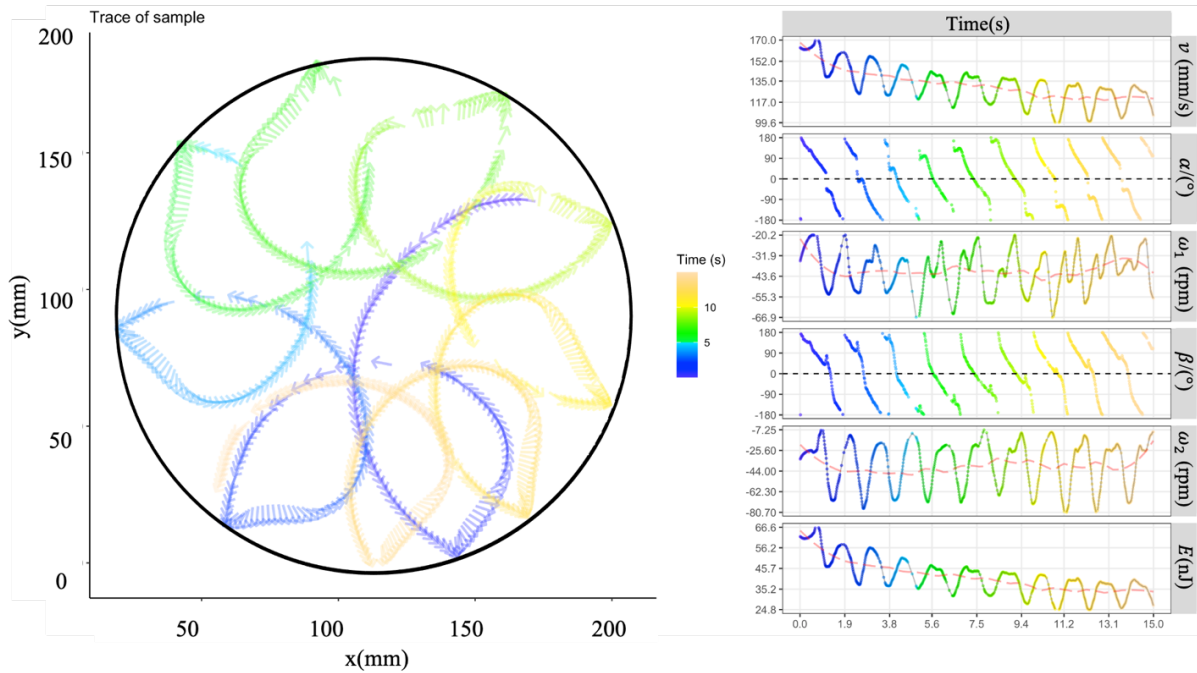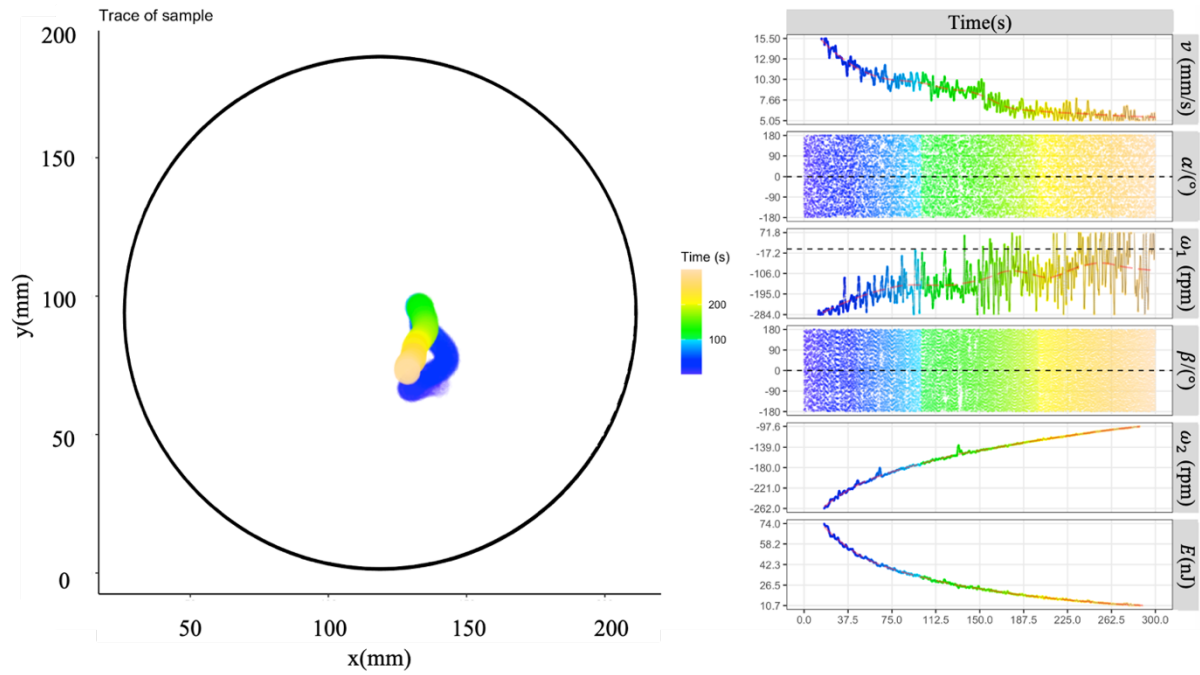
Figure 4.34 Trace (left) and motion parameters (right) including the velocity, orbital speed, spin speed and energy change as the function of time for a rectangle sample with size in 6 mm × 3 mm (sample 2) in the *time period from 0 to 300 second*.

Orbital motion and translational motion of gels are shown in Figure 4.35 – 4.40. Initial velocity of rectangle gel actuators (6 mm × 3 mm) for translational motions ranges from 137mm/s to 188mm/s. While initial velocity of rectangle gel actuators (6 mm × 3 mm) for orbital motion and spin motion were relatively small, which are shown in Table 4.5. Again, it is observed that the velocity reduces when the gel moves towards to the wall, such as at 8.0 second in Figure 4.35, many minimum points in Figure 4.36.
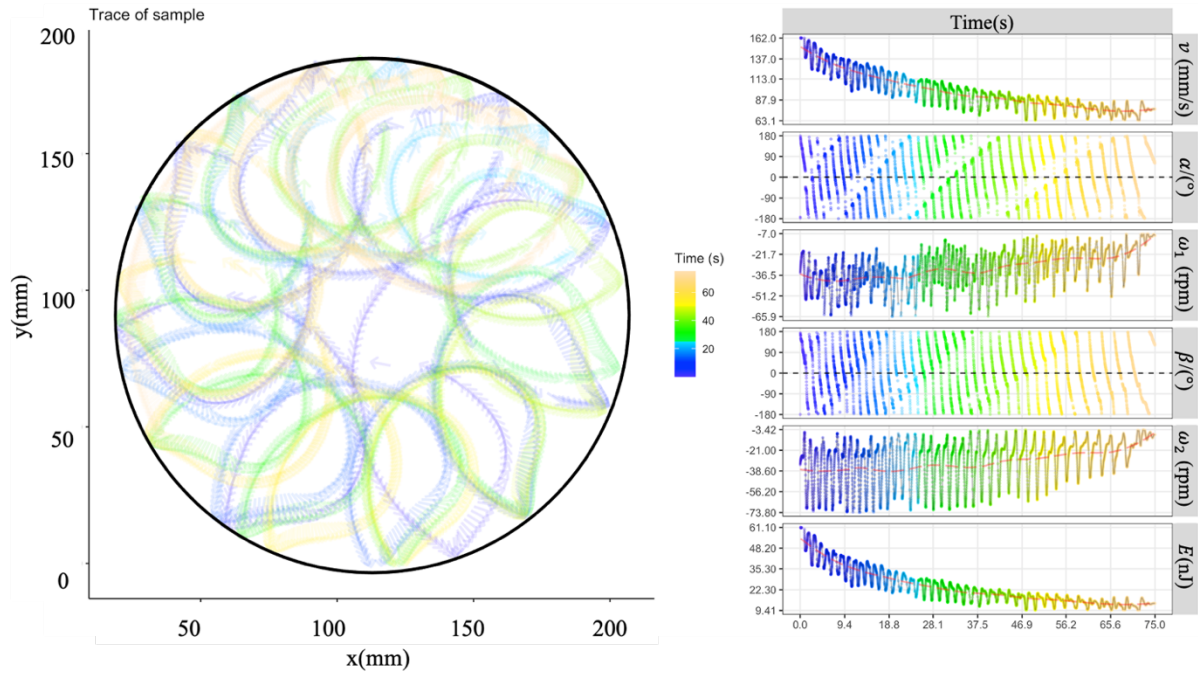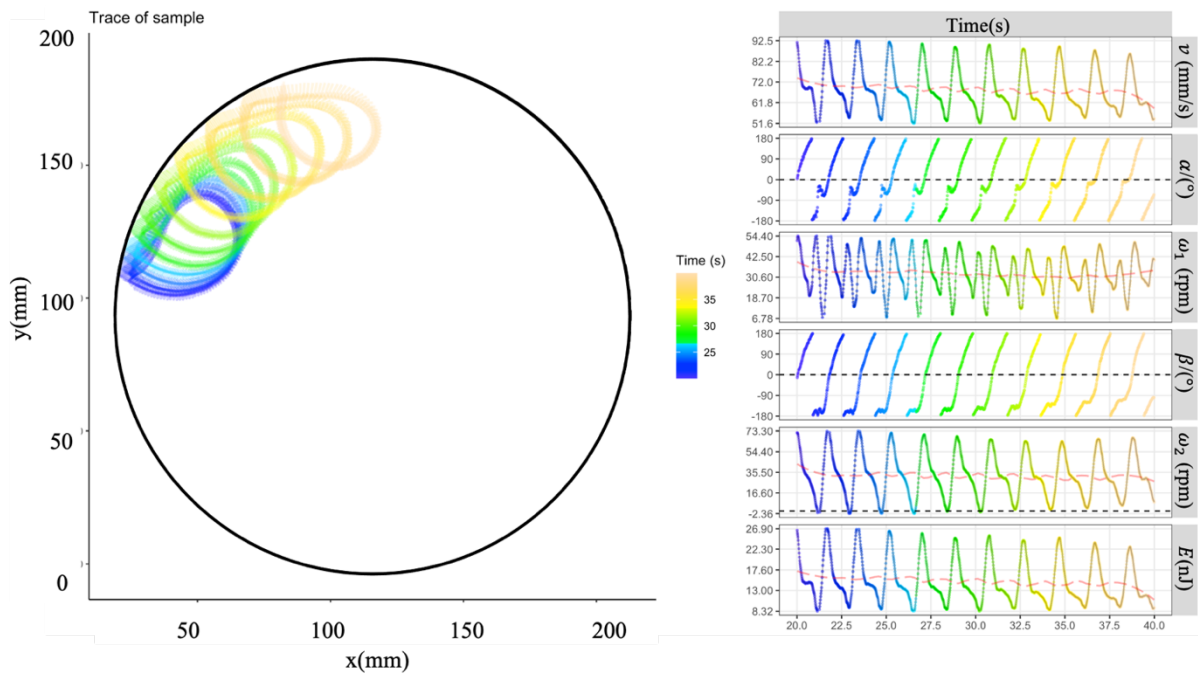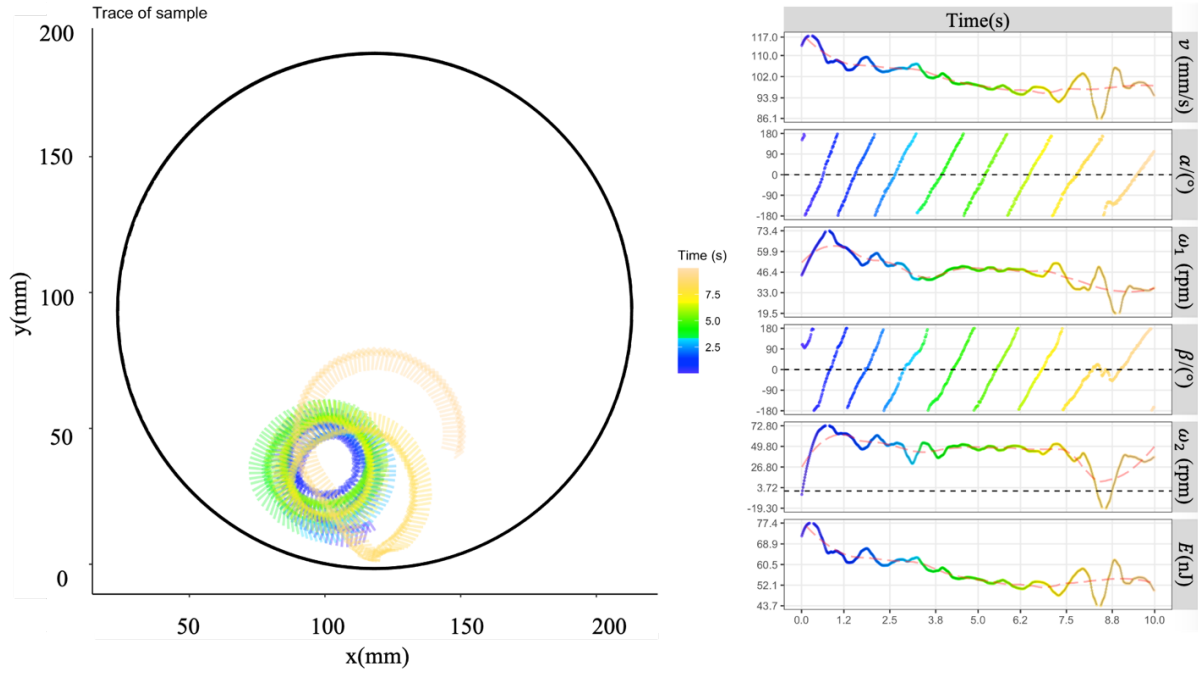
Figure 4.35 Trace (left) and motion parameters (right) including the velocity, orbital speed, spin speed and energy change as the function of time for a rectangle sample with size in 6 mm × 3 mm (sample 4) in the *time period from 0 to 10 second*.

For the gel actuators exhibiting a translational motion, it is found that the velocity decreases when the gel moves towards the wall and increases when the gel moves away from the wall as shown in Figure 4.36 – 4.40.
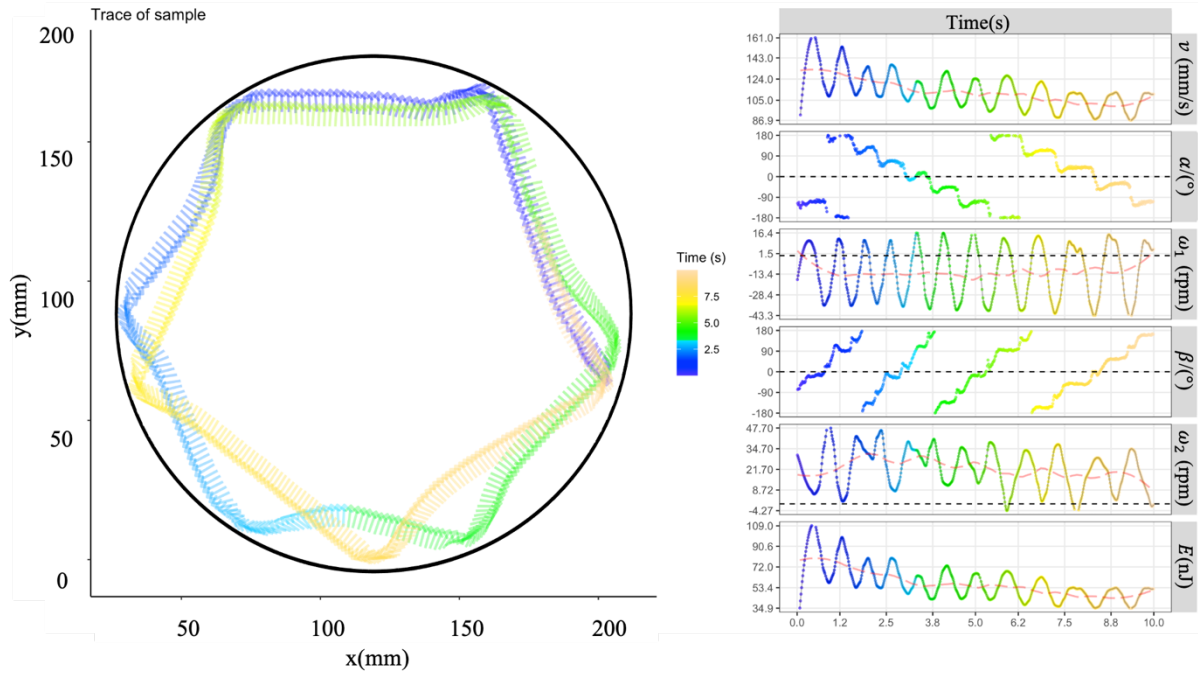
Figure 4.36 Trace (left) and motion parameters (right) including the velocity, orbital speed, spin speed and energy change as the function of time for a rectangle sample with size in 6 mm × 3 mm (sample 6) in the *time period from 0 to 10 second*.
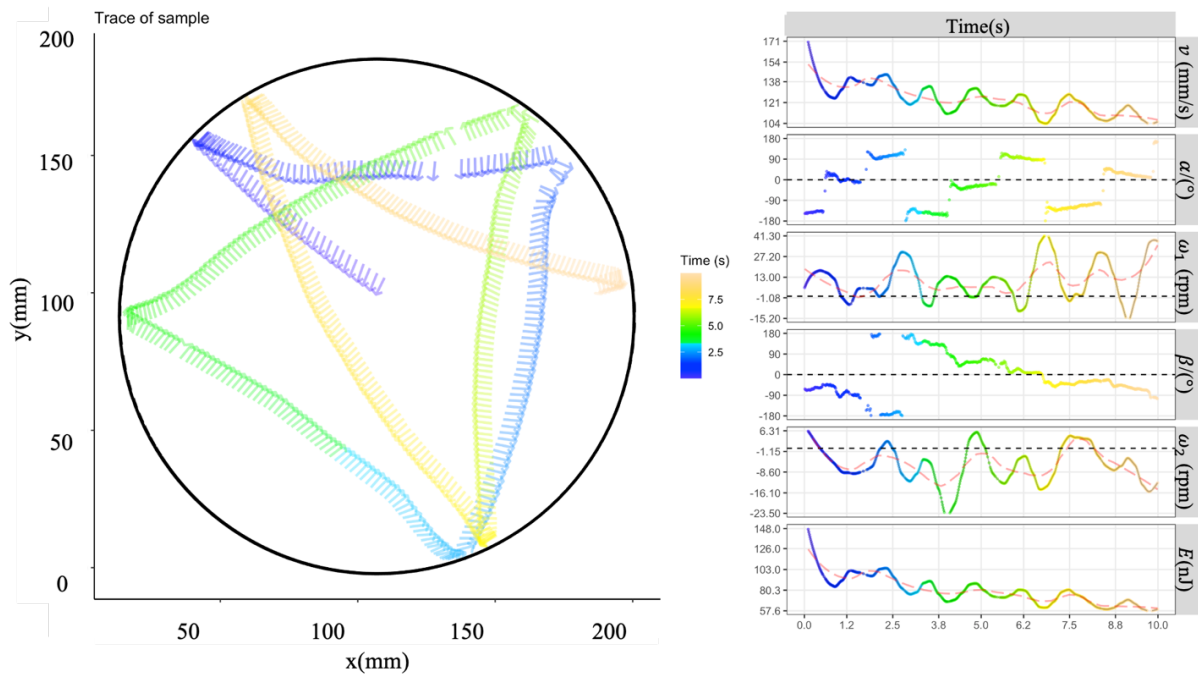
Figure 4.37 Trace (left) and motion parameters (right) including the velocity, orbital speed, spin speed and energy change as the function of time for a rectangle sample with size in 6 mm × 3 mm (sample 8) in the *time period from 0 to 10 second*.
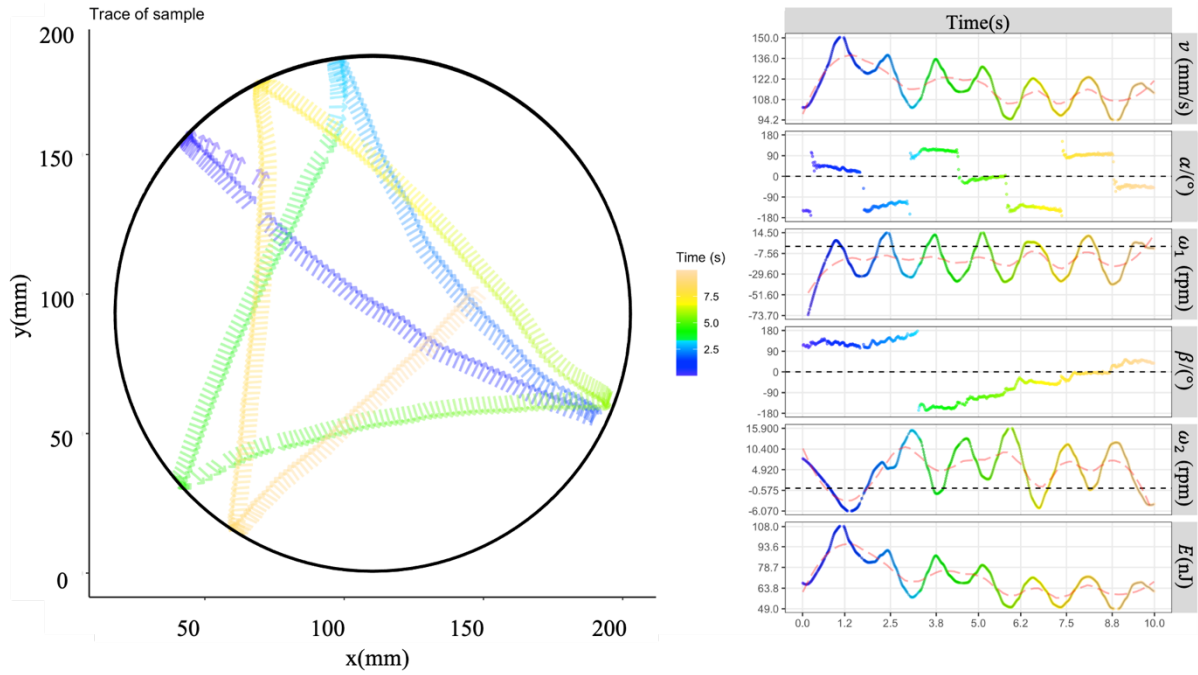
Figure 4.38 Trace (left) and motion parameters (right) including the velocity, orbital speed, spin speed and energy change as the function of time for a rectangle sample with size in 6 mm × 3 mm (sample 9) in the *time period from 0 to 10 second*.
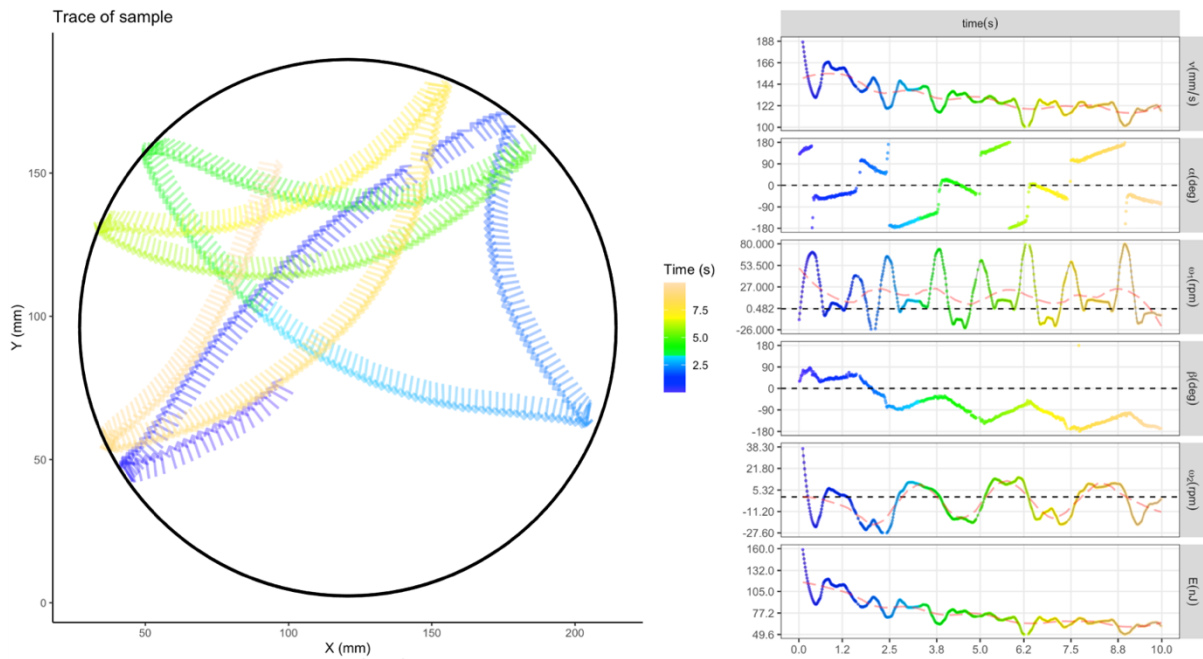
Figure 4.39 Trace (left) and motion parameters (right) including the velocity, orbital speed, spin speed and energy change as the function of time for a rectangle sample with size in 6 mm × 3 mm (sample 15) in the *time period from 0 to 10 second*.
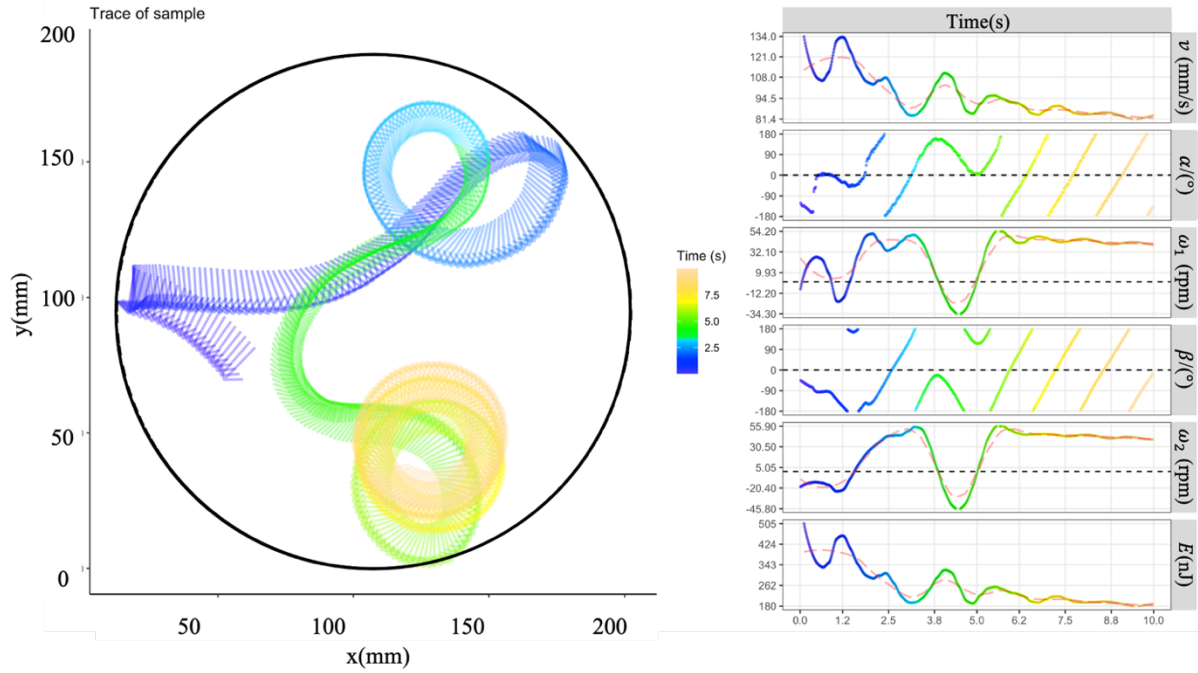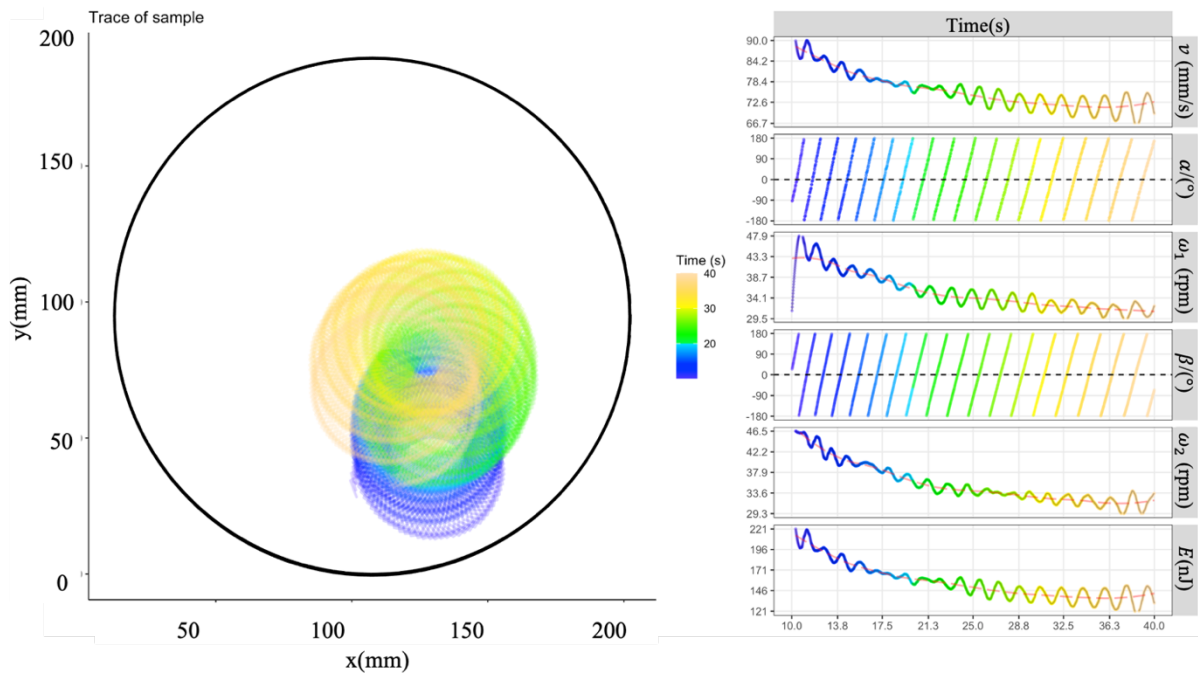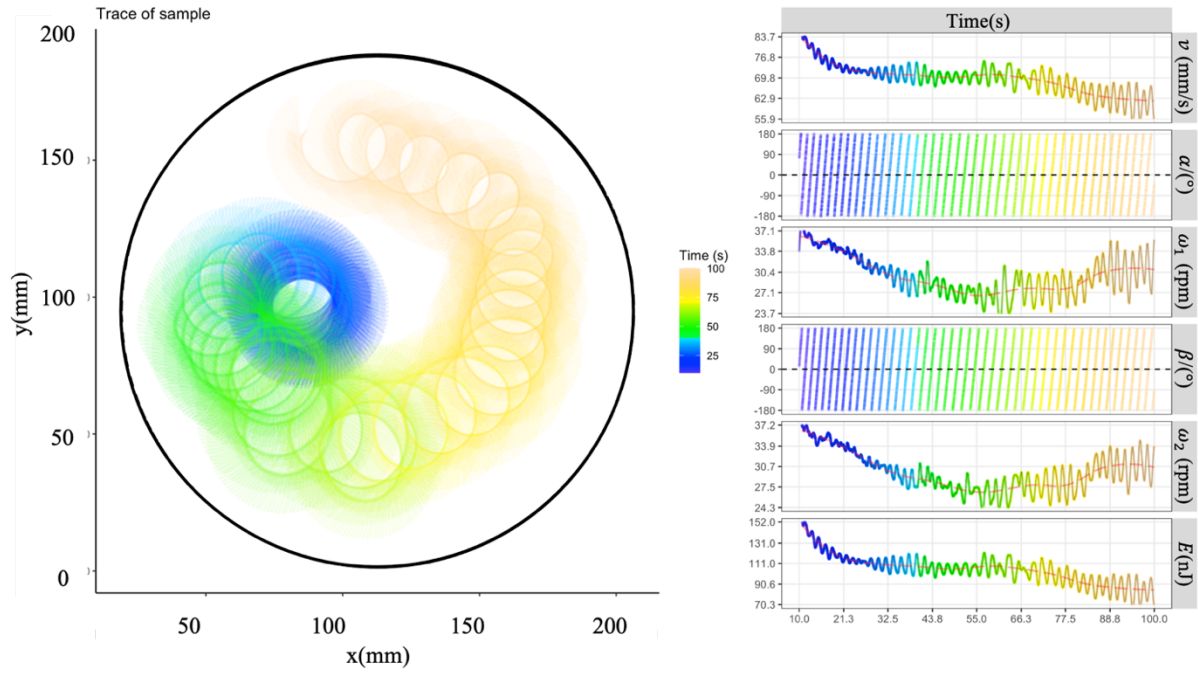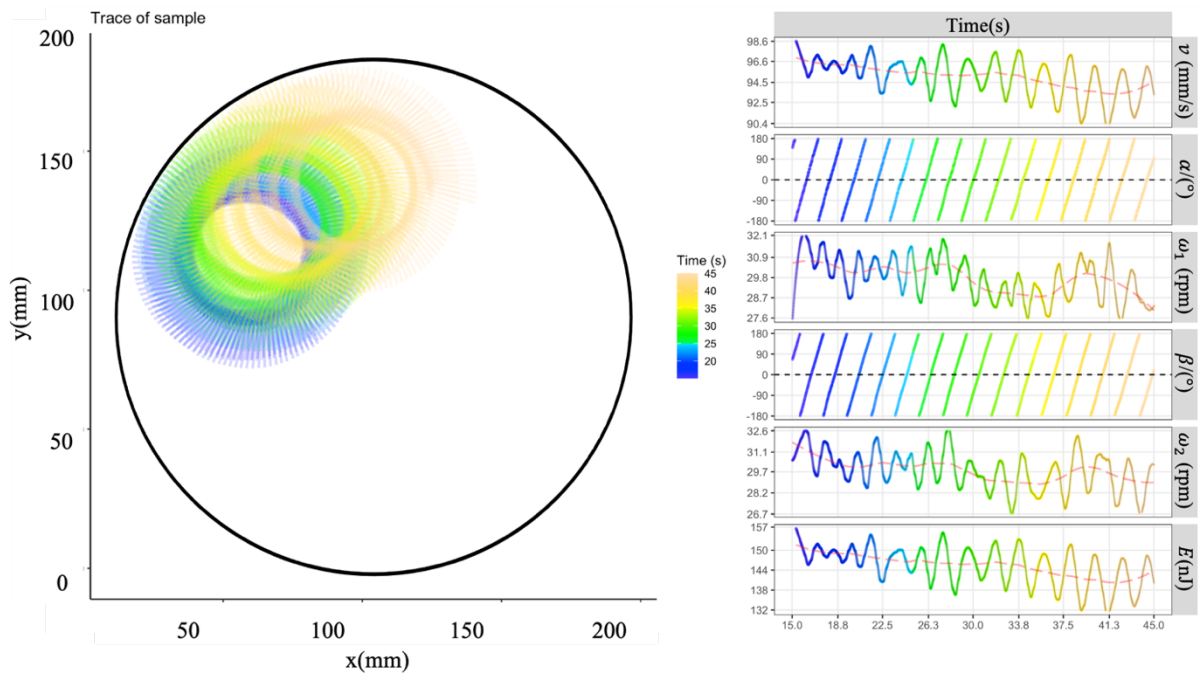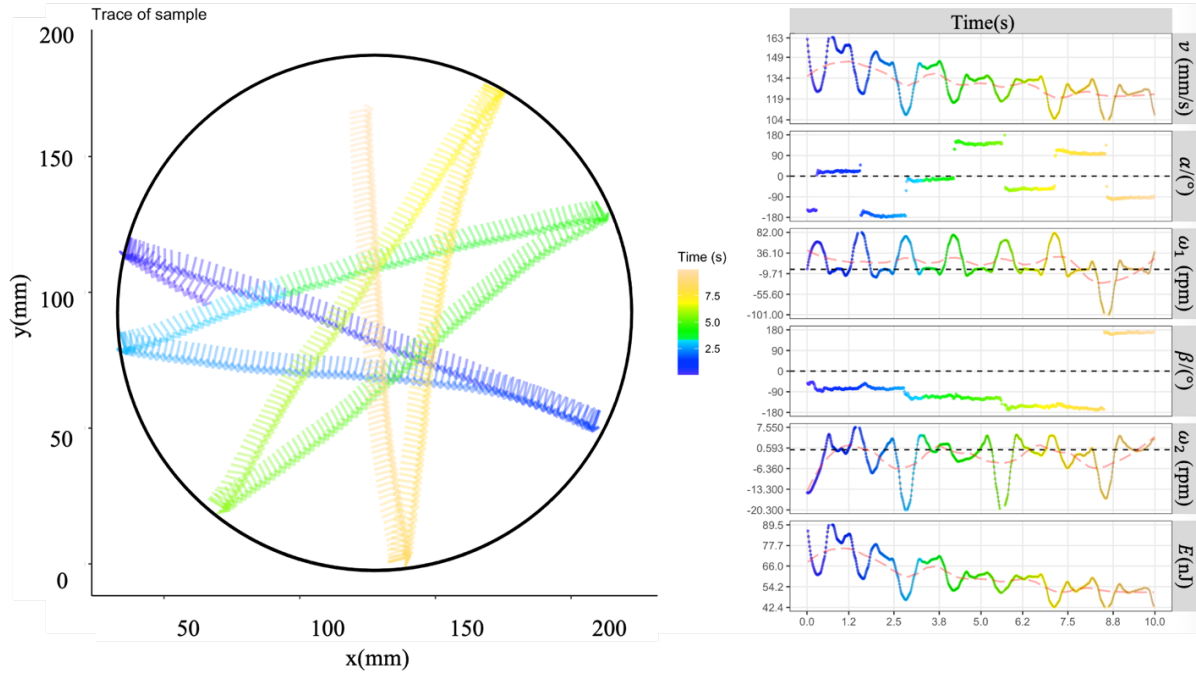
Figure 4.40 Trace (left) and motion parameters (right) including the velocity, orbital speed, spin speed and energy change as the function of time for a rectangle sample with size in 6 mm × 3 mm (sample 16) in the *time period from 0 to 10 second*.

4.2.2 Actuation modes

Experimental results indicated that the motion modes are strongly associated with gel geometry. As discussed in section 4.2.1, the motion modes in the first few seconds are not used. Number of samples exhibited spin, translational motion, orbital motion from different shape of gels was demonstrated in Figure 4.41. Only 1 out of 19 rectangular gel actuators with size of 6 mm × 1 mm exhibited translational motion, the rest of them exhibited spin motion. However, for rectangular gel actuators in size of 6 mm × 3 mm, 18 out of 63 exhibited spin mode, while 40 of them exhibited translational motion and the rest 5 of them exhibited orbital motion. For 27 square gel actuators, 3 exhibited spin motion and the rest of them were orbital motion. 36 out of 37 circular shaped gel

actuators exhibited orbital motion. It seems that higher length/width ratio induce spin mode. Square actuators (i.e., length/width is the smallest, 1) have the tendency of orbital motion.

It has to be mentioned that the motion mode also changes with time during the actuation. For example, it was observed that the spin motion maintained in first few minutes and then changed to translational motion or orbital motion for the rest of time.
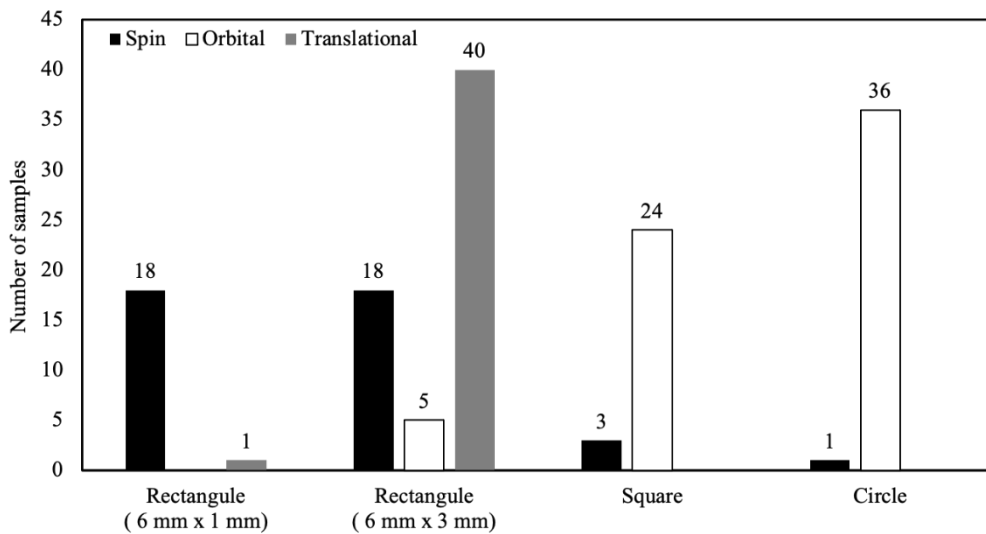
Figure 4.41 Number of gel actuators exhibit spin motion, translational motion and orbital motion.

4.2.3 Friction simulation

To explore the relationship between the friction force and velocity of gel motion at the air-water interface, tests were conducted followed process described in section 2.26. Quantification results of the gel actuators were generated utilizing methods described in Section 4.1. The mass of the gel actuator for this test was 6.1 mg. This sample was a gel that has already actuated till it stopped, which means the difference in the chemical potential of solvent in gel and water, μ_{gel} (T, $n_{s,g}$) $-$ μ_{water} (T, $n_{s,w}$), is so small or even be zero. The initial velocity of gel was generated by a push at time 0 second. Thus, the kinetic energy loses (i.e., the velocity decreases) as the function of time

is the direct results of the friction during the motion. That is, driven force for velocity decreasing is the friction force.

4.2.2.1 Velocity fitting

The time dependence of the velocity of the gel is shown in Figure 4.42, where the results from eight tests are presented.
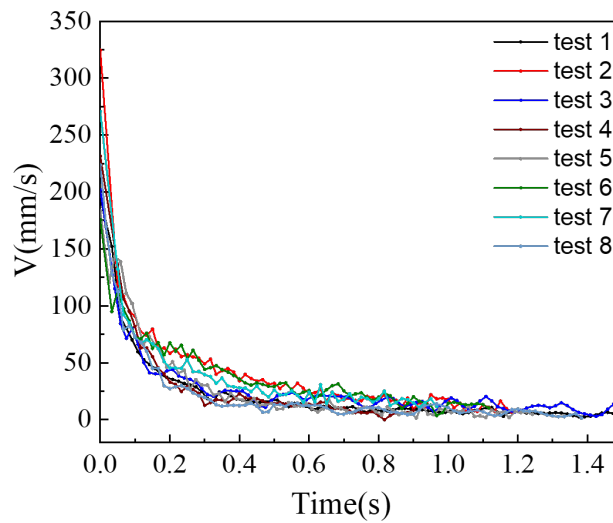
Figure 4.42 Velocity of the gel vs. time. There are eight tests, and the mass of the gel was 6.1 mg.

Relationship between friction force (F) and velocity (v) can be,

$$F = -\alpha v$$

Or

$$F = -\alpha v^2 \qquad \text{Equation 4.7}$$

where F is friction force, α is friction coefficient and v is velocity.

In addition, Newton's second laws can be expressed as following,

$$F = m\frac{dv}{dt} \qquad \text{Equation 4.8}$$

where m is mass of the gel and t is time.

Combine Eq. (4.7) and Eq. (4.8),

$$-\alpha v = m\frac{dv}{dt}$$

Or

$$-\alpha v^2 = m\frac{dv}{dt} \qquad \text{Equation 4.9}$$

So far there is no report on the friction of the gel motions at the air-water surface. Here, we intend

to use experiment results to determine the relationship between the velocity of the gel and friction

force acting on gel when a gel moves at the air-water surface.

4.2.2.1.1 Fitting based on $F = -\alpha v$

Rearrange $-\alpha v = m\frac{dv}{dt}$ and integrate it from t = 0 to t = t,

$$\alpha dt = -m\frac{dv}{v}$$

$$\alpha \int_{t=0}^{t=t} dt = -m\int_{v_0}^{v}\frac{1}{v}dv$$

$$\alpha t = -mlnv + mlnv_0$$

$$lnv = -\frac{\alpha}{m}t + lnv_0 \qquad \text{Equation 4.10}$$

Thus, relationship between velocity and time was shown as Eq. (4.10). Linear fitting can be

conducted by following Eq. (4.11).

$$lnv = A + Bt \qquad \text{Equation 4.11}$$

where $A = lnv_0$, $B = -\frac{\alpha}{m}$.

Eq. (4.10) can be rearranged as following

$$v = e^{-\frac{\alpha}{m}t+lnv_0}$$

$$v = v_0 e^{-\frac{\alpha}{m}t} \qquad \text{Equation 4.12}$$

$$v = ae^{Bt} \qquad \text{Equation 4.13}$$

where $a = v_0, B = -\frac{\alpha}{m}.$
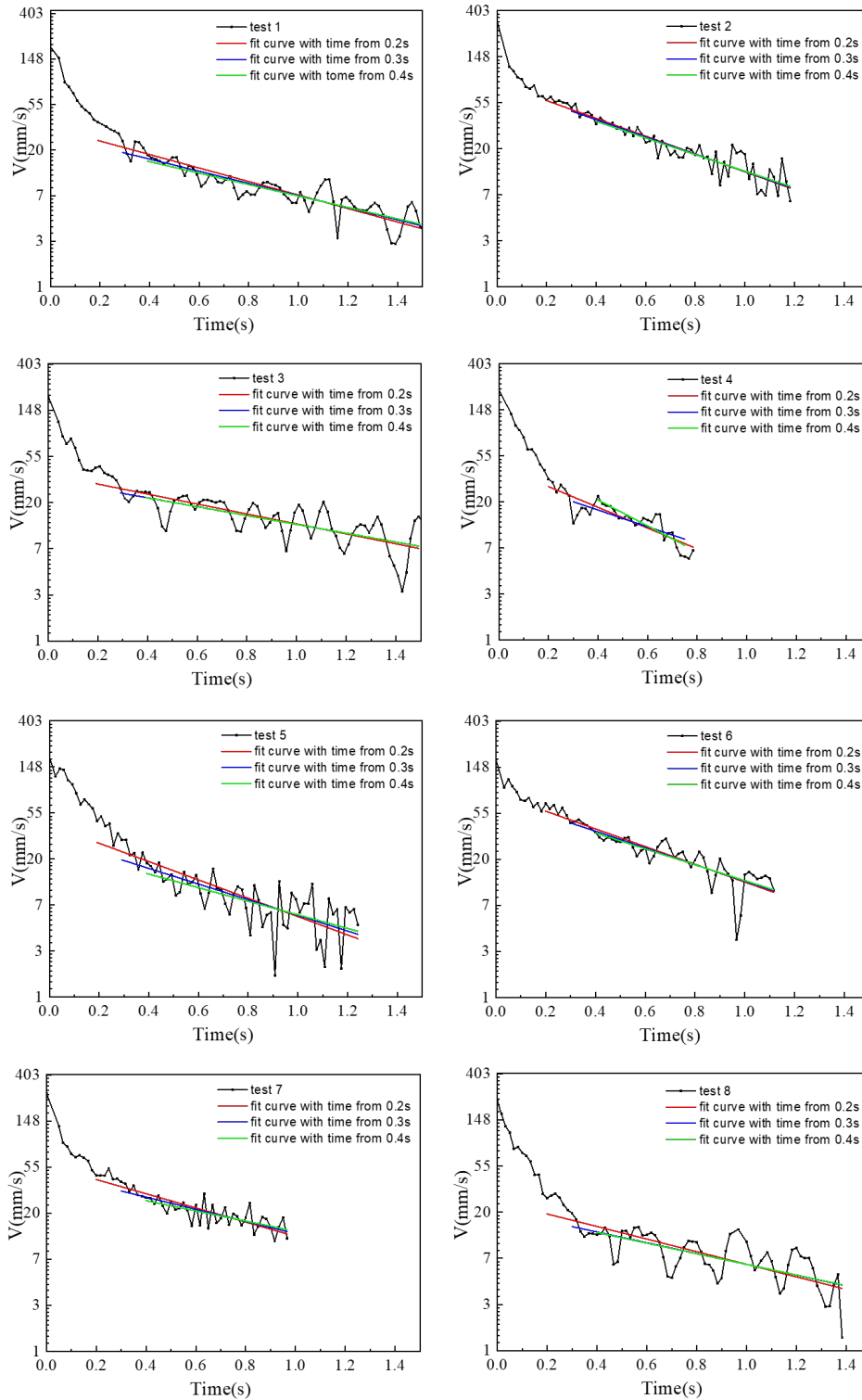
Figure 4.43 Logarithm scale of the velocity as function of time. Fitting using Eq. (4.11).

The time dependence of the velocity for the eight tests of the gel is plotted in Figure 4.43 using logarithm scale for the velocity. Based on Eq. (4.11), there should be a linear relationship between the $\ln(v)$ and the time (t) with the slope is $B = -\frac{\alpha}{m}$. That is, the slope of the curves in Figure 4.43 can be used to determine the α.

From the experiment results, there is two segments for the curves about the slope. For the data analysis, the fitting was conducted by using the experimental data without initial state. In order to figure out which time range should be trusted, data with time ranges from 0.2 second, 0.3 second and 0.4 second to the end were fitted, respectively. Results of fitting were shown in Table 4.6, including coefficient of determination (R^2), slope of linear curve (B), friction coefficient (α), maximum α in the group (α_{max}), minimum α in the group (α_{min}), average of α in the group (α_{avg}) and standard deviation (σ). α_{avg} was calculated by removing α_{max} and α_{min}. The results showed that fitting with time range from 0.2 second was of the smallest standard deviation.

Table 4.6 Fitting results of 8 test using Eq. (4.11)

| Test | The starting time used in the fitting | | | | | | | | |
| | 0.2 s | | | 0.3 s | | | 0.4 s | | |
	R^2	B	α	R^2	B	α	R^2	B	α
1	0.84	-1.48	0.0092	0.80	-1.33	0.0082	0.75	-1.26	0.0077
2	0.88	-1.94	0.0120	0.83	-1.88	0.0115	0.77	-1.81	0.0110
3	0.62	-1.08	0.0066	0.52	-0.96	0.0059	0.46	-0.96	0.0059
4	0.78	-2.26	0.0138	0.56	-1.81	0.0110	0.76	-2.82	0.0172
5	0.67	-1.99	0.0122	0.55	-1.70	0.0104	0.42	-1.48	0.0091
6	0.79	-1.92	0.0117	0.71	-1.80	0.0110	0.60	-1.72	0.0105
7	0.77	-1.54	0.0094	0.65	-1.32	0.0081	0.48	-1.11	0.0068
8	0.63	-1.36	0.0083	0.52	-0.17	0.0010	0.44	-1.16	0.0071
α_{max}			0.0138			0.0115			0.0172
α_{min}			0.0066			0.0010			0.0059
α_{avg}			0.0103			0.0091			0.0087
σ			0.0017			0.0021			0.0018
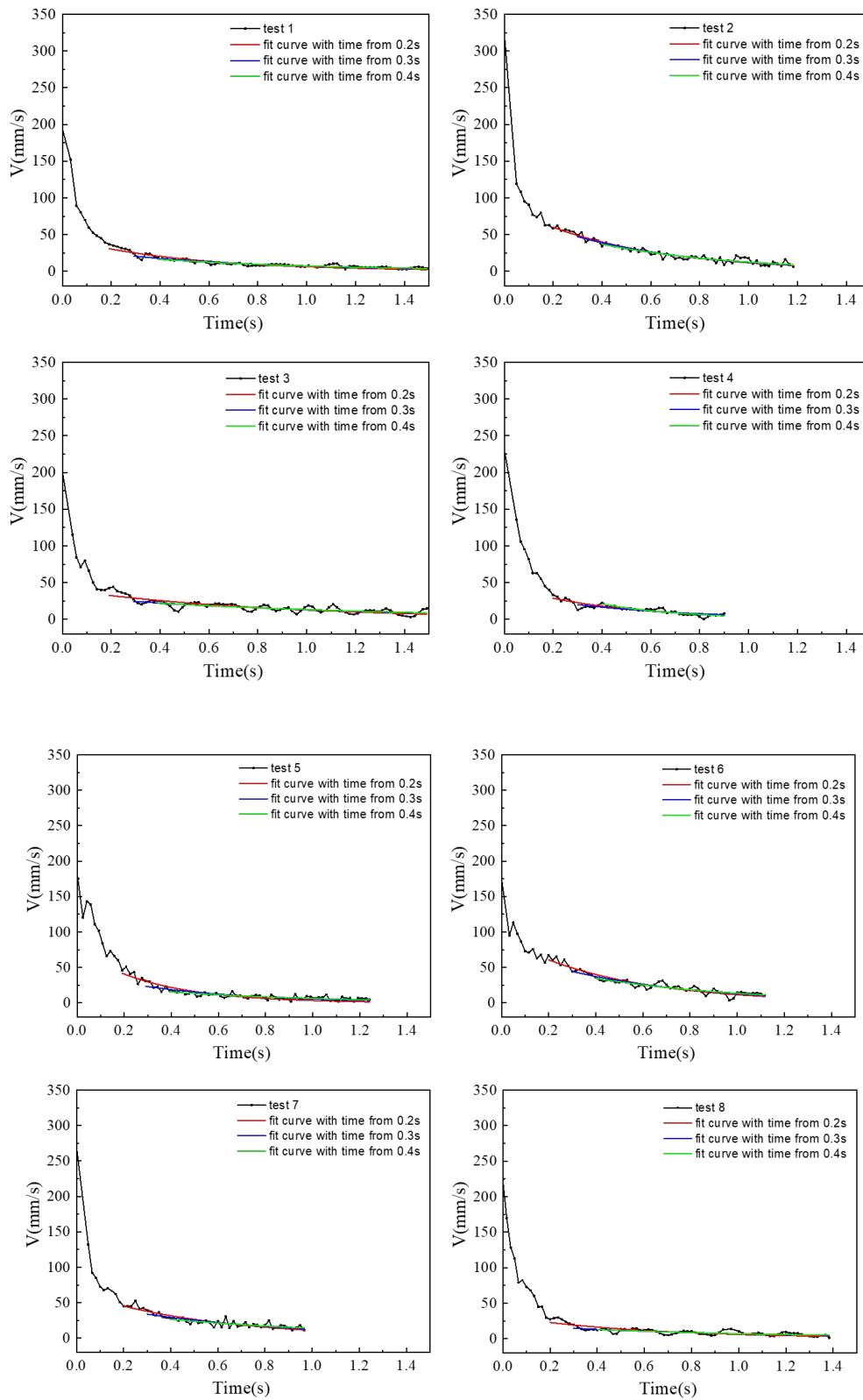
Figure 4.44 Velocity as function of time. Fitting using Eq. (4.13).

Similarly, exponent fitting of 8 tests were conducted using Eq. (4.13) and data with time ranges from 0.2 second, 0.3 second and 0.4 second to the end were fitted, respectively, which are shown in Figure 4.44. Results of fitting were summarized in Table 4.7. The results showed that fitting with time ranges from 0.2 second was of the smallest standard deviation, which is the same as linear fitting result.

Table 4.7 Fitting results of 8 tests using Eq. (4.13)

| | The starting time used in the fitting | | | | | | | | |
| | 0.2 s | | | 0.3 s | | | 0.4 s | | |
Test	R^2	B	α	R^2	B	α	R^2	B	α
1	0.88	-1.97	0.0120	0.85	-1.49	0.0091	0.83	-1.31	0.0080
2	0.95	-2.04	0.0124	0.91	-1.95	0.0119	0.85	-1.79	0.0109
3	0.71	-1.17	0.0071	0.61	-0.88	0.0054	0.51	-0.83	0.0051
4	0.82	-2.36	0.0144	0.66	-1.92	0.0117	0.82	-2.93	0.0179
5	0.84	-3.12	0.0190	0.73	-2.07	0.0126	0.57	-1.50	0.0092
6	0.91	-2.07	0.0126	0.87	-1.76	0.0107	0.77	-1.56	0.0095
7	0.83	-1.77	0.0108	0.70	-1.43	0.0087	0.48	-1.09	0.0066
8	0.70	-1.66	0.0101	0.56	-1.06	0.0065	0.45	-0.98	0.0060
Max			0.0190			0.0126			0.0179
Min			0.0071			0.0054			0.0051
Avg			0.0121			0.0098			0.0084
σ			0.0015			0.0021			0.0019

4.2.2.1.1 Fitting based on $F = -\alpha v^2$

Rearrange $-\alpha v^2 = m\frac{dv}{dt}$ Eq. (4.9) and integrate it from t = 0 to t = t,

$$-\frac{\alpha}{m}t = \frac{1}{v_0} - \frac{1}{v}$$

$$v^{-1} = v_0^{-1} + \frac{\alpha}{m}t \qquad\qquad \text{Equation 4.14}$$

$$v^{-1} = a' + B't \qquad\qquad \text{Equation 4.15}$$

where $a' = v_0^{-1}, B' = \frac{\alpha}{m}$.
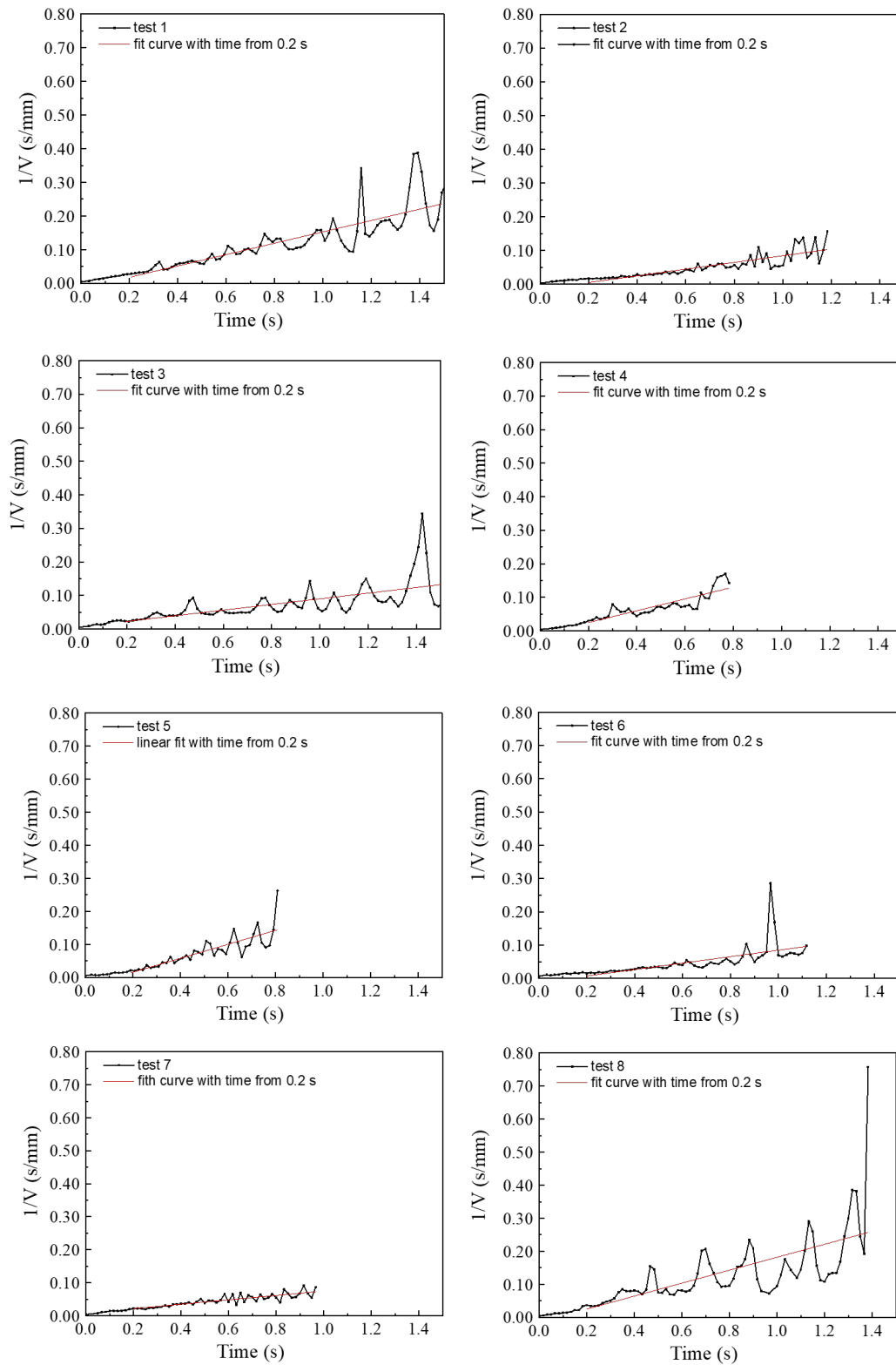
Figure 4.45 Reciprocal of velocity as function of time. Fitting using Eq. (4.15).

Table 4.8 (a) R^2 of fitting results with time starting at 0 s and stop at 0.4 s, 0.5 s and 0.6 s, 0.7 s and 0.8 s.

Test	0.4 s	0.5 s	0.6 s	0.7 s	0.8 s
1	0.87	0.93	0.94	0.94	0.93
2	0.94	0.96	0.95	0.90	0.92
3	0.89	0.80	0.69	0.61	0.68
4	0.81	0.81	0.86	0.85	0.81
5	0.88	0.91	0.88	0.84	0.84
6	0.93	0.94	0.94	0.87	0.90
7	0.96	0.94	0.91	0.85	0.85
8	0.93	0.82	0.72	0.71	0.67
Max	0.96	0.96	0.95	0.94	0.93
Min	0.81	0.80	0.69	0.61	0.67
Avg	0.91	0.89	0.88	0.84	0.83

(b) R^2 of fitting results with time starting at 0.1 s and stop at 0.4 s, 0.5 s and 0.6 s, 0.7 s and 0.8 s.

Test	0.4 s	0.5 s	0.6 s	0.7 s	0.8 s
1	0.80	0.89	0.91	0.92	0.92
2	0.89	0.94	0.93	0.87	0.90
3	0.79	0.73	0.55	0.45	0.56
4	0.72	0.70	0.80	0.78	0.77
5	0.87	0.91	0.85	0.80	0.72
6	0.87	0.91	0.92	0.82	0.87
7	0.93	0.92	0.87	0.80	0.80
8	0.93	0.82	0.59	0.60	0.56
Max	0.93	0.94	0.93	0.92	0.92
Min	0.72	0.7	0.55	0.45	0.56
Avg	0.86	0.86	0.82	0.78	0.77

(c) R^2 of fitting results with time starting at 0.2 s and stop at 0.4 s, 0.5 s and 0.6 s, 0.7 s and 0.8 s.

Test	0.4 s	0.5 s	0.6 s	0.7 s	0.8 s
1	0.56	0.76	0.83	0.87	0.88
2	0.80	0.91	0.90	0.84	0.89
3	0.62	0.67	0.36	0.23	0.42
4	0.26	0.34	0.57	0.63	0.69
5	0.78	0.87	0.78	0.71	0.73
6	0.89	0.95	0.91	0.75	0.82
7	0.87	0.86	0.79	0.71	0.71
8	0.91	0.64	0.32	0.46	0.40
Max	0.91	0.95	0.91	0.87	0.89
Min	0.26	0.34	0.32	0.23	0.4
Avg	0.76	0.79	0.71	0.68	0.71

The time dependence of the velocity for the eight tests of the gel is plotted in Figure 4.45. Based on Eq. (4.15), there should be a linear relationship between the v^{-1} and the time (t) with the slope $B' = \frac{\alpha}{m}$. Then, the slope of the curves in Figure 4.41 can be used to determine the α. Fitting was conducted with time starting at 0 second, 0.1 second and 0.2 second and stopping at 0.4 second, 0.5 second, 0.6 second, 0.7 and 0.8 second based on results above. Fitting results with data from 0.2 second to the end are presented in Table 4.9. α_{avg} from fitting based on $F = -\alpha v^2$ is two orders less than the α_{avg} from fitting based on $F = -\alpha v$.

Table 4.9 Fitting results of 8 tests using Eq. (4.14)

Test	R^2	B'	α
1	0.69	0.169	0.00103
2	0.72	0.099	0.00060
3	0.41	0.088	0.00054
4	0.70	0.176	0.00107
5	0.66	0.211	0.00129
6	0.40	0.097	0.00059
7	0.72	0.067	0.00041
8	0.42	0.196	0.00120
Max			0.00129
Min			0.00041
Avg			0.00084
σ			0.00029

Compare Figure 4.43 and Figure 4.45, fitting based on $F = -\alpha v$ is better for the longer time period, while fitting based on $F = -\alpha v^2$ is better for the short time period and also good for the longer time period. The R^2 is smaller for fitting based on $F = -\alpha v^2$. In addition, the velocity at the early stage is closer to the value of velocity when the gel actuators moving at the air-water interface. Overall, fitting based on $F = -\alpha v^2$ is better.

4.2.2.2 Displacement fitting

As was shown in Figure 4.43, noise of velocity curve after 0.2 s is large. However, relatively less noise was found of the displacement curves, which were shown in Figure 4.46. Both math and physical equation were utilized for displacement fitting.
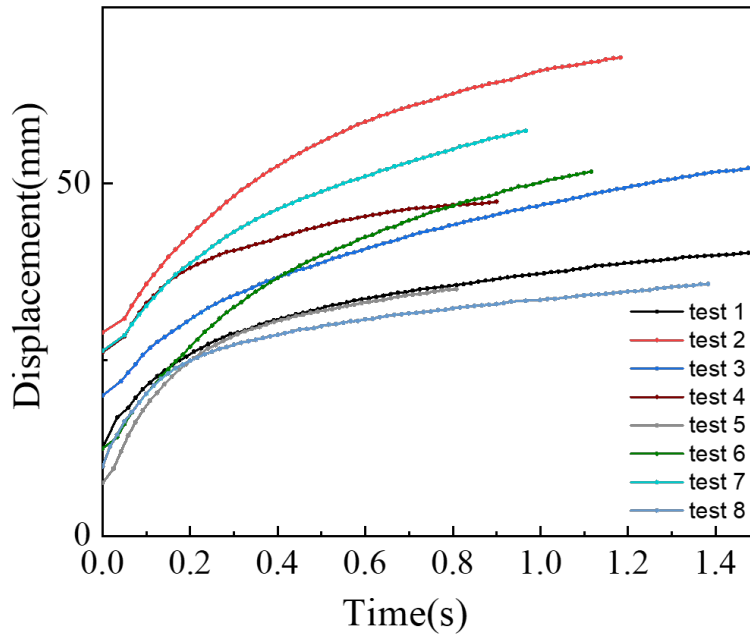
Figure 4.46 Displacement of gel as function of time for 8 tests.

4.2.2.2.1 Math equation and fitting based on $F = -\alpha v$

$$y = B_0 + B_1 x + B_2 x^2 + B_3 x^3 + B_4 x^4 \qquad\qquad \text{Equation 4.16}$$

$$y = B_0 + B_1 x + B_2 x^2 + B_3 x^3 + B_4 x^4 + B_5 x^5 + B_6 x^6 \qquad\qquad \text{Equation 4.17}$$

$$y = B_0 + B_1 x + B_2 x^2 + B_3 x^3 + B_4 x^4 + B_5 x^5 + B_6 x^6 + B_7 x^7 + B_8 x^8 \qquad \text{Equation 4.18}$$

Fitting of experimental displacement results were utilized Eq. (4.15) – (4.17) with time range from 0.2 s to the end. B_i of each equation are obtained from fitting results. Then these equations were

conducted first derivation to obtained Eq. (4.18) – (4.20), which have meaning of velocity as function of time.

$$y' = B_1 + B_2 x + B_3 x^2 + B_4 x^3 \qquad\qquad \text{Equation 4.19}$$

$$y' = B_1 + B_2 x + B_3 x^2 + B_4 x^3 + B_5 x^4 + B_6 x^5 \qquad\qquad \text{Equation 4.20}$$

$$y' = B_1 + B_2 x + B_3 x^2 + B_4 x^3 + B_5 x^4 + B_6 x^5 + B_7 x^6 + B_8 x^7 \qquad \text{Equation 4.21}$$
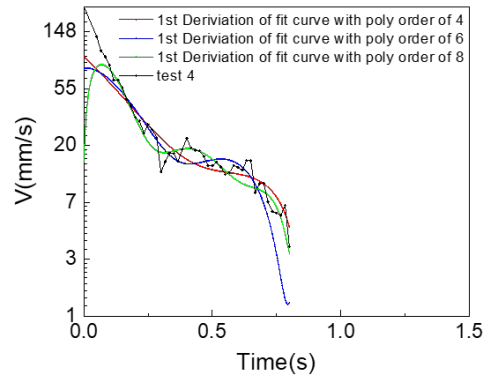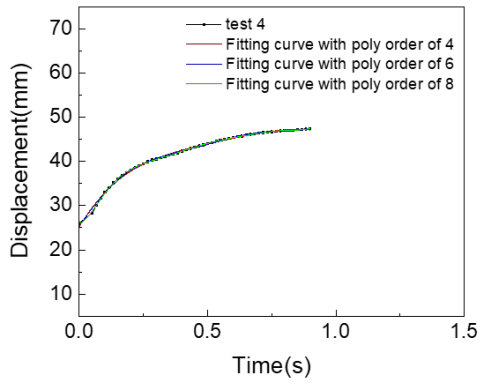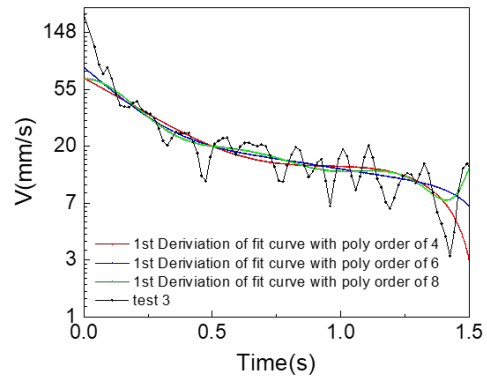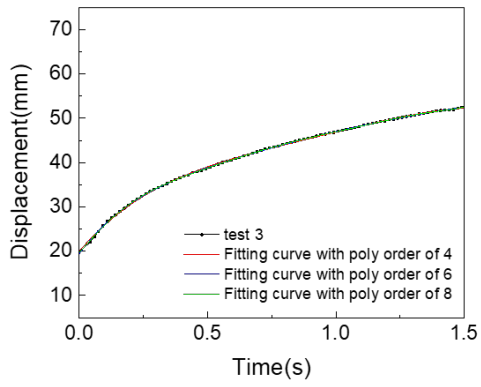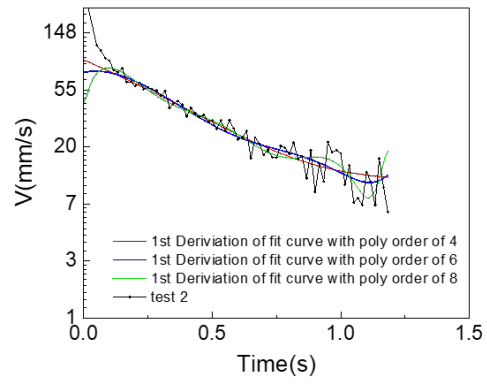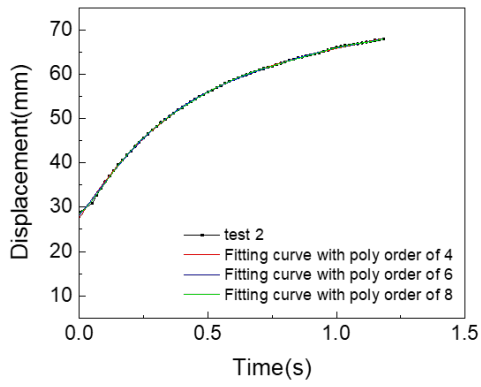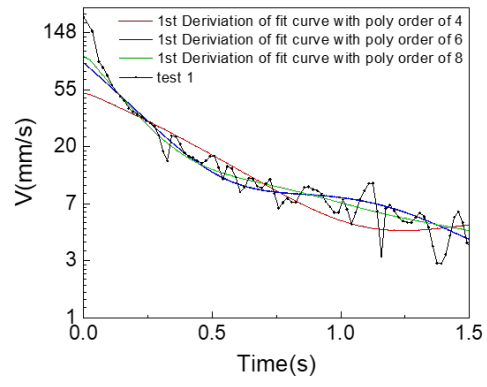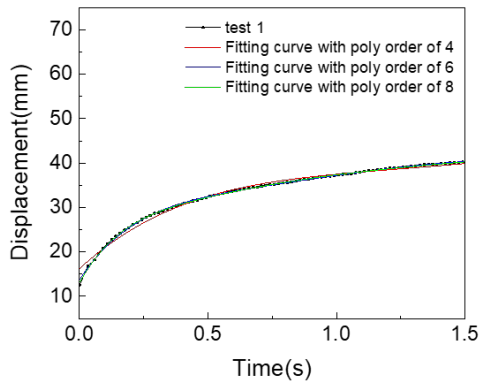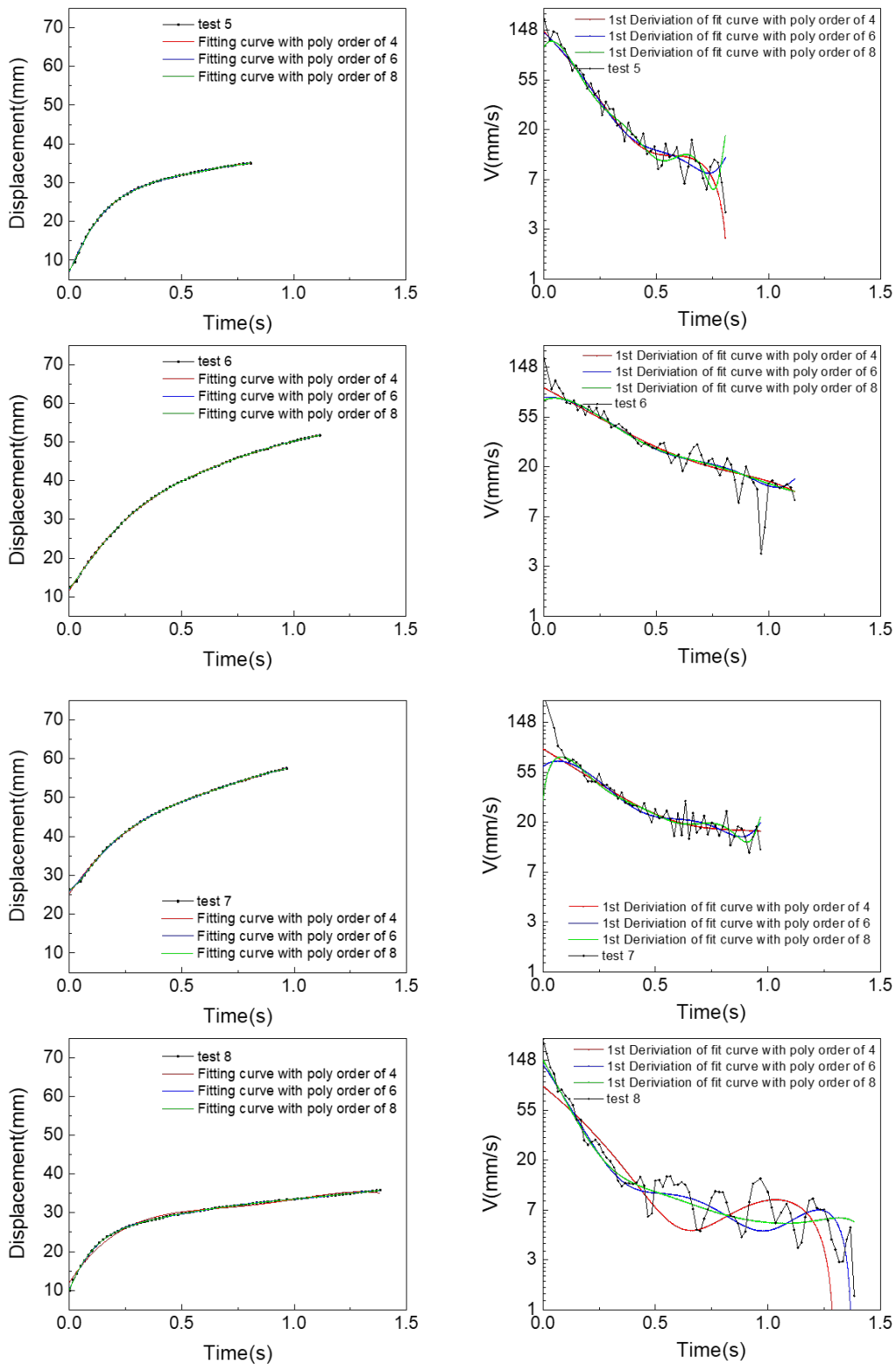
Figure 4.47 Displacement as function of time (left) and Logarithm scale of the velocity as function of time (right).

The experimental results are plotted in Figure 4.47 using logarithm scale for the velocity, accompanied with velocity curve generated using Eq. (4.17) – (4.20). As was shown in Figure 4.47, there are obvious fluctuations on the plots with time after 0.5 second, especially the test 8.

Based on Eq. (4.11), there should be a linear relationship between the $\ln(v)$ and the time (t). And the slope $B = -\frac{\alpha}{m}$ can be used to determine the α. Results of this linear fitting on Eq. (4.19) to (4.21) with time ranges from 0.2 second were shown in Table 4.9. Fitting using Eq. (4.19) has the smallest standard deviation and Eq. (4.19) has larger R^2. Average of α from fitting on Eq. (4.19) is the same as fitting on velocity as function of time using Eq. (4.11).

Table 4.10 Fitting results on velocity of 8 tests using Eq. (4.19)- (4.21)

Test	Equation 4.19			Equation 4.20			Equation 4.21		
	R^2	A	α	R^2	b	α	R^2	b	α
1	0.92	-1.71	0.0104	0.89	-1.33	0.0081	0.95	-1.34	0.0082
2	0.97	-1.76	0.0107	0.98	-1.82	0.0111	0.92	-1.79	0.0109
3	0.84	-1.16	0.0071	0.96	-0.98	0.0060	0.92	-0.95	0.0058
4	0.92	-2.37	0.0145	0.70	-3.62	0.0221	0.88	-2.50	0.0153
5	0.88	-3.05	0.0186	0.89	-2.57	0.0157	0.83	-2.62	0.0160
6	0.98	-1.63	0.0099	0.96	-1.62	0.0099	0.98	-1.65	0.0101
7	0.90	-1.41	0.0086	0.88	-1.43	0.0087	0.89	-1.43	0.0087
8	0.44	-1.25	0.0076	0.73	-1.21	0.0074	0.79	-1.11	0.0068
Max			0.0186			0.0221			0.0160
Min			0.0071			0.0060			0.0058
Avg			0.0103			0.0101			0.0099
σ			0.0024			0.0030			0.0030

4.2.2.2.2 Math equation and fitting based on $F = -\alpha v^2$
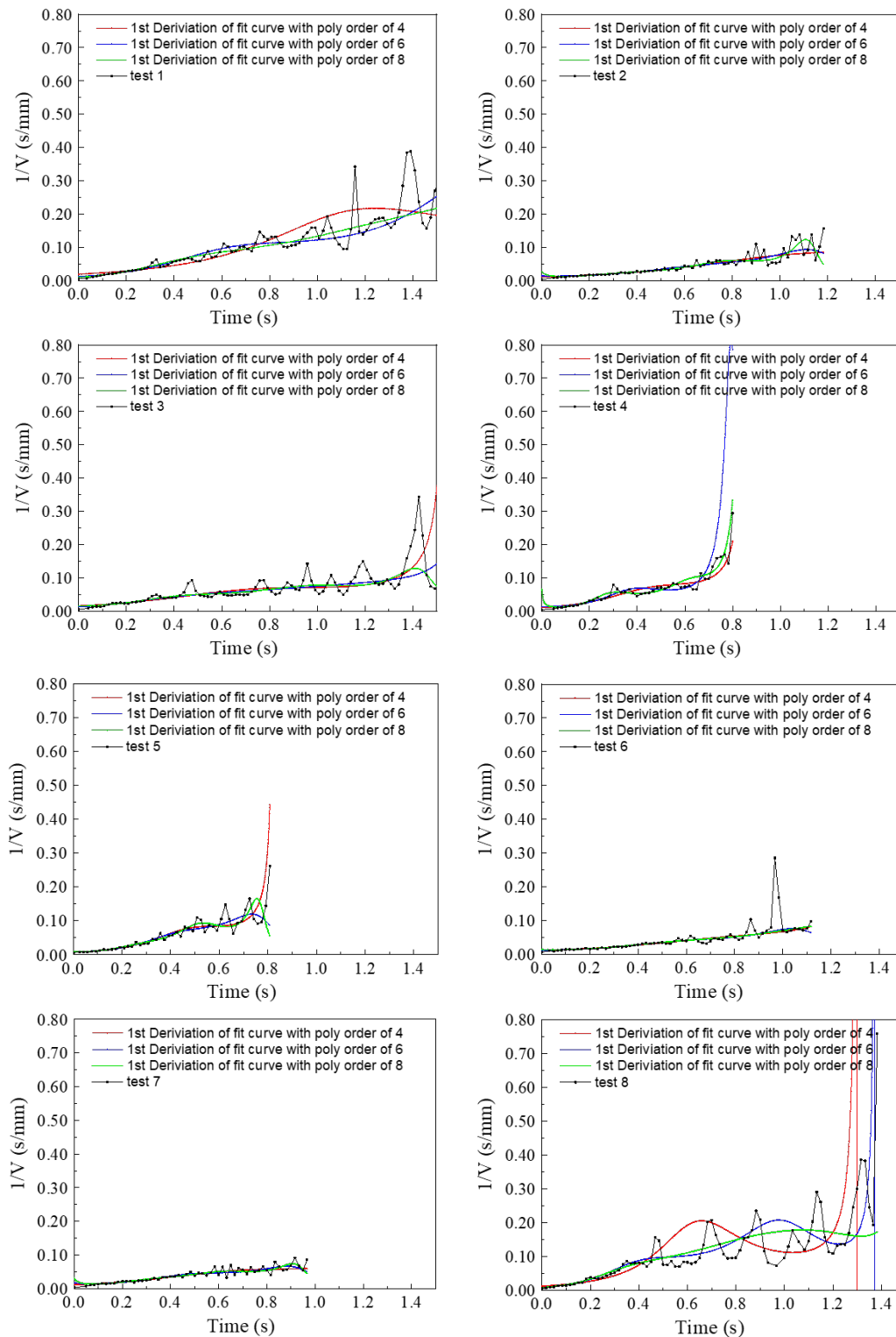
Figure 4.48 Reciprocal of velocity as function of time.

Based on Eq. (4.15), there is linear relationship between the $\frac{1}{v}$ and the time (t) with the slope

$B' = \frac{\alpha}{m}$ as plotted in Figure 4.48. Then, the slope can be used to determine the α. Results of this

linear fitting on Eq. (4.19) to (4.21) with time ranges from 0.2 second were shown in Table 4.11.

Fitting using Eq. (4.19) has the smallest standard deviation. Similarly, α_{avg} from fitting based on F

$= -\alpha v^2$ is two order less than the α_{avg} from fitting based on $F = -\alpha v$. Average of α from fitting on

Eq. (4.19) is close to the fitting on velocity as function of time using Eq. (4.15).

Table 4.11 Fitting results on velocity of 8 tests using Eq. (4.19)- (4.21)

Test	Equation 4.19			Equation 4.20			Equation 4.21		
	R^2	B'	α	R^2	B'	α	R^2	B'	α
1	0.94	0.179	0.00109	0.93	0.135	0.00082	0.99	0.139	0.00085
2	0.99	0.078	0.00048	0.98	0.083	0.00051	0.84	0.086	0.00052
3	0.54	0.095	0.00058	0.95	0.064	0.00039	0.89	0.062	0.00038
4	0.97	0.136	0.00083	0.57	0.187	0.00114	0.88	0.151	0.00092
5	0.60	0.249	0.00152	0.95	0.162	0.00099	0.78	0.214	0.00131
6	0.99	0.067	0.00041	0.98	0.066	0.00040	0.99	0.068	0.00041
7	0.95	0.057	0.00035	0.93	0.058	0.00035	0.91	0.060	0.00037
8	0.29	0.140	0.00085	0.54	0.151	0.00092	0.86	0.196	0.00120
Max			0.00152			0.00114			0.00120
Min			0.00035			0.00035			0.00038
Avg			0.00071			0.00067			0.00071
σ			0.00026			0.00027			0.00030

4.2.2.2.3 Physics equation and fitting based on $F = -\alpha v$

Displacement can be calculated by

$$dl = vdt$$

where l is displacement.

Combine Eq. (4.13),

$$\int_0^l dl = \int_0^t v \, dt = \int_0^t a e^{Bt} \, dt$$

$$l = \frac{a}{B} e^{Bt} \Big|_0^t = \frac{a}{B} e^{Bt} + C \qquad \text{Equation 4.22}$$

where $a = v_0$, $B = -\frac{\alpha}{m}$.
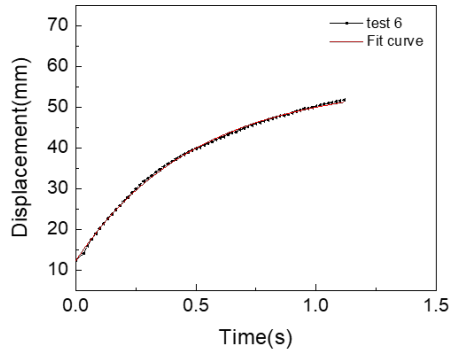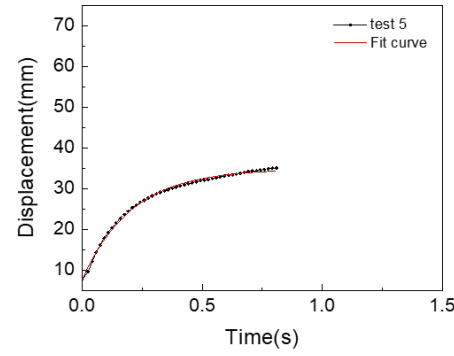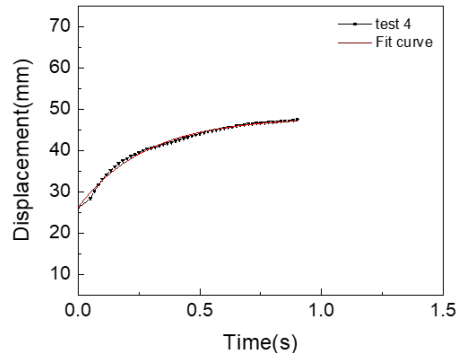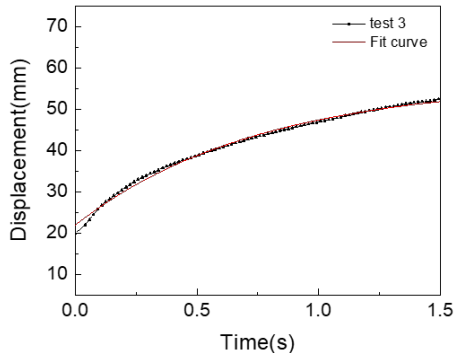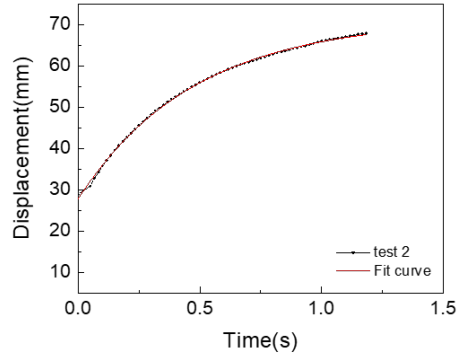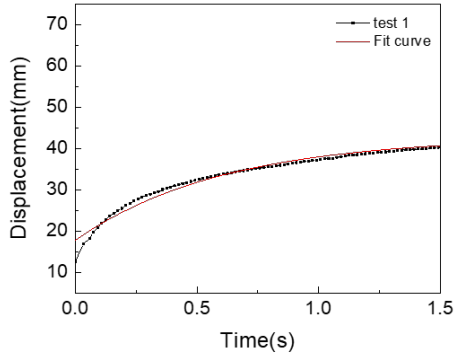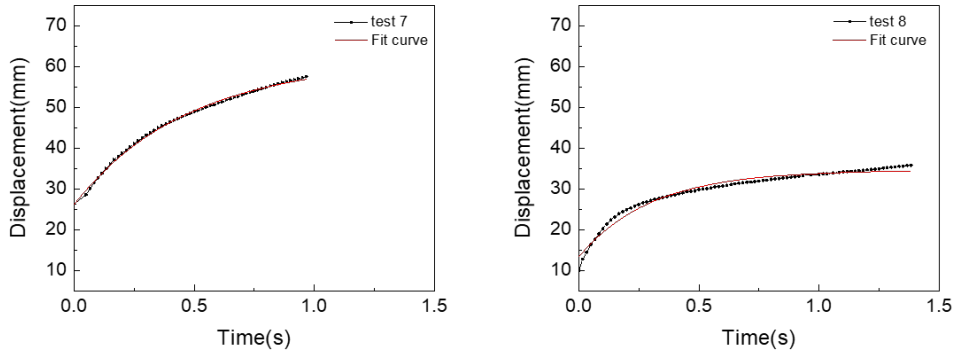
Figure 4.49 Displacement of gel as function of time. Fitting using Eq. (4.22).

The time dependence of the displacement was plotted in Figure 4.49. Displacement curves as function of time were fitted using Eq. (4.22), results of which were presented in Table 4.12. The result is closed to the value of α_{avg} in Table 4.6 and Table 4.10 based on Eq. (4.11). Fitting equation based on Eq. (4.14) for displacement curves as function of time is complex. Fitting on displacement curves will be conducted on next section based on $F = \alpha v^n$, where n can be any value.

Table 4.12 Fitting results on velocity of 8 tests using Eq. (4.21)

Test	R^2	b	α
1	0.98	-1.64	0.0100
2	0.99	-2.08	0.0127
3	0.99	-1.33	0.0081
4	0.99	-3.60	0.0220
5	0.99	-4.86	0.0296
6	0.99	-2.02	0.0123
7	0.99	-2.12	0.0129
8	0.97	-3.30	0.0201
Max			0.0296
Min			0.0081
Avg			0.0150
σ			0.0044

4.2.2.3 Define n

Based on fitting results in Section 4.2.2.1 and Section 4.2.2.2, $F = \alpha v^2$ is better to describe the motion of gel actuators at the air-water interface. To confirm the results, fitting on the experiment results was conducted based on $F = \alpha v^n$ (n can be any value).

$$F = \alpha v^n = -m\frac{dv}{dt} \qquad \text{Equation 4.23}$$

Rearrange and integrate equation 4.24,

$$-\frac{\alpha}{m}\int_0^t dt = \int_{v_0}^v v^{-n}dv$$

$$\frac{1}{v^{n-1}} = (n-1)\frac{\alpha}{m}t + v_0^{-(n-1)} \qquad \text{Equation 4.24}$$

$$\frac{1}{v^{n-1}} = At + B \qquad \text{Equation 4.25}$$

where $A = \frac{(n-1)\alpha}{m}, B = v_0^{-(n-1)}$.

Based on Eq. (4.25), there should be a linear relationship between $\frac{1}{v^{n-1}}$ and the time (t) with the slope is $B = v_0^{-(n-1)}$. Velocity curves as function of time when n = 2, n = 3 and n = 4 were shown in Figure 4.50.
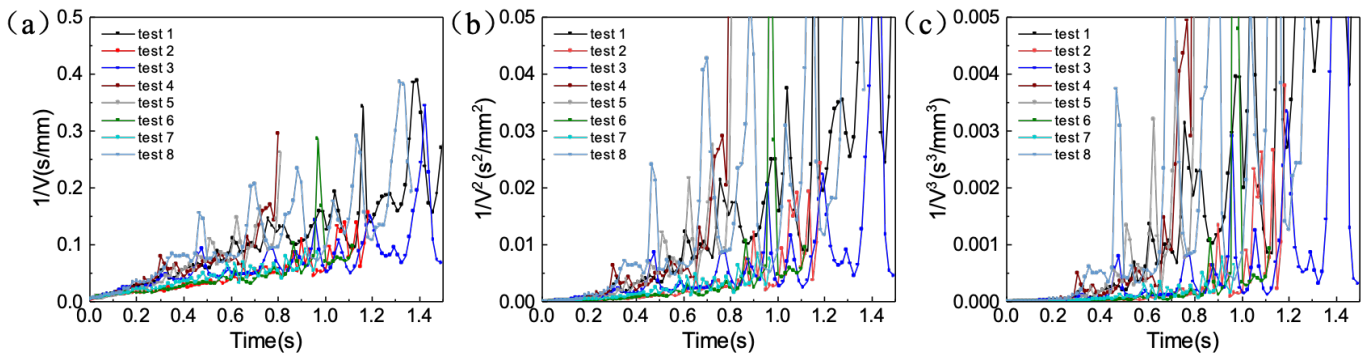
Figure 4.50 Velocity as function of time when (a) n = 2, (b) n = 3 and (c) n = 4.

$$dl = vdt \qquad \text{Equation 4.26}$$

Integrate Equation 4.27 from t=0 to t=t.

$$\int_0^l dl = \int_0^t v\,dt + C$$

where C is the value of $l_{t=0}$ for each test shown in Figure 4.41.

$$l = \int_0^t (At + B)^{-\frac{1}{n-1}}\,dt + C$$

$$= \frac{n-1}{A(n-2)}(At + B)^{\frac{n-2}{n-1}}\big|_{t=0}^{t=t} + C$$

$$l = \frac{n-1}{(n-2)A}\left[(At + B)^{\frac{n-2}{n-1}} - B^{\frac{n-2}{n-1}}\right] + C \qquad \text{Equation 4.27}$$

Relationship between displacement l and time t was shown as Equation 4.28.

Equation 4.28 can be rearranged as following,

$$l + D = \frac{n-1}{(n-2)A}\left[(At + B)^{\frac{n-2}{n-1}}\right]$$

where $D = \frac{n-1}{(n-2)A}B^{\frac{n-2}{n-1}} - C$, let $n^* = \frac{n-2}{n-1}$,

$$l + D = \frac{1}{n^*A}\left[(At + B)^{n^*}\right]$$

$$\ln(l + D) = \ln\frac{1}{n^*A} + n^*\ln(At + B)]$$

$$\ln(l + D) = \ln\frac{1}{n^*A} + n^*\ln A + n^*\ln(t + B/A) \qquad \text{Equation 4.28}$$

To simplify Equation 4.29, let $\ln(l + D) = y$ and $\ln(t + B/A) = x$,

$$y = \ln\frac{1}{n^*A} + n^*\ln A + n^*x$$

$$y = A' + B'x \qquad \text{Equation 4.29}$$

where interception is $A' = \ln\frac{1}{n^*A} + n^*\ln A$ and slope is $B' = n^* = \frac{n-2}{n-1}$,

Thus, a linear fitting can be conducted with Equation 4.30. l and t are two variables in

Equation 4.29, which can be obtained from experimental results. D and B/A were enumerated

conduct fitting and two criteria to evaluate the fitting.

Criterion 1 is R^2 and SSE (sum of squared errors), where large R^2 and small SSE is better.

SSE can be calculated by Equation 4.31.

$$SSE = \sum_{i=1}^{n}(y_i - f(x_i))^2 \qquad\qquad \text{Equation 4.30}$$

Criterion 2 is $\Delta D = |D_{\text{enumerated}} - D_{\text{calculated}}|$ is small. D and B/A were enumerated

independently through the fitting, however, D and B/A has a relationship ($D_{\text{calculated}} =$

$\frac{n-1}{(n-2)A} B^{\frac{n-2}{n-1}} - C$) that was defined in Equation 4.28 and Equation 4.29.

n can be figured out thought slope $n^* = \frac{n-2}{n-1}$. α can be figure out though $ln\frac{1}{n^*A} + n^*lnA$ and

$A = \frac{(n-1)\alpha}{m}$.

Results of fitting were shown in Table 4.13. n in equation F = αv^n was figure out as 2.

Thus, F = αv^2.

Table 4.13 Fitting results of 8 tests using Eq. (4.29)

Test	α	n
1	0.000783	2.003
2	0.000315	2.006
3	0.000393	2.011
4	0.000773	2.027
5	0.000784	2.017
6	0.000308	2.006
7	0.000366	2.006
8	0.001061	2.004
Max	0.001061	2.027
Min	0.000308	2.003
Avg	0.000569	2.008
σ	0.000212	0.004422
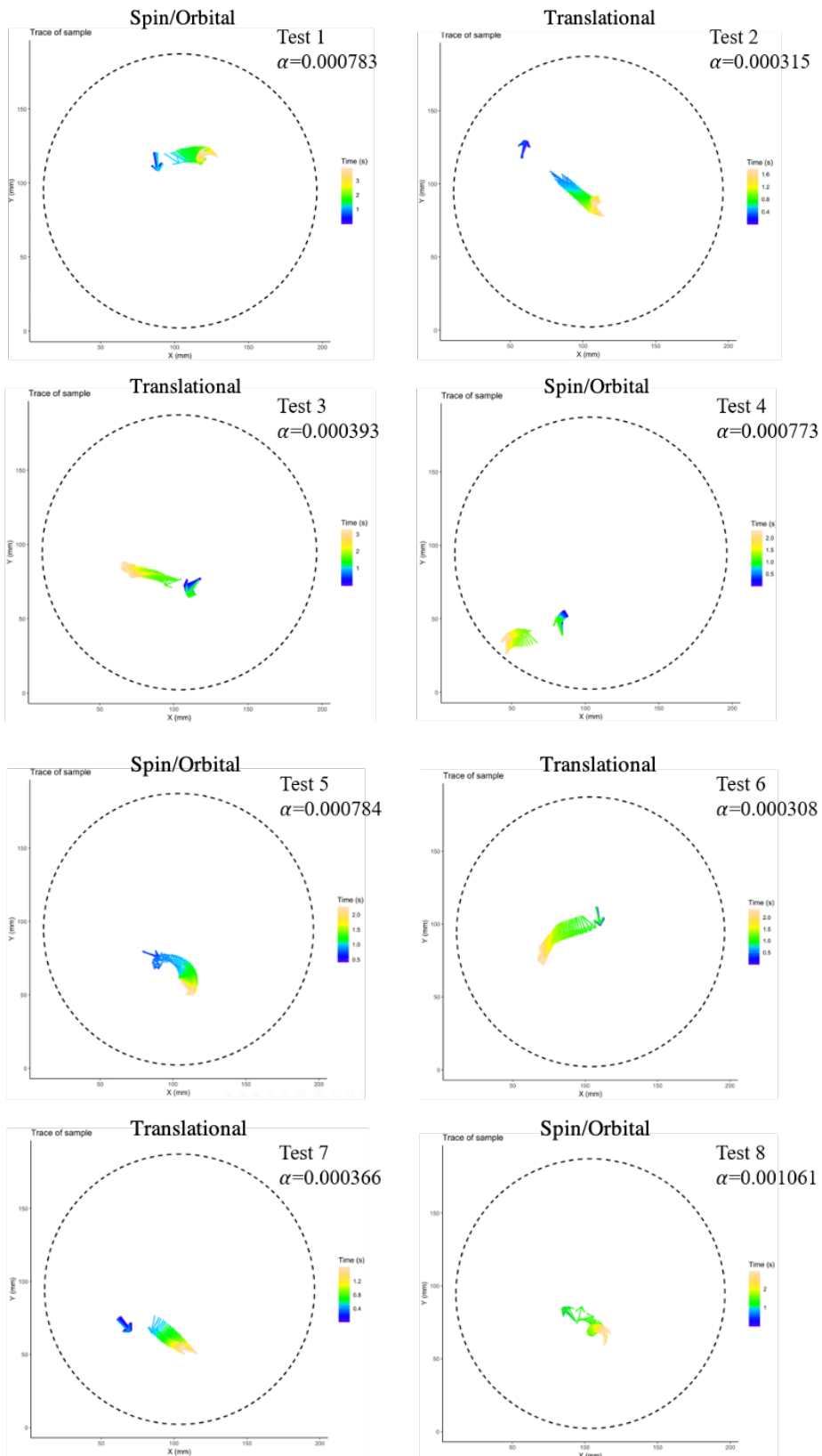
Figure 4.51 Trace and α of the gel on 8 tests

Based on the results and study presented above, it is clear that the friction force (F) acting on a gel moving at air-water surface is $F = \alpha v^2$, where v is the velocity and α is a constant. However, from the results shown in Table 4.13, the value of α changes over a big range. For example, the value of α can be as high as 0.001 and as small as 0.0003. The motion mode for each test is presented in Figure 4.51. Now one can link the value of α with the motion mode. It is found that the translational motion tends to have a small $\alpha_s = 0.000346$ while the motion with orbital or spin tends to have a larger $\alpha_l = 0.000780$. This can be easy to understand since the adding orbital and spin motion to translational motion would require more interaction between the gel and water.

4.3 Conclusion

Three motion modes – spin, translation, orbital motion – were experimentally observed for the gel actuators with different shapes. The motion modes in the first few seconds are not used. Based on the experimental results, it is concluded that the shape/geometry of the gel actuators plays an important role on their motion mode. For example, gel in rectangle shapes with a higher length/width ratio have the tendency of spin motions; gel in circle and square shape have the tendency of orbital motions.

Quantification process was established for output of self-driven motion at the air-water interface. Two markers on the gel actuators are used to determine the coordinate locations as function of time. Variables/parameters about the motion: velocity, acceleration, spin speed, kinetic energy and their time dependence, are able to be obtained. Motion modes of gel actuators in different shape are easy to be clearly illustrated thanks to the trace generated by coordinate points through software.

The periodic fluctuations in the velocity were observed and analyzed. It is concluded that the period fluctuations reflect the interaction between the gel actuator and the glass wall of the container. The velocity of gel actuator decreases as it moves toward the wall of glass beaker, while it increases as it moves away from the wall of glass beaker. Two factors, solvent diffusion and capillary force, may elucidate this phenomenon.

Both relationship between friction force (F) and velocity (v), $F = -\alpha v$ and $F = -\alpha v^2$, were examined by fitting the velocity curve as function of time from 8 tests. α_{avg} from fitting based on $F = -\alpha v^2$ is two order less than the α_{avg} from fitting based $F = -\alpha v$. Fitting based on $F = -\alpha v^2$ is better for overall time period, compared to Fitting based on $F = -\alpha v$. Fitting based on $F = \alpha v^n$, where n can be any value, were also conducted and results show that n = 2. It is concluded that the friction force acting on the gel moving at air-water surface is $F = -\alpha v^2$ and that the value of α is related to the motion mode. For the pure translational mode, the α is the smallest (~0.0003), while for the translational motion with spin/orbital motion, the α is higher (0.0007 ~ 0.001).

Chapter V

Study of energy conversion

Energy conversion through the actuation process was rarely discussed. The input energy of the self-driven actuators is chemical energy stored in the actuators. The chemical energy converts to kinetic energy during the motion of gel at the air-water interface. The consumption of the kinetic energy of a gel during the motion reflects the contribution of the friction force. The research work here is intended to discuss the energy conversion during the motion of a gel, which is a step forward for the understanding of the self-motion actuators.

Kinetic energy of the gel actuators as function of time is obtained from experiment directly using the method shown in Chapter IV. Friction force of the gel actuators on water surface obey $F = -\alpha v^2$ as discussed and concluded in Chapter IV. The chemical energy change of gel actuators can be linked with the mass loss of actuators originated by solvent diffusion.

5.1 Results and discussion

5.1.1 Experimental

Gel was formed in 3D printed mold shown in Figure 2.3. Gel in mold actuators exhibited prolonged translational motion and spin motion with mold shown in Figure 2.3 (a) and (b), respectively. Mass of each mold was measured before gel formation in the molds. And the mass of mold filled with gel was measured before motion at the air-water interface. The mass of mold filled with gel was measured every 60 seconds when the gel actuator is moving at the air-water interface. The mass loss as function of time within 900 seconds is shown in Figure 5.1.
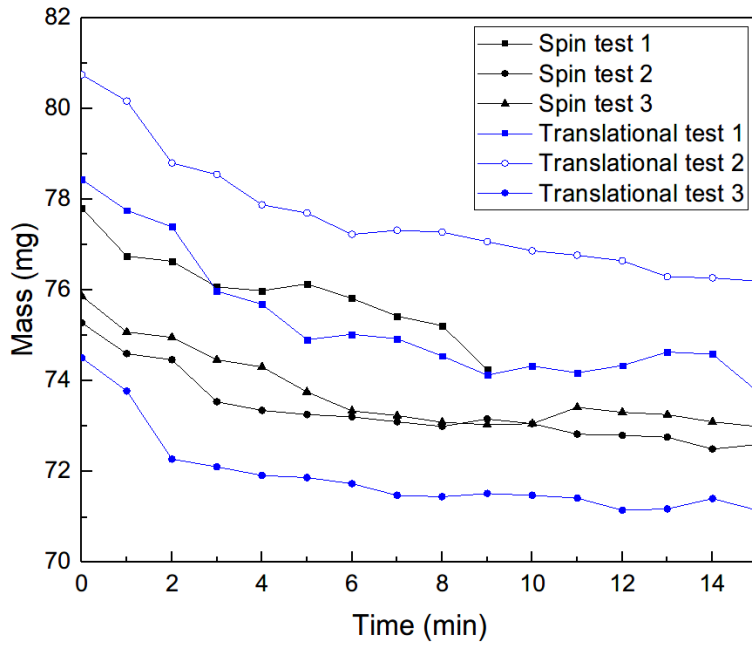
Figure 5.1 Mass of the gel actuator with mold as function of time

5.1.2　Fitting based on an existing model

The mass loss of gel actuator is correlated with solvent diffusion from gel into water. A model is needed to describe the process of solvent diffusion as function of time. Eq. (5.1) describes the concentration as function of location and time for unlimited source diffuses into a semi-infinite bar. The amount of diffusing substance per unit area of surface is denoted as $C(x,t)$. $C_s{}'$ is concentration at the interface. D is diffusion constant of diffusing substance, t is time and x is location from the surface of source.

$$C(x,t) = C_s{}'[1 - \mathrm{erf}\,(\frac{x}{2\sqrt{Dt}})] \qquad \text{Equation 5.1}$$

Amount of substance diffusing into semi-infinite bar at time t is given by integrating Eq. (5.1) with respect to x from 0 to infinite.

$$\int_0^{+\infty} C(x,t)\, dx = \int_0^{+\infty} C_s' \left[1 - \mathrm{erf}\left(\frac{x}{2\sqrt{Dt}}\right)\right] dx$$

$$= C_s' \left[x|_{x=+\infty} - \int_0^{+\infty} \mathrm{erf}\left(\frac{x}{2\sqrt{Dt}}\right) dx\right] \qquad \text{Equation 5.2}$$

Let $z = \frac{x}{2\sqrt{Dt}}$, $0 \le z \le \infty$

$$\int_0^{+\infty} \mathrm{erf}\left(\frac{x}{2\sqrt{Dt}}\right) dx = 2\sqrt{Dt} \int_0^{+\infty} \mathrm{erf}(z)\, dz$$

$$= 2\sqrt{Dt} \times \left[\frac{x}{2\sqrt{Dt}} erf\left(\frac{x}{2\sqrt{Dt}}\right)|_{x=+\infty} - \frac{1}{\sqrt{\pi}}\right] \qquad \text{Equation 5.3}$$

Insert Eq. (5.3) into Eq. (5.2)

$$\int_0^{+\infty} C(x,t)\, dx = C_s \left\{x|_{x=+\infty} - 2\sqrt{Dt} \times \left[\frac{x}{2\sqrt{Dt}} erf\left(\frac{x}{2\sqrt{Dt}}\right)|_{x=+\infty} - \frac{1}{\sqrt{\pi}}\right]\right\}$$

$$= 2C_s'\sqrt{Dt} \times \left[\frac{x}{2\sqrt{Dt}} - \frac{x}{2\sqrt{Dt}} erf\left(\frac{x}{2\sqrt{Dt}}\right)\right]_{x=+\infty} + \frac{2C_s'\sqrt{Dt}}{\sqrt{\pi}} \qquad \text{Equation 5.4}$$

Let $m = \frac{x}{2\sqrt{Dt}}$, $m \to +\infty$ when $x \to +\infty$,

$$\lim_{x \to +\infty} \left[\frac{x}{2\sqrt{Dt}} - \frac{x}{2\sqrt{Dt}} erf\left(\frac{x}{2\sqrt{Dt}}\right)\right] = \lim_{m \to +\infty} [m - m erf(m)] = 0$$

Thus Eq. (5.4) can be rewrite as

$$\int_0^{+\infty} C(x,t)\, dx = \frac{2C_s'\sqrt{Dt}}{\sqrt{\pi}} \qquad \text{Equation 5.5}$$

Mass of substance (m_s) diffused into semi-infinite bar at time t can be calculated using Eq. (5.5).

Therefore, the mass loss curves as function of time of gel actuators can be fitted based on Eq. (5.6), where $a = \frac{2C_s'\sqrt{D}}{\sqrt{\pi}}$.

$$m_s = a\sqrt{t} \qquad \text{Equation 5.6}$$

$$\ln m_s = \ln a + \frac{1}{2} \ln t \qquad \text{Equation 5.7}$$

The time dependence of the mass loss of gel actuators is plotted in Figure 5.2 using logarithm scale for the mass loss and time. Based on Eq. (5.7), there should be a linear relationship between the $ln(m_s)$ and $ln(t)$ with the slope of 0.5.
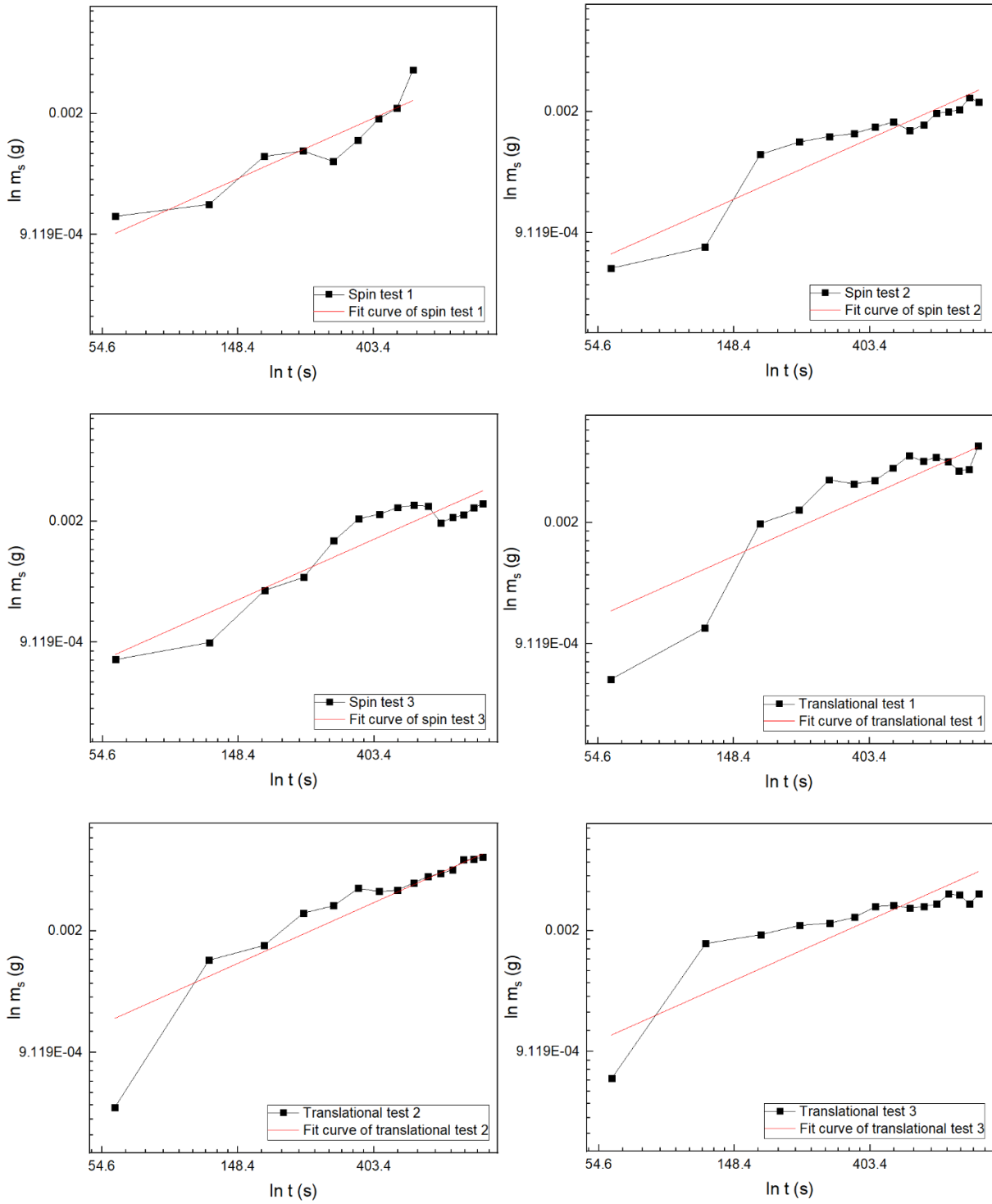
Figure 5.2 Logarithm scale of mass loss of the gel actuator with mold as function of time. Fitting using Eq. (5.7).

Table 5.1 Fitting results of mass loss of the gel actuator with mold using Eq. (5.7). Slope: 0.5.

Test	Intercept	R^2	SSE
Spin test 1	-9.03	0.86	0.16
Spin test 2	-9.22	0.87	0.31
Spin test 3	-9.15	0.89	0.29
Translational test 1	-8.78	0.80	0.82
Translational test 2	-8.77	0.83	0.64
Translational test 3	-8.91	0.71	0.59

The model is not good enough although fitting based on Eq. (5.7) has a high value of R^2 as shown in Table 5.1. Based on the experimental data points, the first one or two points are one order smaller than the rest of data points as shown in Figure 5.2. It is possible that measurements error at the beginning is big. Therefore, the fitting is conducted using a modified equation (i.e., Eq. (5.8)) without the first one or two points marked as hollow square dots in Figure 5.3. Based on Eq. (5.8), there should be a linear relationship between the $ln(m_s)$ and $ln(t)$ with the slope of b, instead of 0.5 in Eq. (5.7).

$$\ln m_s = lna + b\,lnt \qquad\qquad \text{Equation 5.8}$$
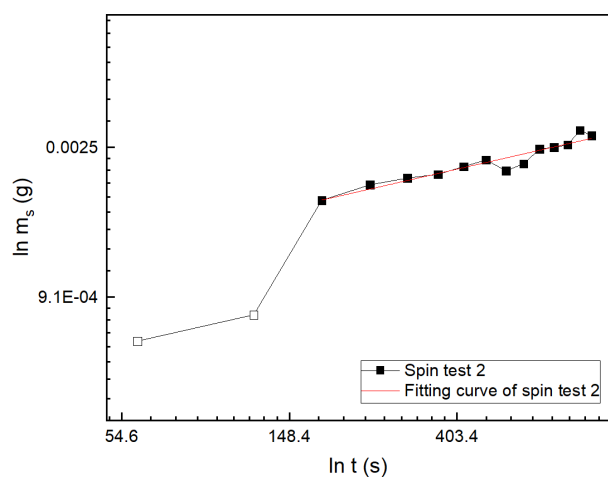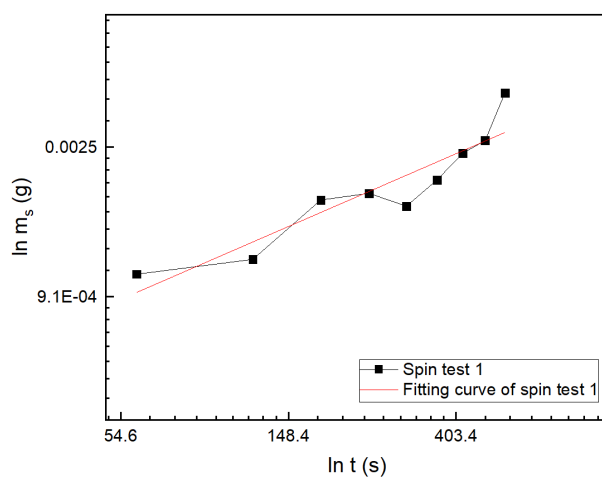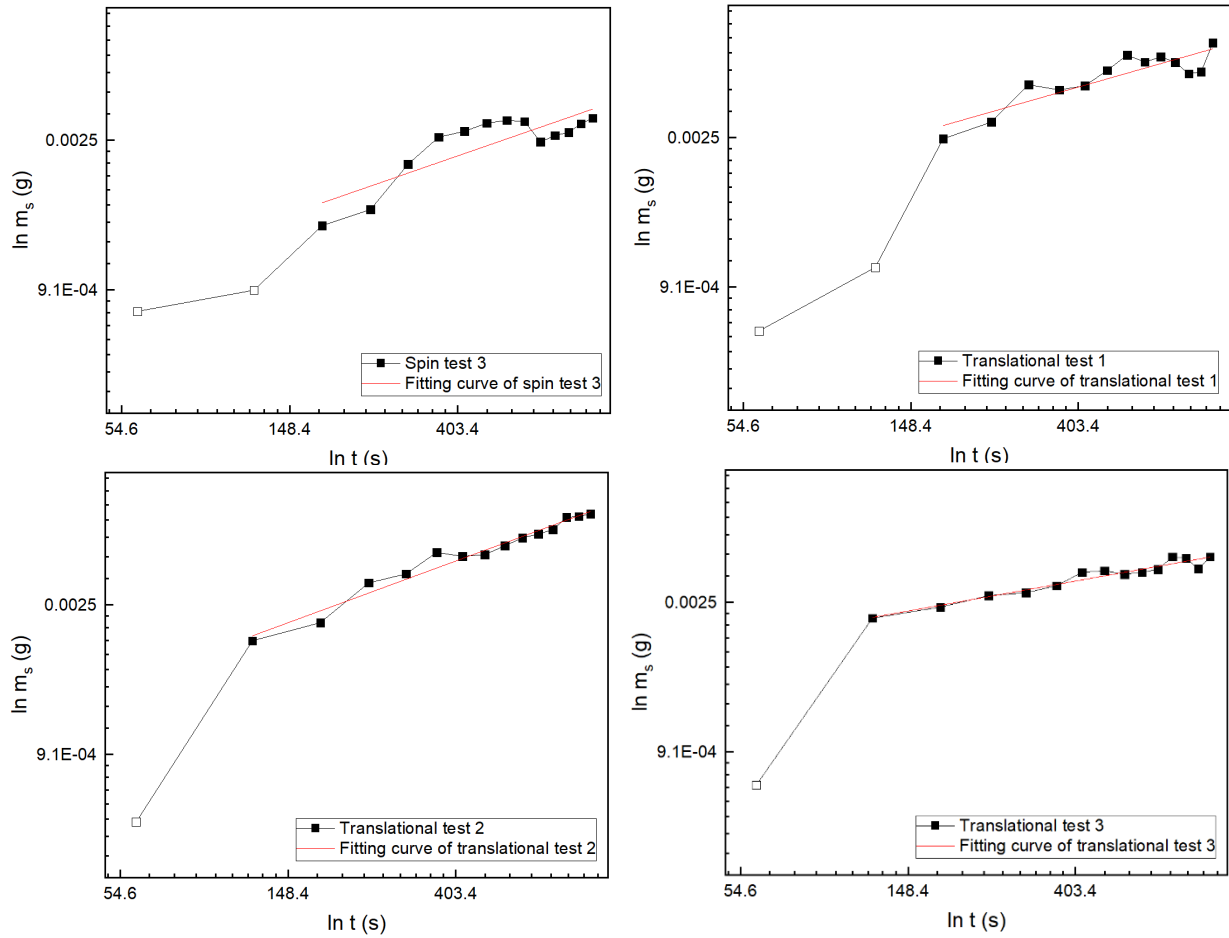
Figure 5.3 Logarithm scale of mass loss of the gel actuator with mold as function of time. Fitting using Eq. (5.8).

Table 5.2 Fitting results of mass loss of the gel actuator with mold using Eq. (5.8).

Test	Intercept	Slope	R^2	SSE
Spin test 1	-8.96	0.49	0.86	0.16
Spin test 2	-7.68	0.26	0.91	0.02
Spin test 3	-8.44	0.39	0.72	0.18
Translational test 1	-7.58	0.32	0.79	0.08
Translational test 2	-8.18	0.41	0.97	0.03
Translational test 3	-7.06	0.20	0.94	0.01

Results shows that the slope varies from 0.3 to 0.49. Fitting based on Eq. (5.8) shows empirical is

better since it has larger value of R^2, compared to the results shown in Table 5.1

The mass loss of gel actuators (gel only) within 24 hours is plotted in Figure 5.4 using logarithm scale for the mass loss and time. Both Eq. (5.7) and Eq. (5.8) state that there is a linear relationship between the $ln(m_s)$ and $ln(t)$ with the one slope, however, there are two slopes of the logarithm scale of mass loss as function of time as shown in Figure 5.4. Period-I (0 to 300 seconds) and Period-II (after 300 seconds) are marked in Figure 5.4. Then, mass loss curves are fitted in Period-I and Period-II using Eq. (5.8), respectively.
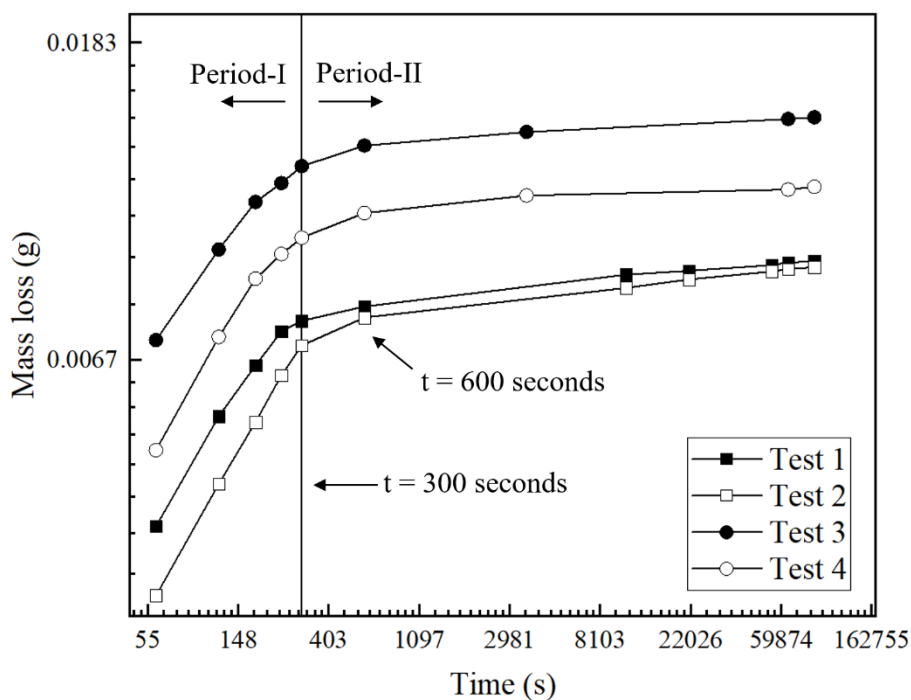
Figure 5.4 Logarithm scale of mass loss of gels (gel only) as function of time. PVDF/ DMF-acetone gel with size in 12 mm × 12 mm.

The results of fitting are shown in Table 5.3 and Table 5.4. The slope of mass loss as function of time in Period-I shown in Figure 5.4 is closed to the slope of mass loss as function of time in Figure 5.2 and Figure 5.3. However, the slope in Period-II is one order less than the slope in Period-I.

Table 5.3 Fitting results of mass loss in Period-I using Eq. (5.8)

Test	Intercept	Slope	R^2	SSE
Test 1	-7.19	0.41	0.98	0.0047
Test 2	-7.76	0.49	0.99	0.0002
Test 3	-6.32	0.34	0.98	0.0032
Test 4	-6.99	0.42	0.98	0.0058

Table 5.4 Fitting results of mass loss in Period-II using Eq. (5.8)

Test	Intercept	Slope	R^2	SSE
Test 1	-5.05	0.032	0.98	0.0006
Test 2	-5.15	0.040	0.96	0.0021
Test 3	-4.49	0.023	0.89	0.0017
Test 4	-4.70	0.023	0.80	0.0036

Figure 3.5 shows one slope of each test until 900 seconds, which is longer than the time of Period-I (0 to 300 seconds) and even longer than the time of first point in Period-II (t = 600 seconds). It should be mentioned that there are two different types of samples. Figure (5.1) – (5.3) shows mass loss of the gel with mold at the air-water interface, while Figure 5.4 shows mass loss of pure gel at the air-water interface, which is the most cases in this study. It is possible that the only two windows on the wall of mold limit solvent diffusion, which postpones the time proceeding to Period-II. That is, 900 seconds is still in Period-I for the case of gel with mold.

5.1.3 Fitting based on a new model

Although attempts were made to modify Eq. (5.7), both Eq. (5.9) and Eq. (5.8) are based on an assumption of unlimited source. In fact, the amount organic solvent in the gel actuator decreases as time. A model is built using the boundary condition of the real situation. A scheme of concentration distribution is shown in Figure 5.5. *C* represents concentration and *x* represents

location. $0 \leq x \leq R$ is region in the gel and $R \leq x \leq \infty$ is region of water. Amount of solvent in the

gel is limited and decreases as time and the solvent accumulate in the water region.
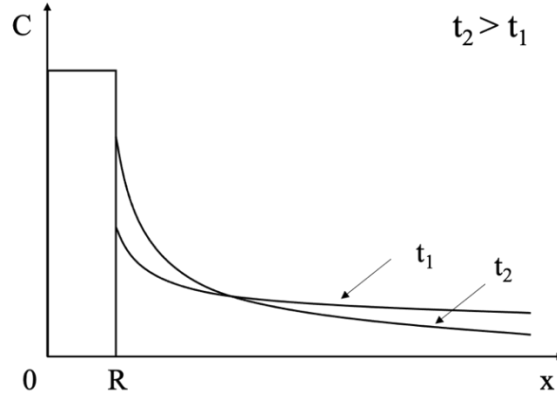
Figure 5.5 Scheme of concentration curves for limited solvent source

Consider the problem of diffusion in a semi-infinite medium. All diffusing substance is

concentrated initially concentrated in a finite region, $0 \leq x \leq R$, Region-I. The diffusing substance

at the initial state is C_s and diffuses into a semi-infinite region, $R \leq x \leq \infty$, Region-II $C(x,t)$ is the

amount of diffusing substance per unit area of surface. D is diffusion coefficient.

$$\frac{\partial C_1(x,t)}{\partial t} = D_1 \frac{\partial^2 C_1(x,t)}{\partial x^2} \ , \ 0 \leq x \leq R \qquad \text{Equation 5.9}$$

$$\frac{\partial C_2(x,t)}{\partial t} = D_2 \frac{\partial^2 C_2(x,t)}{\partial x^2} \ , \ R \leq x \leq \infty \qquad \text{Equation 5.10}$$

Initial state was defined by

$$C_1(x,0) = C_s, C_2(x,0) = 0 \qquad \text{Equation 5.11}$$

Concentrations at the interface$(x = R)$were equal at any time.

$$C_1(R,t) = C_2(R,t) \qquad \text{Equation 5.12}$$

Mass conservation law

$$-D_1 \frac{\partial C_1(R,t)}{\partial x} = -D_2 \frac{\partial C_2(R,t)}{\partial x} \qquad \text{Equation 5.13}$$

Physical condition, no mass transfer to surrounding.

$$\frac{\partial C_2(\infty,t)}{\partial x} = 0 \qquad\qquad \text{Equation 5.14}$$

Laplace's transform of Eq. (5.9)

$$L[D_1 \frac{\partial^2 C_1(x,t)}{\partial x^2}] - L\left[\frac{\partial C_1(x,t)}{\partial t}\right] = 0$$

$$D_1 \frac{\partial^2 W_1(x,s)}{\partial x^2} - [sW_1(x,s) - C_1(x,0)] = 0$$

$$\frac{\partial^2 W_1(x,s)}{\partial x^2} - \left[\frac{s}{D_1} W_1(x,s) - \frac{C_s}{D_1}\right] = 0 \qquad\qquad \text{Equation 5.15}$$

Solution of Eq. (5.15) will be

$$W_1(x,s) = \frac{C_s}{s} + A_1 e^{\sqrt{\frac{s}{D_1}}x} + B_1 e^{-\sqrt{\frac{s}{D_1}}x} \qquad\qquad \text{Equation 5.16}$$

Similarly, Laplace's transform of Eq. (5.10) and solution will be

$$W_2(x,s) = A_2 e^{\sqrt{\frac{s}{D_2}}x} + B_2 e^{-\sqrt{\frac{s}{D_2}}x}$$

Apply physical condition that no mass transfer to surrounding, $A_2 = 0$.

$$W_2(x,s) = B_2 e^{-\sqrt{\frac{s}{D_2}}x} \qquad\qquad \text{Equation 5.17}$$

Combine Eq. (5.16), Eq. (5.17) and Eq. (5.12).

$$W_1(R,s) = W_2(R,s)$$

$$\frac{C_s}{s} + A_1 e^{\sqrt{\frac{s}{D_1}}R} + B_1 e^{-\sqrt{\frac{s}{D_1}}R} = B_2 e^{-\sqrt{\frac{s}{D_2}}R} \qquad\qquad \text{Equation 5.18}$$

Combine Eq. (5.16), Eq. (5.17) and Eq. (5.13).

$$-D_1 \frac{\partial W_1(R,s)}{\partial x} = -D_2 \frac{\partial W_2(R,s)}{\partial x}$$

$$D_1 \sqrt{\frac{s}{D_1}} A_1 e^{\sqrt{\frac{s}{D_1}}R} - D_1 \sqrt{\frac{s}{D_1}} B_1 e^{-\sqrt{\frac{s}{D_1}}R} = -D_2 \sqrt{\frac{s}{D_2}} B_2 e^{-\sqrt{\frac{s}{D_2}}R}$$

$$k[A_1 e^{\sqrt{\frac{s}{D_1}}R} - B_1 e^{-\sqrt{\frac{s}{D_1}}R}] = -B_2 e^{-\sqrt{\frac{s}{D_2}}R} \qquad\qquad \text{Equation 5.19}$$

where $k = \sqrt{\frac{D_1}{D_2}}$

Amount of substance from 0 to infinite is constant and equal to the diffusing substance at the initial

state, C_s.

$$C_s = \int_0^R C_1(x,t)dx + \int_R^{+\infty} C_2(x,t)dx$$

$$C_s/s = \int_0^R W_1(x,s)dx + \int_R^{+\infty} W_2(x,s)dx$$

$$C_s/s = \int_0^R \left[\frac{C_s}{s} + A_1 e^{\sqrt{\frac{s}{D_1}}x} + B_1 e^{-\sqrt{\frac{s}{D_1}}x}\right]dx + \int_R^{+\infty}\left[B_2 e^{-\sqrt{\frac{s}{D_2}}x}\right]dx$$

$$\frac{C_s}{\sqrt{s\,D_2}} = \frac{C_s\,R}{\sqrt{s\,D_2}} + k\left(A_1 e^{\sqrt{\frac{s}{D_1}}R} - B_1 e^{-\sqrt{\frac{s}{D_1}}R} - A_1 + B_1\right) + B_2 e^{-\sqrt{\frac{s}{D_2}}R} \qquad \text{Equation 5.20}$$

Combine Eq. (5.18) – (5.20) to find A_1, B_1 and B_2.

$$A_1 = -\frac{C_s(s - ks - Rs + kRs + e^{R\sqrt{\frac{s}{D_1}}}k\sqrt{D_2 s})}{ks\sqrt{D_2 s}[1 - k + (1+k)e^{2R\sqrt{\frac{s}{D_1}}}]}$$

$$B_1 = -\frac{e^{R\sqrt{\frac{s}{D_1}}}C_s(-e^{R\sqrt{\frac{s}{D_1}}}s - e^{R\sqrt{\frac{s}{D_1}}}ks + e^{R\sqrt{\frac{s}{D_1}}}Rs + e^{R\sqrt{\frac{s}{D_1}}}kRs + k\sqrt{D_2 s})}{ks\sqrt{D_2 s}[1 - k + (1+k)e^{2R\sqrt{\frac{s}{D_1}}}]}$$

$$B_2 = \frac{e^{R\sqrt{\frac{s}{D_2}}}C_s(2e^{R\sqrt{\frac{s}{D_1}}}s - 2e^{R\sqrt{\frac{s}{D_1}}}Rs - k\sqrt{D_2 s} + e^{2R\sqrt{\frac{s}{D_1}}}k\sqrt{D_2 s})}{s\sqrt{D_2 s}[1 - k + (1+k)e^{2R\sqrt{\frac{s}{D_1}}}]}$$

Simplify the results above utilizing Eq. (5.21).

$$\frac{1}{1-x} = \sum_{n=0}^{\infty} x^n \; (|x| < 1) \qquad\qquad \text{Equation 5.21}$$

Denominator for A_1 and B_1 will be rearrange as following,

$$Deno = \frac{1}{ks\sqrt{D_2 s}\left[1 - k + (1+k)e^{2R\sqrt{\frac{s}{D_1}}}\right]}$$

$$Deno = \frac{1}{ks\sqrt{D_2 s}(1+k)e^{2R\sqrt{\frac{s}{D_1}}}\left[\frac{1-k}{1+k}e^{-2R\sqrt{\frac{s}{D_1}}}+1\right]}$$

$$Deno = \frac{1}{ks\sqrt{D_2 s}(1+k)e^{2R\sqrt{\frac{s}{D_1}}}} \times \frac{1}{1-(-he^{-2R\sqrt{\frac{s}{D_1}}})}$$

where $h = \frac{1-k}{1+k}$,

$$Deno = \frac{1}{ks\sqrt{D_2 s}(1+k)e^{2R\sqrt{\frac{s}{D_1}}}} \times \sum_{n=0}^{\infty}(-he^{-2R\sqrt{\frac{s}{D_1}}})^n$$

$$Deno = \frac{1}{ks\sqrt{D_2 s}(1+k)e^{2R\sqrt{\frac{s}{D_1}}}} \times \sum_{n=1}^{\infty}(-he^{-2R\sqrt{\frac{s}{D_1}}})^{n-1}$$

$$Deno = \frac{1}{s\sqrt{D_2 s}k(1+k)} \times \sum_{n=1}^{\infty}(-h)^{n-1}e^{-2nR\sqrt{\frac{s}{D_1}}}$$

Thus,

$$A_1 = -\frac{C_s(1-R)h}{\sqrt{D_2 s}k} \times \sum_{n=1}^{\infty}(-h)^{n-1}e^{-(2n-0)R\sqrt{\frac{s}{D_1}}} - \frac{C_s}{s(1+k)} \times \sum_{n=1}^{\infty}(-h)^{n-1}e^{-(2n-1)R\sqrt{\frac{s}{D_1}}}$$

Equation 5.22

$$B_1 = -\frac{C_s}{s(1+k)} \times \sum_{n=1}^{\infty}(-h)^{n-1}e^{-(2n-1)R\sqrt{\frac{s}{D_1}}} + \frac{C_s(1-R)}{\sqrt{D_2 s}k} \times \sum_{n=1}^{\infty}(-h)^{n-1}e^{-(2n-2)R\sqrt{\frac{s}{D_1}}}$$

Equation 5.23

Similarly, denominator for B_2 will be

$$Deno = \frac{1}{s\sqrt{D_2 s}(1+k)} \times \sum_{n=1}^{\infty}(-h)^{n-1}e^{-2nR\sqrt{\frac{s}{D_1}}}$$

$$B_2 = -\frac{C_s k}{s(1+k)} \times \sum_{n=1}^{\infty} (-h)^{n-1} e^{-2nR\sqrt{\frac{s}{D_1}}+R\sqrt{\frac{s}{D_2}}}$$

$$+\frac{2C_s(1-R)}{\sqrt{D_2}s(1+k)} \times \sum_{n=1}^{\infty} (-h)^{n-1} e^{(-2n+1)R\sqrt{\frac{s}{D_1}}+R\sqrt{\frac{s}{D_2}}}$$

$$+\frac{C_s k}{s(1+k)} \times \sum_{n=1}^{\infty} (-h)^{n-1} e^{(-2n+2)R\sqrt{\frac{s}{D_1}}+R\sqrt{\frac{s}{D_2}}}$$

$$B_2 = -\frac{C_s k}{s(1+k)} \times \sum_{n=1}^{\infty} (-h)^{n-1} e^{\left(-(2n-0)Rk^{-1}+R\right)\sqrt{\frac{s}{D_2}}}$$

$$+\frac{2C_s(1-R)}{\sqrt{D_2}s(1+k)} \times \sum_{n=1}^{\infty} (-h)^{n-1} e^{(-(2n-1)Rk^{-1}+R)\sqrt{\frac{s}{D_2}}}$$

$$+\frac{C_s k}{s(1+k)} \times \sum_{n=1}^{\infty} (-h)^{n-1} e^{(-(2n-2)Rk^{-1}+R)\sqrt{\frac{s}{D_2}}}$$

Equation 5.24

Insert Eq. (5.22) – (5.24) into $W_1(x,s)$ and $W_2(x,s)$.

$$W_1(x,s) = \frac{C_s}{s} - \frac{C_s(1-R)h}{\sqrt{D_2}sk} \times \sum_{n=1}^{\infty} (-h)^{n-1} e^{-[(2n-0)R-x]\sqrt{\frac{s}{D_1}}}$$

$$-\frac{C_s}{s(1+k)} \times \sum_{n=1}^{\infty} (-h)^{n-1} e^{-[(2n-1)R-x]\sqrt{\frac{s}{D_1}}}$$

$$-\frac{C_s}{s(1+k)} \times \sum_{n=1}^{\infty} (-h)^{n-1} e^{-[(2n-1)R+x]\sqrt{\frac{s}{D_1}}}$$

$$+\frac{C_s(1-R)}{\sqrt{D_2}sk} \times \sum_{n=1}^{\infty} (-h)^{n-1} e^{-[(2n-2)R+x]\sqrt{\frac{s}{D_1}}}$$

Equation 5.25

$$W_2(x,s) = -\frac{C_s k}{s(1+k)} \times \sum_{n=1}^{\infty} (-h)^{n-1} e^{(-[(2n-0)Rk^{-1}-R+x])\sqrt{\frac{s}{D_2}}}$$

$$+ \frac{2C_s(1-R)}{\sqrt{D_2}s(1+k)} \times \sum_{n=1}^{\infty} (-h)^{n-1} e^{(-[(2n-1)Rk^{-1}-R+x])\sqrt{\frac{s}{D_2}}}$$

$$+ \frac{C_s k}{s(1+k)} \times \sum_{n=1}^{\infty} (-h)^{n-1} e^{(-[(2n-2)Rk^{-1}-R+x])\sqrt{\frac{s}{D_2}}}$$

<div align="right">Equation 5.26</div>

Inverse Laplace Transform of Eq. (5.25) and Eq. (5.26) using Eq. (5.27). Transform $W_1(x,s)$

and $W_2(x,s)$ to $C_1(x,t)$ and $C_2(x,t)$, respectively.

$$L^{-1}\left[\frac{1}{s}e^{-k\sqrt{s}}\right] = \text{erfc}\left(\frac{k}{2\sqrt{t}}\right) , L^{-1}\left[\frac{1}{\sqrt{s}}e^{-k\sqrt{s}}\right] = \frac{1}{\sqrt{\pi t}}e^{-\frac{k^2}{4t}} \quad \text{Equation 5.27}$$

$$C_1(x,t) = C_s - \frac{C_s(1-R)h}{k\sqrt{D_2\pi t}} \times \sum_{n=1}^{\infty} (-h)^{n-1} e^{-\left[\frac{(2n-0)R-x}{2\sqrt{D_1 t}}\right]^2}$$

$$- \frac{C_s}{1+k}$$

$$\times \left(\sum_{n=1}^{\infty} (-h)^{n-1} \, erfc\left[\frac{(2n-1)R-x}{2\sqrt{D_1 t}}\right] \right.$$

$$+ \sum_{n=1}^{\infty} (-h)^{n-1} \, erfc\left[\frac{(2n-1)R+x}{2\sqrt{D_1 t}}\right] \Bigg)$$

$$+ \frac{C_s(1-R)}{k\sqrt{D_2\pi t}} \times \sum_{n=1}^{\infty} (-h)^{n-1} e^{-\left[\frac{(2n-2)R+x}{2\sqrt{D_1 t}}\right]^2}$$

<div align="right">Equation 5.28</div>

$$C_2(x,t) = -\frac{C_s k}{(1+k)} \sum_{n=1}^{\infty} (-h)^{n-1} \, erfc\left[\frac{(2n-0)Rk^{-1} - R + x}{2\sqrt{D_2 t}}\right]$$

$$+ \frac{2C_s(1-R)}{(1+k)\sqrt{D_2 \pi t}} \sum_{n=1}^{\infty} (-h)^{n-1} \, e^{-\left[\frac{(2n-1)Rk^{-1} - R + x}{2\sqrt{D_2 t}}\right]^2}$$

$$+ \frac{C_s k}{(1+k)} \sum_{n=1}^{\infty} (-h)^{n-1} \, erfc\left[\frac{(2n-2)Rk^{-1} - R + x}{2\sqrt{D_2 t}}\right]$$

<div align="right">Equation 5.29</div>

where $k = \sqrt{\frac{D_1}{D_2}}$, $h = \frac{1-k}{1+k}$.

Eq. (5.28) and Eq. (5.29) describe the case that a limited source diffused into a semi-infinite bar.

Eq. (5.28) depicts the concentration in the Region-I that substance initially concentrated in. Eq. (5.29) depict the concentration in the Region-II. In this work, the Region-I is gel region, and the Region-II is water region. $C_1(x,t)$ and $C_2(x,t)$ are be plotted using MATLAB.
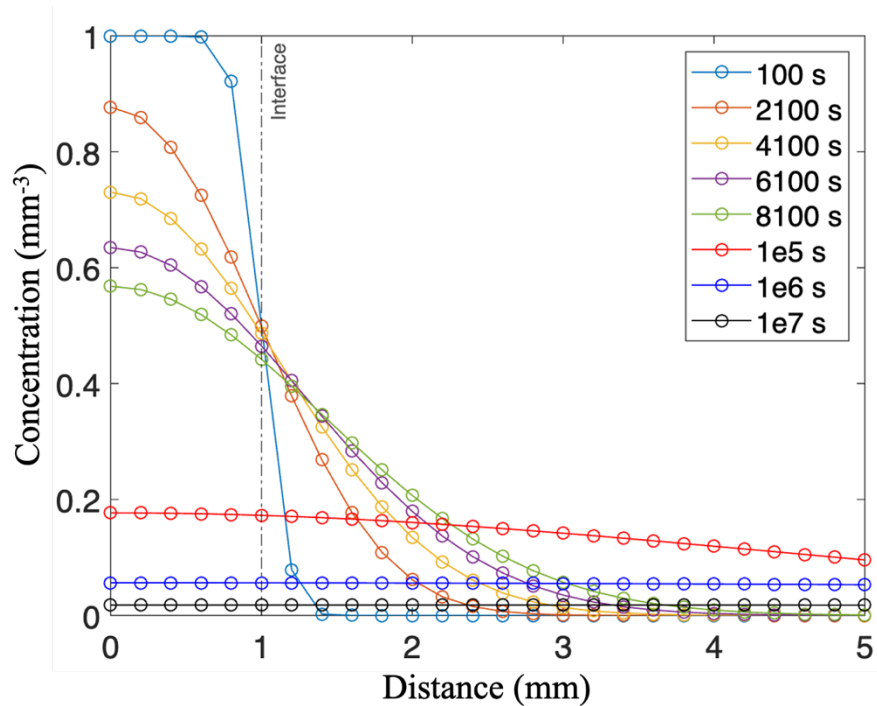
Figure 5.6 Concentration as function of location and time plotted using Eq. (5.28) and Eq. (5.29), $D_1 = D_2 = 1\times10^{-4}$ mm^2/s, $Cs = 1$ mm^{-3} and $R = 1$ mm.

Figure 5.6 illustrated concentration of substance diffused from gel into water as function of time, where $x = 1$ mm is the interface of gel and water. As shown in Figure 5.6, the source of substance in the gel decreases as time, which is one of the purposes to build this model. In addition, the concentration at $x = 2$ mm increases at the beginning and then decreases for long time. The concentration increases because substance diffuses into and accumulates in this region. Then, for long time (i.e., $t = 10^7$ seconds), concentration decreases because the substance in diffuses to infinite area.
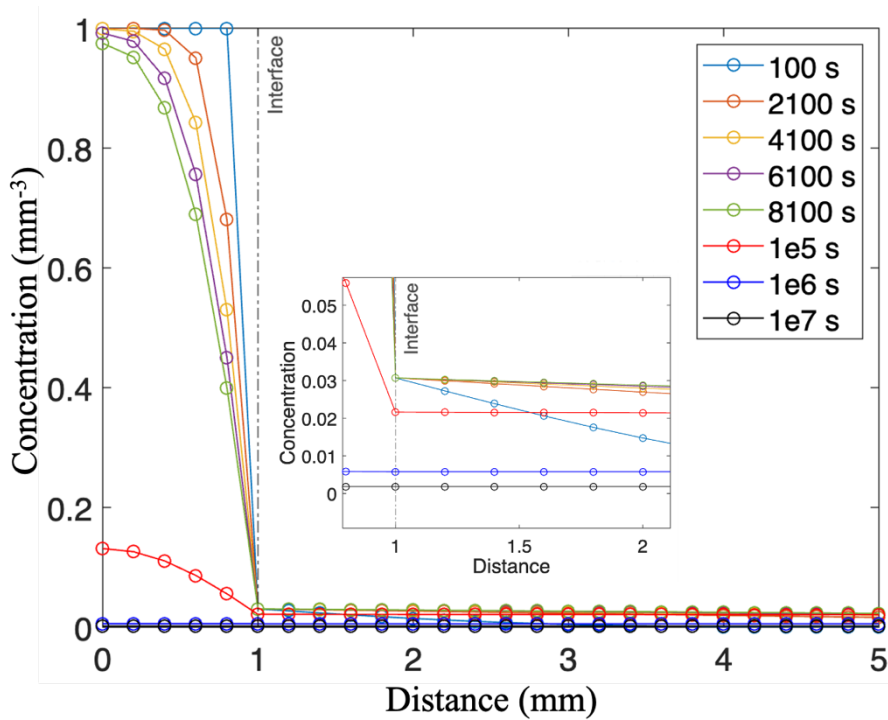
Figure 5.7 Concentration as function of location and time plotted using Eq. (5.28) and Eq. (5.29), $D_1 = 1\times10^{-5}$ mm^2/s, $D_2 = 1\times10^{-2}$ mm^2/s, $Cs=1$ mm^{-3} and $R = 1$ mm.

The concentration at interface is as low as about 0. 1 mm^{-3} when D_1 is three orders less than D_2 as shown in Figure 5.7. While the concentration at interface is in the value that is closed to Cs when D_1 is two orders large than D_2 as shown in Figure 5.8. The concentration curves at $t = 100$ seconds

is plotted when D_1 is fixed at a value of 1×10^{-3} mm^2/s and D_2 varies from 1×10^{-7} mm^2/s to 1×10^0 mm^2/s. The concentration at the interface decreases as D_2 increases as shown in Figure 5.9. In addition, concentration curves in the Region-II are flat and close to $C = 0$ mm^{-3} as D_2 increase, which is similar to the case shown in Figure 5.7. A relatively low concentration in the Region-II is close to the real case in the experiment that gel actuators moving randomly at the air-water interface.
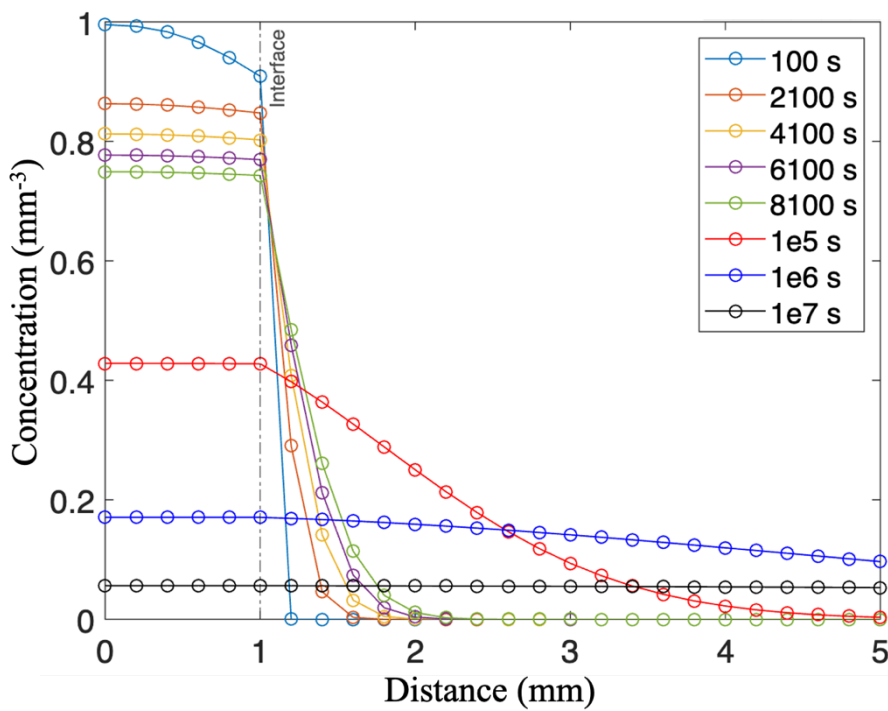
Figure 5.8 Concentration as function of location and time plotted using Eq. (5.28) and Eq. (5.29), $D_1 = 1 \times 10^{-3}$ mm^2/s, $D_2 = 1 \times 10^{-5}$ mm^2/s, $Cs=1$ mm^{-3} and $R = 1$ mm
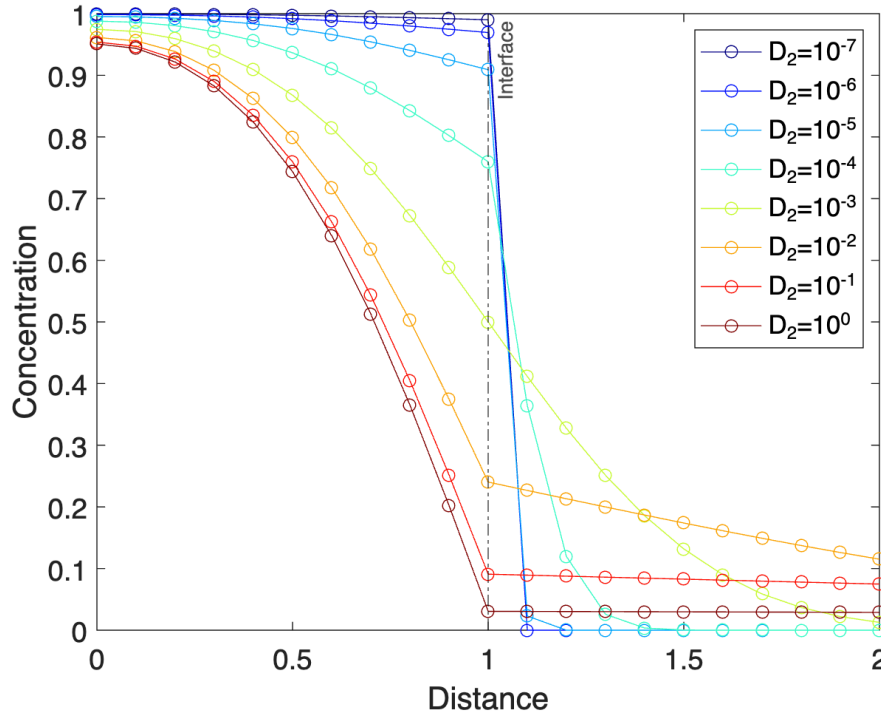
Figure 5.9 Concentration as function of location and time plotted using Eq. (5.28) and Eq. (5.29), $D_1 = 1 \times 10^{-3}\ mm^2/s$, $Cs=1\ mm^{-3}$, $R = 1\ mm$ and t = 100 seconds.

For long time (e.g., t = 10^6 seconds), the concentration curve has a trend to be flat as shown in Figure (5.6) – (5.8). This is a hint to simplify Eq. (5.28) and Eq. (5.29) in two time periods, i.e., short time and long time.

To simplify Eq. (5.28) in the case of short time, both error function and exponential series converges rapidly for all except large values of $D_1 t/R^2$. For example, series of error function and exponential at the $x = 0$ when $D_1 t/R^2 = 1$, where $0 < h = \frac{1-k}{1+k} < 1$.

$$\sum_{n=1}^{\infty} (-h)^{n-1} e^{-\left[\frac{(2n-0)R-x}{2\sqrt{D_1 t}}\right]^2} = 0.1353 - 0.0003h + 1.5230 \times 10^{-8} h^2$$

$$\sum_{n=1}^{\infty} (-h)^{n-1} erfc\left[\frac{(2n-1)R-x}{2\sqrt{D_1 t}}\right] = 0.4795 - 0.0339h + 0.0004h^2 - 7.4310 \times 10^{-8} h^3$$

And when $D_1 t/R^2 = 0.25$

$$\sum_{n=1}^{\infty} (-h)^{n-1} e^{-\left[\frac{(2n-0)R-x}{2\sqrt{D_1 t}}\right]^2} = 0.0183 - 1.2664 \times 10^{-14} h$$

$$\sum_{n=1}^{\infty} (-h)^{n-1} erfc\left[\frac{(2n-1)R-x}{2\sqrt{D_1 t}}\right] = 0.1573 - 2.0000 \times 10^{-5} h + 1.5374 \times 10^{-12} h^2$$

Conservatively, five terms were enumerated for each error function and exponential series.

$$C_1(x,t) = C_s - \frac{C_s(1-R)h}{k\sqrt{D_2 \pi t}} \times \left(e^{-\left[\frac{2R-x}{2\sqrt{D_1 t}}\right]^2} - he^{-\left[\frac{4R-x}{2\sqrt{D_1 t}}\right]^2} \right.$$

$$\left. + h^2 e^{-\left[\frac{6R-x}{2\sqrt{D_1 t}}\right]^2} - h^3 e^{-\left[\frac{8R-x}{2\sqrt{D_1 t}}\right]^2} + h^4 e^{-\left[\frac{10R-x}{2\sqrt{D_1 t}}\right]^2} \right)$$

$$- \frac{C_s}{1+k}$$

$$\times \left(erfc\left(\frac{R-x}{2\sqrt{D_1 t}}\right) - h\, erfc\left(\frac{3R-x}{2\sqrt{D_1 t}}\right) + h^2 erfc\left(\frac{5R-x}{2\sqrt{D_1 t}}\right) \right.$$

$$- h^3 erfc\left(\frac{7R-x}{2\sqrt{D_1 t}}\right) + h^4 erfc\left(\frac{9R-x}{2\sqrt{D_1 t}}\right) + erfc\left(\frac{R+x}{2\sqrt{D_1 t}}\right) - h\, erfc\left(\frac{3R+x}{2\sqrt{D_1 t}}\right)$$

$$\left. + h^2 erfc\left(\frac{5R+x}{2\sqrt{D_1 t}}\right) - h^3 erfc\left(\frac{7R+x}{2\sqrt{D_1 t}}\right) + h^4 erfc\left(\frac{9R+x}{2\sqrt{D_1 t}}\right) \right)$$

$$+ \frac{C_s(1-R)}{k\sqrt{D_2 \pi t}} \times \left(e^{-\left[\frac{x}{2\sqrt{D_1 t}}\right]^2} \right.$$

$$\left. - he^{-\left[\frac{2R+x}{2\sqrt{D_1 t}}\right]^2} + h^2 e^{-\left[\frac{4R+x}{2\sqrt{D_1 t}}\right]^2} - h^3 e^{-\left[\frac{6R+x}{2\sqrt{D_1 t}}\right]^2} + h^4 e^{-\left[\frac{8R+x}{2\sqrt{D_1 t}}\right]^2} \right)$$

<div align="right">Equation 5.30</div>

Amount of substance diffused into region $R \leq x \leq \infty$ at time t is given by integrating Eq. (5.30) with respect to x from 0 to R.

$$m_s = \int_0^R C_1(x,t)\, dx$$

$$\int_0^R C_1(x,t)\,dx = C_s R$$

$$- C_s(1-R)h$$

$$\times \left\{ \left[-erf\left(\frac{R}{2\sqrt{D_1 t}}\right) + erf\left(\frac{R}{\sqrt{D_1 t}}\right) \right] - h\left[-erf\left(\frac{3R}{2\sqrt{D_1 t}}\right) + erf\left(\frac{2R}{\sqrt{D_1 t}}\right) \right] \right.$$

$$+ h^2\left[-erf\left(\frac{5R}{2\sqrt{D_1 t}}\right) + erf\left(\frac{3R}{\sqrt{D_1 t}}\right) \right] - h^3\left[-erf\left(\frac{7R}{2\sqrt{D_1 t}}\right) \right.$$

$$\left. + erf\left(\frac{4R}{\sqrt{D_1 t}}\right) \right] + h^4\left[-erf\left(\frac{9R}{2\sqrt{D_1 t}}\right) + erf\left(\frac{5R}{\sqrt{D_1 t}}\right) \right] \right\}$$

$$- \frac{C_s}{1+k}$$

$$\times \left\{ R + \frac{2\sqrt{D_1 t}}{\sqrt{\pi}} - \frac{2\sqrt{D_1 t}}{\sqrt{\pi}} e^{-\left[\frac{R}{2\sqrt{D_1 t}}\right]^2} - R\,erf\left(\frac{R}{2\sqrt{D_1 t}}\right) \right.$$

$$- h\left[R - R\,erf\left(\frac{R}{\sqrt{D_1 t}}\right) + \frac{2\sqrt{D_1 t}}{\sqrt{\pi}} e^{-\left[\frac{R}{\sqrt{D_1 t}}\right]^2} - \frac{2\sqrt{D_1 t}}{\sqrt{\pi}} e^{-\left[\frac{3R}{2\sqrt{D_1 t}}\right]^2} \right.$$

$$\left. + 3R\,erf\left(\frac{R}{\sqrt{D_1 t}}\right) - 3R\,erf\left(\frac{3R}{2\sqrt{D_1 t}}\right) \right]$$

$$+ h^2\left[R - R\,erf\left(\frac{2R}{\sqrt{D_1 t}}\right) + \frac{2\sqrt{D_1 t}}{\sqrt{\pi}} e^{-\left[\frac{2R}{\sqrt{D_1 t}}\right]^2} - \frac{2\sqrt{D_1 t}}{\sqrt{\pi}} e^{-\left[\frac{5R}{2\sqrt{D_1 t}}\right]^2} \right.$$

$$\left. + 5R\,erf\left(\frac{2R}{\sqrt{D_1 t}}\right) - 5R\,erf\left(\frac{5R}{2\sqrt{D_1 t}}\right) \right]$$

$$- h^3\left[R - R\,erf\left(\frac{3R}{\sqrt{D_1 t}}\right) + \frac{2\sqrt{D_1 t}}{\sqrt{\pi}} e^{-\left[\frac{3R}{\sqrt{D_1 t}}\right]^2} - \frac{2\sqrt{D_1 t}}{\sqrt{\pi}} e^{-\left[\frac{7R}{2\sqrt{D_1 t}}\right]^2} \right.$$

$$\left. + 7R\,erf\left(\frac{3R}{\sqrt{D_1 t}}\right) - 7R\,erf\left(\frac{7R}{2\sqrt{D_1 t}}\right) \right]$$

$$+ h^4\left[R - R\,erf\left(\frac{4R}{\sqrt{D_1 t}}\right) + \frac{2\sqrt{D_1 t}}{\sqrt{\pi}} e^{-\left[\frac{4R}{\sqrt{D_1 t}}\right]^2} - \frac{2\sqrt{D_1 t}}{\sqrt{\pi}} e^{-\left[\frac{9R}{2\sqrt{D_1 t}}\right]^2} \right.$$

$$+ 9R\,erf\left(\frac{4R}{\sqrt{D_1 t}}\right) - 9R\,erf\left(\frac{9R}{2\sqrt{D_1 t}}\right)\Bigg]$$

$$+ \left[R - R\,erf\left(\frac{R}{\sqrt{D_1 t}}\right) - \frac{2\sqrt{D_1 t}}{\sqrt{\pi}}e^{-\left[\frac{R}{\sqrt{D_1 t}}\right]^2} + \frac{2\sqrt{D_1 t}}{\sqrt{\pi}}e^{-\left[\frac{R}{2\sqrt{D_1 t}}\right]^2} - R\,erf\left(\frac{R}{\sqrt{D_1 t}}\right)\right.$$

$$\left. + R\,erf\left(\frac{R}{2\sqrt{D_1 t}}\right)\right]$$

$$- h\left[R - R\,erf\left(\frac{2R}{\sqrt{D_1 t}}\right) - \frac{2\sqrt{D_1 t}}{\sqrt{\pi}}e^{-\left[\frac{2R}{\sqrt{D_1 t}}\right]^2} + \frac{2\sqrt{D_1 t}}{\sqrt{\pi}}e^{-\left[\frac{3R}{2\sqrt{D_1 t}}\right]^2}\right.$$

$$\left. - 3R\,erf\left(\frac{2R}{\sqrt{D_1 t}}\right) + 3R\,erf\left(\frac{3R}{2\sqrt{D_1 t}}\right)\right]$$

$$+ h^2\left[R - R\,erf\left(\frac{3R}{\sqrt{D_1 t}}\right) - \frac{2\sqrt{D_1 t}}{\sqrt{\pi}}e^{-\left[\frac{3R}{\sqrt{D_1 t}}\right]^2} + \frac{2\sqrt{D_1 t}}{\sqrt{\pi}}e^{-\left[\frac{5R}{2\sqrt{D_1 t}}\right]^2}\right.$$

$$\left. - 5R\,erf\left(\frac{3R}{\sqrt{D_1 t}}\right) + 5R\,erf\left(\frac{5R}{2\sqrt{D_1 t}}\right)\right]$$

$$- h^3\left[R - R\,erf\left(\frac{4R}{\sqrt{D_1 t}}\right) - \frac{2\sqrt{D_1 t}}{\sqrt{\pi}}e^{-\left[\frac{4R}{\sqrt{D_1 t}}\right]^2} + \frac{2\sqrt{D_1 t}}{\sqrt{\pi}}e^{-\left[\frac{7R}{2\sqrt{D_1 t}}\right]^2}\right.$$

$$\left. - 7R\,erf\left(\frac{4R}{\sqrt{D_1 t}}\right) + 7R\,erf\left(\frac{7R}{2\sqrt{D_1 t}}\right)\right]$$

$$+ h^4\left[R - R\,erf\left(\frac{5R}{\sqrt{D_1 t}}\right) - \frac{2\sqrt{D_1 t}}{\sqrt{\pi}}e^{-\left[\frac{5R}{\sqrt{D_1 t}}\right]^2} + \frac{2\sqrt{D_1 t}}{\sqrt{\pi}}e^{-\left[\frac{9R}{2\sqrt{D_1 t}}\right]^2}\right.$$

$$\left.\left. - 9R\,erf\left(\frac{5R}{\sqrt{D_1 t}}\right) + 9R\,erf\left(\frac{9R}{2\sqrt{D_1 t}}\right)\right]\right\}$$

$$+ C_s(1 - R)$$

$$\times \left\{erf\left(\frac{R}{2\sqrt{D_1 t}}\right)\right.$$

$$- h\left[erf\left(\frac{3R}{2\sqrt{D_1 t}}\right) - erf\left(\frac{R}{\sqrt{D_1 t}}\right)\right] + h^2\left[erf\left(\frac{5R}{2\sqrt{D_1 t}}\right)\right.$$

$$- erf\left(\frac{2R}{\sqrt{D_1 t}}\right)\right] - h^3 \left[erf\left(\frac{7R}{2\sqrt{D_1 t}}\right) - erf\left(\frac{3R}{\sqrt{D_1 t}}\right)\right] + h^4 \left[erf\left(\frac{9R}{2\sqrt{D_1 t}}\right)\right.$$

$$\left. - erf\left(\frac{4R}{\sqrt{D_1 t}}\right)\right]\right\}$$

$$= C_s R - C_s(1 - R)h$$

$$\times \left\{\left[-erf\left(\frac{R}{2\sqrt{D_1 t}}\right) + erf\left(\frac{R}{\sqrt{D_1 t}}\right)\right] - h\left[-erf\left(\frac{3R}{2\sqrt{D_1 t}}\right) + erf\left(\frac{2R}{\sqrt{D_1 t}}\right)\right]\right.$$

$$+ h^2 \left[-erf\left(\frac{5R}{2\sqrt{D_1 t}}\right) + erf\left(\frac{3R}{\sqrt{D_1 t}}\right)\right] - h^3 \left[-erf\left(\frac{7R}{2\sqrt{D_1 t}}\right)\right.$$

$$\left. + erf\left(\frac{4R}{\sqrt{D_1 t}}\right)\right] + h^4 \left[-erf\left(\frac{9R}{2\sqrt{D_1 t}}\right) + erf\left(\frac{5R}{\sqrt{D_1 t}}\right)\right]\right\}$$

$$- \frac{C_s}{1 + k}$$

$$\times \left\{R + \frac{2\sqrt{D_1 t}}{\sqrt{\pi}} - h\left[R + \frac{2\sqrt{D_1 t}}{\sqrt{\pi}}e^{-\left[\frac{R}{\sqrt{D_1 t}}\right]^2} + 2R\, erf\left(\frac{R}{\sqrt{D_1 t}}\right)\right]\right.$$

$$+ h^2 \left[R + \frac{2\sqrt{D_1 t}}{\sqrt{\pi}}e^{-\left[\frac{2R}{\sqrt{D_1 t}}\right]^2} + 4R\, erf\left(\frac{2R}{\sqrt{D_1 t}}\right)\right]$$

$$- h^3 \left[R + \frac{2\sqrt{D_1 t}}{\sqrt{\pi}}e^{-\left[\frac{3R}{\sqrt{D_1 t}}\right]^2} + 6R\, erf\left(\frac{3R}{\sqrt{D_1 t}}\right)\right]$$

$$+ h^4 \left[R + \frac{2\sqrt{D_1 t}}{\sqrt{\pi}}e^{-\left[\frac{4R}{\sqrt{D_1 t}}\right]^2} + 8R\, erf\left(\frac{4R}{\sqrt{D_1 t}}\right)\right]$$

$$+ \left[R - \frac{2\sqrt{D_1 t}}{\sqrt{\pi}}e^{-\left[\frac{R}{\sqrt{D_1 t}}\right]^2} - 2R\, erf\left(\frac{R}{\sqrt{D_1 t}}\right)\right]$$

$$- h\left[R - \frac{2\sqrt{D_1 t}}{\sqrt{\pi}}e^{-\left[\frac{2R}{\sqrt{D_1 t}}\right]^2} - 4R\, erf\left(\frac{2R}{\sqrt{D_1 t}}\right)\right]$$

$$+ h^2 \left[R - \frac{2\sqrt{D_1 t}}{\sqrt{\pi}}e^{-\left[\frac{3R}{\sqrt{D_1 t}}\right]^2} - 6R\, erf\left(\frac{3R}{\sqrt{D_1 t}}\right)\right]$$

$$-h^3\left[R-\frac{2\sqrt{D_1 t}}{\sqrt{\pi}}e^{-\left[\frac{4R}{\sqrt{D_1 t}}\right]^2}-8R\,erf\left(\frac{4R}{\sqrt{D_1 t}}\right)\right]$$

$$+h^4\left[R-\frac{2\sqrt{D_1 t}}{\sqrt{\pi}}e^{-\left[\frac{5R}{\sqrt{D_1 t}}\right]^2}-10R\,erf\left(\frac{5R}{\sqrt{D_1 t}}\right)\right]\right\}$$

$$+C_s(1-R)$$

$$\times\left\{erf\left(\frac{R}{2\sqrt{D_1 t}}\right)\right.$$

$$-h\left[erf\left(\frac{3R}{2\sqrt{D_1 t}}\right)-erf\left(\frac{R}{\sqrt{D_1 t}}\right)\right]+h^2\left[erf\left(\frac{5R}{2\sqrt{D_1 t}}\right)\right.$$

$$\left.-erf\left(\frac{2R}{\sqrt{D_1 t}}\right)\right]-h^3\left[erf\left(\frac{7R}{2\sqrt{D_1 t}}\right)-erf\left(\frac{3R}{\sqrt{D_1 t}}\right)\right]+h^4\left[erf\left(\frac{9R}{2\sqrt{D_1 t}}\right)\right.$$

$$\left.\left.-erf\left(\frac{4R}{\sqrt{D_1 t}}\right)\right]\right\}$$

<div align="right">Equation 5.31</div>

Fitting of mass loss as function of time using Eq. 5.31 is shown in Figure 5.10. Curve fitting was failed for spin test 1 due to the lack of data points. Fitting results are summarized in Table 5.5. Take both R^2 and *SSE* into consideration, fitting of mass loss as function of time using Eq. (5.31) is better than linear fitting based on Eq. 5.7.
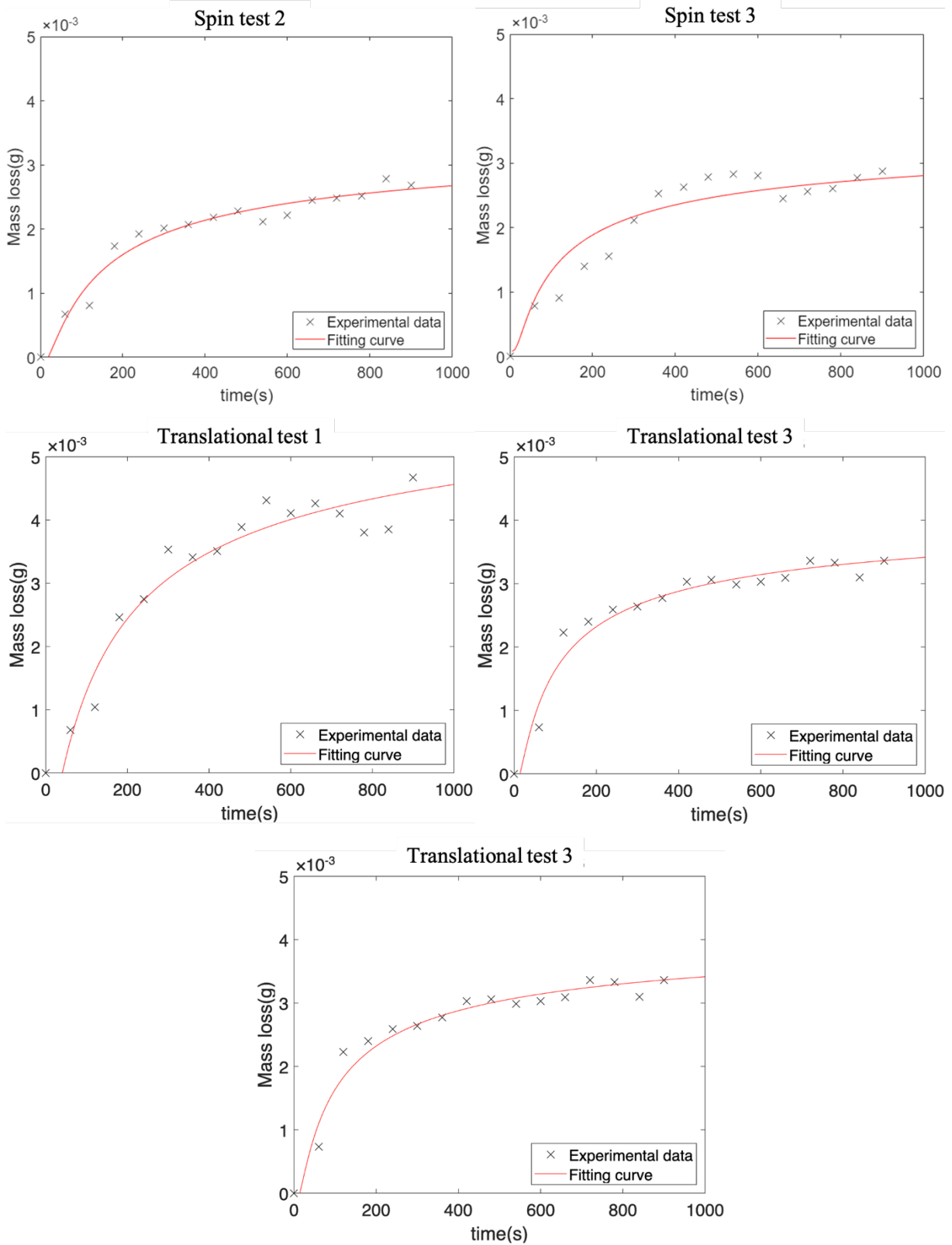
Figure 5.10 Mass loss as function of time. Fitting using Eq. (5.31).

Table 5.5 Fitting results of mass loss curve using Eq. (5.31)

	D_1	R	k	C_s	R^2	SSE $(\times 10^{-7})$
Spin test 1	-	-	-	-	-	-
Spin test 2	171.9	15.8	4.6	0.002	0.88	6.14
Spin test 3	272.9	19.6	3.6	0.002	0.83	12.24
Translational test 1	141.5	15.9	3.6	0.005	0.86	26.31
Translational test 2	528.4	27.5	3.7	0.003	0.92	12.63
Translational test 3	630.9	27.9	2.9	0.005	0.97	2.00

Parameters of translational test 3 from fitting results is selected to insert Eq. (5.31) due to a large

value of R^2 and low value of SSE.

$$\int_0^R C_1(x,t)\,dx = 0.140$$

$$- 0.066$$

$$\times \left\{ \left[-erf\left(\frac{0.555}{\sqrt{t}}\right) + erf\left(\frac{1.111}{\sqrt{t}}\right)\right] + 0.487\left[-erf\left(\frac{1.666}{\sqrt{t}}\right) + erf\left(\frac{2.222}{\sqrt{t}}\right)\right] \right.$$
$$+ 0.237\left[-erf\left(\frac{2.777}{\sqrt{t}}\right) + erf\left(\frac{3.332}{\sqrt{t}}\right)\right]$$
$$+ 0.116\left[-erf\left(\frac{3.888}{\sqrt{t}}\right) + erf\left(\frac{4.443}{\sqrt{t}}\right)\right]$$
$$\left. + 0.056\left[-erf\left(\frac{5.998}{\sqrt{t}}\right) + erf\left(\frac{5.554}{\sqrt{t}}\right)\right]\right\}$$

$$- 0.0013$$

$$\times \left\{ 27.9 + 28.342\,\sqrt{t} + 0.487\left[27.9 + 28.342\,\sqrt{t}\,e^{-\left[\frac{1.111}{\sqrt{t}}\right]^2} + 55.8\,erf\left(\frac{1.111}{\sqrt{t}}\right)\right]\right.$$

$$+ 0.237\left[27.9 + 28.342\,\sqrt{t}\,e^{-\left[\frac{2.222}{\sqrt{t}}\right]^2} + 111.6\,erf\left(\frac{2.222}{\sqrt{t}}\right)\right]$$

$$+ 0.116\left[27.9 + 28.342\,\sqrt{t}\,e^{-\left[\frac{3.332}{\sqrt{t}}\right]^2} + 167.4\,erf\left(\frac{3.332}{\sqrt{t}}\right)\right]$$

$$+ 0.056\left[27.9 + 28.342\,\sqrt{t}\,e^{-\left[\frac{4.443}{\sqrt{t}}\right]^2} + 223.2\,erf\left(\frac{4.443}{\sqrt{t}}\right)\right]$$

$$+ \left[27.9 - 28.342\,\sqrt{t}\,e^{-\left[\frac{1.111}{\sqrt{t}}\right]^2} - 55.8\,erf\left(\frac{1.111}{\sqrt{t}}\right)\right]$$

$$+ 0.487\left[27.9 - 28.342\,\sqrt{t}\,e^{-\left[\frac{2.222}{\sqrt{t}}\right]^2} - 111.6\,erf\left(\frac{2.222}{\sqrt{t}}\right)\right]$$

$$+ 0.237\left[27.9 - 28.342\,\sqrt{t}\,e^{-\left[\frac{3.332}{\sqrt{t}}\right]^2}\right.$$

$$\left. - 167.4\,erf\left(\frac{3.332}{\sqrt{t}}\right)\right] + 0.116\left[27.9 - 28.342\,\sqrt{t}\,e^{-\left[\frac{4.443}{\sqrt{t}}\right]^2}\right.$$

$$- 223.2 \, erf\left(\frac{4.443}{\sqrt{t}}\right)\Big]$$

$$+ 0.056 \left[27.9 - 28.342 \sqrt{t} \, e^{-\left[\frac{5.554}{\sqrt{t}}\right]^2} - 279 \, erf\left(\frac{5.554}{\sqrt{t}}\right)\right]\Bigg\}\Bigg]$$

$$- 0.135$$

$$\times \Bigg\{ erf\left(\frac{0.555}{\sqrt{t}}\right) + 0.487 \left[erf\left(\frac{1.666}{\sqrt{t}}\right) - erf\left(\frac{1.111}{\sqrt{t}}\right)\right]$$

$$+ 0.237 \left[erf\left(\frac{2.777}{\sqrt{t}}\right) - erf\left(\frac{2.332}{\sqrt{t}}\right)\right] + 0.116 \left[erf\left(\frac{3.888}{\sqrt{t}}\right) - erf\left(\frac{3.332}{\sqrt{t}}\right)\right]$$

$$+ 0.056 \left[erf\left(\frac{4.998}{\sqrt{t}}\right) - erf\left(\frac{4.443}{\sqrt{t}}\right)\right]\Bigg\}\Bigg]$$

$$= 4.46 \times 10^{-3}$$

$$- \Bigg[0.029 \, erf\left(\frac{0.57}{\sqrt{t}}\right) - 0.013 \, erf\left(\frac{1.14}{\sqrt{t}}\right) + 0.017 \, erf\left(\frac{1.71}{\sqrt{t}}\right)$$

$$+ 0.015 \, erf\left(\frac{2.28}{\sqrt{t}}\right) + 9.57 \times 10^{-3} erf\left(\frac{2.86}{\sqrt{t}}\right) - 0.013 \, erf\left(\frac{3.43}{\sqrt{t}}\right)$$

$$+ 5.51 \times 10^{-3} \, erf\left(\frac{4.00}{\sqrt{t}}\right) - 9.87 \times 10^{-3} \, erf\left(\frac{4.57}{\sqrt{t}}\right)$$

$$+ 3.19 \times 10^{-3} \, erf\left(\frac{5.14}{\sqrt{t}}\right) - 0.013 \, erf\left(\frac{5.71}{\sqrt{t}}\right)\Bigg]$$

$$- \Bigg[0.015\sqrt{t} - 6.617 \times 10^{-3} \sqrt{t} \, e^{-\left[\frac{1.14}{\sqrt{t}}\right]^2} - 3.693 \times 10^{-3} \sqrt{t} \, e^{-\left[\frac{2.28}{\sqrt{t}}\right]^2}$$

$$- 2.154 \times 10^{-3}\sqrt{t} \, e^{-\left[\frac{3.43}{\sqrt{t}}\right]^2}$$

$$- 1.231 \times 10^{-3}\sqrt{t} \, e^{-\left[\frac{4.57}{\sqrt{t}}\right]^2} - 1.697 \times 10^{-3}\sqrt{t} \, e^{-\left[\frac{5.71}{\sqrt{t}}\right]^2}\Bigg]$$

<div align="right">Equation 5.32</div>

For long time (i.e., very large times), both the exponentials and error-function complements in $C_l(x,t)$ may all be replaced by unity[216,217].

Thus, both $\sum_{n=1}^{\infty}(-h)^{n-1} e^{-\left[\frac{(2n-0)R-x}{2\sqrt{D_1 t}}\right]^2}$ and $\sum_{n=1}^{\infty}(-h)^{n-1} erfc\left[\frac{(2n-1)R-x}{2\sqrt{D_1 t}}\right]$ can be

approximated as $\sum_{n=1}^{\infty}(-h)^{n-1}$, where $0 < h = \frac{1-k}{1+k} < 1$.

$$\sum_{n=1}^{\infty}(-h)^{n-1} = \frac{1}{1+h}$$

Equation 5.33

Combine Eq. (5.28) and Eq. (5.33)

$$C_1(x,t) = C_s - \left[\frac{C_s(1-R)(1+h)}{k\sqrt{D_2 \pi t}} - \frac{2C_s}{1+k}\right] \times \frac{1}{1+h}$$

Equation 5.34

Amount of substance diffused into region $R \le x \le \infty$ at time t is given by integrating Eq. (5.34)

with respect to x from 0 to R.

$$\int_0^R C_1(x,t)\, dx = C_s R\left(1 + \frac{1}{(1+k)(1+h)}\right) - \left(\frac{C_s R(1+R)}{k\sqrt{D_2 \pi}}\right) \times \frac{1}{\sqrt{t}}$$

Equation 5.35

Thus, mass of substance (m_s) diffused into water, or mass loss as function of time can be fitted

using Eq. (5.36).

$$m_s = \int_0^R C_1(x,t)\, dx = a + b\frac{1}{\sqrt{t}}$$

Equation 5.36

where $a = C_s R\left(1 + \frac{1}{(1+k)(1+h)}\right)$ and $b = \frac{C_s R(1+R)}{k\sqrt{D_2 \pi}}$.

194
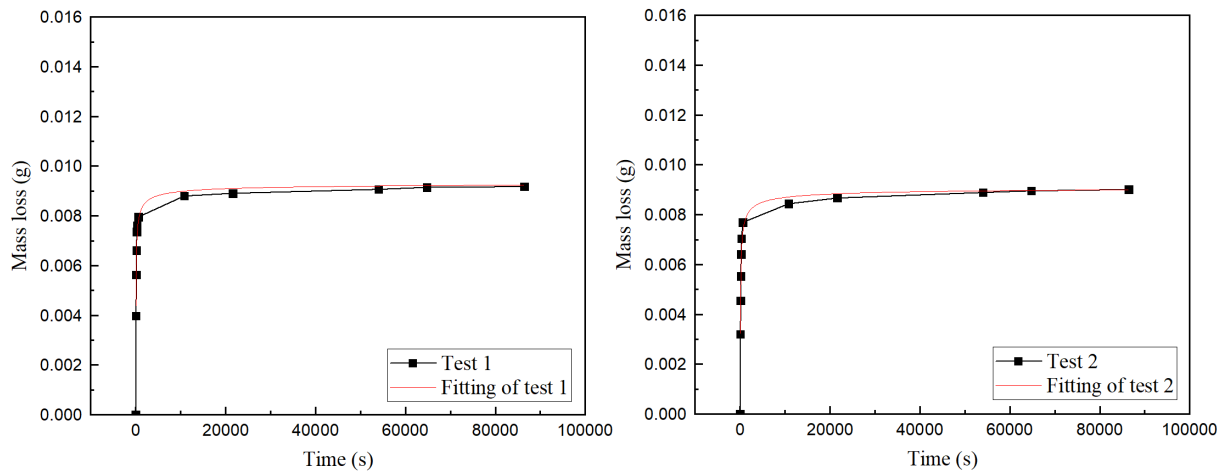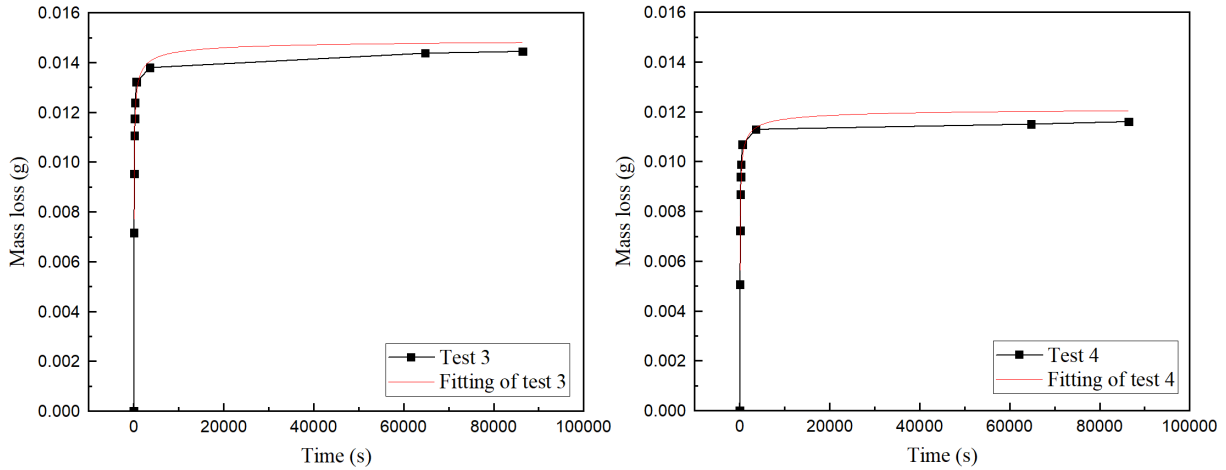
Figure 5.11 Mass loss as function of time. PVDF/ DMF-acetone gel with size in 12 mm × 12 mm. Fitting using Eq. (5.36).

Mass loss as function of time and their fitting using Eq. (5.36) is shown in Figure 5.11. Results in Table 5.6 shows that the fitting using Eq. (5.36) has large value of R^2 and small SSE. The assumption of Eq. (5.34) is for very large times, while the data in Figure 5.11 includes mass loss from t = 0 second to t = 86400 seconds (24 hours).

Table 5.6 Fitting results of mass loss curves using Eq. (5.36)

	a	b	R^2	SSE (×10^{-7})
Test 1	0.00937	-0.0387	0.99	8.09
Test 2	0.00915	-0.0459	0.99	8.25
Test 3	0.0150	-0.0565	0.99	21.09
Test 4	0.0122	-0.0510	0.98	23.35

The time dependence of the mass loss of the gel actuators is plotted in Figure 5.12 using $\frac{1}{\sqrt{t}}$ for time. Based on Eq. (5.36), there should be a linear relationship between the mass loss and $\frac{1}{\sqrt{t}}$. Period-I and Period-II are marked in Figure 5.12. Instead of a full time, the mass loss as function

195

of time is fitted using Eq. (5.36) in Period-II as shown in Figure 5.13. Fitting results are in Table 5.7.
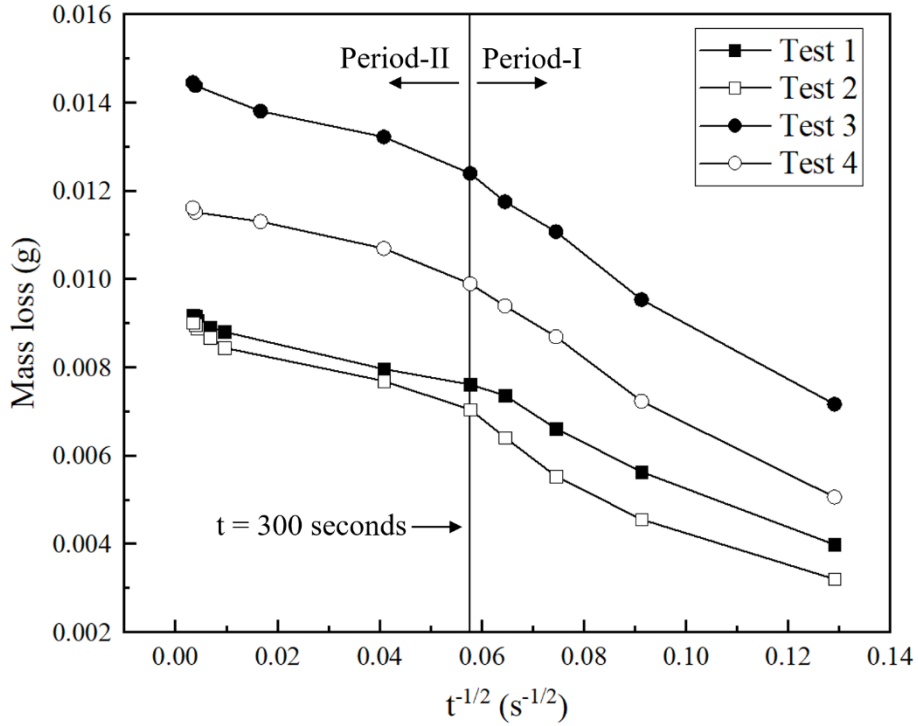
Figure 5.12 Mass loss of gel actuators as function of time. PVDF/ DMF-acetone gel with size in 12 mm × 12 mm.
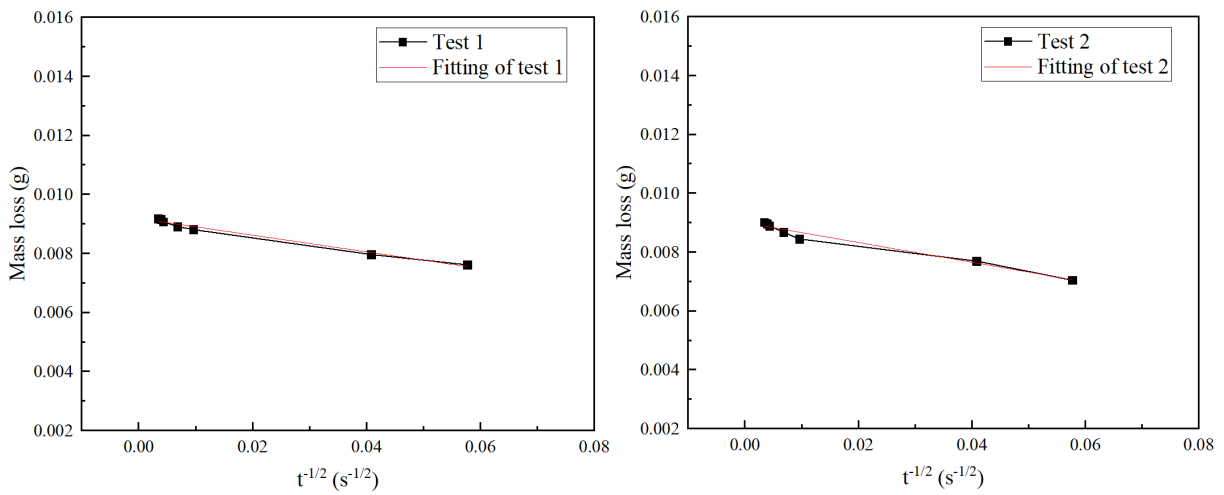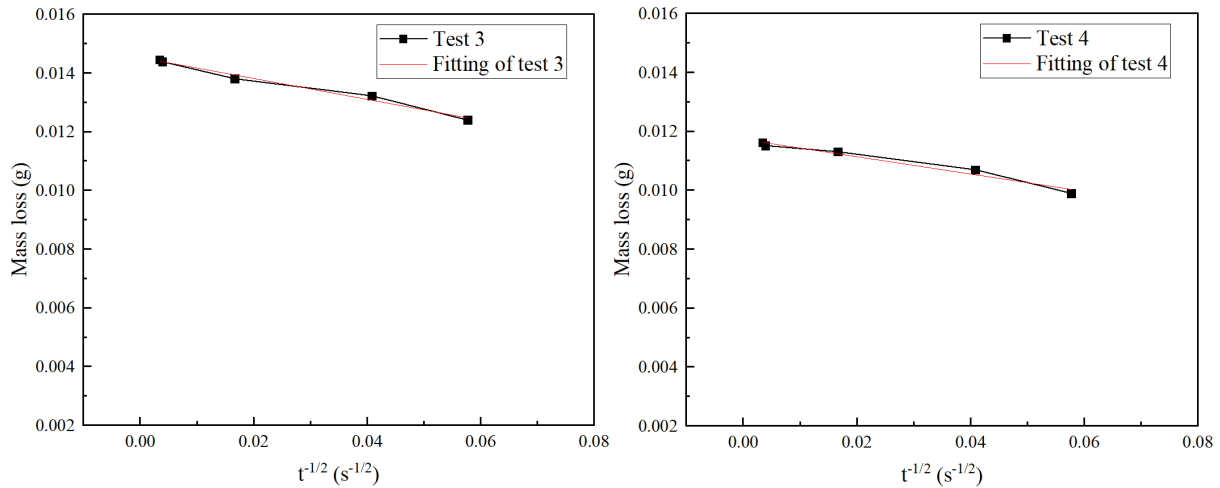
Figure 5.13 Mass loss as function of time in Period-II. PVDF/ DMF-acetone gel with size in 12 mm × 12 mm. Fitting using Eq. (5.36).

Table 5.7 Fitting results of mass loss curves in Period-I using Eq. (5.36)

	a	b	R^2	SSE ($\times 10^{-7}$)
Test 1	0.0106	-0.0517	0.99	8.22
Test 2	0.0097	-0.0522	0.96	4.15
Test 3	0.0165	-0.0732	0.99	1.09
Test 4	0.0137	-0.0682	0.99	1.07

Similarly, Period-I in Figure 5.12 is fitting using Eq. (5.36) to obtain an empirical equation. Fitting

results are in Table 5.8.

Table 5.8 Fitting results of mass loss curves in Period-II using Eq. (5.36)

	a	b	R^2	SSE ($\times 10^{-8}$)
Test 1	0.0092	-0.0283	0.98	4.18
Test 2	0.0090	-0.0336	0.97	9.53
Test 3	0.0145	-0.0356	0.98	4.77
Test 4	0.0117	-0.0294	0.97	6.05

Combine Table 5.7 and Table 5.8, fitting results (i.e., a and b) from Test 3 are selected because of

large R^2 and small SSE in both Period-I and Period-II. Eq. (5.37) and Eq. (5.38) can be used to

predict mass loss of gel actuators as function of time in Period-I and Period-II in future analytical solution, where m_s is mass loss and t is time.

$$m_s = 0.0165 - 0.0732\frac{1}{\sqrt{t}} \qquad \text{Equation 5.37}$$

$$m_s = 0.0145 - 0.0356\frac{1}{\sqrt{t}} \qquad \text{Equation 5.38}$$

Eq. (5.28) and Eq. (5.29) describe the case that a limited source diffused into a semi-infinite bar. It considers one dimensional diffusion which is not the real case in the experiments. However, this model can help us understand the trend of mass loss as function of time. Eq. (5.28) is simplified based on two time periods, short time and long time, which can be used to fit Period-I and Period-II. Mass loss fitting was conducted using integration of the simplified equations with respect to x from 0 to R. Thanks to the fitting using simplified Eq. (5.28), Eq. (5.32) can be used to describe mass loss as function of time in Period-I. Similarly, Eq. (5.37) can be used to describe mass loss as function of time in Period-II.

All in all, it was observed that the mass loss as function of time has two segments of time, i.e., Period – I and Period – II. A set of equation were derived to describe the mass loss in the two time period. An empirical equation based on Eq. (5.8) can be used to predict mass loss as function of time in Period – I and a simplified equation from Eq. (5.28) can be used to predict mass loss as function of time in Period – II.

5.2 Energy conversion

The self-driven motion of gel actuators at air-water interface is driven by the solvent diffusion. Self-driven gels convert stored chemical energy into mechanic motions and will convert to heat

finally. The driven force act on gel actuators is denoted as F_d. The friction force, denoted as F_f, of self-driven motion of gel actuators at the air-water interface Thus, net force act on the gel actuators, denoted as F_n, can be expressed by Eq. 5.39.

$$F_n = F_d - F_f$$
<div align="right">Equation 5.39</div>

The velocity and mechanical energy of gel actuators at any time are obtained from experiments data using digitalized methods motioned in Section 4.2.1. Friction force is given by $F_f = -\alpha v^2$ as discussed in Section 4.2.2. Therefore, the driven force of gel motion at the air-water interface can be calculated.

5.3 Conclusion

Based on the experimental results, it is concluded that the time dependence of the mass loss can be separated into in time period: short time period (Period-I) and long time period (Period-II). An existing model, unlimited source diffused into a semi-infinite bar, was utilized to fit the mass loss curve of gel actuators. Based on this model, there should be a linear relationship between the $ln(m_s)$ and $ln(t)$ with the slope of 0.5. This model is not good enough, especially the long times. The equation was modified by change the slope of 0.5 to b, which can be used to fitted mass loss as function of time in both Period-I and Period-II. A new model describes the case that a limited source diffused into a semi-infinite bar is built. Eq. (5.28) is simplified based on two time periods, short time and long time, which can be used to fit mass loss curves in Period-I and Period-II.

A set of equation were derived to describe the mass loss in the two time periods. An empirical equation based on Eq. (5.8) can be used to predict mass loss as function of time in Period – I and

a simplified equation from Eq. (5.28) can be used to predict mass loss as function of time in Period – II. The equations to describe the time dependence of the mass loss can be used for the future study to determine the velocity of solvent eject by the gel actuators, which is a step forward for the understanding of self-driven gels.

Chapter VI

Future work

Self-driven motion of the gel actuators at the air-water interface was studied. The duration of gel actuators increases as mass of gel increases. In Section 3.2.6, it was showed that the motion of gel actuator stops when the difference in chemical potential of solvent in gel and water is so small or even be zero, rather than the solvent in gel actuator is empty. This result indicates that a gel actuator would have a longer motion duration in a container with more water. If there is a semipermeable membrane that allows solvents diffusing out and keep water inside, the certain amount of water can keep clean for longer time. Thus, the longer motion is possible to be obtained with certain amount of water.

The motion of gel actuators in a plastic beaker is harder. Self-driven motion of gel actuators at the air-water interface are in the glass beaker in this study. However, no motion was observed when a gel is placed at the air-water interface in a plastic beaker. The gel can move at the air-water interface in a glass beaker after it was taken out from the plastic one. The gel actuator is able to move slowly if the plastic beaker is washed 10 days using DI water. A droplet of PVDF polymer solution can move rapidly when placed at the air-water interface in plastic beaker, no need to be washed. The mechanisms are still not clear to explain this phenomenon by our experiments. If the mechanisms are understood, the on-off switch of the gel motion at the air-water interface can be obtained by taking advantage of this phenomenon.

Quantification process was established for output of self-driven motion at the air-water interface. Thanks to the digitalized results, velocity, acceleration, kinetic energy and their time dependence are able to be obtained for the motion of gel actuators. The velocity of gel actuator decreases as it moves toward the wall of glass beaker was observed. This phenomenon can be attributed to the surface tension issues. Anyway, there is external effect slowing down the gel actuators, while there is no external effect speeding up the gel actuators. Therefore, the red dash-dotted line as shown in Figure 6.1 can be used to predict the velocity of gel actuator acquired from the solvent diffusion at any time.
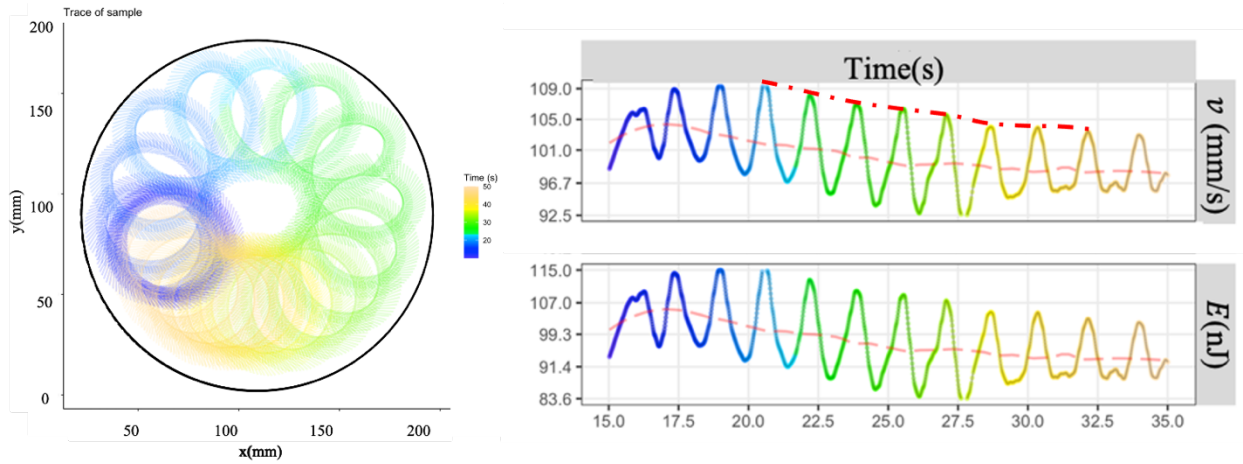
Figure 6.1 Trace (left) and motion parameters (right) including the velocity energy change as the function of time for a circle sample with diameter in 7.82 mm in the *time period from 15 to 35 second*.

Relationship between friction force and velocity is studied. It is confirmed that friction force of gel motion at the air-water interface obeys $F = -\alpha v^2$. As discussed, the self-driven motion of gel actuators at air-water interface is driven by the solvent diffusion. Self-driven gels convert stored chemical energy into mechanic motions and will convert to heat finally. The driven force act on gel actuators can be calculated using Eq. (6.1).

$$F_d = F_n + F_f \qquad \text{Equation 6.1}$$

At time t, the mass of solvent ejected by the gel actuator, m_{sl}, can be calculated Eq. (5.37) and Eq. (5.38). Momentum of eject mass, P_{sl}, can be calculated using Eq. (6.2), where v_{sl} is the velocity of ejected mass, a is the acceleration.

$$P_{sl} = m_{sl} \times v_{sl} \qquad \text{Equation 6.2}$$

$$\frac{d\,P_{sl}}{d\,t} = m_{sl}\frac{d\,v_{sl}}{d\,t} = m\,a = F_d \qquad \text{Equation 6.3}$$

The derivation of P_{sl} can also be expressed as Eq. (6.4).

$$\frac{d\,P_{sl}}{d\,t} = m_{sl}dv_{sl} + v_{sl}dm_{sl} \qquad \text{Equation 6.4}$$

Combine Eq. (6.1), Eq. (6.3) and Eq. (6.4),

$$F_n + F_f = m_{sl}dv_{sl} + v_{sl}dm_{sl} \qquad \text{Equation 6.5}$$

Analytic solution of Eq. (6.5) can be used to predict the velocity of solvent eject by the gel actuators, which is a step forward for the understanding of self-driven gels.

Reference

[1] Paek, Jungwook, Inho Cho, and Jaeyoun Kim. "Microrobotic tentacles with spiral bending capability based on shape-engineered elastomeric microtubes." *Scientific reports* 5 (2015): 10768.

[2] Immerstrand, Charlotte, et al. "Conjugated-polymer micro-and milliactuators for biological applications." *MRS bulletin* 27.6 (2002): 461-464.

[3] Wang, Shurong, et al. "Organic/inorganic hybrid sensors: A review." *Sensors and Actuators B: Chemical* 182 (2013): 467-481.

[4] Takahashi, Sadayuki. "Multilayer piezoelectric ceramic actuators and their applications." *Japanese Journal of Applied Physics* 24.S2 (1985): 41.

[5] Pelrine, Ron, Roy Kornbluh, and Guggi Kofod. "High-strain actuator materials based on dielectric elastomers." *Advanced Materials* 12.16 (2000): 1223-1225.

[6] Polygerinos, Panagiotis, et al. "Modeling of soft fiber-reinforced bending actuators." IEEE Transactions on Robotics 31.3 (2015): 778-789.

[7] Hines, Lindsey, et al. "Soft actuators for small-scale robotics." Advanced materials 29.13 (2017): 1603483.

[8] Voit, Walter, et al. "High-Strain Shape-Memory Polymers." *Advanced functional materials* 20.1 (2010): 162-171.

[9] Oh, Sang-Keun, Masaru Nakagawa, and Kunihiro Ichimura. "Photocontrol of liquid motion on an azobenzene monolayer." *Journal of Materials Chemistry* 12.8 (2002): 2262-2269.

[10] Mohammed, Mohammed, Rishi Sundaresan, and Michael D. Dickey. "Self-running liquid metal drops that delaminate metal films at record velocities." *ACS applied materials & interfaces* 7.41 (2015): 23163-23171.

[11] Stuart, Martien A. Cohen, et al. "Emerging applications of stimuli-responsive polymer materials." *Nature materials* 9.2 (2010): 101.

[12] Di, Chunfeng, et al. "Multi-responsive polymer nanoparticles from the amphiphilic poly (dimethylsiloxane)(PDMS)-containing poly (ether amine) (PDMS-gPEA) and its potential application for smart separation." *Journal of Materials Chemistry* 21.12 (2011): 4416-4423.

[13] Yan, Xuzhou, et al. "A multiresponsive, shape-persistent, and elastic supramolecular polymer network gel constructed by orthogonal self-assembly." *Advanced Materials* 24.3 (2012): 362-369.

[14] Cheng, Ru, et al. "Dual and multi-stimuli responsive polymeric nanoparticles for programmed site-specific drug delivery." *Biomaterials* 34.14 (2013): 3647-3657.

[15] Uchino, Kenji, and Sadayuki Takahashi. "Multilayer ceramic actuators." *Current Opinion in Solid State and Materials Science* 1.5 (1996): 698-705.

[16] Jeyaseelan, A. Antony, et al. "Smart Piezo-ceramic Coating for Multifunctional Applications." *Materials Today: Proceedings*5.1 (2018): 3056-3063.

[17] Kras, A., et al. "ADVANTAGES OF LARGE PIEZOELECTRIC ACTUATORS AND HIGH POWER DRIVERS FOR FATIGUE AND FRETTING TEST."

18 Kim, Jaehwan, and Yung B. Seo. "Electro-active paper actuators." Smart Materials and Structures 11.3 (2002): 355.

[19]Carpi, Federico, et al. "Electroactive polymer actuators as artificial muscles: are they ready for bioinspired applications?." *Bioinspiration & biomimetics* 6.4 (2011): 045006.

[20] Wang, Fan, et al. "Ecofriendly electroactive polymer actuator using highly porous carboxylated bacterial cellulose." *Electrical Engineering/Electronics, Computer, Telecommunications and Information Technology (ECTI-CON), 2017 14th International Conference on*. IEEE, 2017.

[21] Maeda, Shingo, et al. "Active polymer gel actuators." *International journal of molecular sciences* 11.1 (2010): 52-66.

[22] Hamedi, Mahiar M., et al. "Electrically activated paper actuators." *Advanced Functional Materials* 26.15 (2016): 2446-2453.

[23] Fuchigami, Yuuta, Toshikazu Takigawa, and Kenji Urayama. "Electrical actuation of cholesteric liquid crystal gels." *ACS Macro Letters* 3.8 (2014): 813-818.

[24] Shankar, Ravi, Tushar K. Ghosh, and Richard J. Spontak. "Electroactive nanostructured polymers as tunable actuators." *Advanced Materials* 19.17 (2007): 2218-2223.

[25] Smela, Elisabeth. "Conjugated polymer actuators for biomedical applications." *Advanced materials* 15.6 (2003): 481-494.

[26] Zhang, Q. M., et al. "An all-organic composite actuator material with a high dielectric constant." *Nature* 419.6904 (2002): 284.

[27] Must, Indrek, et al. "Ionic and capacitive artificial muscle

 for biomimetic soft robotics." *Advanced Engineering Materials* 17.1 (2015): 84-94.

[28] Wang, Hyuck Sik, et al. "High-Performance Electroactive Polymer Actuators Based on Ultrathick Ionic Polymer–Metal Composites with Nanodispersed Metal Electrodes." *ACS applied materials & interfaces* 9.26 (2017): 21998-22005.

[29] Sun, Li, et al. "Stimulus-responsive shape memory materials: a review." *Materials & Design* 33 (2012): 577-640.

[30] Butera, Francesco. "Shape memory actuators." *Advanced Materials & Processes* 166.3 (2008): 37-40.

[31] Seelecke, Stefan, and Ingo Muller. "Shape memory alloy actuators in smart structures: Modeling and simulation." *Applied Mechanics Reviews* 57.1 (2004): 23-46.

[32] Huang, W. "On the selection of shape memory alloys for actuators." *Materials & design* 23.1 (2002): 11-19.

[33] Mohd Jani, Jaronie, Martin Leary, and Aleksandar Subic. "Designing shape memory alloy linear actuators: A review." *Journal of Intelligent Material Systems and Structures* 28.13 (2017): 1699-1718.

[34] Behl, Marc, et al. "Temperature-memory polymer actuators." *Proceedings of the National Academy of Sciences* 110.31 (2013): 12555-12559.

[35] Lv, Haibao, et al. "Shape-memory polymer in response to solution." *Advanced Engineering Materials* 10.6 (2008): 592-595.

[36] Huang, W. M., et al. "Water-driven programmable polyurethane shape memory polymer: demonstration and mechanism." *Applied Physics Letters* 86.11 (2005): 114105.

[37] Lendlein, Andreas, et al. "Light-induced shape-memory polymers." *Nature* 434.7035 (2005): 879.

[38] Jiang, H. Y., Steffen Kelch, and Andreas Lendlein. "Polymers move in response to light." *Advanced Materials* 18.11 (2006): 1471-1475.

[39] Maitland, Duncan J., et al. "Photothermal properties of shape memory polymer micro-actuators for treating stroke." *Lasers in Surgery and Medicine* 30.1 (2002): 1-11.

[40] Cho, Jae Whan, et al. "Electroactive shape-memory polyurethane composites incorporating carbon nanotubes." *Macromolecular Rapid Communications* 26.5 (2005): 412-416.

[41] Paik, Il Hyun, et al. "Development and application of conducting shape memory polyurethane actuators." *Smart Materials and Structures* 15.5 (2006): 1476.

[42] Liu, Yanju, et al. "Review of electro-active shape-memory polymer composite." *Composites Science and Technology*69.13 (2009): 2064-2068.

[43] Buckley, Patrick R., et al. "Inductively heated shape memory polymer for the magnetic actuation of medical devices." *IEEE transactions on biomedical engineering* 53.10 (2006): 2075-2083.

[44] Leng, J. S., et al. "Significantly reducing electrical resistivity by forming conductive Ni chains in a polyurethane shape-memory polymer/carbon-black composite." *Applied Physics Letters*92.20 (2008): 204101.

[45] Schattling, Philipp, Florian D. Jochum, and Patrick Theato. "Multi-stimuli responsive polymers–the all-in-one talents." *Polymer Chemistry* 5.1 (2014): 25-36.

[46] Yu, Yuan-Yuan, et al. "Facile synthesis of triple-stimuli (photo/pH/thermo) responsive copolymers of 2-diazo-1, 2-naphthoquinone-mediated poly (N-isopropylacrylamide-co-N-hydroxymethylacrylamide)." *Journal of Polymer Science Part A: Polymer Chemistry* 47.11 (2009): 2763-2773.

[47] Jiang, Weitao, et al. "Photoresponsive soft-robotic platform: biomimetic fabrication and remote actuation." *Advanced Functional Materials* 24.48 (2014): 7598-7604.

[48] Van Oosten, Casper L., Cees WM Bastiaansen, and Dirk J. Broer. "Printed artificial cilia from liquid-crystal network actuators modularly driven by light." *Nature materials* 8.8 (2009): 677-682.
[49] Ercole, Francesca, Thomas P. Davis, and Richard A. Evans. "Photo-responsive systems and biomaterials: photochromic polymers, light-triggered self-assembly, surface modification, fluorescence modulation and beyond." Polymer Chemistry 1.1 (2010): 37-54.

[50] Wei, Jia, and Yanlei Yu. "Photodeformable polymer gels and crosslinked liquid-crystalline polymers." *Soft Matter* 8.31 (2012): 8050-8059.

[51] Hu, Ying, et al. "A graphene-based bimorph structure for design of high performance photoactuators." *Advanced Materials* 27.47 (2015): 7867-7873.

[52] Satoh, Taku, et al. "Fast-reversible light-driven hydrogels consisting of spirobenzopyran-functionalized poly (N-isopropylacrylamide)." *Soft Matter* 7.18 (2011): 8030-8034.

[53] Liang, Jiajie, et al. "Infrared-triggered actuators from graphene-based nanocomposites." The Journal of Physical Chemistry C 113.22 (2009): 9921-9927.

[54] White, Timothy J., et al. "A high frequency photodriven polymer oscillator." *Soft Matter* 4.9 (2008): 1796-1798.

[55] Harris, Kenneth D., et al. "Large amplitude light-induced motion in high elastic modulus polymer actuators." *Journal of Materials Chemistry* 15.47 (2005): 5043-5048.

[56] Iamsaard, Supitchaya, et al. "Conversion of light into macroscopic helical motion." *Nature chemistry* 6.3 (2014): 229-235.

[57] Mu, Jiuke, et al. "A multi-responsive water-driven actuator with instant and powerful performance for versatile applications." *Scientific reports* 5 (2015): 9503.

[58] Kumar, Kamlesh, et al. "A chaotic self-oscillating sunlight-driven polymer actuator." *Nature communications* 7 (2016): 11975.

[59] Diller, Eric, et al. "Six-degree-of-freedom magnetic actuation for wireless microrobotics." *The International Journal of Robotics Research* 35.1-3 (2016): 114-128.

[60] Garstecki, Piotr, et al. "Propulsion of flexible polymer structures in a rotating magnetic field." *Journal of Physics: Condensed Matter* 21.20 (2009): 204110.

[61] Diller, Eric, et al. "Continuously distributed magnetization profile for millimeter-scale elastomeric undulatory swimming." *Applied Physics Letters* 104.17 (2014): 174101.

[62] Chen, Ching-Yao, W-L. Wu, and José A. Miranda. "Magnetically induced spreading and pattern selection in thin ferrofluid drops." *Physical Review E* 82.5 (2010): 056321.

[63] Li, Hao, et al. "Magnetic actuated pH-responsive hydrogel-based soft micro-robot for targeted drug delivery." *Smart Materials and Structures* 25.2 (2016): 027001.

[64] Tasoglu, S., et al. "Untethered micro-robotic coding of three-dimensional material composition." Nature communications 5.1 (2014): 1-9.

[65] Zhao, Yan, et al. "Magnetic liquid marbles: manipulation of liquid droplets using highly hydrophobic Fe3O4 nanoparticles." *Advanced materials* 22.6 (2010): 707-710.

[66] Murase, Yoko, et al. "Design of a mass transport surface utilizing peristaltic motion of a self-oscillating gel." *Langmuir* 25.1 (2009): 483-489.

[67] Yoshida, Ryo, et al. "In-phase synchronization of chemical and mechanical oscillations in self-oscillating gels." *The Journal of Physical Chemistry A* 104.32 (2000): 7549-7555.

[68] Chen, Irene Chou, et al. "Mechanical resuscitation of chemical oscillations in Belousov–Zhabotinsky gels." *Advanced Functional Materials* 22.12 (2012): 2535-2541.

[69] Suematsu, Nobuhiko J., et al. "Oscillation of speed of a self-propelled Belousov–Zhabotinsky droplet." *The journal of physical chemistry letters* 7.17 (2016): 3424-3428.

[70] Hara, Yusuke, Yoshinori Yamaguchi, and Hiroyuki Mayama. "Switching the BZ Reaction with a Strong-Acid-Free Gel." *The Journal of Physical Chemistry B* 118.2 (2014): 634-638.

[71] Nakata, Satoshi, et al. "Periodic reciprocating motion of a polymer gel on an aqueous phase synchronized with the Belousov–Zhabotinsky reaction." *Langmuir* 30.2 (2014): 517-521.

[72] Maeda, Shingo, et al. "Control of the Dynamic Motion of a Gel Actuator Driven by the Belousov-Zhabotinsky Reaction." *Macromolecular Rapid Communications* 29.5 (2008): 401-405.

[73] Tabata, Osamu, et al. "Ciliary motion actuator using self-oscillating gel." *Sensors and Actuators A: Physical* 95.2-3 (2002): 234-238

[74] Maeda, Shingo, et al. "Self-walking gel." *Advanced Materials*19.21 (2007): 3480-3484.

[75] Shiraki, Yusuke, and Ryo Yoshida. "Autonomous Intestine-Like Motion of Tubular Self-Oscillating Gel." *Angewandte Chemie International Edition* 51.25 (2012): 6112-6116.

[76] Yoshida, Ryo. "Self-oscillating gels driven by the Belousov–Zhabotinsky reaction as novel smart materials." *Advanced Materials* 22.31 (2010): 3463-3483.

[77] Kim, Youn Soo, et al. "Recent developments in self-oscillating polymeric systems as smart materials: from polymers to bulk hydrogels." *Materials Horizons* 4.1 (2017): 38-54.

[78] Zhao, Qiang, et al. "An instant multi-responsive porous polymer actuator driven by solvent molecule sorption." *Nature communications* 5.1 (2014): 1-8.

[79] Zhang, Kai, et al. "Moisture-responsive films of cellulose stearoyl esters showing reversible shape transitions." *Scientific reports* 5 (2015): 11011.

[80] Cheng, Huhu, et al. "Moisture-Activated Torsional Graphene-Fiber Motor." *Advanced Materials* 26.18 (2014): 2909-2913.

[81] Mikhailov, Alexander S., and Vera Calenbuhr. *From cells to societies: models of complex coherent action*. Springer Science & Business Media, 2013.

[82] Yoshinaga, Natsuhiko, et al. "Drift instability in the motion of a fluid droplet with a chemically reactive surface driven by Marangoni flow." *Physical Review E* 86.1 (2012): 016108.

[83] Suematsu, Nobuhiko J., et al. "Collective behavior of inanimate boats." *Physical Review E* 81.5 (2010): 056210.

[84] He, Ximin, et al. "Synthetic homeostatic materials with chemo-mechano-chemical self-regulation." *Nature* 487.7406 (2012): 214-218.

[85] Saita, Ei-ichiro, et al. "Simple mechanism whereby the F1-ATPase motor rotates with near-perfect chemomechanical energy conversion." *Proceedings of the National Academy of Sciences* 112.31 (2015): 9626-9631.

[86] Osada, Yoshihito, Hidenori Okuzaki, and Hirofumi Hori. "A polymer gel with electrically driven motility." *Nature* 355.6357 (1992): 242.

[87] Vikrant, K. S. N., William C. Chueh, and R. Edwin García. "Charged interfaces: electrochemical and mechanical effects." *Energy & Environmental Science* 11.8 (2018): 1993-2000.

[88] Osada, Yoshihito. "Conversion of chemical into mechanical energy by synthetic polymers (chemomechanical systems)." *Polymer Physics*. Springer, Berlin, Heidelberg, 1987. 1-46.

[89] Kitahata, Hiroyuki, et al. "Spontaneous motion of a droplet coupled with a chemical wave." *Physical Review E* 84.1 (2011): 015101.

[90] Izri, Ziane, et al. "Self-propulsion of pure water droplets by spontaneous Marangoni-stress-driven motion." *Physical review letters* 113.24 (2014): 248302.

[91] De Gennes, Pierre-Gilles, Françoise Brochard-Wyart, and David Quéré. *Capillarity and wetting phenomena: drops, bubbles, pearls, waves*. Springer Science & Business Media, 2013.

[92] Kovalchuk, N. M., and D. Vollhardt. "Effect of substance properties on the appearance and characteristics of repeated surface tension auto-oscillation driven by Marangoni force." *Physical Review E* 69.1 (2004): 016307.

[93] Stoilov, Yuri Yu. "Fluorocarbons as volatile surfactants." *Langmuir* 14.20 (1998): 5685-5690.

[94] Alpers, Werner, and Heinrich Hühnerfuss. "Radar signatures of oil films floating on the sea surface and the Marangoni effect." *Journal of Geophysical Research: Oceans* 93.C4 (1988): 3642-3648.

[95] Dupeyrat, Me, and E. Nakache. "205-direct conversion of chemical energy into mechanical energy at an oil water Interface." *Bioelectrochemistry and Bioenergetics* 5.1 (1978): 134-141.

[96] Davis, Stephen H. "Thermocapillary instabilities." *Annual Review of Fluid Mechanics*. Annual Reviews Inc, 1987. 403-435.

[97] Ouenzerfi, Safouene, and Souad Harmand. "Experimental droplet study of inverted Marangoni effect of a binary liquid mixture on a nonuniform heated substrate." *Langmuir* 32.10 (2016): 2378-2388.

[98] Gugliotti, Marcos, Mauricio S. Baptista, and Mario J. Politi. "Surface tension gradients induced by temperature: The thermal Marangoni effect." *Journal of chemical education* 81.6 (2004): 824.

[99] Arafune, Koji, and Akira Hirata. "Thermal and solutal Marangoni convection in In–Ga–Sb system." *Journal of Crystal Growth* 197.4 (1999): 811-817.

[100] Arafune, Koji, and Akira Hirata. "Interactive solutal and thermal Marangoni convection in a rectangular open boat." *Numerical Heat Transfer, Part A Applications* 34.4 (1998): 421-429.

[101] Chen, J., C. Yang, and Z-S. Mao. "The interphase mass transfer in liquid–liquid systems with Marangoni effect." *The European Physical Journal Special Topics* 224.2 (2015): 389-399.

[102] Xu, Xuefeng, and Jianbin Luo. "Marangoni flow in an evaporating water droplet." *Applied Physics Letters* 91.12 (2007): 124102.

[103] Karpitschka, Stefan, Ferenc Liebig, and Hans Riegler. "Marangoni contraction of evaporating sessile droplets of binary mixtures." *Langmuir* 33.19 (2017): 4682-4687.

[104] Barmi, Meysam R., and Carl D. Meinhart. "Convective flows in evaporating sessile droplets." *The Journal of Physical Chemistry B* 118.9 (2014): 2414-2421.

[105] Daniel, Susan, Manoj K. Chaudhury, and John C. Chen. "Fast drop movements resulting from the phase change on a gradient surface." *Science* 291.5504 (2001): 633-636.

[106] Matar, O. K., and R. V. Craster. "Models for Marangoni drying." *Physics of Fluids* 13.7 (2001): 1869-1883.

[107] Xiao, Meng, Yiming Xian, and Feng Shi. "Precise macroscopic supramolecular assembly by combining spontaneous locomotion driven by the marangoni effect and molecular recognition." *Angewandte Chemie* 127.31 (2015): 9080-9084.

[108] Čejková, Jitka, et al. "Dancing performance of organic droplets in aqueous surfactant solutions." *Colloids and Surfaces A: Physicochemical and Engineering Aspects* 566 (2019): 141-147.

[109] Zhao, Haoyan, et al. "Fabrication of highly oriented large-scale TIPS pentacene crystals and transistors by the Marangoni effect-controlled growth method." *Physical Chemistry Chemical Physics* 17.9 (2015): 6274-6279.

[110] Ding, Zijing, et al. "Breakup of ultra-thin liquid films on vertical fiber enhanced by Marangoni effect." *Chemical Engineering Science* 199 (2019): 342-348.

[111] Herminghaus, Stephan, et al. "Interfacial mechanisms in active emulsions." *Soft matter* 10.36 (2014): 7008-7022.

[112] Deegan, Robert D., et al. "Capillary flow as the cause of ring stains from dried liquid drops." *Nature* 389.6653 (1997): 827.

[113] Kang, Saeed Jafari, et al. "Alternative mechanism for coffee-ring deposition based on active role of free surface." *Physical Review E* 94.6 (2016): 063104.

[114] Miniewicz, A., et al. "Marangoni effect visualized in two-dimensions Optical tweezers for gas bubbles." *Scientific reports* 6.1 (2016): 1-8.

[115] Hu, Hua, and Ronald G. Larson. "Marangoni effect reverses coffee-ring depositions." *The*

*Journal of Physical Chemistry B*110.14 (2006): 7090-7094.

[116] Ouenzerfi, Safouene, and Souad Harmand. "Experimental droplet study of inverted Marangoni effect of a binary liquid mixture on a nonuniform heated substrate." *Langmuir* 32.10 (2016): 2378-2388.

[117] Poulard, C., and P. Damman. "Control of spreading and drying of a polymer solution from Marangoni flows." *EPL (Europhysics Letters)* 80.6 (2007): 64001.

[118] Girard, F., M. Antoni, and K. Sefiane. "On the effect of Marangoni flow on evaporation rates of heated water drops." *Langmuir* 24.17 (2008): 9207-9210.

[119] Yunker, Peter J., et al. "Suppression of the coffee-ring effect by shape-dependent capillary interactions." *Nature* 476.7360 (2011): 308.

[120] Arendt, B., and R. Eggers. "Interaction of Marangoni convection with mass transfer effects at droplets." *International Journal of Heat and Mass Transfer* 50.13-14 (2007): 2805-2815.

[121] Garcia-Cordero, Jose L., and Z. Hugh Fan. "Sessile droplets for chemical and biological assays." *Lab on a Chip* 17.13 (2017): 2150-2166.

[122] Fatouros, Dimitrios G., et al. "Lipid-like self-assembling peptide nanovesicles for drug delivery." *ACS applied materials & interfaces* 6.11 (2014): 8184-8189.

[123] McBride, Samantha A., Susmita Dash, and Kripa K. Varanasi. "Evaporative crystallization in drops on superhydrophobic and liquid-impregnated surfaces." *Langmuir* 34.41 (2018): 12350-12358.

[124] Osada, Yoshihito, and Jian-Ping Gong. "Soft and wet materials: polymer gels." *Advanced Materials* 10.11 (1998): 827-837.

[125] Osada, Yoshihito, et al. "Spontaneous motion of amphoteric polymer gels on water." *Japanese journal of applied physics* 34.4B (1995): L511.

[126] Gong, J. P., et al. "Motion of polymer gels by spreading organic fluid on water." *The Journal of Physical Chemistry* 100.26 (1996): 11092-11097.

[127] Matsuda, Atsushi, et al. "Order-disorder transition of a hydrogel containing an n-alkyl acrylate." *Macromolecules* 27.26 (1994): 7695-7698.

[128] Mitsumata, Tetsu, et al. "Controlled motion of solvent-driven gel motor and its application as a generator." Langmuir 16.2 (2000): 307-312.

[129] Mitsumata, Tetsu, et al. "Controlled motion of solvent-driven gel motor and its application as a generator." *Langmuir* 16.2 (2000): 307-312.

[130] Bassik, Noy, Beza T. Abebe, and David H. Gracias. "Solvent driven motion of lithographically fabricated gels." *Langmuir* 24.21 (2008): 12158-12163.

[131] Zhao, Guanjia, and Martin Pumera. "Macroscopic self-propelled objects." *Chemistry–An Asian Journal* 7.9 (2012): 1994-2002.

[132] Zhao, Guanjia, Tzu Hui Seah, and Martin Pumera. "External-energy-independent polymer capsule motors and their cooperative behaviors." *Chemistry–A European Journal* 17.43 (2011): 12020-12026.

[133] Brochard, Françoise. "Motions of droplets on solid surfaces induced by chemical or thermal gradients." *langmuir* 5.2 (1989): 432-438.

[134] Ichimura, Kunihiro, Sang-Keun Oh, and Masaru Nakagawa. "Light-driven motion of liquids on a photoresponsive surface." *Science* 288.5471 (2000): 1624-1626.

[135] Nakata, Satoshi, et al. "Mercury drop "attacks" an oxidant crystal." *The Journal of Physical Chemistry B* 104.15 (2000): 3589-3593.

[136] Chao, Shih-hui, and Deirdre R. Meldrum. "Spontaneous, oscillatory liquid transport in surface tension-confined microfluidics." *Lab on a Chip* 9.7 (2009): 867-869.

[137] Magome, Nobuyuki, and Kenichi Yoshikawa. "Nonlinear oscillation and ameba-like motion in an oil/water system." *The Journal of Physical Chemistry* 100.49 (1996): 19102-19105.

[138] Toyota, Taro, et al. "Self-propelled oil droplets consuming "fuel" surfactant." *Journal of the American Chemical Society* 131.14 (2009): 5012-5013.

[139] Ban, Takahiko, et al. "pH-dependent motion of self-propelled droplets due to Marangoni effect at neutral pH." *Langmuir* 29.8 (2013): 2554-2561.

[140] Dos Santos, Fabrice Domingues, and Thierry Ondarcuhu. "Free-running droplets." *Physical Review Letters* 75.16 (1995): 2972.

[141] Zhang, Lidong, et al. "Marangoni effect-driven motion of miniature robots and generation of electricity on water." *Langmuir* 33.44 (2017): 12609-12615.

[142] Nagai, Ken, et al. "Mode selection in the spontaneous motion of an alcohol droplet." *Physical Review E* 71.6 (2005): 065301.

[143] Takabatake, Fumi, et al. "Spontaneous mode-selection in the self-propelled motion of a solid/liquid composite driven by interfacial instability." *The Journal of chemical physics* 134.11 (2011): 114704.

[144] Nagai, Ken, Yutaka Sumino, and Kenichi Yoshikawa. "Regular self-motion of a liquid droplet powered by the chemical marangoni effect." *Colloids and Surfaces B: Biointerfaces* 56.1-2 (2007): 197-200.

[145] Sumino, Yutaka, et al. "Self-running droplet: Emergence of regular motion from nonequilibrium noise." *Physical Review Letters* 94.6 (2005): 068301.

[146] Francis, Wayne, et al. "Self-propelled chemotactic ionic liquid droplets." *Chemical Communications* 51.12 (2015): 2342-2344.

[147] Chen, Yong-Jun, Yuko Nagamine, and Kenichi Yoshikawa. "Self-propelled motion of a droplet induced by Marangoni-driven spreading." *Physical Review E* 80.1 (2009): 016303.

[148] Albernaz, Daniel L., Gustav Amberg, and Minh Do-Quang. "Simulation of a suspended droplet under evaporation with Marangoni effects." *International Journal of Heat and Mass Transfer* 97 (2016): 853-860.

[149] Hanczyc, Martin M., et al. "Fatty acid chemistry at the oil− water interface: self-propelled oil droplets." *Journal of the American Chemical Society* 129.30 (2007): 9386-9391.

[150] Oshima, Shogo, et al. "Surface tension gradient around an alcohol droplet moving spontaneously on a water surface." *Analytical Sciences* 30.4 (2014): 441-444.

[151] Tomlinson, Charles. "II. On the motions of camphor on the surface of water." *Proceedings of the Royal Society of London* 11 (1862): 575-577..

[152] Kohira, Masahiro I., et al. "Synchronized self-motion of two camphor boats." *Langmuir* 17.22 (2001): 7124-7129.

[153] Bechinger, Clemens, et al. "Active particles in complex and crowded environments." *Reviews of Modern Physics* 88.4 (2016): 045006.

[154] Hayashima, Yuko, et al. "Self-motion of a camphoric acid boat sensitive to the chemical environment." *Physical Chemistry Chemical Physics* 4.8 (2002): 1386-1392.

[155] Nakata, Satoshi, et al. "pH-sensitive self-motion of a solid scraping on an aqueous phase." *The Journal of Physical Chemistry B* 102.38 (1998): 7425-7427.

[156] Nakata, Satoshi, and Yuko Hayashima. "Spontaneous motion of a solid is sensitive to the pH of an aqueous phase." *Langmuir* 15.5 (1999): 1872-1875.

[157] Nakata, Satoshi, and Mai Murakami. "Self-motion of a camphor disk on an aqueous phase depending on the alkyl chain length of sulfate surfactants." *Langmuir* 26.4 (2010): 2414-2417.

[158] Nakata, Satoshi, et al. "Self-motion of a camphanic acid disk on water with different types of surfactants." *The Journal of Physical Chemistry B* 110.42 (2006): 21131-21134.

[159] Nakata, Satoshi, Masahiro I. Kohira, and Yuko Hayashima. "Mode selection of a camphor boat in a dual-circle canal." *Chemical Physics Letters* 322.5 (2000): 419-423.

[160] Nakata, Satoshi, et al. "Self-rotation of a camphor scraping on water: new insight into the old problem." *Langmuir* 13.16 (1997): 4454-4458.

[161] Nakata, Satoshi, Yuko Hayashima, and Haruhisa Komoto. "Spontaneous switching of camphor motion between two chambers." *Physical Chemistry Chemical Physics* 2.10 (2000): 2395-2399.

[162] Nakata, Satoshi, and Shin-ichi Hiromatsu. "Intermittent motion of a camphor float." *Colloids and Surfaces A: Physicochemical and Engineering Aspects* 224.1-3 (2003): 157-163.

[163] Suematsu, Nobuhiko J., et al. "Mode-switching of the self-motion of a camphor boat depending on the diffusion distance of camphor molecules." *The Journal of Physical Chemistry C* 114.21 (2010): 9876-9882.

[164] Hayashima, Yuko, Masaharu Nagayama, and Satoshi Nakata. "A camphor grain oscillates while breaking symmetry." *The Journal of Physical Chemistry B* 105.22 (2001): 5353-5357.

[165] Nakata, Satoshi, Yukie Doi, and Hiroyuki Kitahata. "Synchronized sailing of two camphor boats in polygonal chambers." *The Journal of Physical Chemistry B* 109.5 (2005): 1798-1802.

[166] Nagayama, Masaharu, et al. "A theoretical and experimental study on the unidirectional motion of a camphor disk." *Physica D: Nonlinear Phenomena* 194.3-4 (2004): 151-165.

[167] Nakata, Satoshi, Yukie Doi, and Hiroyuki Kitahata. "Synchronized motion of a mobile boundary driven by a camphor fragment." *Journal of colloid and interface science* 279.2 (2004): 503-508.

[168] Nakata, Satoshi, Yukie Doi, and Yuko Hayashima. "Intermittent motion of a camphene disk at the center of a cell." *The Journal of Physical Chemistry B* 106.44 (2002): 11681-11684.

[169] Kitahata, Hiroyuki, et al. "Self-motion of a camphor disk coupled with convection." *Physical Chemistry Chemical Physics* 6.9 (2004): 2409-2414.

[170] Matsuda, Yui, et al. "Acceleration or deceleration of self-motion by the Marangoni effect." *Chemical Physics Letters* 654 (2016): 92-96.

[171] Soh, Siowling, Michal Branicki, and Bartosz A. Grzybowski. "Swarming in shallow waters." *The Journal of Physical Chemistry Letters* 2.7 (2011): 770-774.

[172] Karasawa, Yuichiro, et al. "Simultaneous measurement of surface tension and its gradient around moving camphor boat on water surface." *Chemistry Letters* 43.7 (2014): 1002-1004.

[173] Nepomnyashchy, Alexander A., Manuel G. Velarde, and Pierre Colinet. *Interfacial phenomena and convection*. CRC Press, 2001.

[174] Ikura, Yumihiko S., et al. "Suppression and regeneration of camphor-driven Marangoni flow with the addition of sodium dodecyl sulfate." *The Journal of Physical Chemistry B* 116.3 (2012): 992-996.

[175] Nakata, Satoshi, et al. "Marangoni flow around a camphor disk regenerated by the interaction between camphor and sodium dodecyl sulfate molecules." *Colloids and Surfaces A: Physicochemical and Engineering Aspects* 466 (2015): 40-44.

[176] Kitahata, Hiroyuki, et al. "Oscillation of a water surface in contact with a fixed camphor disk." *Chemical Physics Letters* 457.1-3 (2008): 254-258.

[177] Suematsu, Nobuhiko J., et al. "Quantitative estimation of the parameters for self-motion driven by difference in surface tension." *Langmuir* 30.27 (2014): 8101-8108.

[178] Kitahata, Hiroyuki, and Natsuhiko Yoshinaga. "Effective diffusion coefficient including the marangoni effect." *The Journal of chemical physics* 148.13 (2018): 134906.

[179] Mills, Allan. "The coefficient of friction, particularly of ice." *Physics Education* 43.4 (2008): 392.

[180] Gong, Jianping, and Yoshihito Osada. "Gel friction: a model based on surface repulsion and adsorption." *The Journal of chemical physics* 109.18 (1998): 8062-8068.

[181] Nanjundiah, Kumar, Ping Yuan Hsu, and Ali Dhinojwala. "Understanding rubber friction in the presence of water using sum-frequency generation spectroscopy." *The Journal of chemical physics* 130.2 (2009): 024702.

[182] Gong, Jianping, et al. "Friction of gels." *The Journal of Physical Chemistry B* 101.28 (1997): 5487-5489.

[183] Kurokawa, Takayuki, et al. "Elastic− hydrodynamic transition of gel friction." *Langmuir* 21.19 (2005): 8643-8648.

[184] Pucci, Giuseppe, Ian Ho, and Daniel M. Harris. "Friction on water sliders." *Scientific reports* 9.1 (2019): 1-7.

[185] Gong, Jian Ping. "Friction and lubrication of hydrogels—its richness and complexity." *Soft matter* 2.7 (2006): 544-552.

[186] Gong, Jianping, et al. "Friction of gels. 3. Friction on solid surfaces." *The Journal of Physical Chemistry B* 103.29 (1999): 6001-6006.

[187] Ghajar, Mohammad Hossein, Mahmoud Mosavi Mashhadi, and Hadi Ghattan Kashani. "Dynamic mechanical analysis of bucky gel actuator electrolyte by molecular dynamics simulation." *Computational Materials Science* 149 (2018): 379-385.

[188] Kang, Guo-dong, and Yi-ming Cao. "Application and modification of poly (vinylidene fluoride)(PVDF) membranes–a review." *Journal of Membrane Science* 463 (2014): 145-165.

[189] Ueberschlag, Pierre. "PVDF piezoelectric polymer." *Sensor review* (2001).

[190] Chen, Yong, and Chwen-Yang Shew. "Theoretical studies of the conformational behavior of chain molecules containing polar groups: simulations of a poly (vinylidene fluoride) model." *Journal of molecular modeling* 9.6 (2003): 379-389.

[191] Liu, Fu, et al. "Progress in the production and modification of PVDF membranes." *Journal of Membrane Science* 375.1-2 (2011): 1-27.

[192] Pickford, Tom, et al. "Effects of an ionic liquid and processing conditions on the β-polymorph crystal formation in poly (vinylidene fluoride)." *CrystEngComm* 21.36 (2019): 5418-5428.

[193] Ma, Wenzhong, et al. "Crystalline Phase Formation of Poly (vinylidene fluoride) from Tetrahydrofuran/N, N-dimethylformamide Mixed Solutions." *Journal of Macromolecular Science®, Part B: Physics* 47.3 (2008): 434-449.

[194] Wang, Xuyun, et al. "Formation mechanism and crystallization of poly (vinylidene fluoride) membrane via immersion precipitation method." *Desalination* 236.1-3 (2009): 170-178.

[195] Cho, Jae Whan, Ha Yool Song, and Sang Yong Kim. "Thermoreversible gelation of poly (vinylidene fluoride) in γ-butyrolactone solution." *Polymer* 34.5 (1993): 1024-1027.

[196] Xie, Yunchuan, et al. "Fabrication of stretchable nanocomposites with high energy density and low loss from cross-linked PVDF filled with poly (dopamine) encapsulated BaTiO3." *ACS applied materials & interfaces* 9.3 (2017): 2995-3005.

[197] Tazaki, Michiko, et al. "Crystallization and gelation of poly (vinylidene fluoride) in organic solvents." *Journal of applied polymer science* 65.8 (1997): 1517-1524.

[198] Wu, Qing-Yun, et al. "Interactions between polyacrylonitrile and solvents: density functional theory study and two-dimensional infrared correlation analysis." The Journal of Physical Chemistry B 116.28 (2012): 8321-8330.

[199] Rahaman, Muhammad Syukri Abdul, Ahmad Fauzi Ismail, and Azeman Mustafa. "A review of heat treatment on polyacrylonitrile fiber." *Polymer degradation and Stability* 92.8 (2007): 1421-1432.

[200] Tan, Lianjiang, Ding Pan, and Ning Pan. "Gelation behavior of polyacrylonitrile solution in relation to aging process and gel concentration." Polymer 49.26 (2008): 5676-5682.

[201] Roberts, A. D., and A. G. Thomas. "The adhesion and friction of smooth rubber surfaces." *Wear* 33.1 (1975): 45-64.

［202］ Persson, Bo NJ, et al. "On the nature of surface roughness with application to contact mechanics, sealing, rubber friction and adhesion." *Journal of physics: Condensed matter* 17.1 (2004): R1.

[203] Kim, Jaehwan, et al. "Durable and water-floatable ionic polymer actuator with hydrophobic and asymmetrically laser-scribed reduced graphene oxide paper electrodes." *Acs Nano* 8.3 (2014): 2986-2997.

[204] Simaite, Aiva, et al. "Hybrid PVDF/PVDF-graft-PEGMA membranes for improved interface strength and lifetime of PEDOT: PSS/PVDF/ionic liquid actuators." *ACS applied materials & interfaces* 7.36 (2015): 19966-19977.

[205] Wang, Miao, et al. "Sensitive Humidity-Driven Reversible and Bidirectional Bending of Nanocellulose Thin Films as Bio-Inspired Actuation." *Advanced Materials Interfaces* 2.7 (2015): 1500080.

[206] He, Jiang, et al. "Highly efficient actuator of graphene/polydopamine uniform composite thin film driven by moisture gradients." *Advanced Materials Interfaces* 3.14 (2016): 1600169.

[207] Arazoe, Hiroki, et al. "An autonomous actuator driven by fluctuations in ambient humidity." *Nature materials* 15.10 (2016): 1084-1089.

[208] Dong, Wutao, Songlin Nie, and Anqing Zhang. "Tribological behavior of PEEK filled with CF/PTFE/graphite sliding against stainless steel surface under water lubrication." Proceedings of

the Institution of Mechanical Engineers, Part J: Journal of Engineering Tribology 227.10 (2013): 1129-1137.

[209] Chen, Jinyu, et al. "Velocity dependence of friction and hydrogen bonding effects." *Physical review letters* 96.23 (2006): 236102.

[210] Van Rossum, Guido and Fred L. Drake. Python 3 Reference Manual. ScottsValley, CA: CreateSpace, 2009. Print.

[211] R Core Team.R: A Language and Environment for Statistical Computing. Vi-enna, Austria, 2020. Web.<https://www.R-project.org/>.

[212] Bradski, G. "The OpenCV Library".Dr. Dobb's Journal of Software Tools(2000). Print.

[213] Kralchevsky, Peter A., and Nikolai D. Denkov. "Capillary forces and structuring in layers of colloid particles." Current opinion in colloid & interface science 6.4 (2001): 383-401.

[214] Di Leonardo, R., F. Saglimbeni, and G. Ruocco. "Very-long-range nature of capillary interactions in liquid films." *Physical review letters* 100.10 (2008): 106103.

[215] Vella, Dominic, and L. Mahadevan. "The "cheerios effect"." *American journal of physics* 73.9 (2005): 817-825.

[216] Jaeger, John Conrad, and Horatio Scott Carslaw. Conduction of heat in solids. Clarendon P, 1959, Page 322.

[217] Crank, John. *The mathematics of diffusion*. Oxford university press, 1979,Page 41.